ATMOSPHERIC ICE NUCLEATION ABILITY OF MARINE PHYTOPLANKTON AND VIRUSES

A Dissertation

by

ELISE KATHERINE WILBOURN

Submitted to the Office of Graduate and Professional Studies of
Texas A&M University
in partial fulfillment of the requirements for the degree of

DOCTOR OF PHILOSOPHY

Chair of Committee,	Daniel C.O. Thornton
Co-Chair of Committee,	Sarah D. Brooks
Committee Members,	Shari Yvon-Lewis
	Jason Sylvan
Head of Department,	Shari Yvon-Lewis

December 2019

Major Subject: Oceanography

ABSTRACT

Ice nucleating particles (INP) are aerosol particles that catalyze the freezing of atmospheric water at temperatures warmer than homogeneous freezing, which occurs at -36 °C. INP contained in marine sea spray aerosols may be important drivers of atmospheric ice formation in clean marine areas with low concentrations of terrestrial INP. The characteristics of these INP and how they are formed is not well understood and may be linked to phytoplankton populations in the underlying water. Three phytoplankton batch cultures were grown in a marine aerosol reference tank (MART): *Thalassiosira weissflogii*, *Synechococcus elongatus*, and *Emiliania huxleyi*. Aerosols generated from the phytoplankton cultures were measured for INP activity. All taxa of marine phytoplankton investigated produce INP early in their growth, with maximum average freezing temperatures ranging from -18.0 ± 2.3 °C to -24.6 ± 1.9 °C. There was no link between INPs and chlorophyll *a* concentrations, unlike past studies. High ice nucleation temperatures occurred at times with a high growth rate. Three types of icosahedral marine phytoplankton viruses (31 nm to 170 nm diameter) were also tested for ice nucleation ability. These viruses froze at temperatures between -25.4 ± 0.6 °C and -20.8 ± 1.6 °C, showing the first evidence of viruses acting as INP.

Field samples were taken to compare the INP activity of phytoplankton sampled during the spring phytoplankton bloom as part of the North Atlantic Aerosols and Marine Ecosystems Study (NAAMES). Samples showed the same moderate INP activity seen in the MART samples taken at times of fast growth. Samples were also removed

from natural seawater samples by flow cytometry. These samples each contained a single group of phytoplankton (*Synechococcus*, nanoeukaryotes, and picoeukaryotes). The sorted samples had average freezing temperatures between -33.8 ± 1.5 °C and -22.1 ± 0.9 °C. Diluted samples showed an increase of the INP activity, demonstrating that the salt contained in the samples lowered the freezing temperature of the samples by up to 10 °C. Although not every sample tested had freezing temperatures above homogeneous freezing, these results show that many groups of phytoplankton and viruses produce INP that are active at atmospherically relevant temperatures.

ACKNOWLEDGEMENTS

I would like to thank my committee chairs, Drs. Thornton and Brooks, and my committee members, Dr. Sylvan and Dr. Yvon-Lewis for their guidance and support throughout the course of this research. I would also like to thank everyone who helped me collect and analyze samples during the MART and NAAMES projects.

Thanks also go to my friends and colleagues and the department faculty and staff for making my time at Texas A&M University a great experience.

Finally, thanks to Mom, Dad, Ed and Phyllis for their encouragement.

CONTRIBUTORS AND FUNDING SOURCES

Contributors

This work was supervised by a dissertation committee consisting of Professor Daniel C. O. Thornton (chair), Professor Shari Yvon-Lewis, and Professor Jason Sylvan of the Department of Oceanography and Professor Sarah D. Brooks (co-chair) of the Department of Atmospheric Science. Some of the data analyzed for Chapters 3, 4, and 5 was provided by Jessica Mirrielees in the Department of Atmospheric Science and Gerardo Gold Bouchot, Daniel Thornton, Alyssa Alsante, Kimberley Saypraysith, and Andrew Whitesell in the Department of Oceanography. Samples analyzed in Chapter 7 were taken in collaboration with Patricia Quinn, Timothy Bates, and Jason Graff. Viruses analyzed in Chapter 6 were provided by Kay Bidle. All other work conducted for the dissertation was completed by the student independently.

Funding Sources

Graduate study was made possible in part by the National Science Foundation under Grant Numbers ACP1539881 and DUE1355807 and the National Aeronautics and Space Association under Grant Number M1501775. Funding was also provided by the Department of Oceanography through the following scholarships: the Louis & Elizabeth Scherck Scholarship, the Webber Scholarship, and the Sharp Graduate Scholarship. Its contents are solely the responsibility of the authors and do not necessarily represent the official views of the Texas A&M University.

NOMENCLATURE

ASW	Artificial seawater
CCN	Cloud condensation nucleus
CDOM	Colored/chromophoric dissolved organic matter
Chl a	Chlorophyll *a*
Chlide a	Chlorophyllide *a*
CPC	Condensation particle counter
CSP	Coomassie staining particles
DMA	Differential mobility analyzer
DOC	Dissolved organic carbon
EPS	Exopolymeric substances
INP(s)	Ice nucleating particle(s)
NAAMES	North Atlantic Aerosols and Marine Ecosystem Study
OM	Organic matter
PCD	Programmed cell death
POM	Particulate organic matter
Ppt	Parts per thousand
TEP	Transparent exopolymer
UHP	Ultra high purity
VLP	Virus-like particle

TABLE OF CONTENTS

Page

LIST OF FIGURES

Page

LIST OF TABLES

Page

1. INTRODUCTION

Marine phytoplankton blooms produce large quantities of organic material as cell fragments and exudates (Falkowski et al., 2000), a portion of which are then aerosolized through winds and wave action (Prather et al., 2013; Quinn et al., 2014; Quinn, Collins, Grassian, Prather, & Bates, 2015). Seawater also contains small bacterial and viral particles that can be aerosolized and transported across kilometer-scale distances (Michaud et al., 2018; Reche, D'Orta, Mladenov, Winget, & Suttle, 2018). Marine aerosols contain cloud ice nucleating particles, but it is currently not fully understood what those INP are composed of or how they are produced. This dissertation aims to gather more detailed information on which groups of marine microorganisms (including viruses) produce INPs and whether there is link between physiological stress and INP production.

1.1. Cloud Types and Aerosol Interactions

Cloud properties driven by aerosols can have major climate effects, and yet are one of the most poorly understood aspects of atmospheric science (Boucher et al., 2013; Brooks & Thornton, 2018; Lee, Reddington, & Carslaw, 2016; Seinfeld et al., 2016; Zhao et al., 2016). Aerosols can indirectly effect the climate by changing the radiative effects of clouds including albedo and cloud lifetimes (DeMott et al., 2010; Jensen & Toon, 1997; Lohmann, 2002), or directly affect the amount and type of precipitation (Teller, Xue, & Levin, 2012). There are three main types of clouds, each composed of either solid ice or liquid droplets. Warm clouds contain only liquid water, and their water

droplets grow either due to high water supersaturation or the presence of cloud condensation nuclei (CCN), which initiate droplet formation by lowering the critical supersaturation, allowing condensation (Rogers & Yau, 1996). Ice clouds contain solid ice particles that freeze either at temperatures below -36 °C through the process of homogeneous freezing or due to the presence of ice nucleating particles (INPs) during heterogeneous freezing processes (Heymsfield & Sabin, 1989; Hoose & Mohler, 2012; Vali, 1971). Mixed phase clouds contain both liquid water and ice crystals. The type of cloud that forms over an area is dependent on relative humidity, altitude (and therefore temperature), and the type and concentration of aerosols present (Pruppacher & Klett, 2012).

At any given point in time it is estimated that two thirds of the globe is covered in clouds (Boucher et al., 2013; Mace et al., 2009). Measurements of cloud cover are made by satellites including Cloud-Sat and CALIPSO (Cloud-Aerosol Lidar and Infrared Pathfinder Satellite Observations). These data are then used in small-scale, high resolution models to characterize cloud properties. However, data from individual clouds are not used directly in large-scale global circulation models, which typically have a grid size of kilometers or larger, much larger than the size of an individual cloud. Due to difficulties in including individual cloud processes, including albedo and precipitation, this information must instead be well-characterized by smaller-scale models so that it can be accurately represented by large-scale GCMs (Boucher et al., 2013). This is one of the main reasons it is so important to remove as much uncertainty as possible from measurements of aerosol effects and models of cloud microphysics.

1.2. Ice Nucleation Mechanisms

In the absence of any ice nucleating particles (INP), atmospheric water droplets do not freeze at 0 °C due to the small size of the droplets (Hoose, Kristjansson, Chen, & Hazra, 2010; Koop, 2004). Atmospheric water droplets are 1-2 μL and smaller (Yau & Rogers, 1996), so freezing must overcome the effects of this small size before ice crystals can form. Since atmospheric ice nucleation is a semi-stochastic process, the physics of freezing are not fully defined (Hoose & Mohler, 2012; Lohmann & Ferrachat, 2010; Morrison & Milbrandt, 2015). However, it is known that part of the reason ice forms at much colder temperatures with decreasing droplet diameter is due to the effect of the droplet surface tension. The smaller the droplet, the greater the effect the curvature of the edge has on the freezing process. In the absence of any outside nucleation catalyst, ice crystals in the atmosphere form at approximately -36 °C (Hoose & Mohler, 2012). This process is known as homogeneous nucleation (figure 1.1A).

There are four mechanisms by which INP catalyze freezing at temperatures warmer than homogeneous nucleation: immersion, condensation, deposition, and contact freezing (Pruppacher & Klett, 2012; Vali, 1985) (see Figure 1.1 B-E). These mechanisms are atmospherically important because of their ability to lower the altitude of formation of clouds containing ice crystals. The radiative effect of an ice cloud is very different from that of a warm cloud that forms at the same altitude (Lohmann & Diehl, 2006; Vergara-Temprado et al., 2018), so it is important to understand the processes that change the altitude of formation of ice clouds.

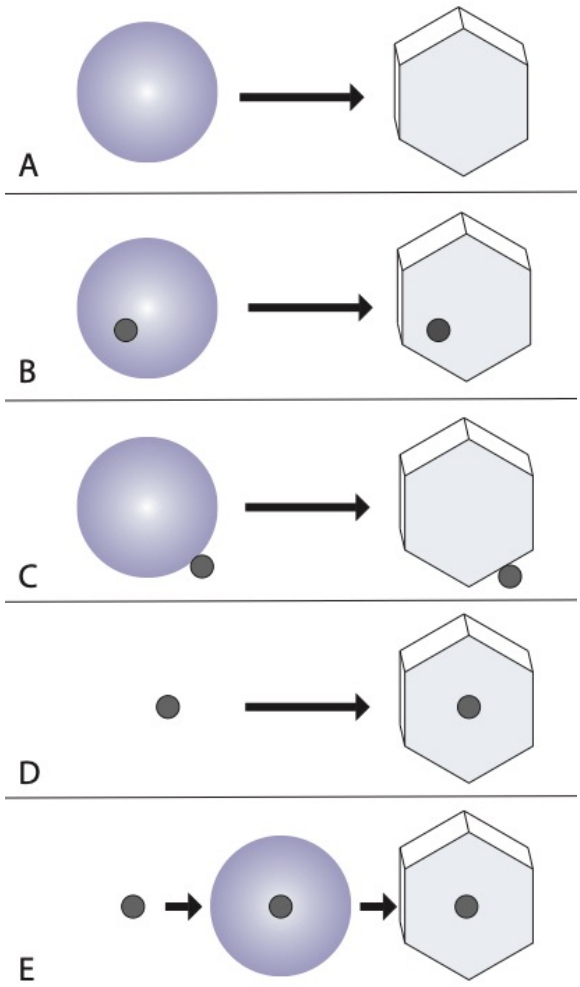

Figure 1.1: Ice nucleation mechanisms: A) homogeneous nucleation without ice nucleating particles, B) immersion freezing, C) contact freezing, D) deposition freezing, and E) condensation freezing

Condensation freezing involves the INP first activating as a CCN, followed by freezing of the condensation that forms around the particle. Deposition freezing is similar but ice deposits onto the INP directly from the vapor phase rather than liquid water forming around a nucleus and freezing. Contact freezing occurs when the INP is in

direct contact with the edge of the droplet, which nucleates freezing. The final freezing mechanism is immersion freezing. During the process of immersion freezing, a particle inside a water droplet catalyzes freezing. In some cases condensation freezing is considered a discrete freezing mechanism as the droplet may have fully formed before the particle was immersed in water (Hoose & Mohler, 2012), but other parameterizations regard condensation freezing as part of immersion or deposition nucleation processes (Diehl & Mitra, 1998; Field et al., 2012). Contact freezing may occur at warmer temperatures than deposition or condensation freezing (Diehl, Matthias-Maser, Jaenicke, & Mitra, 2002; Gokhale & Goold Jr, 1968; Levin & Yankofsky, 1983; Pitter & Pruppacher, 1973) but relies on the INP impacting with a water droplet. Estimates of freezing mechanisms based on field measurements and modeling suggest that contact and condensation/immersion freezing are the dominant freezing modes (Cooper & Vali, 1981). However, ice nucleation process measurements in clouds are difficult to measure directly, so there are no available estimates of the exact rates at which each freezing process is occurring (Durant & Shaw, 2005).

1.3. Ice Nucleating Particles

It is mostly unknown what characteristics of an aerosol particle make it able to effectively catalyze freezing at temperatures warmer than homogeneous freezing. The first atmospheric ice nucleation studies assumed that the particles must be hexagonal and as close to the crystalline structure of water as possible. The first well-studied INP was silver iodide (AgI) (Vonnegut, 1947), followed by other iodine-containing molecules such as lead iodide (Hogan, 1967; Morgan & Allee, 1968; Schaefer, 1966). Silver iodide

has a hexagonal crystal structure and catalyzes freezing at temperatures as high as -3 °C. Following studies assumed that this hexagonal crystal structure was both necessary and characteristic of compounds that act as INP, but Fukuta (1958) showed that compounds can act as INP without a hexagonal crystal structure and compounds with hexagonal structures are not necessarily good INP. Recent work has shown that glassy solids without a defined crystal structure can also act as INP (Murray et al., 2010; Wilson et al., 2012). Many of the initial conclusions about ice nucleation have been shown to only be true in certain cases rather than applicable to all INP.

Currently known INP are produced both by natural and anthropogenic processes. Mineral dust is both a large source of aerosols and a large source of INP. Deserts are a major source of mineral dust, including potassium feldspar (K-feldspar) (Kiselev et al., 2017; Mason & Maybank, 1958), which can nucleate freezing below -15 °C (Atkinson et al., 2013). K-feldspar can be found in mineral dust worldwide, with an ice nucleation ability that is dependent on its mineral group (Welti, Lohmann, & Kanji, 2019). K-feldspar minerals that have a more ordered tetrahedral crystal structure may catalyze atmospheric ice nucleation at higher temperatures, although increases in ice nucleation temperature have also been linked to surface properties of individual particles (Whale et al., 2017). This increase in INP activity is due the higher level of order in K-feldspar crystals from groups such as microcline that form at comparatively low temperatures (Welti et al., 2019). Other natural sources of INP are volcanic sulfate emissions and soot and black carbon from wildfires and biomass burning (Durant, Shaw, Rose, Mi, & Ernst, 2008; Fullerton, Garcia, & Langer, 1975; Seifert et al., 2011; Steinke et al., 2011),

although some studies suggest that volcanic ash are generally poor INPs (Hoyle et al., 2011). Anthropogenic INP sources include manufacturing and transportation processes. These processes produce black carbon and organic materials that are somewhat effective INP (Crawford et al., 2011; DeMott, Chen, Kreidenweis, Rogers, & Sherman, 1999; Friedman et al., 2011; Jensen & Toon, 1997; Knopf, Wang, Laskin, Moffet, & Gilles, 2010; Möhler et al., 2005). Biological matter can also be a source of INP, including pollen, (Diehl et al., 2002; Hader, Wright, & Petters, 2014) bacteria, (Amato et al., 2015; Kim, Orser, Lindow, & Sands, 1987; Lindow, Arny, & Upper, 1978; Maki, Galyan, Chang-Chien, & Caldwell, 1974; Morris, Georgakopoulos, & Sands, 2004), fungi (Fröhlich-Nowoisky et al., 2016; Iannone, Chernoff, Pringle, Martin, & Bertram, 2011; Morris et al., 2013; Pouleur, Richard, Martin, & Antoun, 1992), lichens (Kieft, 1988; Kieft & Ahmadjian, 1989; Moffet, Getti, Henderson-Begg, & Hill, 2015), individual biological molecules like cellulose and oxalic acid (Hiranuma et al., 2019; Hiranuma et al., 2015; Zobrist et al., 2006), and marine microorganisms including phytoplankton and bacteria (DeMott et al., 2016; Irish et al., 2017; Ladino et al., 2016; Vergara-Temprado et al., 2017; Wilson et al., 2015; Wolf et al., 2019).

1.4. Marine Aerosols

Marine aerosols can generally be classified as containing a mixture of two major chemical groups: sea salt aerosols and marine organic aerosols (Ault et al., 2013; Quinn et al., 2015). These types of aerosols vary not just in composition but in size (Gantt & Meskhidze, 2013). Generally, marine organic aerosols have a greater number of very small Aitken-mode particles (approximately 45 nm diameter) when compared with sea

salt aerosols, and some studies have reported an increase in 200-300 nm particles compared with sea salt aerosols (Cavalli et al., 2004; Keene et al., 2007). Since marine INP have an average diameter of 300 nm (Wilson et al., 2015), this suggests an organic source for these INP.

When characterizing sea spray aerosols (SSA), it is not known exactly what drives organic enrichment in aerosols relative to underlying water but is has been proposed that the sea surface microlayer (SML) is a major source of aerosolized organics. The SML is a thin (μm-scale) layer of hydrophobic organic matter that collects on the surface of the ocean (Cunliffe et al., 2013; Engel et al., 2017). The microlayer is enriched in organics, bacteria, and viruses compared with the underlying waters (Aller, Kuznetsova, Jahns, & Kemp, 2005; Engel et al., 2017). Some studies have reported enrichment of polysaccharides and gel particles in the SML (Aller et al., 2005; Cunliffe et al., 2013; Thornton, Brooks, & Chen, 2016). Gel particles have also been found in aerosols (Leck & Bigg, 2005). As bubbles pass through this layer, organic material is adsorbed to the surface of the bubble and ejected into the air as the bubble bursts (Marks, Górecka, McCartney, & Borkowski, 2019; Wang et al., 2017). Chance et al. (2018) found that the SML contained more efficient INP than the underlying seawater as well as spatially variable enrichment in some ions (which were likely biological in origin). Irish et al. (2017) also found INP-active particles in SML samples.

1.4.1. Marine Aerosols as Ice Nucleating Particles

There are relatively few studies on INP generated from marine aerosols (Alpert, Aller, & Knopf, 2011a; DeMott et al., 2016; DeMott et al., 2018; Irish et al., 2017;

Knopf, Alpert, Wang, & Aller, 2011; Ladino et al., 2016; McCluskey et al., 2016; McCluskey, Hill, et al., 2018; McCluskey, Ovadnevaite, et al., 2018; Prather et al., 2013; Vergara-Temprado et al., 2017; Wilson et al., 2015), and fewer on specifically the role of biological processes on INP generation (DeMott et al., 2018; McCluskey et al., 2016; McCluskey, Hill, et al., 2018; McCluskey, Ovadnevaite, et al., 2018). However, as the oceans cover 71% of the planet, they are a major source of aerosols, some of which act as INP. Although other INP sources including aeolian dust have a larger atmospheric impact (Burrows, Hoose, Pöschl, & Lawrence, 2013; Hoose, Kristjansson, & Burrows, 2010), an underestimation of INPs present leads to incorrect calculation of the radiative effect of the clouds present, so it is important to determine the INP concentration in marine aerosols.

Open ocean waters contain up to 10^5 phytoplankton mL^{-1} seawater, 10^6 bacterial cells mL^{-1}, and 10^8 viruses mL^{-1} (Lalli & Parsons, 1997; Suttle, 2005; Whitman, Coleman, & Wiebe, 1998), although concentrations vary widely. Michaud et al. (2018) measured on the order of 10^7 virus-like particles (VLP) per cubic meter of air when sampling sea spray aerosols, ranging from 0.07 to 1.13 times the VLP in corresponding bulk water samples (also on the order of 10^7 VLP mL^{-1} of seawater). They also reported an enrichment of specific bacterial taxa at amounts up to an order of magnitude higher than bulk water samples, suggesting selective aerosolization of marine bacteria. There does not seem to be a straightforward relationship between bacteria and plankton biomass and rates of aerosol production (Irish, Hanna, Xi, et al., 2019). Although organic aerosol concentrations generally increase with increasing seawater organic

concentrations (O'Dowd et al., 2015; Rastelli et al., 2017; Schmitt-Kopplin et al., 2012), it is also unlikely that there would be a linear relationship between increasing numbers of VLP in the underlying water and INP concentration. INPs in the surface seawater probably include organic matter other than just whole cells or viruses, as organisms are a major source of dissolved and particulate carbon in the ocean (Brooks & Thornton, 2018; Falkowski et al., 2000).

1.5. Ocean Nutrient Cycling

Phytoplankton play a vital role in the oceanic carbon cycle (referring to the movement and transformation of carbon through biotic and abiotic processes) as they are the only organisms capable of transforming carbon dioxide into carbon sources like sugars that can be utilized by heterotrophic organisms (Falkowski, Barber, & Smetacek, 1998). Carbon dioxide in the ocean is either atmospheric carbon dioxide that dissolves in the ocean or carbon dioxide produced through bacterial remineralization (Emerson & Hedges, 2008). Current estimates of phytoplankton carbon uptake suggest that they are responsible for approximately half the global uptake, with uptake increasing as atmospheric CO_2 rises (Riebesell et al., 2007).

Carbon fixed by phytoplankton enters the marine ecosystem as dissolved and particulate organic material (DOM and POM, operationally defined as larger and smaller than 0.7 μm respectively) through consumption of the phytoplankton themselves or their death (Calbet & Landry, 2004). Viral infection and subsequent lysis is also an important pathway for increased dissolved organic matter increases (Jiao et al., 2010; Suttle, 2007). Some of the OM produced by phytoplankton moves throughout the trophic web as it is

consumed by zooplankton and other larger organisms, but some sinks through the water column. Unless this sinking material is uplifted by physical mixing processes, it can be buried in seafloor sediment for hundreds or thousands of years. However, the total amount of atmospheric carbon that is sequestered is only a small percentage of the CO_2 that is taken up by phytoplankton (Berner, 1982; Duarte & Cebrián, 1996; Müller & Suess, 1979).

Phytoplankton also require nutrients other than carbon for photosynthesis, including nitrogen, phosphorous, silicon, and other micronutrients (Lalli & Parsons, 1997). Nutrient requirements vary by species. These nutrients enter the marine system through weathering of continental material and deposition of aeolian desert dust (Fan, Moxim, & Levy, 2006; Mahowald et al., 2005). Nitrogen and phosphorous especially in coastal waters may also be sourced from agricultural runoff (Beman, Arrigo, & Matson, 2005; Carlsson & Granéli, 1993), and nitrogen may also be fixed into a utilizable form by bacteria, including some species of cyanobacteria (Bullerjahn & Post, 2014; Fay, 1992). Nutrients are cycled through the ocean waters through physical processes including upwelling (Thurman, Trujillo, Abel, & McConnell, 1999). Limitation of specific required nutrients can help explain the phytoplankton species present in a region, although there are other environmental factors that also impact this (DiTullio, Hutchins, & Bruland, 1993; Frey & Small, 1980).

1.6. Phytoplankton Growth Processes

As a phytoplankton population grows, it goes through several different growth phases (Buchanan, Whiting, & Damert, 1997; Hogg, 2005; Zwietering, Jongenburger,

Rombouts, & van 't Riet, 1990). These growth phases are seen both in populations of individual species and multi-species populations under ideal conditions but are most apparent in single-species laboratory-based cultures that do not include grazing processes by zooplankton, variable environmental conditions and nutrient concentrations, or viral infection.

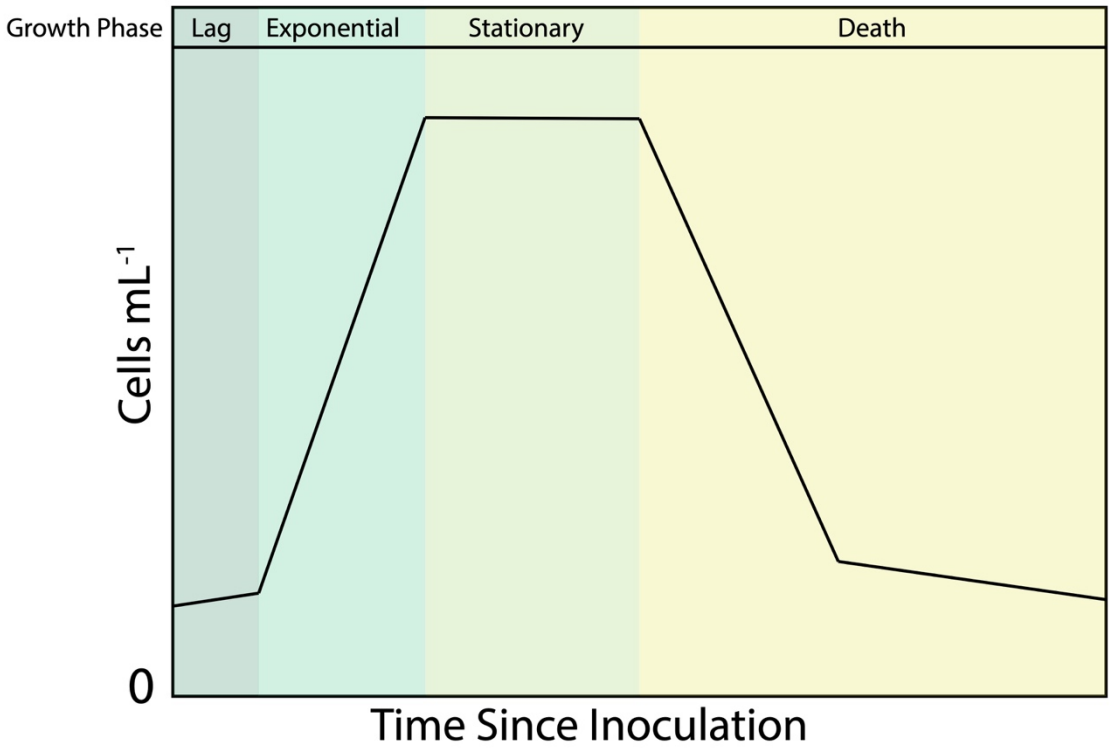

Figure 1.2: Idealized microbial growth, including relative cell concentration (cells mL^{-1}) and growth phases.

Growth phases can best be defined using growth rates, calculated from the following equation:

$$\mu = \frac{\ln(X_0) - \ln(X_1)}{t} \quad (1)$$

where μ is growth rate (day^{-1}), X_0 is the initial concentration (number of cells), X_1 is the final concentration, and *t* is time in days (Hogg, 2005). The first growth, lag phase, occurs as the cells adjust to different environmental conditions, including temperature, salinity, light levels, and nutrient concentrations, and is characterized by a slightly positive growth rate as division rates are slightly higher than death rates. Lag phase is not always clear in cell concentration plots if the population adjusts to environmental conditions at a faster rate than sampling occurs. Exponential growth follows the lag phase, where cells are dividing rapidly due to suitable environmental conditions and few cells are dying. Exponential phase corresponds with a large, positive growth rate as the cell concentration is increasing exponentially. Following exponential growth, the death rate begins to increase until it is nearly equal to the division rate and the culture enters stationary phase, which has a growth rate of nearly zero. Some studies include a time of declining growth rate following exponential growth and prior to stationary phase (Monod, 1949), but this phase is not included in all models. Following stationary phase is the death phase (Kono, 1968; Whiting & Cygnarowicz-Provost, 1992; Zwietering et al., 1990). The death rate continues to increase until it is much higher than the rate of division and the culture is said to be in death phase, where the growth rate is very negative. This negative growth rate generally continues until the cell concentration is low but not zero, at which point the death rate will decrease but remain higher than the

division rate. An ideal plot of growth rates and cell concentrations is plotted in Figure 1.2. In batch cultures there is a limited nutrient concentration unless more nutrients are added, so eventually the nutrients will be consumed and even a small population of phytoplankton cells cannot be supported, leading to complete death of the population.

In real-world settings, drivers of phytoplankton population concentrations include environmental conditions include light availability, temperature, and nutrient concentrations, as well the rate of grazing and death due to viral infection (Gunnar Bratbak, Egge, & Heldal, 1993; Brussaard, 2004; Eppley, 1972; Lalli & Parsons, 1997). As climate change continues in the future, ocean acidification will also be an important factor in phytoplankton health, especially those species with more soluble calcium carbonate cell walls (Behrenfeld et al., 2006; Iglesias-Rodriguez et al., 2008; McCarthy, Rogers, Duffy, & Campbell, 2012; Passow & Laws, 2015; Riebesell & Tortell, 2011). All of these factors can be varied in laboratory settings, but for the studies described in this dissertation nutrient limitation will be the major driver of cell death. There are no zooplankton included in any of the marine aerosol reference tank (MART) experiments, and grazing is not considered in field samples. As well, viral infection is not addressed in any of the chapters of this dissertation. Light and temperature were held steady, and a single dose of nutrients was added at the beginning of each MART experiment and subsequently consumed by the growing phytoplankton population. See Chapter 3, 4, and 5 for further details on the amount of nutrients added to the tank each time.

As the culture moves through the different growth phases, there are corresponding changes in individual cell physiology and condition, although the health

of an individual cell remains much less important than the overall population health since any given cell may only live one or two days (Behrenfeld, Halsey, & Milligan, 2008). Many of these changes are very species-specific and can also vary within species based on environmental conditions (Behrenfeld et al., 2008; Owens & Esaias, 1976). However, there are some changes that occur within all the groups studied here (diatoms, cyanobacteria, and coccolithophores).

One possible physiological change that may occur as culture health declines that could have major atmospheric implications is an increase in cellular membrane permeability. A healthy cell will have processes to tightly regulate movement of molecules through the cell membrane. As the cell ages and becomes less healthy the membrane permeability increases (Veldhuis, Kraay, & Timmermans, 2001). Once the cell dies, there is no regulation of movement through the membrane and the material inside the cell is released, first through the membrane and then freely after the cell membrane ruptures. This increase in membrane permeability can be monitored through the use of stains such as SYTOX Green (Lebaron, Catala, & Parthuisot, 1998), and may be a source of atmospheric organic material as the exuded material joins the pool of marine dissolved organic matter (DOM) (O'Dowd et al., 2015).

As the cell health decreases, it also releases a larger quantity of exopolymeric material in some phytoplankton species (Berman-Frank, Rosenberg, Levitan, Haramaty, & Mari, 2007; Bidle, 2015; Chen & Thornton, 2015; Fukao, Kimoto, & Kotani, 2010; Thornton & Chen, 2017), which as discussed earlier may be a source of INP. Some studies have found an increase in INP concentration following phytoplankton bloom

decline that was attributed to an increase in cell leakiness (DeMott et al., 2016; McCluskey, Hill, et al., 2018; McCluskey, Ovadnevaite, et al., 2018), but these studies did not measure cell permeability or exopolymer production and instead linked a decline in chlorophyll *a* with the end of the bloom.

Pigment concentrations in each cell and in the culture as a whole may also increase and decrease as the culture health changes. All photosynthetic plankton contain chlorophyll *a* as their main photosynthetic pigment, accompanied by a variety of accessory pigments. Generally, a higher pigment concentration is associated with a healthier culture, but it should be noted that chlorophyll and accessory pigment concentrations can also increase or decrease as the culture photoacclimates (Dubinsky & Stambler, 2009; Perry, Talbot, & Alberte, 1981). The amount of photosynthetic pigment is also associated with how efficiently the cell is able to photosynthesize (Falkowski, 1980), so generally the closer the culture is to death phase, the lower the chlorophyll concentration and the less efficiently the culture can utilize the energy from sunlight. However, in some cases photosynthetic efficiency can increase in response to light limitation (Falkowski, 1980).

The culture stoichiometry also changes as the culture moves through growth phases, with some studies suggesting that nutrient utilization is moving toward the Redfield ratio (universal C:N:P ratio of 106:16:1, [Redfield, 1934, 1958]) (Goldman, 1980). Species with a higher growth rate are generally found to produce a greater proportion of protein relative to their rate of carbohydrate production (Veldhuis, Admiraal, & Colijn, 1986). This high rate of protein synthesis is maintained by high

concentrations and production rates of rRNA (Elser et al., 2000; Sterner, 1995), which in turn pushes the ratio of N:P lower as more P is used in building the rRNA. Nutrient limitation can change this ratio in natural seawater systems, but in a system that is not nutrient-limited and follows a standard growth curve higher rates of protein production are seen during exponential growth, followed by higher rates of carbohydrate production during later growth phases. A lower N:P ratio is also associated with higher rates of extracellular polysaccharides (Myklestad, 1995).

1.7. Dissertation Hypotheses and Research Motivation

Although it was first hypothesized in the 1980s that marine phytoplankton could play a role in atmospheric processes (Charlson, Lovelock, Andreae, & Warren, 1987), there are a very limited number of studies looking at the role of phytoplankton biological processes in the formation of ice-containing clouds. This dissertation aims to determine the role of several phytoplankton taxa in ice cloud formation by testing the following hypotheses:

1. Phytoplankton and material produced by phytoplankton act as ice nucleating particles (INPs) at atmospherically relevant temperatures.
2. Different phytoplankton taxa change ice nucleation temperatures and INP concentrations.
3. There is a link between the processes associated with cell growth and physiological status and ice nucleation ability of cells and associated material.
4. Viruses act as ice nucleating particles in seawater samples.

Current research suggests that most of the phytoplankton species tested produce

INPs (Alpert et al., 2011a; Alpert, Aller, & Knopf, 2011b; Knopf et al., 2011; Ladino et al., 2016; Wilson et al., 2015) and freeze at temperatures well above -36 °C where homogeneous freezing occurs. However, there are only five studies addressing INP production from single-species cultures (Alpert et al. 2011a and 2011b; Knopf et al., 2011; Wilson et al., 2015; Wolf et al., 2019). Wolf et al. (2019) only reports the deposition mode INP activity of the particles produced from *Prochlorococcus*, while the other four studies contain data on either solely immersion mode INPs or a combination of immersion and deposition mode INP data (Alpert et al., 2011a and 2011b; Knopf et al., 2011; Wilson et al. 2015). One of these studies (Alpert et al., 2011b) reported freezing temperatures from *Emiliania huxleyi* that were much closer to homogeneous freezing (suggesting that the material tested contained poor INPs). An extensive examination of immersion mode INP production by phytoplankton, which are ubiquitous globally, is needed to determine the potential impact of phytoplankton-influenced aerosols.

Once it has been determined whether all tested phytoplankton groups produce INPs, the INP concentration produced by each group should be studied. Phytoplankton are phylogenetically diverse with extremely variable morphologies and chemical compositions. This dissertation will aim to test several of the most ubiquitous phytoplankton taxa for INP production.

Phytoplankton, like all organisms, change over the course of their life cycle. These changes may change the chemical composition and ice nucleating activity of the aerosols that are produced over the water containing phytoplankton blooms, but no

current research has tracked the INP production of a phytoplankton bloom from beginning to death.

Seawater contains more than just phytoplankton, including bacteria and viruses that are aerosolized along with phytoplankton-based material. Marine phytoplankton viruses are a similar size to other known INPs. Although past research concluded that viruses are poor INP, only one species of virus out of the many found in seawater was tested (Junge & Swanson, 2007). Further testing of marine phytoplankton viruses is justified based on the diversity of shapes and sizes of virus particles (Suttle, 2005).

The species studied in this dissertation were studied across the entire growth cycle of the culture from bloom to death in large-volume batch cultures in a marine aerosol reference tank (MART). The three groups studied were chosen to represent a large proportion of the phytoplankton found in the open ocean and include a ubiquitous diatom species, one of the most common cyanobacterial species, and the most environmentally important coccolithophore species. As well as phytoplankton species, three types of marine viruses were tested for ice nucleating ability. In addition to laboratory-based single species experiments, this dissertation will include results from samples taken in the North Atlantic during the May 2016 North Atlantic Aerosols and Marine Ecosystems Study (NAAMES) research cruise.

2. METHODS

2.1. Introduction

This section describes the methods used in the experiments described in chapters 3, 4, and 5. Each of these experiments focuses on a single species grown in a Marine Aerosol Reference Tank (MART). Aerosols were generated inside the tank and water and air samples were taken concurrently to characterize how the aerosols changed as the phytoplankton culture progressed through each of the growth phases. All of the methods described in this chapter were used in at least two out of three of the experiments. Any changes to the methods or additional methods used are described at the beginning of each subsequent chapter, and if the sampling or analysis was performed by anyone else this is also noted. Due to the quantity and variety of samples taken each day during each MART experiment, at least three people gathered and analyzed samples daily.

2.2. Experimental Setup

Single-species cultures were grown in artificial seawater and aerosols were generated from the water containing nutrients, phytoplankton, and bacterial populations. Previous MART experiments have used natural seawater and natural phytoplankton populations (McCluskey et al., 2016; McCluskey, Hill, et al., 2018; McCluskey, Ovadnevaite, et al., 2018; Wang et al., 2015). Although natural seawater would contain more representative bacterial populations, it is more difficult to determine drivers of results and changes in aerosols produced from natural seawater. By closely monitoring a single-species culture, we hoped to be able to directly link biological processes such as

cell death and exudate production to changes in aerosol production and characteristics. As well, three ubiquitous species were chosen to represent their respective taxa and determine what if anything is driving taxon-level differences in INP production.

2.2.1. Tank Parameters

A rectangular acrylic aquarium with 200 L capacity was first sprayed down with 70% isopropanol and then rinsed three times with ultra-high purity (UHP) water. The tank was then filled with 63 L of artificial seawater (described in section 2.2.1.1 and table 2.1) and modified L1 nutrients (individual nutrient amounts for each experiment are described in chapters 3, 4, and 5). A single-species culture of phytoplankton was added to the seawater, the tank was closed using a shaped acrylic sheet as a lid and sealed with gasket tape, and the sealed edge of the tank was then wrapped with Parafilm (Bemis Corp., Inc.). Unless aerosol sampling was occurring, three 4-cm long stir bars constantly mixed the water (180 rpm) in the MART to prevent organisms from settling to the bottom of the tank. The tank was illuminated with two LED lights that ran the length of the front and the back of the tank 10 cm above the bottom of the tank. The lights provided 170 μmol s^{-1} m^{-2} of light (measured with a LiCor 250A light meter) on a 14 hour light: 10 hour dark cycle. All water and aerosol samples were taken when the tank was illuminated, and each type of sample was taken at approximately the same time after the lights turned on each day. Biological sampling occurred one hour after the lights turned on each day, and aerosol generation began one hour after this (two hours after the lights turned on), with pumping occurring every 2 hours for the next six hours. Aerosols were generated using a peristaltic pump to pump water from a 2 cm hole in the

bottom of the tank up to a waterfall made of 3 cm PVC pipe 35.6 cm above the water surface. All water samples were drawn from a 2 cm sample port in the top of the tank using a 60 mL syringe (VWR). The port was sealed with an airtight plug unless sampling was occurring. Aerosol sampling was also from the top of the tank, as seen in figure 2.1. See section 2.6 for more detail on aerosol sample types and methods. After the tank was sealed it was not reopened until the experiment was over to prevent contamination.

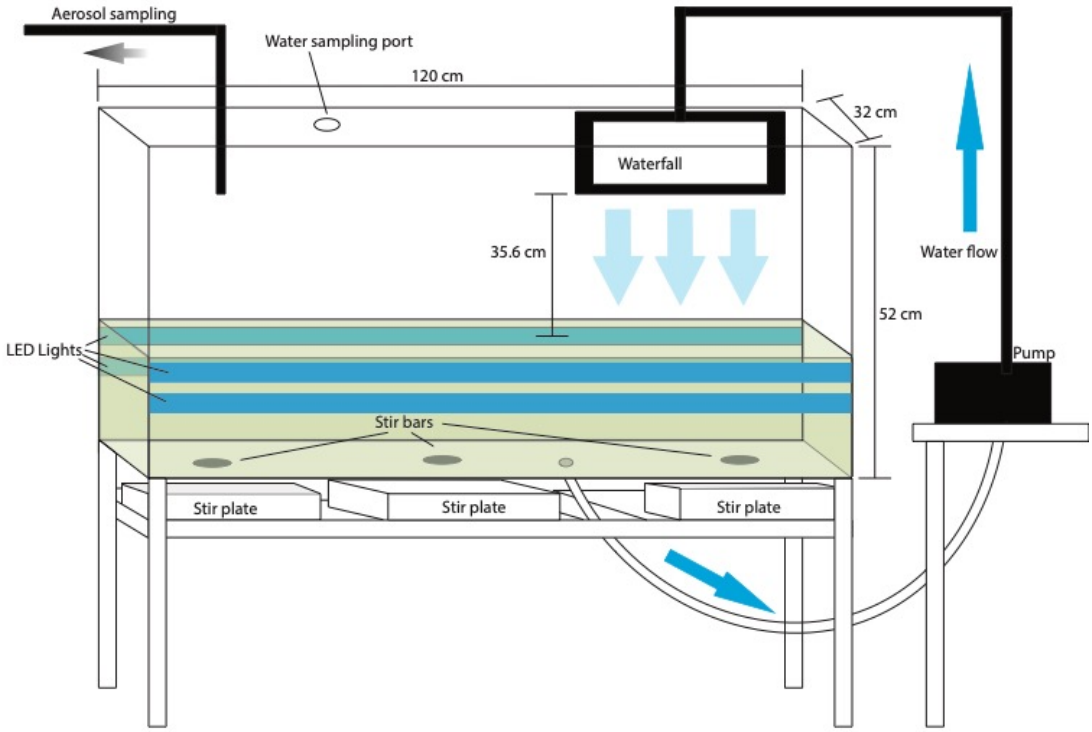

Figure 2.1: Setup of the marine aerosol reference tank (MART) and peristaltic pump. During each experiment 63 L ASW + modified L1 media was placed into the tank along with the phytoplankton culture. LED lights illuminated the tank and aerosols were generated using a peristaltic pump to create a waterfall. Aerosol and water sampling occurred via the top of the tank.

2.2.1.1. Artificial Seawater

Artificial seawater (ASW) was made following the formula given in Harrison, Waters, and Taylor (1980) and updated in Berges and Franklin (2001). All seawater was made with ultra high purity (UHP) water. For all MART experiments, the NaCl was combusted for at least six hours at 500 °C to remove any organic contamination. The following recipe was used to make 5L of artificial seawater, and any larger batches were scaled appropriately:

Table 2.1: Recipe for 1 L of artificial seawater following Berges et al., 2001. All salts were purchased from VWR. Sodium chloride was combusted (500 °C, 6 hours) to remove organic material. All ASW was made with UHP water.

Chemical	Amount (g)
Anhydrous Salts	
Sodium chloride (NaCl)	21.19
Sodium sulfate (Na_2SO_4)	3.55
Potassium chloride (KCl)	0.599
Sodium bicarbonate ($NaHCO_3$)	0.174
Potassium bromide (KBr)	0.0863
Boric acid (H_3BO_3)	0.023
Sodium fluoride (NaF)	0.0028
Hydrated Salts	
Magnesium chloride ($MgCl_2 \cdot 6H_2O$)	9.59
Calcium chloride ($CaCl_2 \cdot 6H_2O$)	1.344
Strontium chloride ($SrCl_2 \cdot 6H_2O$)	0.0218

Table 2.2: Nutrients, vitamins, and trace mineral molar concentrations in L1 media. Nutrient concentrations varied between experiments and are described in further detail in the chapters describing each individual experiment. Nutrient salts and vitamins were purchased from VWR and prepared in UHP water, while the trace metal solution was purchased from the National Center for Marine Algae and Microbiota at Bigelow Laboratories. *Concentrations for individual MART experiments are given in chapters 3, 4, and 5

Chemical	Concentration (M)
Nutrients*	
Sodium nitrate ($NaNO_3$)	N/A*
Monosodium phosphate ($NaH_2PO_4 \cdot H_2O$)	N/A*
Sodium silicate ($Na_2SiO_3 \cdot 9H_2O$)	N/A*
Vitamins	
Thiamine	2.96×10^{-7}
Biotin	2.05×10^{-9}
Cyanocobalamin	3.69×10^{-10}
Trace Metals	
$Na_2EDTA \cdot 2H_2O$	1.17×10^{-5}
Iron (III) chloride ($FeCl_3 \cdot 6H_2O$)	1.17×10^{-5}
Manganese (II) chloride ($MnCl_2 \cdot 4H_2O$)	9.09×10^{-7}
Zinc sulfate ($ZnSO_4 \cdot 7H_2O$)	8.00×10^{-8}
Cobalt (II) chloride ($CoCl_2 \cdot 6H_2O$)	5.00×10^{-8}
Copper (II) sulfate ($CuSO_4 \cdot 5H_2O$)	1.00×10^{-8}
Sodium molybdate ($Na_2MoO_4 \cdot 2H_2O$)	8.22×10^{-8}
Selenious acid (H_2SeO_3)	1.00×10^{-8}
Nickel (II) sulfate ($NiSO_4 \cdot 6H_2O$)	1.00×10^{-8}
Sodium orthovanadate (Na_3VO_4)	1.00×10^{-8}
Potassium chromate (K_2CrO_4)	1.00×10^{-8}

All anhydrous and hydrated salts were purchased from VWR, and the trace metals solution was purchased from the National Center for Marine Microbiota and Algae (NCMA) at Bigelow Laboratory for Ocean Science. The sodium chloride used in the artificial seawater was combusted for six hours at 500 °C to remove any organic contaminants. Following preparation of the ASW the solution was allowed to dissolve at room temperature (20-25 °C) for at least 24 hours and was then adjusted to a pH of 8.2 using a 2 M sodium hydroxide solution.

2.2.2. MART Experiment Samples

Daily water and aerosol samples were taken to monitor the status of the phytoplankton culture and measure the quantity and characteristics of aerosols produced from the water containing phytoplankton cells and byproducts (e.g. exudates, exopolymers, and dead cells and fragments). These samples are described both in chapter 2 and in further detail in chapters 3, 4, and 5 (if needed). Table 2.3 shows the samples taken during each experiment and is separated to distinguish between water samples and aerosol samples. If the sample was taken or analyzed by anyone else, that is denoted by a "*" and noted in the results section regarding each sample in Chapter 3, 4, and 5.

Table 2.3: A comparison of three experiments consisting of cultures grown in the MART tank, and the samples taken during each experiment. Further details of each method can be found either following in this chapter or in the individual chapters for each experiment. Water measurements were taken on samples drawn from the bulk water, while aerosol samples were taken following generation of daily aerosol populations. *Samples taken or analyzed by someone else

Species Grown	*Thalassiosira weissflogii*	*Synechococcus elongatus*	*Emiliania huxleyi*
Water measurements	CCMP 1051	CCMP 1379	CCMP 374
	Cell counts	Cell counts	Cell counts
	Bulk protein concentration	Bulk protein concentration	Bulk protein concentration
	Bulk carbohydrate concentration*		Bulk carbohydrate concentration
	Quantum yield of photosystem II (dark-adapted)	Quantum yield of photosystem II (light- and dark-adapted)	Quantum yield of photosystem II (light- and dark-adapted)
	Cell membrane permeability	Cell membrane permeability	Cell membrane permeability
	Caspase-3-like enzyme activity	Caspase-3-like enzyme activity	Caspase-3-like enzyeme activity
	β-glucosidase activity*		β-glucosidase activity*
	Transparent exopolymer particle area and concentration*	Transparent exopolymer particle area and concentration*	Transparent exopolymer particle area and concentration
	Coomassie-staining particle area and concentration*	Coomassie-staining particle area and concentration*	Coomassie-staining particle area and concentration
		Bacterial counts*	Bacterial counts*
	Colored dissolved organic material*	Colored dissolved organic material*	Colored dissolved organic material*
	Chlorophyll *a* concentration	Chlorophyll *a* concentration*	Chlorophyll *a* concentration*
		Prokaryotic community composition*	Prokaryotic community composition*
Aerosol measurements	Total aerosol concentration*	Total aerosol concentration*	Total aerosol concentration*
	Cloud-condensation nucleus concentration*	Cloud-condensation nucleus concentration*	Cloud-condensation nucleus concentration*
		Particle size distributions**	Particle size distributions**
	Ice nucleation activity	Ice nucleation activity	Ice nucleation activity

2.3. Biological Measurements

Biological sampling occurred via a 2 cm port in the top of the tank, which was sealed with a silicone rubber bung between water sampling events. Water was removed from the tank with a 60-mL syringe that was acid-washed in 10% HCl daily and rinsed three times with UHP prior to sampling. All biological samples were taken between 8 and 10 am when the LED lights had been on for approximately two hours but before the daily aerosol generation and measurements.

2.3.1. Biomass Measurements

Methods described in this section were performed on bulk water samples without any further processing to induce cell lysis or filtration. Although this gives the best picture of changes in culture biomass over time, it also includes not just the phytoplankton population but any contaminating bacteria. Although the MART was sealed, it was not kept axenic at any point during the experiments. Bacterial counts are given in Chapter 4 and 5 but were not successful for the experiment described in Chapter 3. Growth phases were defined for each experiment based on chlorophyll *a* concentration as this is the only biomass data that is available for all three MART experiments.

2.3.1.1. Phytoplankton Counts

Cell counts were taken each day to give the most accurate estimate of phytoplankton biomass. Samples were preserved for cell counts in 2 mL glass bottles with 2 drops of Lugol's iodine. Bottles were placed in the dark at 4 °C and stored for no more than two weeks prior to counting. Cell count methods are based on (Guillard &

Sieracki, 2005). Before the sample was removed from the bottle for counting, the bottle was gently shaken to ensure cells were evenly suspended within the liquid. Cells were counted at 100x magnification with a light microscope (Spencer microscope, American Optical). Cultures were placed in a Fuchs-Rosenthal hemocytometer (VWR) with a disposable glass pipette (VWR) and at least 400 cells were counted. The volume of each grid square is 1.25 x 10^{-4} mL. The cell concentration was calculated using the following formula:

$$\text{cells mL}^{-1} = \frac{\text{cells counted}}{\text{grid squares}} \cdot 80{,}000 \quad (1)$$

Three cell counts were taken from each sample and the average was reported as the daily cell concentration ± standard deviation, n = 3.

The growth rate can be calculated from biomass measurements including cell counts and chlorophyll *a* concentrations, using the following equation:

$$\mu\ (d^{-1}) = \frac{\ln(N_1 - N_0)}{T_1 - T_0} \quad (2)$$

where μ is the growth rate (per day), and N is the biomass at the beginning and end of a unit of time (T). The biomass N is either the total chlorophyll per mL seawater or the cell concentration per mL of seawater, but must remain the same measure of biomass (either chlorophyll or cells) for the entire experiment so that data can be compared between days.

2.3.1.2. Bacteria Counts

Bacteria were counted during the experiments covered in Chapter 4 and 5 by Alyssa Alsante. Each day, a single 15 mL sample of water was placed into a sterile 50

mL centrifuge tube (VWR) and fixed with 300 mL 0.2 µm-filtered formalin (VWR, 37-39% wt/v formaldehyde solution). Samples were stored in the dark at 4 °C for at least 10 minutes or until slides were prepared (no more than one hour). Following slide preparation the tube was flash frozen with liquid nitrogen and stored at -20 °C.

To prepare slides for bacterial counts, a known concentration of fixed culture was filtered onto 0.02 µm 25 mm Anodisc filters (VWR). Three filters were made from each daily sample. Each filter was placed into a sterile petri dish and 100 µL SYBR Green stain (1:200 dilution prepared with UHP water, Thermo Fisher) was dropped onto the slide. The filter was then left to dry and stain for at least 18 minutes in the dark at 20 °C. once the filter was dry it was mounted onto a glass slide (VWR) with SlowFade Diamond Antifade Mountant (Invitrogen) and stored at -20 °C until the bacteria were counted with an epifluorescence microscope (Zeiss Axioplan 2). At least 400 cells were counted from each slide.

2.3.2. Bulk Protein Measurements

Bulk measurements of the protein concentration in both culture medium and cells were measured using methods from (Bradford, 1976). Samples were placed into sterile 1.5 mL microcentrifuge tubes (VWR) and stored in the dark at -20 °C for no more than one month prior to measurement. A protein standard was made with bovine serum albumin (BSA, VWR) at known protein concentrations between 0 and 20 mg mL^{-1}, and a calibration was performed at the same time as the sample measurements. Absorbance was plotted against protein concentration to construct a calibration curve. Samples were placed into disposable polycarbonate microcuvettes (VWR) at a 1:1 ratio with Bradford

Reagent (Sigma Aldrich). Cuvettes were incubated in the dark at 25 °C for between 30 and 40 minutes. Sample absorbance was read with a spectrophotometer (Shimadzu UV-mini 1240) at 595 nm. All samples and standards were measured as fast as possible and always within 10 minutes of each other. Sample protein concentration was determined from the BSA calibration curve. Protein measurements in Chapter 5 were performed with assistance from Kimberly Sayprasith.

2.3.3. Bulk Carbohydrate Measurements

Carbohydrate analysis was based off methods from DuBois, Gilles, Hamilton, Rebers, and Smith (1956). Samples were placed in 1.5 mL microcentrifuge tubes and stored at -20 °C in the dark for no more than six months prior to analysis. Just prior to analysis 0.8 mL of the sample was placed into combusted boiling tubes (Pyrex) and 0.4 mL 5% phenol was added to the tube. Sulfuric acid was then rapidly added to the tubes, followed by resting for 30 minutes. The sample absorbance was then read at 485 nm. The measured absorbance was compared with a calibration curve prepared with D-glucose and UHP water prior to analysis (with concentrations ranging from 1 to 100 μg mL^{-1}). Absorbance was read with a spectrophotometer (Shimadzu UV-mini 1240). Carbohydrate measurements made for Chapter 3 were taken by Andrew Whitesell.

2.4. Physiological Measurements

While measurements described in section 2.3 give an approximation of culture biomass and bulk water characteristics, methods described in this section give more detailed information about cellular functions, including photosynthesis and membrane integrity. This gives a clearer picture of the physiological status of the phytoplankton in

the culture, including how efficiently photosynthesis is occurring, what materials are being taken up and exuded, and the activity of specific enzymes. The data collected using these methods is used to confirm when the culture enters and leaves each growth phase, and focuses especially on cell death processes as a time when large quantities of organic material may be exuded and thus aerosolized (O'Dowd et al., 2015).

2.4.1. Pulse Amplitude Modulation (PAM) Fluorometry

The maximum quantum yield of photosystem II was measured with a PAM fluorometer (Walz Phyto-PAM) as an indicator of photosynthetic efficiency (Schreiber, 2004). This instrument allows for several simultaneous measurements on the same sample. Fluorescence measurements are made based on the cellular response to four colored lights (470 nm, 520 nm, 645 nm, and 665 nm). The sample (4 mL) was placed into a clean quartz glass cuvette (Hellma Analytics and placed in the dark at room temperature (23-25 °C) for 30 minutes to dark-adapt the sample. To ensure the measurements could be taken in triplicate, identical quartz glass cuvettes were used for all measurements. The background fluorescence was determined by filtering 4 mL of culture with a 0.2 μm pore size filter attached to a sterile syringe (VWR). The filtrate was placed into one of the glass cuvettes and this was placed into the PAM fluorometer and the background fluorescence was measured and set for the sample. It was assumed that all three samples taken concurrently had the same background fluorescence. After dark adaptation for 30 minutes at 20 °C, the sample was then quickly placed into the emitter-detector chamber (Walz) and a measurement was taken.

Samples were dark-adapted for 30 minutes at 20 °C to measure the maximum quantum yield of photosystem II (F_v/F_m) (Klughammer & Schreiber, 2008; van Kooten & Snel, 1990). Dark adaptation limits the amount of non-photochemical quenching by measuring the response of fully relaxed reaction centers to light (Schreiber, Schliwa, & Bilger, 1986). Although measurements were recorded at all four wavelengths, only the measurements from dark-adapted samples from 665 nm are reported here. The 665 nm wavelength was chosen as it is representative of chlorophyll *a*, which all of the different phytoplankton studied contain. However, the fluorescent yield is not directly proportional to chlorophyll *a* concentrations in the sample as the PAM fluorometer applies a photomultiplier gain to account for biomass differences. The fluorometer has the capability to measure chlorophyll concentrations and account for the gain but has to be calibrated against each species to be accurate.

2.4.2. Cell Membrane Permeability

Cell membrane permeability was determined based on staining with SYTOX green (5 mM solution in DMSO, Invitrogen) (Veldhuis, Cucci, & Sieracki, 1997). This stains DNA with a molecule that fluoresces green (523 nm) under 450-490 nm light. The SYTOX molecule is too large to pass through a healthy cell membrane, but as the cell ages the membrane becomes more permeable (Thornton & Chen, 2017). Eukaryotic cells have two different stages of health that are visible with SYTOX green. Healthy cells only show red fluorescence (from the chlorophyll *a*). In the first stage, the outer cell membrane is permeable enough to allow SYTOX green molecules to pass into the cell, but the cell still has an intact nuclear membrane enclosing all the DNA. Cells observed

in this stage still show some red fluorescence from the chlorophyll *a*, but the nucleus is also visible as a small green area. As cells become unhealthier, the nuclear envelope ruptures and DNA is spread throughout the cell. At this stage, cells appear entirely green under the fluorescent microscope.

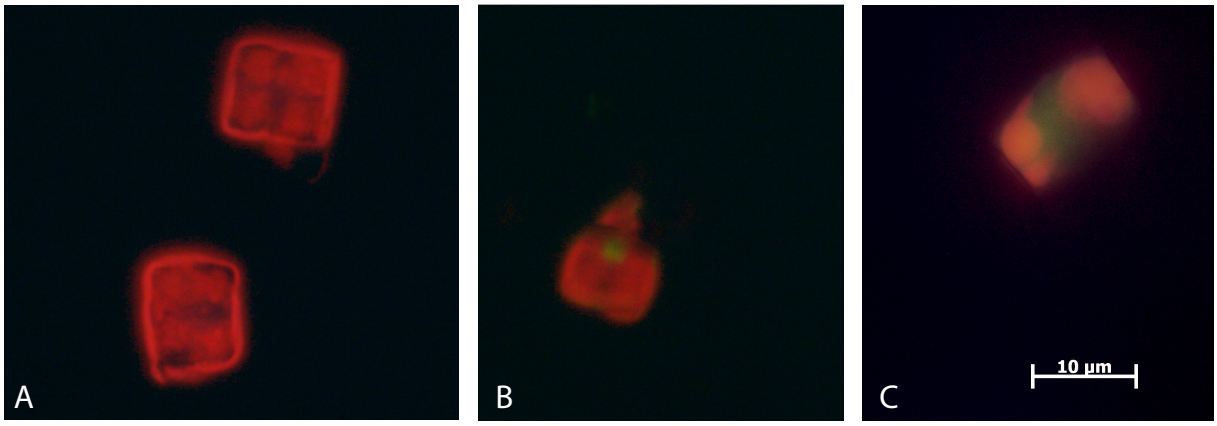

Figure 2.2: A) *Thalassiosira weissflogii* cells showing red chlorophyll fluorescence B) *Thalassiosira weissflogii* cell showing chlorophyll fluorescence (red) and SYTOX Green fluorescence by genetic material in the nucleus (green) C) *Thalassiosira weissflogii* cell showing fluorescence of chlorophyll (red) and genetic material (green). All images were taken with an epifluorescence microscope.

To stain cells with SYTOX green, the stain was diluted from 5 mM to 0.5 µM with UHP water. This working solution was stored in 1 mL aliquots in sterile microcentrifuge tubes in the dark at -20 °C until use. Cell culture samples (1 mL) were placed in sterile microcentrifuge tubes along with 40 µL diluted SYTOX green (1.92 µM). The culture and stain were incubated at 20 °C in the dark for 30 minutes. The

stained culture was then diluted with 1 mL UHP water and filtered onto a polycarbonate filter (0.4 µm pore size, Nuclepore). The stained cells were counted at 400x magnification with an epifluorescence microscope (Zeiss Axioplan 2). At least 400 cells were counted from each sample and classified as either unstained, partially stained (only the nucleus was stained), or completely stained. In the case of prokaryotic cells, only two classes were counted due to lacking a nucleus. Three replicate slides of filtered sample were counted each day.

2.4.3. Caspase-3-like Enzyme Activity

Caspase-like enzyme activity was measured using methods modified from Bouchard and Purdie (2011) and further described in Thornton and Chen (2017). Samples in 15 mL sterile centrifuge tubes were first centrifuged for 20 minutes at 4000 *g* to create a pellet of cells (12 tubes total, four for each sample due to the size of the centrifuge rotor). Each sample consisted of 60 mL of starting culture, and pellets from four tubes (60 mL starting volume) were combined into one 15 mL centrifuge tube following the first centrifugation. Pellets were resuspended in 15 mL phosphate-buffered saline (PBS). The sample was then centrifuged for 20 minutes at 4000 *g* to pelletize the cells. The washing process was repeated three times. Following the final centrifugation, overlying PBS was pipetted off and the pellet was stored at -20 °C in the dark for no more than one month prior to analysis with the EnzChek™ Caspase-3 Assay Kit #1 (ThermoFisher). This kit uses the substrate Z-Asp-Glu-Val-Asp-7-amino-4-methylcoumarin (Z-DEVD-AMC), which is fluorescent once cleaved by caspase-3 and other caspase-like enzymes. To break open the cells, samples were sonicated with a

probe sonicator (QSonica Model CL-18, 125 watts, 20kHz) in 1X cell lysis buffer according to the kit instructions and samples and standards were placed into a 96-well plate (Grenier, 50 µL per well). The following samples and controls were tested: sample alone, sample and substrate, sample and DMSO (to ensure no background fluorescence by the DMSO contained in the substrate), and UHP water. Fluorescence was read every 5 minutes for at least 12 hours with a fluorescent plate reader (SpectraMax GEMINI EM; Molecular Devices). Excitation was measured at 342 nm and emission at 441 nm, with a cutoff at 420 nm. The amount of protein in each sample was measured using the method described in Section 2.3.2 from Bradford (1976) to give final units of pmol μg^{-1} protein hr^{-1}.

2.4.4. β-glucosidase Measurements

Measurements of β-glucosidase activity were made on samples with 2 mM 4-methylumbelliferone-β-D-glucopyranoside as a substrate (Hoppe, 1983; Marx, Wood, & Jarvis, 2001) without adjusting the pH. The samples were also compared to a heat-killed control (prepared by incubation of a 10 mL sample at 90-95 °C for 15 minutes). The samples were placed into a Grenier opaque white 96-well plate (200 µL in each well) with the following controls: artificial seawater, UHP water, cultures filtered through a GF/C filter, and samples filtered through a GF/C filter and a 0.2 µm syringe filter (VWR). Standards of methylumbelliferone (MUF) at concentrations ranging from 0-1 µM were run at the same time and used to prepare a calibration curve. The plate of samples was analyzed with SoftMax Pro 4.8 software reading emission and excitation from a fluorescent plate reader (SpectraMax Gemini EM) with an excitation of 346 nm,

emission at 460 nm, and a cutoff at 435 nm. The samples were mixed for 5 seconds prior to reading and a reading was taken every 2.5 minutes for at least 12 hours. Measurements of β-glucosidase activity for Chapter 3 were made by Daniel Thornton, and for Chapter 5 were made by Alyssa Alsante.

2.4.5. Exopolymer Particle Measurements

Transparent exopolymer (TEP) measurements were based on methods from Passow and Alldredge (1995) and Alldredge, Passow, and Logan (1993)and Coomassie staining particles were measured based on methods in (Long & Azam, 1996). These methods were also described in Thornton et al. (2016) and Chen and Thornton (2015). Transparent exopolymers are composed of acidic polysaccharides, while Coomassie staining particles are proteinaceous. TEP and CSP samples were prepared with the same method; only the stain used differed. As both stains are blue-colored, the same filter could not be stained with both dyes. Alcian blue (Sigma Aldrich) was used to stain the TEP samples, while Coomassie brilliant blue (CBB, Sigma Aldrich) was used for the CSP samples. Alcian blue was prepared as a 0.02% solution in UHP water and 0.06 % glacial acetic acid (VWR) and was then adjusted to a ph of 2.5 with more acetic acid. The CBB stock solution was prepared with 1 g of CBB in 100 mL UHP water, and was further diluted each day with a ratio of 1:25 stock solution: UHP water. Both stains were filtered through 0.2 μm syringe filters prior to use. To prepare a filter, 2 mL sample was filtered onto a 0.4 μm pore size polycarbonate filter (Nuclepore, VWR) at a very slow rate to prevent breakup of exopolymeric material. The sample or stain (1 mL) was then filtered through the same filter at a rate of approximately one drop per 30 seconds to

stain the exopolymers. The filter was then rinsed with 1 mL of water two times, again at a rate of approximately one drop every 30 seconds. Once the filter was dry, it was mounted onto a white glass Cytoclear slide (GE Water and Process Technologies) with Type FF immersion oil (Cargille) and covered with a 25 mm glass cover slip (VWR). Three slides each of TEP and CSP samples were prepared for each sample. Slides were stored vertically in the dark at -20 °C until analysis. Exopolymer particle measurements for Chapter 3 were made by Andrew Whitesell, and for Chapter 4 were made by Alyssa Alsante.

Ten photographs were taken of each slide. Each photograph was processed with Image J software (NIH). First the color channels were split into red, green, and blue. The red channel was then transformed into a binary scale using the software to threshold the image such that only the colored particles were chosen. These particles were analyzed for number and area concentration if they were larger than 10 μm.

2.5. Statistical Methods

All statistical analysis was performed in SigmaPlot (SyStat Software, Inc.). If a sample was run multiple times on the ice microscope, the pooled mean and pooled standard deviation are reported. All other data points ($n \geq 3$) are reported as the mean ± standard deviation. Correlations are given as Pearson's correlation coefficients (r) and correlations are only reported as significant if $p < 0.05$. Data was confirmed to be unique by performing a 1-way repeated measures analysis of variance test (ANOVA, Shapiro-Wilk Normality Test, $P < 0.05$, equal variance test, $P < 0.05$, and pairwise multiple comparison via Holm-Sidak method) with an overall significance level at 0.05.

2.6. Aerosol Measurements

All aerosol samples were taken by Jessica Mirrielees, who also analyzed all aerosol measurements other than the ice nucleation activity. Aerosols were generated using a peristaltic pump (Watson-Marlow 550Dz) to send 70 x 1 L doses of water through 2 cm tubing (internal diameter) to a PVC pipe with a 4-cm slot in it to generate a waterfall (see Figures 2.1 and 2.2). The waterfall was 35.6 cm above the surface of the water. Each round of 70 doses took approximately 30 minutes. Stir bars (3 cm, VWR) were used to mix the tank during times when aerosol sampling was not occurring. There were four periods of aerosol sampling on each day, and the pump was run to generate aerosols prior to each aerosol sampling period. Aerosol generation occurred starting two hours after the LED lights turned on each day. Aerosol sampling occurred from a PVC pipe attached to 1.5 cm internal diameter tubing.

During each sampling period, aerosols were pumped through a desiccant tube (TSI) to lower the relative humidity of the sampled air to 50% or below, followed by passing through a metal mixing chamber, where the sample was split. The sample then either was collected with impaction samplers (PIXE) to be tested for ice nucleation or sized through a differential mobility analyzer (Grimm or TSI) and then counted with a butanol-based condensation particle counter (CPC, Grimm). During the second and third sampling times the setup is slightly different, with the sample split between a water-based CPC (TSI) or another mixing tube that leads to both the same butanol-based CPC (Grimm) and a condensation particle counter (Droplet Measurement Technologies

[DMT] CCNC-100). Figure 2.2 shows the setup used to take samples that are later tested for ice nucleation activity.

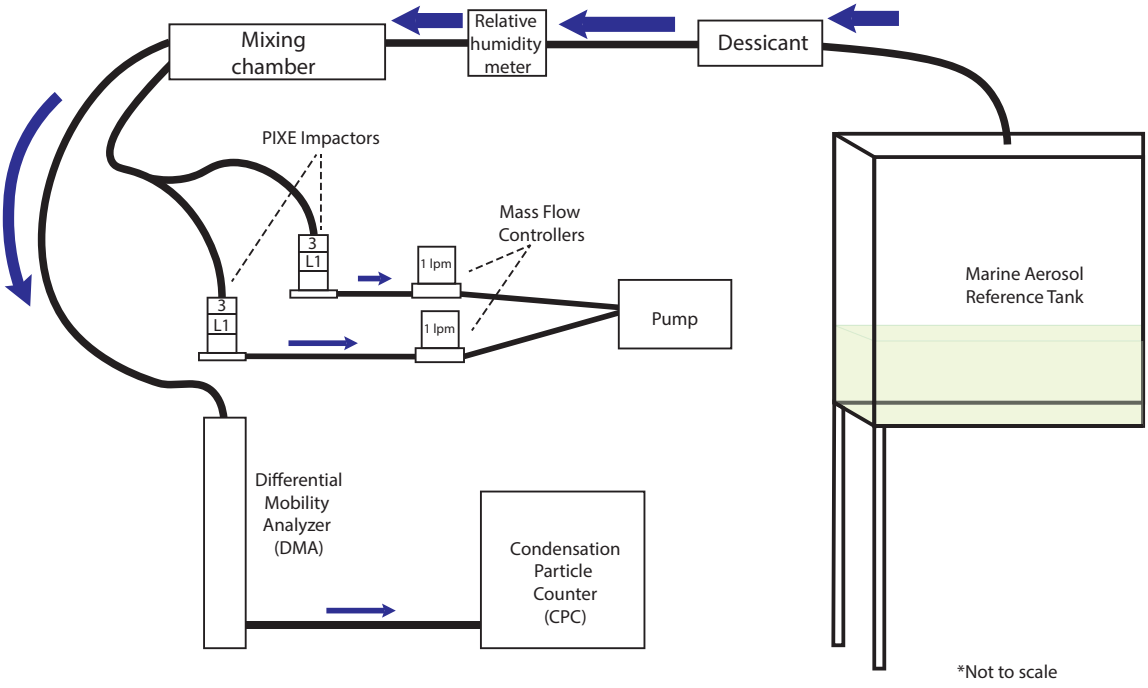

Figure 2.3: Aerosol sampling setup. Aerosols are generated by a waterfall, dried in a desiccant tube (TSI), and sampled into either an impaction sampler (PIXE) or a differential mobility analyzer (DMA, Grimm).

2.6.1. Total Aerosol Concentrations

Total aerosol concentrations were measured with a condensation particle counter (CPC, TSI Inc. Model 3786). Aerosols generated from the MART were dried by passing through a desiccant tube (TSI) to a relative humidity of no higher than 50% with a flow rate of 1 liter per minute (lpm). Particle concentrations were read for the entire two-hour

sampling period and an average particle concentration was found from measurements taken at one second intervals. Any times when the CPC gave an error message were not included in this average calculation.

2.6.2. Ice Nucleation Measurements

All ice nucleation measurements were made with a custom microscope (referred to as an ice microscope) equipped with a cooling stage capable of reaching temperatures colder than -36 °C (the temperature of homogeneous freezing). This setup was first described in Fornea, Brooks, Dooley, and Saha (2009), and further details can be found in Collier and Brooks (2016). Samples are either liquid or aerosol samples. Aerosol samples were collected with impaction samplers (PIXE, Inc.) using the L1 stage (0.06 μm – 1 μm size range) onto aluminum foil discs (25 mm). The aluminum foil was first combusted at 500 °C for at least six hours to remove all organic contamination, followed by mounting onto polycarbonate disks (PIXE Inc.). Further detail on aerosol sample collection is found in individual chapters.

Liquid samples (2 μL) were run on silanized slides, while samples collected with an impaction sampler onto aluminum foil were placed under a 2 μL droplet of UHP water. The aluminum foil disc was then placed onto a silanized slide. Slides were prepared by soaking clear slides (VWR) in 2% Aquasil solution (VWR) for 60 seconds, followed by rinsing with methanol (VWR) and drying before use. If dilutions were needed, the sample was diluted with UHP water.

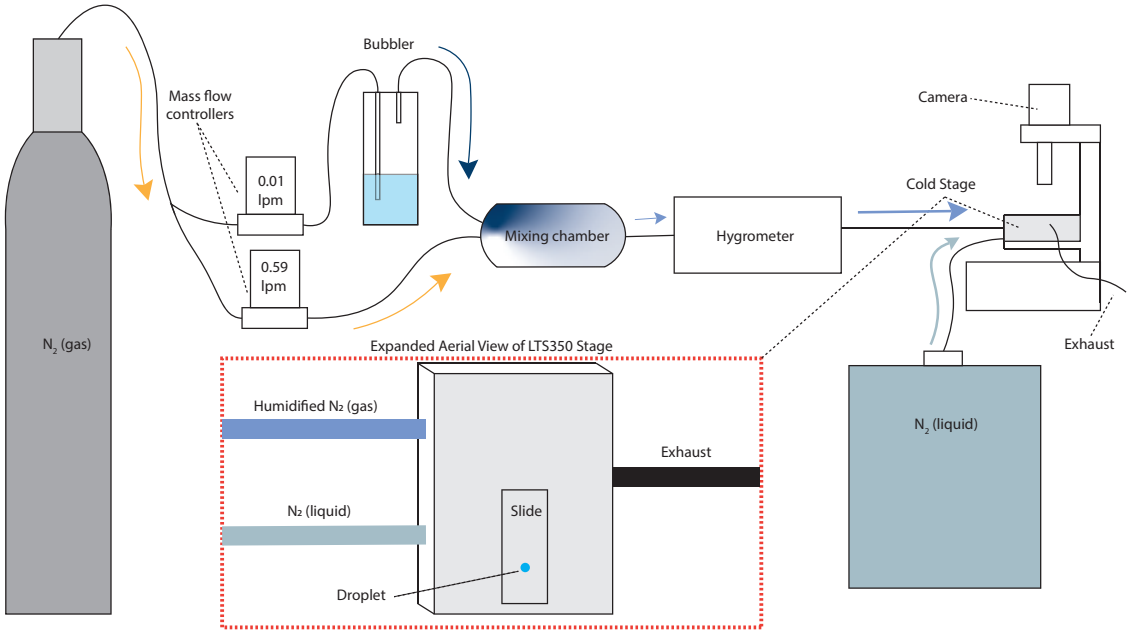

Figure 2.4: Ice microscope apparatus used to test ice nucleation temperatures. A sample droplet is sealed inside a Linkam LTS350 stage which is cooled via a flow of liquid nitrogen to temperatures between 5 and -40 °C. The droplet is maintained via a flow of humidified N_2 gas (mixed in the mixing chamber and measured with the dew point hygrometer), and freezing events are recorded with a camera mounted on the microscope.

The ice microscope setup is shown in figure 2.3. The microscope (Olympus BX51M) is equipped with a cold stage (LTS350, Linkam) capable of reaching temperatures as low as -80 °C, although samples are only tested to -40 °C as anything below -36 °C shows homogeneous freezing rather than heterogeneous freezing processes. The stage is cooled with liquid nitrogen, and the flow of liquid nitrogen is controlled by a Linkam LN95 system controller. Once the 2 µL droplet is placed onto the slide or filter, the sample is sealed inside the cooling stage. The stage is temperature-controlled using Linksys 32 software (Linkam) and the droplet is cooled and warmed

repeatedly following a programmed sequence. To maintain the droplet, the nitrogen gas flowing through the cooling stage is humidified (monitored with a hygrometer [EdgeTech Dew Prime 2000]) by passing the air through the headspace of a bubbler filled with UHP water at a set flow rate (between 0.05 and 0.10 lpm). By humidifying the air over the droplet, a single droplet can be frozen and thawed up to 30 times in a single run. The stage is cooled at a rate of 1 °C per minute, and the droplet is photographed (Q-Imaging Micropublisher RTV camera) every six seconds, or 0.1 °C. These images are then examined to determine the temperature freezing occurred. Figure 2.4 shows an example of a freezing event, as the droplet visibly becomes opaque between a single image and the next.

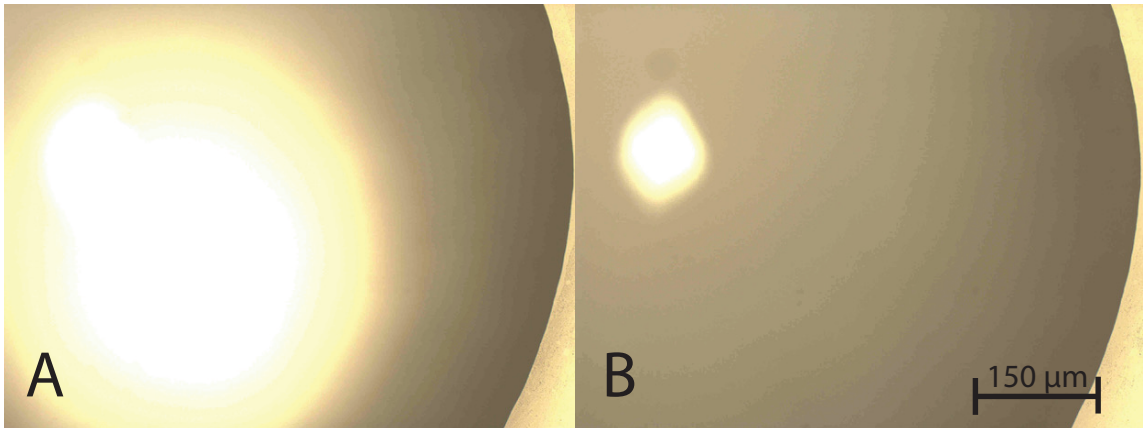

Figure 2.5: Image A shows a single unfrozen 2 µL droplet. The dark curved area to the right side of the image is the edge of the droplet, and the bright area in the middle is due to light reflection off the droplet. Image B shows the same droplet once frozen. Image A was taken six seconds before image B at a temperature 0.1 °C warmer.

Metadata for each image records the temperature the image was taken at, so freezing temperature can be determined very accurately.

2.6.3. Ice Nucleating Particle Concentration Calculations

The fraction of droplets frozen at a given temperature can be used to display both the onset freezing temperature of each sample as well as the spread of freezing temperatures for each droplet. The frozen fraction can be calculated as:

$$Fraction\ frozen\ (T) = \frac{N_f(T)}{N_a} \quad (3)$$

Where $N_f(T)$ is the number of droplets frozen at a temperature and N_a is the total number of freezing events for the sample. The fraction unfrozen can also be calculated by replacing $N_f(T)$ with $N_u(T)$, the number of unfrozen droplets at a temperature (T).

The freezing temperature of a sample was used to calculate the INP concentration (N_{INP}, L^{-1} air) in the droplet across the range of tested freezing temperatures (0 °C to -40 °C) using an equation from DeMott et al. (2016), modified from Vali (1994):

$$n_{INP\_A}(T) = -\ln\left(\frac{N_u(T)}{N_a}\right)\left(\frac{V_w}{V_a V_s}\right) \quad (4)$$

where $N_u(T)$ is the number of unfrozen droplets at a given temperature, N_a is the total number of freezing events of a sample, V_a is the aliquot volume (0.002 mL), V_w is the total volume in mL of all water droplets (calculated by multiplying V_a by the number of freezing events), and V_s is the volume of sampled air (L). The number of INPs per sample was then normalized to the total number of aerosols sampled, calculated by

multiplying the sampling time by the total number of aerosols per cubic centimeter as measured with a condensation particle counter (CPC, TSI Model 3010).

Equation 2 is only applicable to aerosol samples, so a modified equation was used to calculate the INP concentration (L^{-1} water) in liquid samples:

$$n_{INP\_B}(T) = -\ln\left(\frac{N_u(T)}{N_a}\right)\left(\frac{1}{V_a}\right) \quad (5)$$

where V_w/V_s is substituted with 1. Equation 3 was used to calculate the INP concentration in bulk water samples from the MART containing *Thalassiosira weissflogii* as well as the single-group samples produced with flow cytometry during the North Atlantic Aerosols and Marine Ecosystems Study (NAAMES). The INP concentrations per L water calculated with Equation 3 were not normalized to aerosol concentrations over the sample as the relationship between ambient aerosols or the aerosols produced by the MART were not directly related to the number of INP in the water.

From the INP concentration the fraction of INPs activated at any given temperature can be calculated as:

$$A_f(T) = \frac{INP_T}{INP_{max}} \quad (6)$$

where INP_T is the INP concentration at a given temperature (T) and INP_{max} is the maximum number of INP that activate for the sample.

The INP concentration can then be used to calculate the number of surface active sites (N_s, cm^{-2}) (DeMott et al., 2016):

$$N_s(T) = n_{INP}(T) \cdot \frac{10^5}{S_{tot}} \quad (7)$$

where the average aerosol particle count and size can be used to calculate S_{tot}, the total surface area of aerosols collected. Equation 7 can only be used for aerosol samples, as the average particle size is not known for liquid samples.

3. PRODUCTION OF ICE NUCLEATING PARTICLES IN A MARINE AEROSOL REFERENCE TANK BY THE DIATOM *THALASSIOSIRA WEISSFLOGII*

3.1. Introduction

One possible marine source of INPs are marine phytoplankton, including both photosynthetic bacteria (cyanobacteria) and eukaryotic taxa such as diatoms. Diatoms are photosynthetic stramenopiles. They are abundant in the modern marine environment and are well-preserved in the fossil record starting approximately 190 million years ago (Kooistra, Gersonde, Medlin, & Mann, 2007). Diatoms are one of the most important phytoplankton groups, as they are responsible for between 25 and 40% of global carbon fixation (Bopp, Aumont, Cadule, Alvain, & Gehlen, 2005; Field, Behrenfeld, Randerson, & Falkowski, 1998; Leblanc et al., 2012; Nelson, Treguer, Brzezinski, Leynaert, & Queguiner, 1995) and greater than 50% of global C export and burial (Dugdale & Wilkerson, 1998). Diatoms do not have flagella and cannot swim against currents, although some benthic species can move via exopolymer secretion (Cohn & Weitzell, 1996). They are found in nearly every environment, including freshwater, surface seawater, coastal sediments, caves, and moist terrestrial environments including wet rock surfaces (Furey, Lowe, & Johansen, 2007; Graham, Graham, Wilcox, & Cook, 2016; Johansen, 2010; Kociolek, Stepanek, Lowe, Johansen, & Sherwood, 2013). Mann and Vanormelingen (2013) estimated that there could be up to 100,000 different species of diatoms (although this number is somewhat variable depending on how species are defined). However, most estimates are more conservative, ranging from 1,400 to 1,800

marine planktonic diatom species (Sournia, Chrdtiennot-Dinet, & Ricard, 1991) to more than 4,700 marine diatom species (Malviya et al., 2016).

Diatom species are characterized by the structure of their siliceous cell walls called frustules (Graham et al., 2016). The structure of these frustules is species-specific and highly variable but is always symmetric (either centrally or laterally) and composed of amorphous hydrated silica ($SiO_2 \cdot H_2O$). There are two halves to a diatom frustule, the epitheca and hypotheca, which fit together like a petri dish with the hypotheca inside the epitheca. Although diatoms can reproduce both sexually and asexually, they are unique in that asexual reproduction results in sequentially smaller cells (Graham et al., 2016; Macdonald, 1869; Pfitzer, 1869). This is because as the diatom is dividing, the frustule splits into its two parts. In one of the daughter cells the epitheca remains as the largest part of the frustule and the diatom is the same size as the parent cell. In the second daughter cell the hypotheca of the parent cell becomes the epitheca of the daughter cell, resulting in a slightly smaller cell. Subsequent generations will grow smaller and smaller, but there seems to be a limit to this process where the population will shift to sexual reproduction.

Although whole diatom cells (μm diameter) are much larger than most atmospheric INP (nm diameter) and are unlikely to act as INP when whole, fragments of cells or material from lysed cells could be aerosolized by wave action and bubble bursting to act as INP (DeMott et al., 2016; Irish et al., 2017; Wilson et al., 2015). Past studies have shown that although crystalline silicates such as those found in mineral dust are somewhat efficient INP (Zimmermann et al., 2008), amorphous opal is a poor INP

(Kumar, Marcolli, & Peter, 2019), so it is unlikely that the cell wall fragments alone will act as INP. However, there are studies on the ice nucleating ability of diatoms that indicate that diatoms freeze at temperatures between -24 °C and -30 °C (Alpert et al., 2011a and 2011b; Knopf et al., 2011; Wilson et al., 2015). All past studies have focused on *Thalassiosira pseudonana*, a centric marine diatom ranging from 5-15 μm in diameter (Ferguson, Collier, & Meeter, 1976; Sumper & Brunner, 2008). This species is structurally very similar to *Thalassiosira weissflogii* that is grown in this chapter.

Diatoms are a well-studied producer of exopolymeric material (Chen & Thornton, 2015; Thornton & Chen, 2017; Yamada, Tomaru, Fukuda, & Nagata, 2018). These exopolymers can be found in high concentrations in the sea surface microlayer (Cunliffe et al., 2013; Engel et al., 2017), and are produced in the greatest amounts when the phytoplankton have high stress levels (Berman-Frank et al., 2007). This study aims to determine if the INP activity of primary aerosols are affected by the growth phase of the diatom culture living in the waters that the aerosols are generated from. Previous studies have suggested enhanced ice nucleation during culture decline, which are times of high exopolymer production (Aller et al., 2017; McCluskey, Hill, et al., 2018; McCluskey, Ovadnevaite, et al., 2018; Wang et al., 2015). These exopolymers can be found in high concentrations in the sea surface microlayer (Cunliffe et al., 2013; Engel et al., 2017), and are produced in the greatest amounts when the phytoplankton have high stress levels (Berman-Frank et al., 2007; Thornton & Chen, 2017). Therefore, the diatom culture was sampled to determine 1) if the diatoms and the organic matter in the MART can enhance ice nucleation activity and 2) if there was a link between diatom physiology

and culture health and ice nucleation activity. As well, a comparison of diatom ice nucleation ability and the other groups studied in Chapters 4 and 5 will be made in Chapter 8.

3.2. Methods

Methods for physiological measurements and aerosol measurements are given in Chapter 2. Aerosol samples were made by Jessica Mirrielees, and some of the water measurements were made by Alyssa Alsante, Daniel Thornton, and Andrew Whitesell. It is noted in the respective sections whether a sample was collected or analyzed by anyone other than the author.

3.2.1. Marine Aerosol Reference Tank Nutrients and Measurements

Cultures of *Thalassiosira weissflogii* (CCMP 1051) were grown in artificial seawater made from combusted and/or analytical grade and ultra high purity (UHP) water (Hahn & Blobel, 1968; Harrison et al., 1980), described in section 2.2.1.1. Nutrients were added following a modified recipe for L1 media with the following macronutrient concentrations: 60 μM $NaNO_3$, 50 μM NaH_2PO_4, and 60 μM Na_2SiO_3 (Hahn & Blobel, 1968; Harrison et al., 1980). The tank was inoculated with 630 mL of culture with 8.6 x 10^4 cells mL^{-1}, giving an initial cell concentration of 857 cells mL^{-1} on Day 0 just following inoculation.

The following water samples were taken during this MART experiment:

Table 3.1: Measurements and samples taken during MART sampling. See section 2.2.2 and Table 2.1 for samples that were taken by others. Not all results will be reported on in this chapter.

Sample Name	Sample type	Replications	Reference Section
Bulk carbohydrates	Bottle, microcentrifuge	3	2.3.3
Cell counts	Bottle	3	2.3.1.1
Fluorescence	Measurement	3	2.4.1
Z_{off}	Measurement	1	2.4.1
Bulk ice	Microcentrifuge tube	3	2.6.2
Pigments	Filter (GF/C)	3	3.2.2
TEP	Filter (polycarbonate)	3	2.4.5
CSP	Filter (polycarbonate)	3	2.4.5
SYTOX green	Filter (polycarbonate)	3	2.4.2
Caspase	Pellet	3	2.4.3
CDOM	Bottle, filter (GF/F)	3	
β-glucosidase	Microcentrifuge tube	3	2.4.4

As well, measurements of aerosols were made to determine total aerosol concentration and cloud condensation nucleus concentration, and aerosol samples were collected to test for ice nucleation ability.

3.2.2. Chlorophyll *a* Measurements

Unlike the results from Chapters 4 and 5, chlorophyll *a* was measured with a spectrophotometer rather than a fluorometer due to the availability of a calibrated instrument. Bulk water chlorophyll was determined first, followed by chlorophyll *a* concentration per cell (using cell counts taken simultaneously with the sample collected for chlorophyll *a* analysis. A known volume of culture was filtered with a GF/F filter (VWR) until the white filter was visibly green. This filter was then placed inside a microcentrifuge tube (VWR), taking care to ensure that the filtered material was folded

to the inside of the filter so that none was touching the wall of the tube. The filters were then stored at -20 °C in the dark for no more than one month prior to analysis.

To extract the chlorophyll *a*, each filter was placed in a 15 mL sterile polypropylene centrifuge tube along with 5 mL of HPLC-grade acetone (VWR). The filter and acetone was sonicated (QSonica, Q125, 125 watts) at 10kHz three times. Each round of sonication consisted of one minute of sonication in 10 second bursts with 10 seconds' rest to ensure the sample didn't heat up too much. The samples were held on ice during the sonication process, and there was approximately five minutes' rest between each round of sonication. The tubes containing filters and acetone were then held for at least 12 hours in the dark at 4 °C to extract the chl *a*. The acetone containing chl *a* was then measured using spectrophotometry (Arar, 1997; Jeffrey & Humphrey, 1975).

To measure the chlorophyll *a* concentration, 2 mL of the acetone and extracted pigment was placed in a glass cuvette (VWR). Prior to use the cuvette was cleaned with HPLC-grade acetone. The absorbance was measured at 664 nm, 647 nm, and 630 nm with a spectrophotometer (Shimadzu UV-mini 1240). The following equation from Jeffrey and Humphrey (1975) was then used to calculate the chl *a* concentration:

$$\text{chl } a = 11.85 \cdot abs_{664} - 1.54 \cdot abs_{647} - 0.08 \cdot abs_{630} \quad (3.1)$$

3.3. Results

The culture grew quickly for the first four days following inoculation (Figure 3.2) with positive growth rates. The culture began to grow exponentially as soon as it was added to the tank and did not show a lag phase. The exponential phase lasted from

Day 0 to Day 4, the stationary phase was from Day 5 to Day 10, and death phase lasted from Day 11 to the end of the experiment on Day 29.

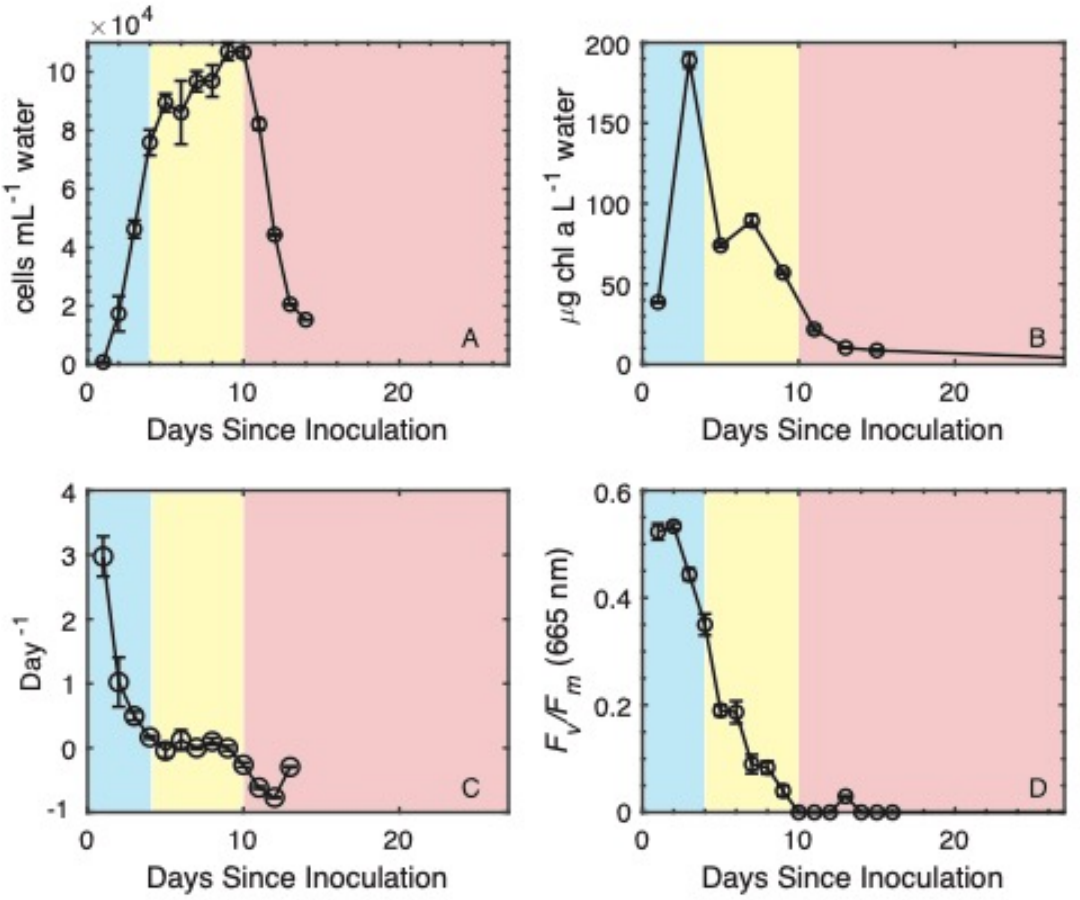

Figure 3.1: Physiological measurements of the diatom culture: A) cell concentration, mL^{-1}, B) bulk water chlorophyll *a* concentration, µg chl a mL^{-}, C) growth rate, day^{-1}, and D) photosynthetic yield, F_v/F_m. Exponential phase is highlighted in blue, stationary phase in yellow, and death phase in red. Each data point represents the mean ± standard deviation, n = 3.

The maximum growth rate was seen during the exponential phase on Day 1, at 2.9 day^{-1}. Days 9 and 10 had the highest cell counts seen in the experiment: 1.1 x 10^5 ± 3010.0 cells mL^{-1}. The cell count was approximately the same during the stationary phase, particularly toward the end of stationary phase on Days 9 and 10, followed by a steep decrease in cell concentration as death phase began and continuing from Days 10 to 13. The cell count decreased by a smaller amount between Days 13 and 14, and likely continued a slow rate of decline between Days 14 and 30 although no cell counts were taken between Day 13 and the end of the experiment.

The maximum quantum yield of photosystem II (F_v/F_m) was highest during the beginning of the exponential phase on Days 1 and 2 (0.5 ± 0.006) and then decreased steeply during the rest of exponential phase and continuing into stationary phase until Day 7. From Days 7 through 11 the yield was slightly lower each day, reaching a minimum of 0.02 ± 0.01 on Day 11 as death phase began. Days 11 through 13 the yield increased slightly each day, reaching 0.04 ± 0.01 on Day 13. Although these values are low, the chlorophyll content was well above the detection limit of 0.1 µg chl L^1, so the slight variation is likely due to slight physiological differences rather than being an instrument artifact (Schreiber, 1998). Measurements on Days 14 through 16 did not show any pattern, and the standard deviation was higher than most previous days, possibly due to increasing the instrumental gain as a result of low cell concentrations. Following Day 16 measurements were not possible because the background fluorescence (Z_{off}) from dissolved matter was higher than the measurement.

Figure 3.1B shows the bulk chlorophyll *a* measurements. The highest chlorophyll *a* was seen on Day 3 in both the bulk water and the chlorophyll *a* per cell. Bulk chlorophyll *a* on Day 3 was 188 ± 4.8 µg L^{-1}, or 2.5 pg chlorophyll *a* $cell^{-1}$. There was a steep decrease in chlorophyll *a* between Day 3 and Day 5, followed by a slight increase between Days 5 and 7. Following Day 7 throughout the rest of stationary phase and throughout death phase the bulk chlorophyll continued to decrease until the end of the experiment on Day 29. In contrast, the chlorophyll *a* per cell only decreased at the end of stationary phase through the first few days of death phase between Days 7 and 13 to a minimum of 0.49 pg chlorophyll *a* $cell^{-1}$. On Day 13 the chlorophyll *a* content per cell increased by 72% to 0.68 pg chl *a* $cell^{-1}$. Chlorophyll *a* content per cell is not available past Day 13 due to a lack of cell counts. Although bulk chlorophyll *a* and chlorophyll per cell vary together for the first nine days, later in the experiment the chlorophyll per cell increases while the bulk chlorophyll *a* decreases.

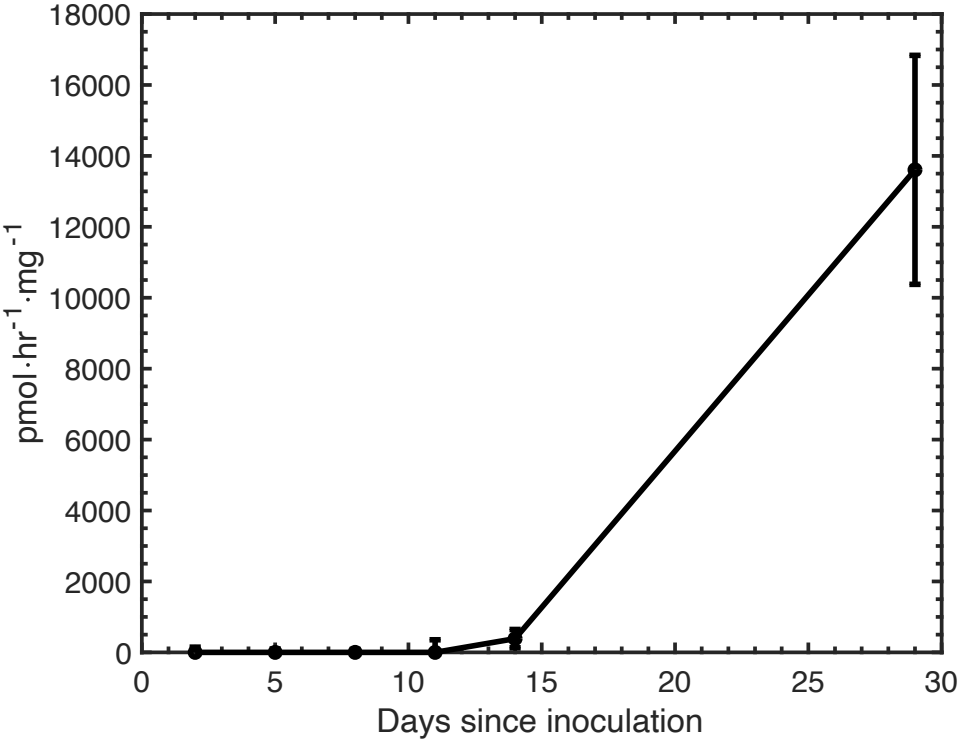

Figure 3.2: Caspase-like enzyme activity (pmol Caspase-3 hr^{-1} mg $protein^{-1}$) measured using EnzChek™ Caspase-3 Assay Kit #1 (Invitrogen). Data points are means ± standard deviation (n = 3).

Caspase-like enzyme activity (Figure 3.2) was not present during the exponential and stationary phases, and was only measurable during death phase on Day 14 and Day 29 (of the days sampled), as shown in Figure 3. No samples were taken between Day 14 and Day 29. The rate of enzyme activity was 0 on Days 2, 5, 8, and 11, and was highest on Day 29, with a rate of 0.146 pmol hr^{1} mg^{-1}.

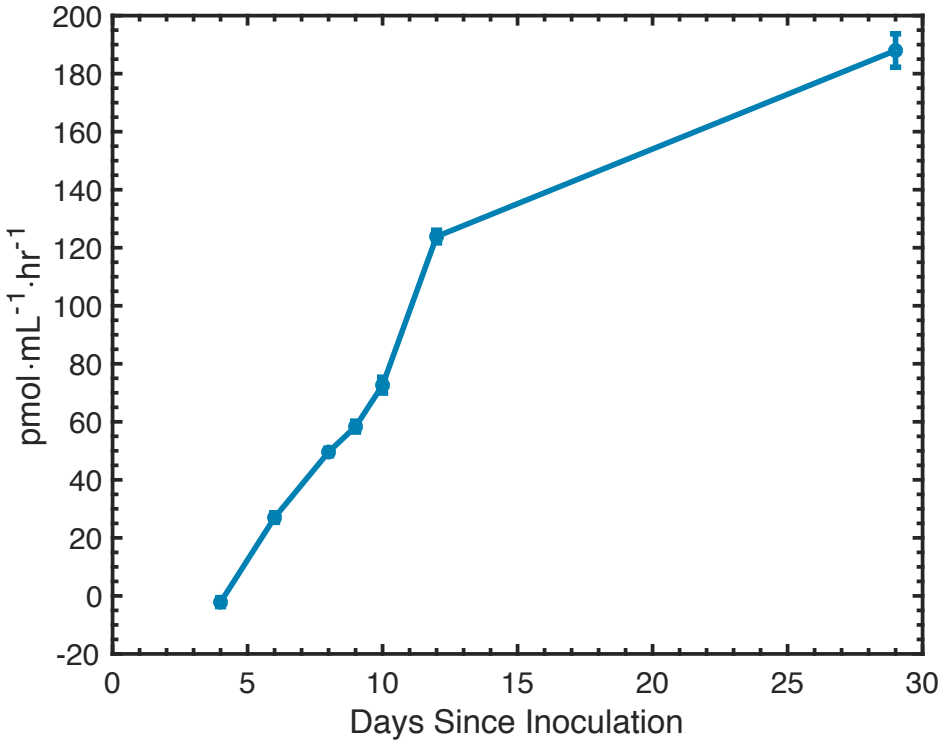

Figure 3.3: Mean β-glucosidase activity (pmol MUG hr^{-1} mL^{-1}) ± standard deviation, n = 3.

β-glucosidase activity (Figure 3.3) was measured every two days starting at the end of exponential phase. Activity increased for the length of the experiment. The highest rate measured was on Day 29, at 188 ± 5.8 pmol MUG mL^{-1} hr^{-1}. β-glucosidase has been correlated with bacterial activity (Hoppe, 1983).

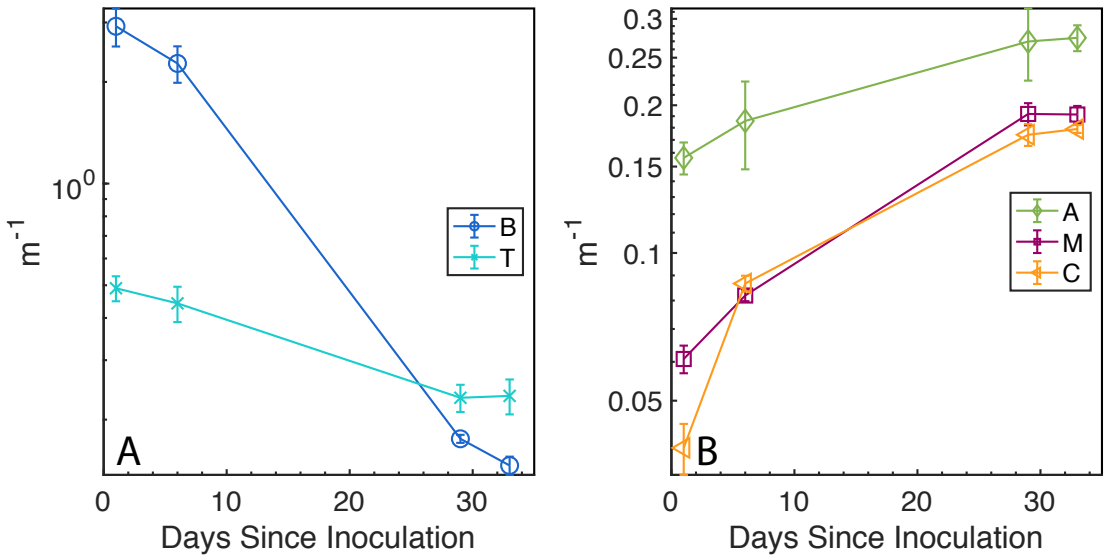

Figure 3.4: a) Colored dissolved organic matter (CDOM) fluorescent components (m^{-1}) ± standard deviation (n=3), with A) line B showing tyrosine-like material and T showing tryptophan-like material and B) humic-like materials, where A and C are humic-like materials, and M is marine-humic like material.

Colored dissolved organic matter (CDOM) components are shown in Figure 3.4. Generally, the humic-like components (peaks A, M, and C) increased as the culture grew and protein-like components (peaks B and T) decreased. The tyrosine-like component showed the greatest change, with a maximum value of 2.9 m^{-1} on Day 1 and a minimum of 0.1 m^{-1} on Day 33. Of the three humic-like components, peak C showed the greatest increase, from 0.04 m^{-1} to 0.2 m^{-1} from Days 1 to 33.

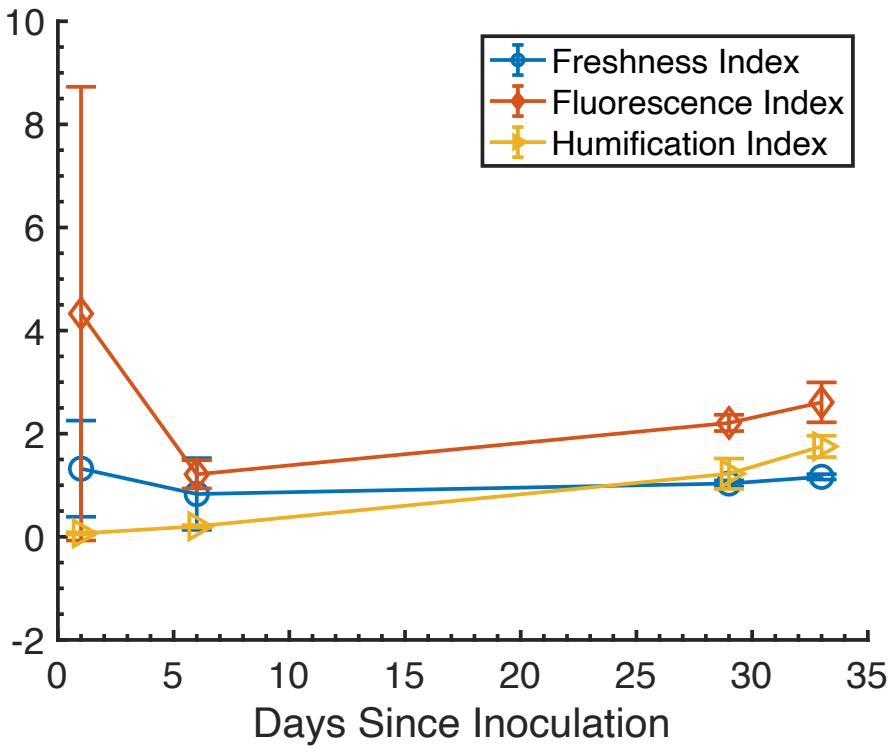

Figure 3.5: Mean fluorescent material indices for colored dissolved organic matter (unitless, ± standard deviation, n = 3).

Figure 3.5 shows several different unitless ratios of these components. Only the humification index (HIX) changed significantly between Day 1 and Day 33, with an increase from 0.07 to 1.75.

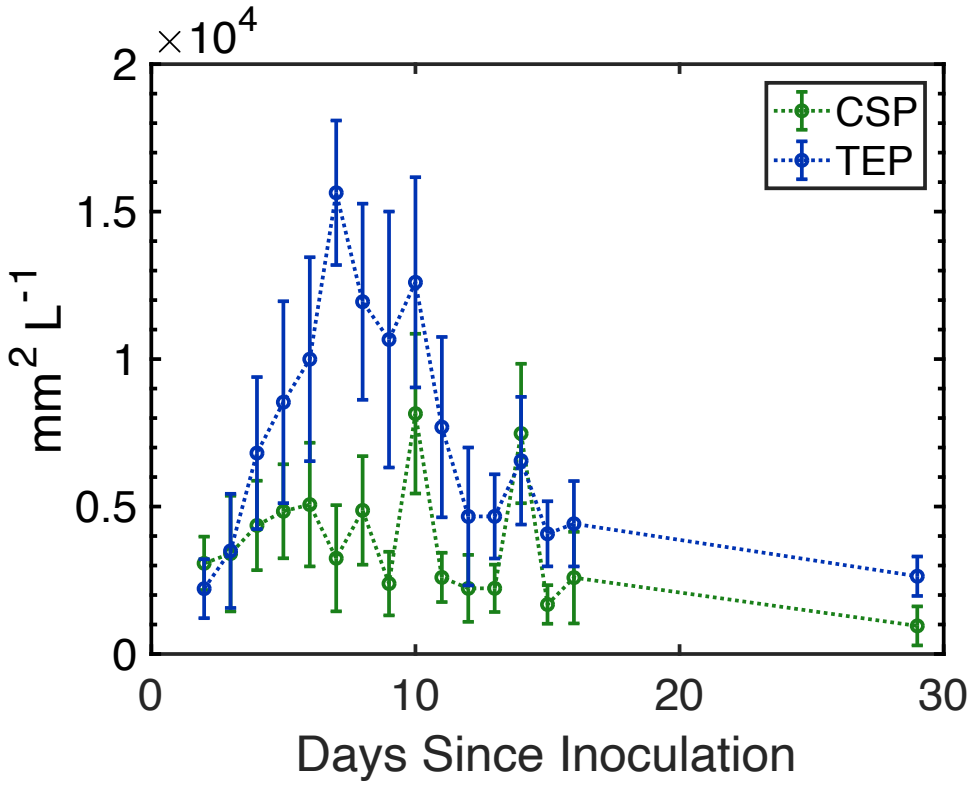

Figure 3.6: Transparent exopolymer (TEP) and Coomassie staining particle (CSP) concentration, measured from bulk water samples. Each data point shows the mean abundance ± a single standard deviation, n = 3.

TEP concentrations ($mm^2\ L^{-1}$) are plotted in Figure 3.6. An increasing concentration of TEP weakly correlates with cell counts ($r^2 = 0.59$, $p < 0.05$, $n = 18$), with the peak TEP concentration of $1.6 \times 10^5\ mm^2\ L^{-1}$ on Day 7 during stationary phase. Carbohydrate concentration (Figure 3.7) correlates with TEP concentration (Pearson correlation, $r^2 = 0.67$, $p < 0.05$, $n = 18$), which is to be expected since TEP contains a high proportion of acid polysaccharides (Alldredge et al., 1993; Thornton & Chen, 2017). Although the highest carbohydrate concentrations (Figure 3.7) were measured on

Day 5 (20.5 µg mL^{-1}), Days 5 through 7 had approximately the same carbohydrate concentration. Coomassie staining particles (CSP, Figure 6) were also measured and peaked on Day 10, but there is no correlation between CSP production and any other measured component.

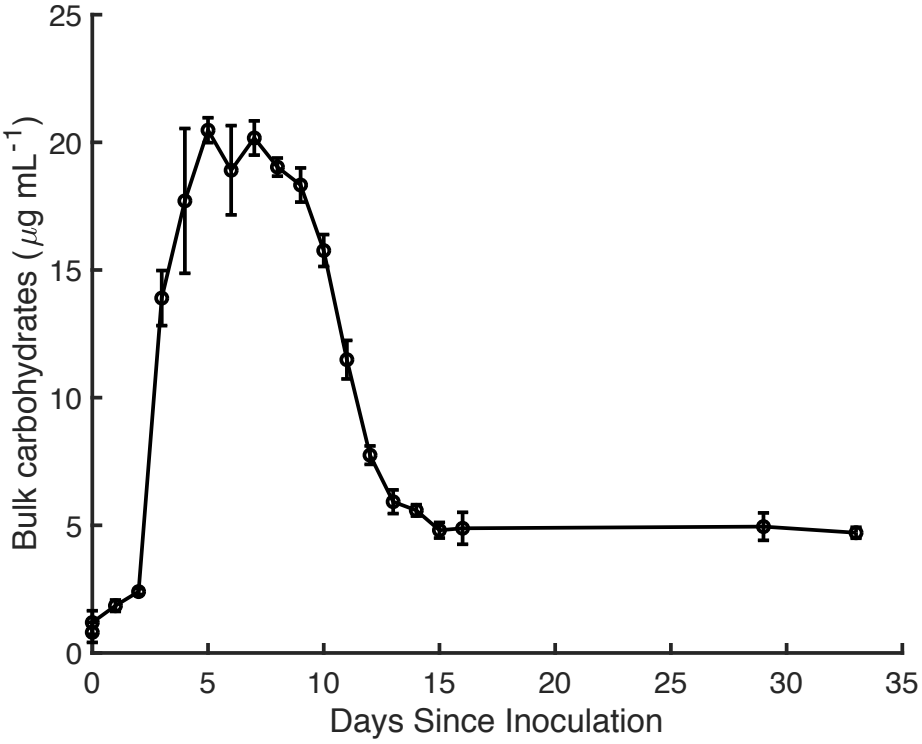

Figure 3.7: Mean bulk carbohydrate concentrations (µg mL^{-1} [glucose equivalents]) ± standard deviation, n = 3.

Figure 3.7 shows the bulk carbohydrate concentration which peaked two days prior to the peak TEP concentration. Bulk carbohydrate concentrations account for all carbohydrates within the culture, not just gel-like acidic polysaccharide particles that are

measured as TEP. The carbohydrate concentration increased throughout exponential phase. The highest concentrations were seen throughout the stationary phase, and the concentration decreased from Days 10 through 14 as death phase began, then held steady for the remainder of the experiment.

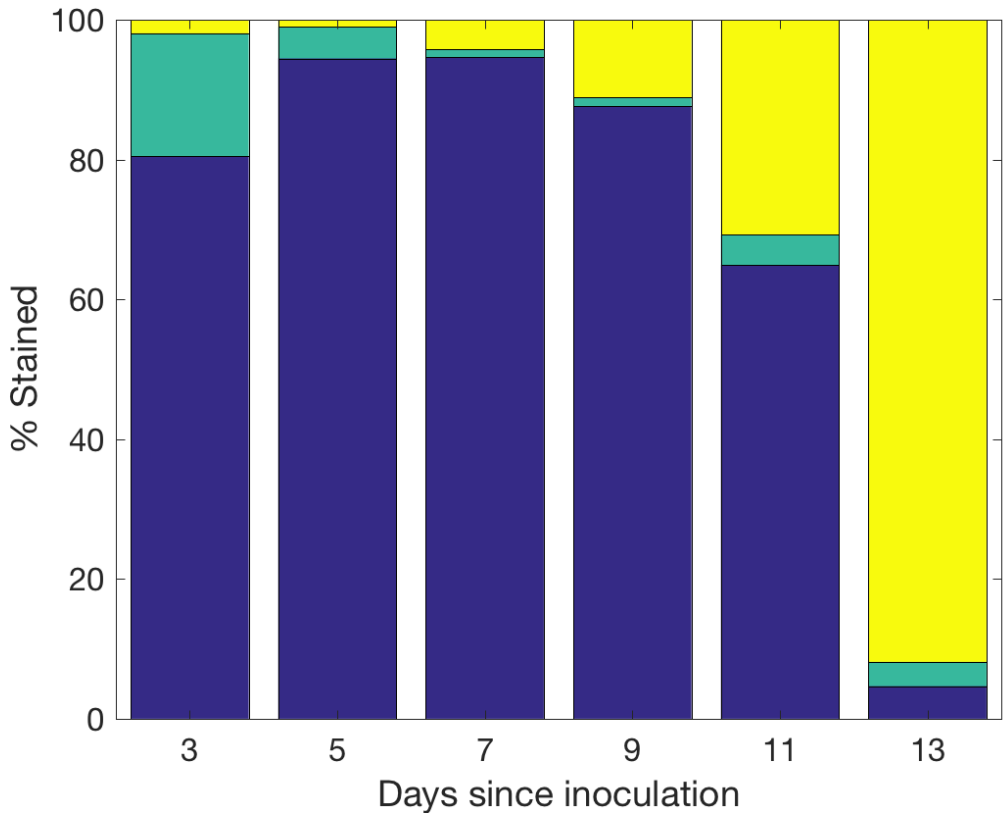

Figure 3.8: Proportion of SYTOX Green-staining *Thalassiosira weissflogii* cells in the MART tank, based on counts of 400 cells on each day. The proportion of unstained cells is represented with blue, the proportion with only the nucleus stained with green, and the proportion of fully stained cells with yellow. Bars represent the mean proportion, n = 3.

SYTOX Green staining (Figure 3.8) was measured every other day following inoculation. There was an increase in the proportion of fully stained cells each day the measurement was taken following Day 3 from only 1% on Day 5 to 92% on Day 13. The concentration of unstained cells increased from Day 3 at the end of exponential phase with 80.5 ± 2.9% to the middle of stationary phase on Day 7, which had the highest proportion of unstained cells with 94.7 ± 4.8% unstained. From Day 7 onwards the proportion of unstained cells decreased rapidly, with the lowest proportion seen on during death phase on Day 13 (4.5 ± 2.7%). Other than the first day of measurements (the only measurement taken during exponential phase), the proportion of cells with only a stained nucleus was less than 5% of the observed cells. Day 3 had the highest proportion with 17.6 ± 2.3% of the cells observed to have only the nucleus stained.

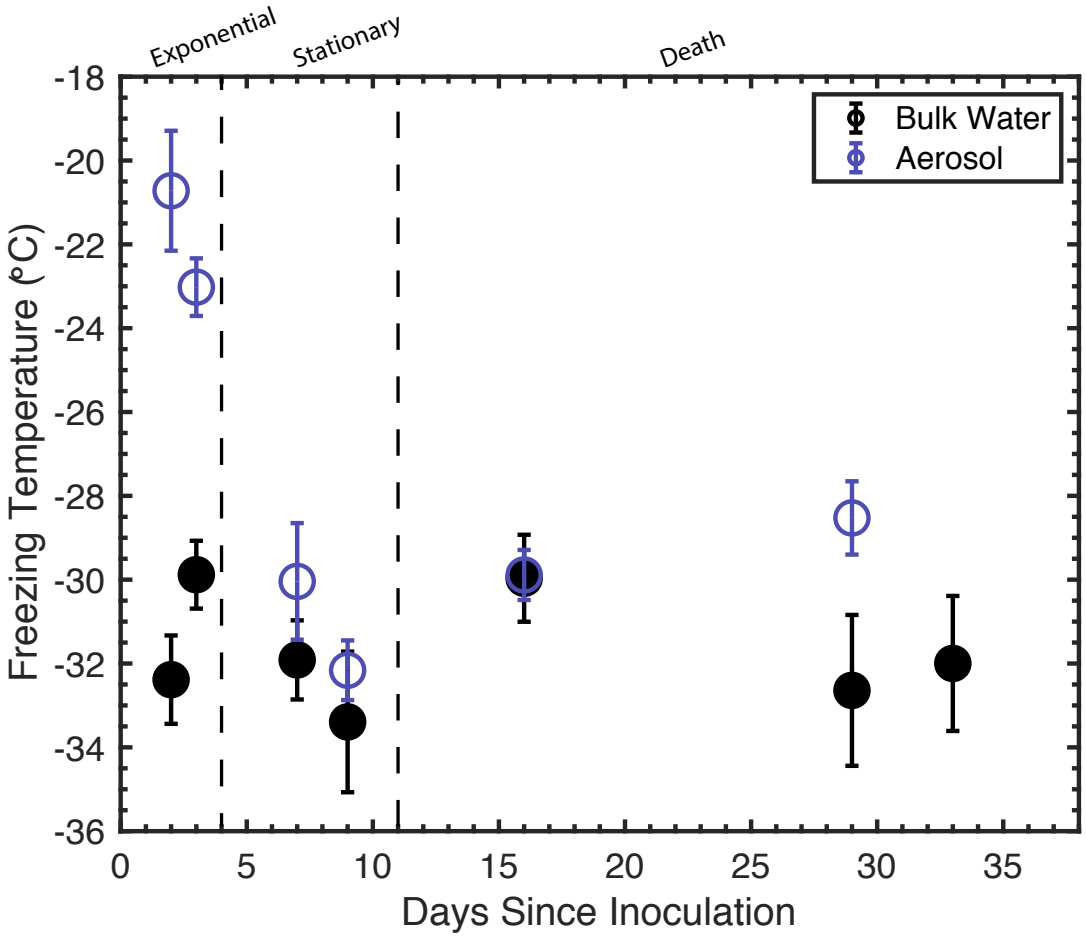

Figure 3.9: Average ice nucleation temperature (°C) of aerosol and bulk water samples. Aerosol freezing temperatures are plotted in blue, with bulk water samples plotted in black. Growth phases are shown with dashed lines. Data points show mean ± standard deviation (n ≥ 5).

Mean freezing temperatures of bulk water and aerosol samples across the three growth phases are shown in Figure 3.9, and INP concentrations per liter of air are shown in Figure 3.11. Nearly all the samples of both types have freezing temperatures that suggest very low INP activity. Most of the samples freeze at temperatures below -28 °C,

and seven of the samples have average nucleation temperatures below -30 °C. The aerosol sample taken during the exponential phase on Day 2 froze at the warmest temperature of -20.7 °C, while the aerosol sample taken on Day 3 froze at -23.0 °C. There was a significant correlation between the mean freezing temperature of the aerosol samples and the photosynthetic yield ($r = 0.987$, $p < 0.01$, $n = 5$). The higher yields correlated with higher freezing temperatures. In contrast, there was a negative correlation between cell concentration and aerosol freezing temperatures ($r = -0.99$, $p < 0.01$, $n = 4$). However, on many of the freezing runs data points had to be discarded, generally either due to droplets shrinking or due to visible condensation, leading to low numbers of data points for some samples (Days 2, 3, and 7 aerosol samples especially had lower repetition numbers.

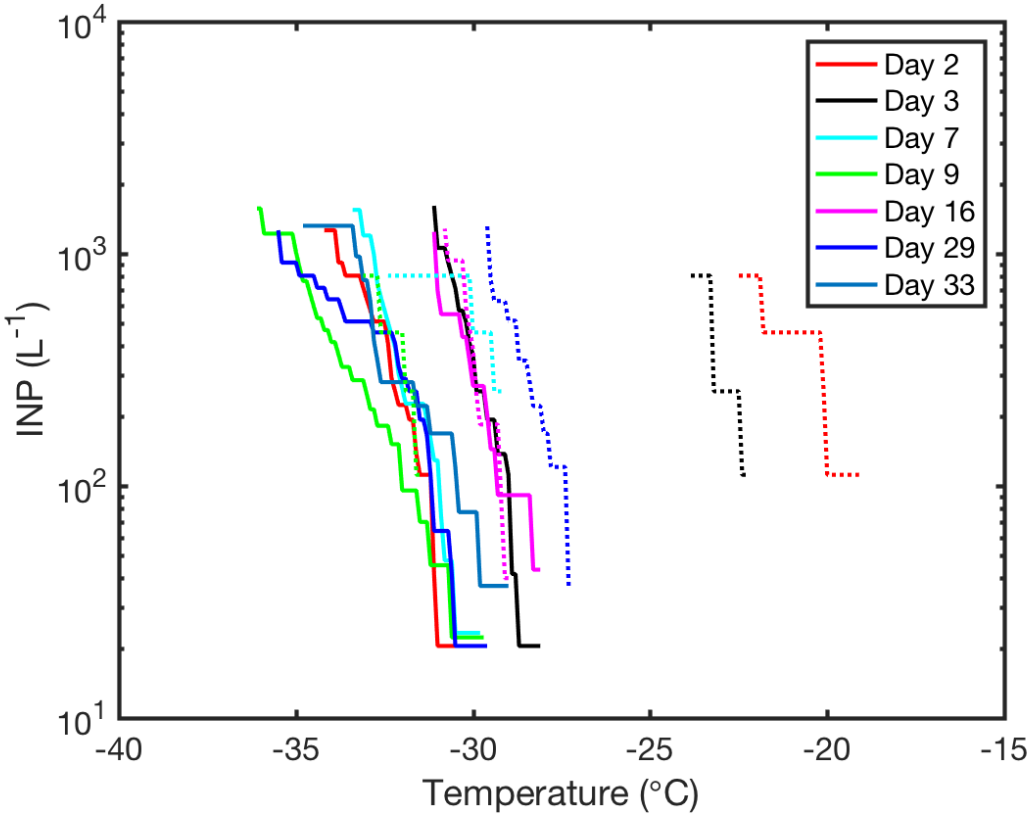

Figure 3.10: Ice nucleating particle (INP) concentrations (L^{-1} seawater) for all samples, calculated from Equation 1. The color of the line represents sampling day, with aerosol samples plotted with dashed lines and bulk water samples as solid lines. Note that there is no aerosol sample on Day 33.

Figure 3.10 shows the concentration of INP per liter of seawater at a given temperature. Each day of sampling is represented by a different colored line, and the bulk water samples are represented with a solid line while the aerosol samples are represented with a dashed line. None of the bulk water samples had INP that were active at temperatures higher than -28 °C, and the highest INP concentration at -30 °C was on

Day 3, which had a concentration of 367.0 L^{-1}. Of the aerosol samples, Day 29 had the highest INP concentration at -30 °C, with 1319.5 L^{-1}. However, Days 2 and 3 did have higher INP concentrations at -25 °C, and the aerosol sample from Day 2 was the only sample that had INP active at -20 °C, with a concentration of 111.6 L^{-1}.

There are not aerosol concentrations available for all samples, but Figure 3.11 shows the INP concentration per liter of air following normalization to the total number of aerosols collected on each impactor sample. The colors represent the growth phases, with exponential phase plotted in blue and death phase plotted in black. There are no data points available from stationary phase.

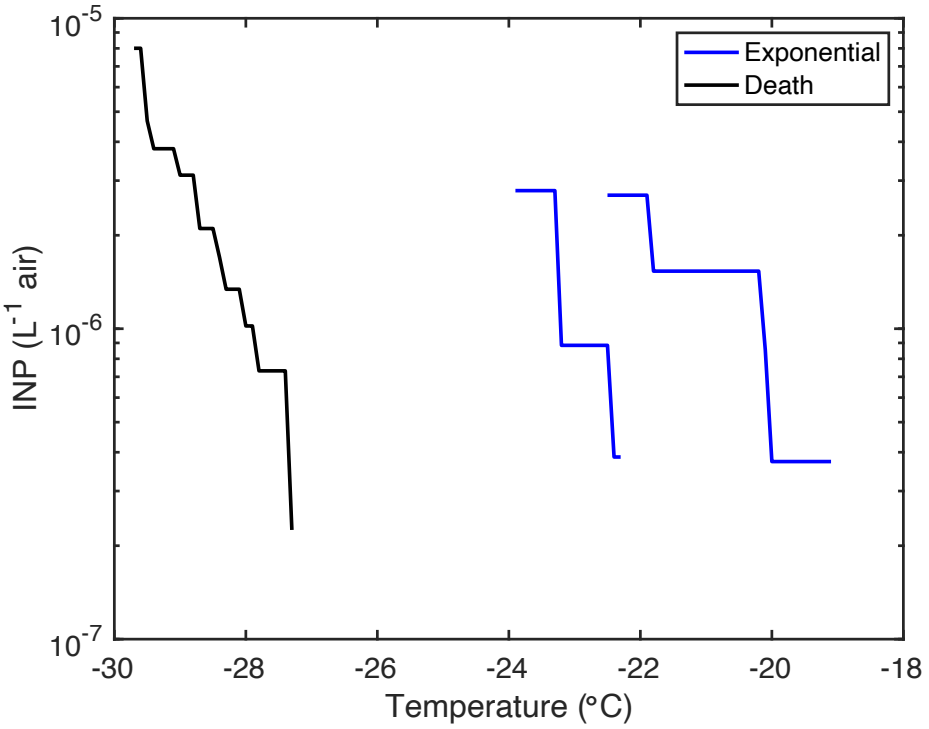

Figure 3.11: INP concentrations per liter of air, calculated with Equation 4 given in Section 2.6. Blue lines represent samples from times of exponential growth, and black lines represent data from death phase.

At -25 °C, only the samples from exponential phase had INPs that were active, with both samples containing 2.8 x 10^{-6} INP per liter of air. At -30 °C the death phase sample contained more INPs, with 8.0 x 10^{-6} INPs per liter of air.

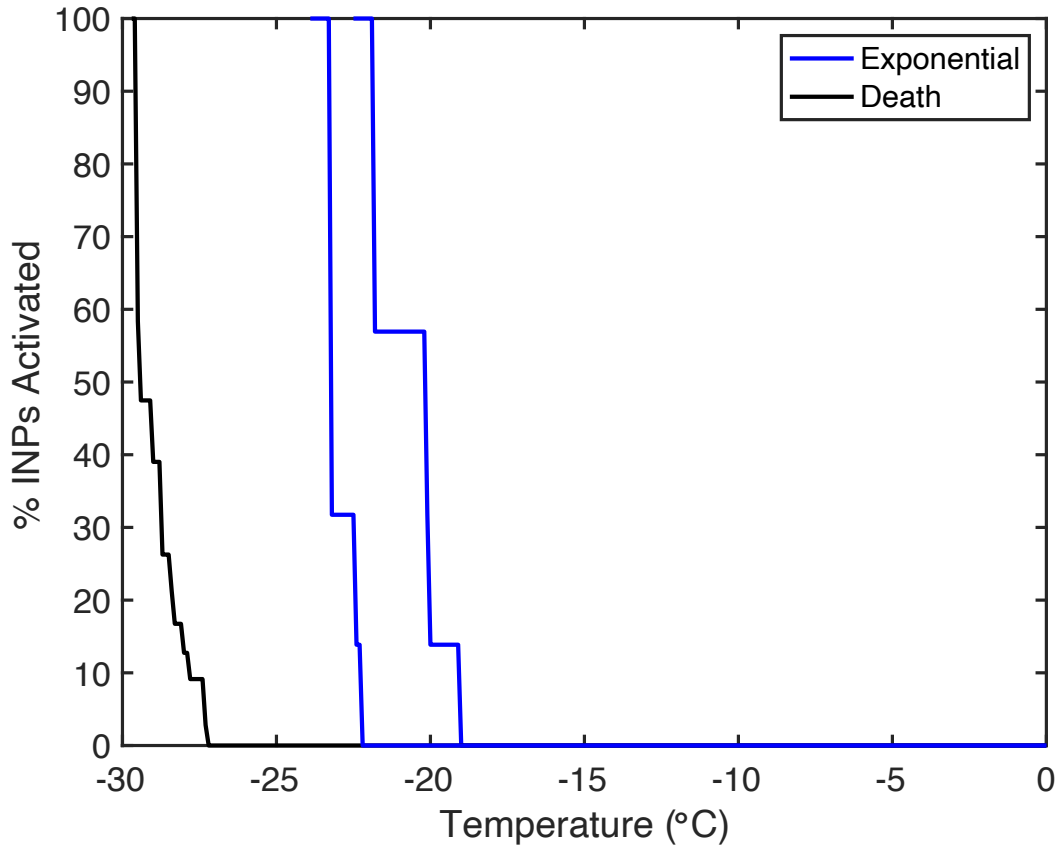

Figure 3.12: Percentage of aerosols activated in a sample at a temperature (°C). Samples taken during exponential phase are plotted in blue and the sample from death phase is plotted in black.

Figure 3.11 shows the fraction of INP per liter of air that have activated at each temperature. The two exponential-phase samples are fully activated at -23.9 °C, which is a warmer temperature than the sample from death phase, which does not fully activate until -29.7 °C.

3.4. Discussion

There was a high rate of growth seen at the beginning of the experiment during exponential phase, which occurred at the same time as a high yield. During this time, the diatoms were efficiently photosynthesizing and had high concentrations of chlorophyll *a* per cell. Together, this is due to the high nutrient concentrations in the tank at the beginning of the experiment, leading to a very healthy culture with a fast rate of division and growth. Growth rate decreased each day for the first five days of the experiment as nutrients were consumed and cell concentration increased, decreasing the light available for photosynthesis due to increased turbidity.

Peak chlorophyll *a* levels in the MART were approximately an order of magnitude higher than most open ocean blooms (Uitz, Claustre, Morel, & Hooker, 2006), which rarely have concentrations higher than 10 $\mu g\ L^{-1}$. Bulk chlorophyll *a* decreased across the entirety of the experiment, which is expected as the culture grows and uses up the available nutrients. Chlorophyll *a* per cell also decreased each day except for Day 7 and Day 13. The two slight increases in chlorophyll *a* concentration on Days 3 and 7 were likely due to acclimation of the phytoplankton to decreased light levels (Post, Dubinsky, Wyman, & Falkowski, 1984), as lower nutrient concentrations typically lead to lower chlorophyll *a* concentrations (Hou, Huang, Cao, Chen, & Hong, 2007), as seen with the overall trend toward lower chlorophyll *a* concentrations as the experiment progressed. The quantum yield of photosystem II also generally decreased over time, again likely due to lower nutrient concentrations (Parkhill, Maillet, & Cullen, 2001). It has also been observed in diatoms that the yield decreases with increasing light

levels as a result of photoacclimation (Anning et al., 2000; van de Poll, Alderkamp, Janknegt, Roggeveld, & Buma, 2006). The high standard deviation on yield measurements on days 14 through 16 is an instrument artifact. While the instrument is capable of measuring photosynthetic activity at chlorophyll *a* concentrations above 0.1 $\mu g\ L^{-1}$, to compensate for lower chlorophyll concentrations, the instrument increases the gain. This in turn increases the variability and decreases the precision of measurements, leading to a higher standard deviation among multiple measurements (Schreiber, 1998, 2004).

The caspase-3-like enzyme activity was either not present or very low for the majority of the measured days, which is interpreted as low rates of programmed cell death (PCD). However, the growth rate was consistently negative and the cell concentration decreased past Day 10 as the culture entered death phase, so there was cell death occurring via other pathways than PCD. We cannot exclude the possibility that bacteria contributed to the observed caspase-like enzyme activity as the culture was not axenic, and bacterial activity increased as over time, using β-glucosidase activity as a proxy for bacterial activity (Hoppe, 1983). This increase in bacterial activity is likely due the increase in cell death past Day 10 (as indicated by the very negative growth rates), as the dead cells and the material they release after they lyse provides material for bacterial remineralization. An increase in humification in marine samples has also been linked to bacterial remineralization of organic matter produced by senescent phytoplankton (Shimotori, Omori, & Hama, 2009). Peak C in particular has been linked to bacterial consumption of exudates, and the peak generally increases with an increase in bacterial

activity (Romera-Castillo et al., 2011). As shown in in Figure 3.4B peak C increases across the length of the experiment, but especially at the end of death phase on Days 29 and 33. This helps explain the decrease in TEP and CSP that is seen in Figure 3.6 as bacteria likely consumed the exopolymer particles. It is also likely that the TEP and CSP settled out over time; although the tank was being stirred at any point sampling was not occurring, there was visible detritus on the bottom of the tank that was not captured in bulk water samples. An increase in cell death is also supported by the proportions of cells stained by SYTOX Green. Figure 3.8 shows an increasing proportion of cells with permeable membranes after Day 7, representing an increase in cell stress and a decrease in the overall health of the *T. weissflogii* culture. We would expect to see this high proportion continue across the rest of the death phase.

Table 3.2: Bulk water ice nucleation descriptions. All bulk water samples had a salinity of 35 ppt. Cells per droplet were calculated from bulk water cell counts as the number of cells contained in each 2 µL droplet.

Sample number (days since inoculation)	Cells droplet^{-1}	Freezing runs	Average freezing temperature	Growth rate (day^{-1})
2	925	25	-32.4 ± 1.1	1.02
3	1520	25	-29.9 ± 0.8	0.49
7	1940	22	-31.9 ± 0.9	0.00
9	2130	23	-33.4 ± 1.7	0.00
16	-	12	-30.0 ± 1.0	-
29	-	25	-32.6 ± 1.8	-
33	-	14	-32.0 ± 1.6	-

This is the only experiment where undiluted water samples with 30 ppt salt concentrations was tested for ice nucleation activity (shown in Table 3.2) due to difficulty determining the actual ice nucleation activity at the same time the salt concentration was driving down the freezing temperatures. Whole-cell bulk water samples have low freezing temperatures around -30 °C, suggesting that the presence of entire cells is not enough to raise the freezing temperature and overcome the high salt concentrations in the water. Assuming that during immersion freezing processes the particle first activates as a cloud condensation nucleus and then freezes, a rough calculation of dilution can be made. The salinity of an activated CCN can be calculated at the point of freezing assuming a starting concentration of 35 parts per thousand salt, a mean sea spray particle radius of 0.05 μm (from Clarke, Owens, and Zhou [2006]), and a mean CCN radius of 0.15 μm. With an initial volume of 5.24×10^{-22} m^3 and a final volume of 1.41×10^{-20} m^3, the final salt concentration is approximately 1.3 parts per thousand.

Koop and Zobrist (2009) proposed a method to calculate freezing point depressions from the calculated activity of the water droplet that has been applied in several studies (Irish et al., 2017; Irish, Hanna, Xi, et al., 2019). However, Whale, Holden, Wilson, O'Sullivan, and Murray (2018) showed that this correction likely underestimates the amount of freezing point depression that occurs by several degrees. For this reason, we chose to test freezing temperatures of both bulk water and generated aerosols on Al foil discs. Aerosol samples have a lower salinity as the aerosol samples have been suspended within UHP water with a salinity of 0 ppt. It is likely that dissolved

organic material within the water is aerosolized and acting as INP in the aerosol samples. However, this organic material within the aerosols is not quantified using current methods.

Table 3.3: Aerosol ice nucleation sample information. Particle concentration was measured in the ambient air with a condensation particle counter (CPC, TSI 3786) and mean freezing temperature (n ≥ 5) was measured with an offline ice nucleation microscope. Note that growth rate is based on cell counts and thus only available for Days 1-13.

Sample Number (Days Since Inoculation)	Aerosol particle Size (nm)	Ambient particle concentration (particles·cm^{-3})	Freezing Runs	Average Freezing Temperature (°C)	Growth Rate (day^{-1})
2	60-1000	-	5	-20.7 ± 1.4	1.02
3	60-1000	1740	5	-23.0 ± 0.7	0.49
7	60-1000	-	5	-30.0 ± 1.4	0.00
9	60-1000	786	6	-32.2 ± 0.7	0.00
16	60-1000	889	13	-29.9 ± 0.6	-
29	60-1000	1280	14	-28.5 ± 0.9	-

The high freezing temperatures of aerosol samples (Table 3.3) from Days 2 and 3 suggest that the particles gathered are acting as INP due to high concentrations of INP-active organic material (Brooks & Thornton, 2018; Wilson et al., 2015). Although the range of INP concentrations at 25 °C on Days 2 and 3 is higher than very clean marine conditions, which may have as few as 10^{-5} particles per liter of air (Irish et al., 2017; Wilson et al., 2015), it is within previously reported field measurements of marine INP concentrations (DeMott et al., 2016).

Days 2 and 3 of sampling occurred during a time when the culture was rapidly growing during exponential phase. This is in contrast with recent studies that have

suggested that senescent organisms have a larger impact on atmospheric processes (McCluskey, Hill, et al., 2018; O'Dowd et al., 2015). Our results instead find a link between the highest growth rates and high INP activity. Peak INP concentrations at -20 °C on Day 2 of the aerosol samples are also approximately an order of magnitude higher than those reported from field samples (McCluskey et al., 2016). However, there is not a direct relationship between culture biomass and INP concentrations. Due to high biomass grown in the MART, higher INP concentrations were produced, but it cannot be said that higher biomass always leads to a higher INP concentration. Our results instead find a relationship between the highest growth rates and high INP activity.

3.5. Conclusions

Three of my initial hypotheses can be addressed by this chapter (as well as the next two chapters covering other MART results), although a comparison of the three organisms grown in the MART will be included in Chapter 8. First, the freezing temperatures on Days 2 and 3 of the aerosol samples show that phytoplankton are acting as INP at atmospherically relevant temperatures. Second, as the freezing temperature is different as the culture grows, it can be concluded that there is a link between cell growth and physiological status and INP production. Our results suggest that there may be a link between phytoplankton populations with a high growth rate and increased ice nucleation activity. Our results show the highest levels of ice nucleation activity during times of growth when the cell concentration is quickly increasing, but is overall quite low. Freezing temperatures were as much as 10 °C higher at the beginning of the experiment when growth rates are highest, cell concentrations are lowest, and cells are

physiologically healthiest (based on photosynthetic yield). In open ocean settings, these times of high diatom growth occur at the beginning of a bloom when nutrient levels are high, and this study may link high ice nucleation activity to the beginning of blooms in clean marine settings. This directly contrasts previous studies, which found cell senescence seemed to lead to high INP concentrations.

4. ICE NUCLEATING PARTICLES GENERATED BY *SYNECHOCOCCUS ELONGATUS* GROWN IN A MARINE AEROSOL REFERENCE TANK

4.1. Introduction

Synechococcus is one of the most abundant organisms in marine waters. It has been found from the arctic (Dvořák, Hindák, Hašler, Hindakova, & Poulíčková, 2014) to the tropics (Erwin & Thacker, 2008; Usher, Fromont, Sutton, & Toze, 2004) to hot springs (Robertson, Tezuka, & Watanabe, 2001). Although it can survive in waters with low temperature and low salinity (Dvořák, Casamatta, et al., 2014) and is seen in samples from oligotrophic oceans (DuRand, Olson, & Chisholm, 2001; Partensky, Blanchot, & Vaulot, 1999) it is generally one of the dominant cyanobacteria genera in nutrient-rich ocean waters, as it seems to thrive in waters with high nitrogen concentrations (Partensky et al., 1999). However, it is ubiquitous and can be found in low concentrations (10^3 cells mL^{-1}) in low nutrient regions (Blanchot & Rodier, 1996; Blanchot, Rodier, & Le Bouteiller, 1992; Campbell & Vaulot, 1993; Li, 1995; Olson, Chisholm, Zettler, & Armbrust, 1990), cold waters (Shapiro & Haugen, 1988), and low salinity waters (Jochem, 1988; Vaulot & Xiuren, 1988). *Synechococcus* was first discovered due to the strong orange fluorescence of the accessory pigment phycoerythrin under epifluorescence microscopy (Murphy & Haugen, 1985; Olson, Chisholm, Zettler, & Armbrust, 1988; Waterbury, Watson, Guillard, & Brand, 1979). Prior to the discovery of *Prochlorococcus*, *Synechococcus* was assumed to be the only photosynthetic organism with a diameter <1 μm, but it is still one of the smallest photosynthetic

organisms, ranging in size from 0.5 to 6 μm (Dvořák, Casamatta, et al., 2014; Partensky et al., 1999).

Although INP activity generally increases with increasing size (Welti, Lüönd, Stetzer, & Lohmann, 2009) most *Synechococcus* cells are larger than the estimated size for ice nucleating particles, which are generally considered to be less than 1 μm (Möhler et al., 2006). However, they produce organic matter including exopolymeric material that may be aerosolized (W. Deng, Cruz, & Neuer, 2016; O'Dowd et al., 2015; Quinn & Bates, 2011; Thornton & Chen, 2017) and may nucleate as INP. There are many studies of non-photosynthetic bacteria as INP (Amato et al., 2015; Hill et al., 2014; Maki et al., 1974; Niehaus, Becker, Kostinski, & Cantrell, 2014), primarily focusing on the production by these bacteria of ice nucleating proteins (Graether & Jia, 2001; Ling et al., 2018; Schmid et al., 1997). There are no studies of *Synechococcus* as an ice nucleating particle (although Chapter 7 includes the ice nucleating ability of *Synechococcus* cells collected in the North Atlantic with flow cytometry). However, there is one study of the ice nucleating ability of *Prochlorococcus.* Wolf et al. (2019) found that material generated from lysed cultures of *Prochlorococcus* contained material capable of catalyzing heterogeneous nucleation, and that smaller 200 nm particles (which contained a higher proportion of organic material) were more efficient INP than larger particles (500 nm). However, direct comparison of *Prochlorococcus* and *Synechococcus* ice nucleating ability is difficult, as Wolf et al. (2019) tested the ice nucleation ability of *Prochlorococcus* during deposition mode nucleation rather than immersion mode, as is reported on in this chapter. This chapter will compare the effectiveness of INP produced

from a single-species culture of *Synechococcus* grown in a marine aerosol reference tank across the extent of the bloom, as well as the biology of the bloom itself.

4.2. Methods

The following samples were analyzed using methods previously described in chapter 2: photosynthetic yield, bulk protein concentrations, TEP and CSP concentrations, caspase-like enzyme activity, colored dissolved organic matter concentrations and ratios, and ice nucleation temperatures and calculations. SYTOX-stained samples were prepared and counted using the previously described methods, but the cells were only categorized as stained or unstained as *Synechococcus* is a prokaryotic organism and does not have a nucleus. The MART was inoculated with 630 mL of fast-growing culture on the morning of Day 0.

Table 4.1: Water samples taken during this MART experiment. Note that not all sample results are reported in this chapter. See Table 2.1 for a complete list of MART samples.

Sample Name	Sample type	Replications	Reference Section
Bacterial counts	Bottle, filter	3	2.3.1.2
Bulk carbohydrates	Bottle, microcentrifuge	3	2.3.3
Cell counts	Bottle	3	2.3.1.1
Fluorescence	Measurement	3	2.4.1
Zoff	Measurement	1	2.4.1
Bulk ice	Microcentrifuge tube	3	2.6.2
Chlorophyll *a*	Filter (GF/C)	3	4.2.2
TEP	Filter (polycarbonate)	3	2.4.5
CSP	Filter (polycarbonate)	3	2.4.5
SYTOX green	Filter (polycarbonate)	3	2.4.2
Caspase	Pellet	3	2.4.3
CDOM	Bottle, filter (GF/F)	3	

TEP and CSP concentrations and bacterial counts were performed by Alyssa Alsante. Aerosol measurements were made by Jessica Mirrielees.

4.2.1. Chlorophyll *a* Measurements

Chlorophyll *a* samples were taken using methods previously described in Section 3.2.1. Samples were taken on GF/C filters and stored frozen at -20 °C prior to extraction with 90% acetone. Chlorophyll *a* concentrations were measured fluorometrically using a Turner Designs Fluorometer (TD700). The extracted sample was placed into a quartz glass cuvette (Fisher Scientific) and placed into the calibrated fluorometer. The fluorometer was calibrated with a known concentration of chlorophyll *a* in acetone (Spinach chlorophyll *a*, HPLC-grade acetone, VWR).

4.3. Results

Most of the measured biological parameters showed two peaks, including both biomass measurements and indicators of physiological status. There were two periods of exponential growth (seen in an increase in biomass and high growth rates). Growth rates plotted in Figure 4.1A were calculated using chlorophyll *a* as a representative of biomass since cell counts were not available. However, as chlorophyll *a* measurements were only made every two days, the growth rate could only be calculated for the preceding two days rather than one day as in Chapters 3 and 5. The growth rate calculated from chlorophyll *a* concentration (Figure 4.1A) did not show two roughly equal peaks, unlike many other measurements, and instead sharply decreased from the highest rate of 1.3 day^{-1} on Day 4 to a negative growth rate of -0.1 on Day 6 during the only death phase seen. There was an increase during the second exponential phase to a second peak of 0.2

day^{-1} on Day 12, much lower than the highest calculated growth rate. The maximum quantum yield of photosystem II (Figure 1B) showed 2 nearly equal peaks, one on Day 5 just following the first exponential phase and one on Day 11 during the second exponential phase. The first day of death phase on Day 5 had a yield of 0.48 ± 0.005, while the yield on Day 11 during the second exponential phase was 0.45 ± 0.01. The bulk water chlorophyll *a* concentration (figure 4.1C) peaked on Day 4 at the end of the first exponential phase with 34.1 ± 0.2 μg L^{-1}, followed by a declining concentration during the death phase for the next four days and then an increasing concentration between Days 8 and 22 during the next exponential phase and the stationary phase. Cell counts are not available so these numbers have not been normalized to cell concentrations. Figure 4.1D shows the total bacterial concentrations, which steadily increase across the experiment to their highest value of 1.7 x 10^{8} cells mL^{-1} on Day 22.

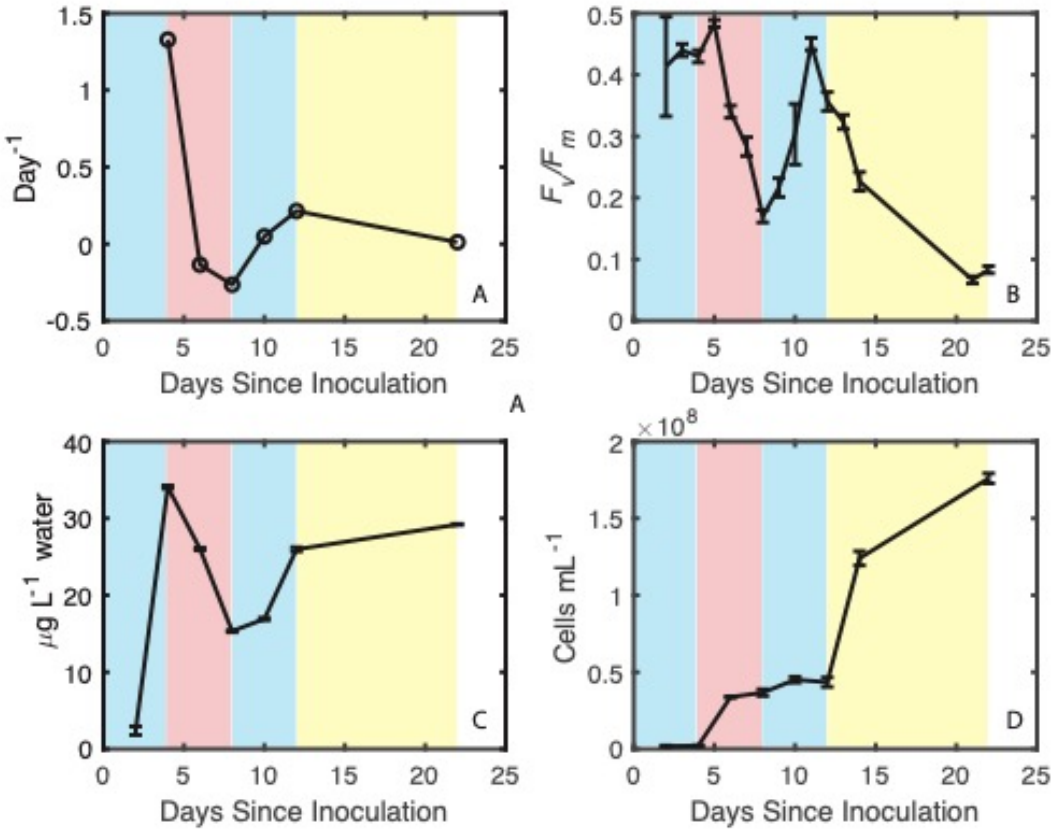

Figure 4.1: A) Growth rates calculated using chlorophyll a concentrations B) mean photosynthetic yield ± standard deviation C) mean chlorophyll *a* ± standard deviation, and D) total bacterial cell concentration ± standard deviation (d). N =3 for all measurements. Exponential phases are highlighted in blue, death phase in red, and stationary phase in yellow.

The bulk protein concentrations in the tank (shown in Figure 4.2) were very low during the first five days of the experiment during the first exponential phase. The concentration decreased for the first three days, and the concentration on Days 3 and 4 was measured as 0 μg mL^{-1}. Following the end of the first exponential phase Day 4 the concentration increased and reached its maximum value of 1.41 μg mL^{-1} on Day 9 at the

beginning of the next exponential phase. The concentration decreased during the second exponential phase but remained approximately 1 μg mL^{-1} until the end of the experiment on Day 24.

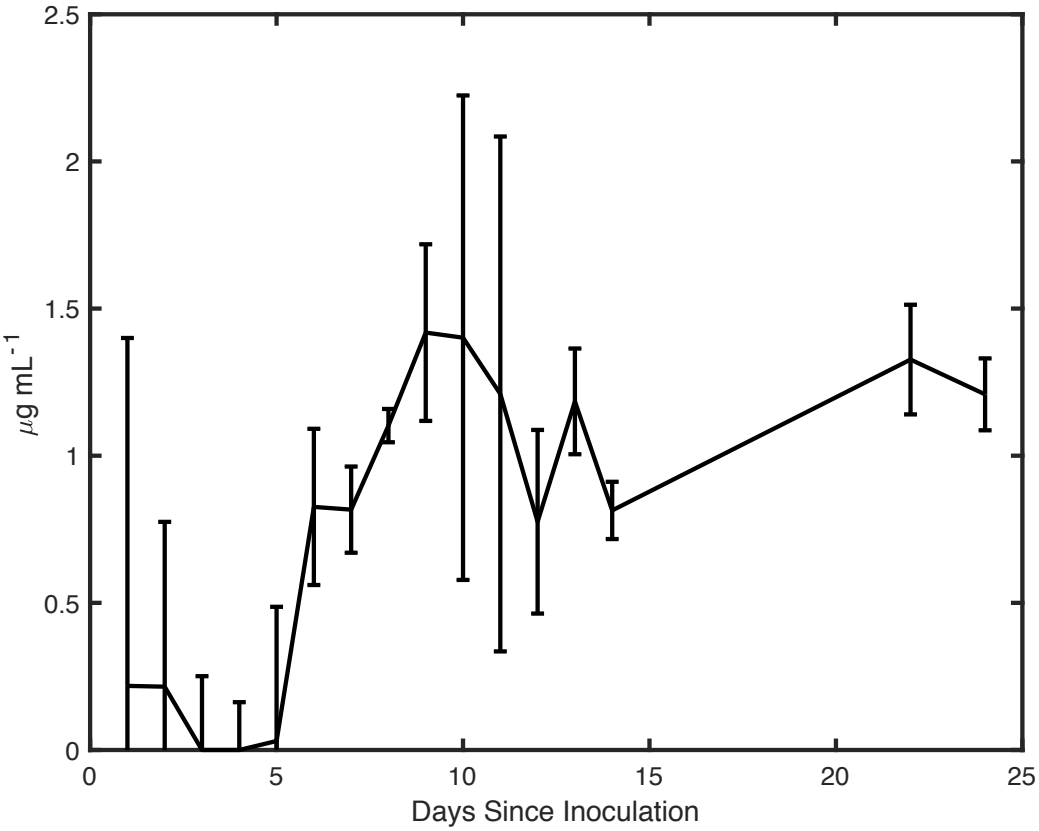

Figure 4.2: Mean bulk water protein concentration ± standard deviation, n = 3.

Two types of exopolymers were measured from the bulk water, transparent exopolymers (TEP) and Coomassie staining particles (CSP) and are shown in Figure 4.3. TEP concentrations peak on the first day of death phase on Day 5 and during the

stationary phase on Day 22. The highest measurement was near the end of the experiment during stationary phase on Day 22, with 6.7 ± 3.7 μg mL^{-1}, but there was not a steady increase prior to this peak. CSP concentrations peak much earlier, with a maximum value of 5.3 ± 1.7 μg mL^{-1} during the second exponential phase. Both the TEP and CSP concentrations are highly variable, with standard deviations up to 60% of the measured concentration.

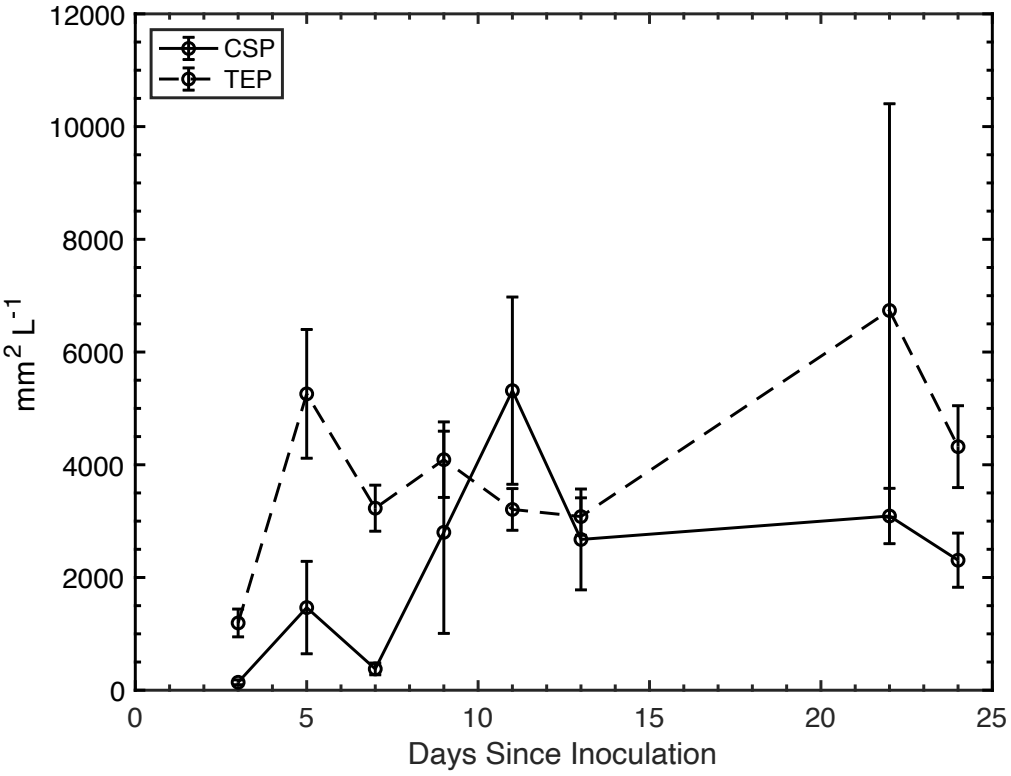

Figure 4.3: Mean transparent exopolymer (TEP) and Coomassie staining particle (CSP) concentrations in water ± standard deviation, n = 3.

SYTOX Green staining is plotted in Figure 4.4. As the only two categories measured were stained cells and unstained healthy cells (due to the lack of a nucleus in cyanobacteria), the two categories vary opposite each other. The peak proportion of stained cells was during the death phase with 86.7 ± 9.5% of cells stained on Day 5, followed by a sharp decrease during the second exponential phase to 28.3 ± 6.1% on Day 9. Although the proportion of stained cells remained around 30% during the second exponential phase, by the end of the stationary phase on Day 22 the proportion of stained cells decreased to 7.8 ± 0.2%.

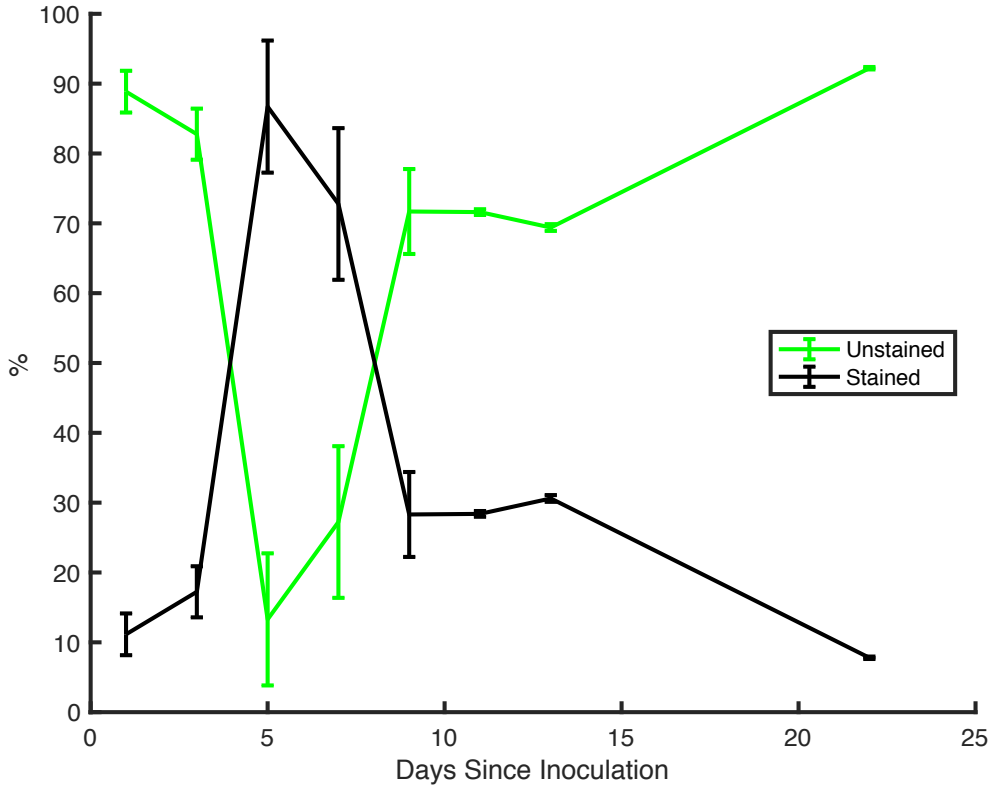

Figure 4.4: Proportion of cells stained with SYTOX Green. Each data point is mean ± standard deviation, n = 3. At least 400 cells were counted for each measurement.

Caspase-like enzyme activity (Figure 4.5) was only above zero on two of the days measured, once during death phase on Day 6 and once during stationary phase on Day 22, with values of 0.09 and 0.11 pmol μg^{-1} hr^{-1} respectively. The measured levels of caspase during this experiment were much lower than the levels measured during the other two MART experiments.

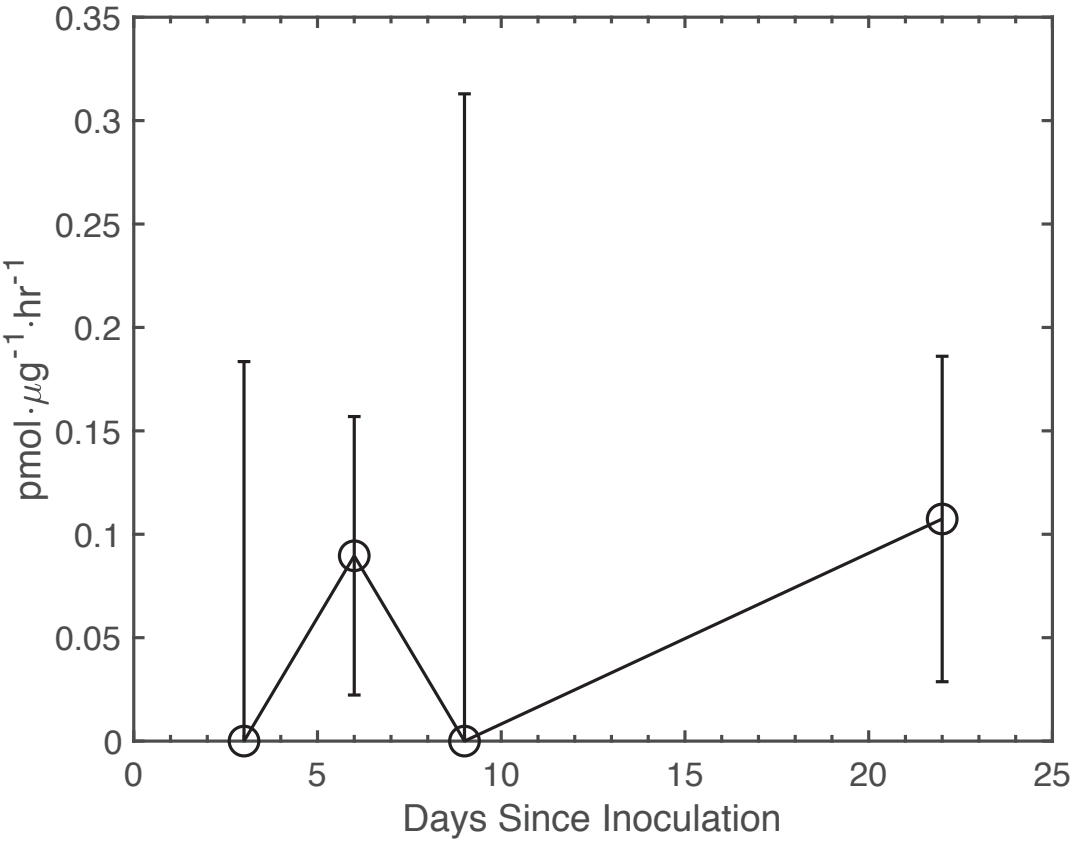

Figure 4.5: Mean caspase-like enzyme activity normalized to bulk protein concentrations, n = 3.

Five types of colored dissolved organic matter are plotted in Figure 4.6. The fluorescent peaks (Coble, 1996, 2007) representing protein-like materials are plotted in Figure 4.6A, while humic-like materials are plotted in Figure 4.6B. The concentration of tyrosine (peak B) increases across the course of the experiment, with the greatest rate of increase seen during stationary phase between Days 22 and 24. The tryptophan concentrations are more variable, first increasing sharply between Days 1 and 6 followed by decreasing concentrations between Days 6 and 22. However, like the tyrosine concentration the tryptophan concentration increased sharply during the stationary phase between Days 22 and 24. The two peaks representing terrestrial humic-like material, peaks A and C, did not increase or decrease together. Instead the terrestrial humic material represented by peak A showed a pattern of variability similar to the tryptophan concentrations, first increasing between Days 1 and 6 and then decreasing for the next 16 days until it began to increase between Days 22 and 24. The terrestrial humic material represented by peak C increased between Days 1 and 13, followed by a very minor decrease until Day 22 and a slight increase between Days 22 and 24. Peak M increased steadily across the experiment.

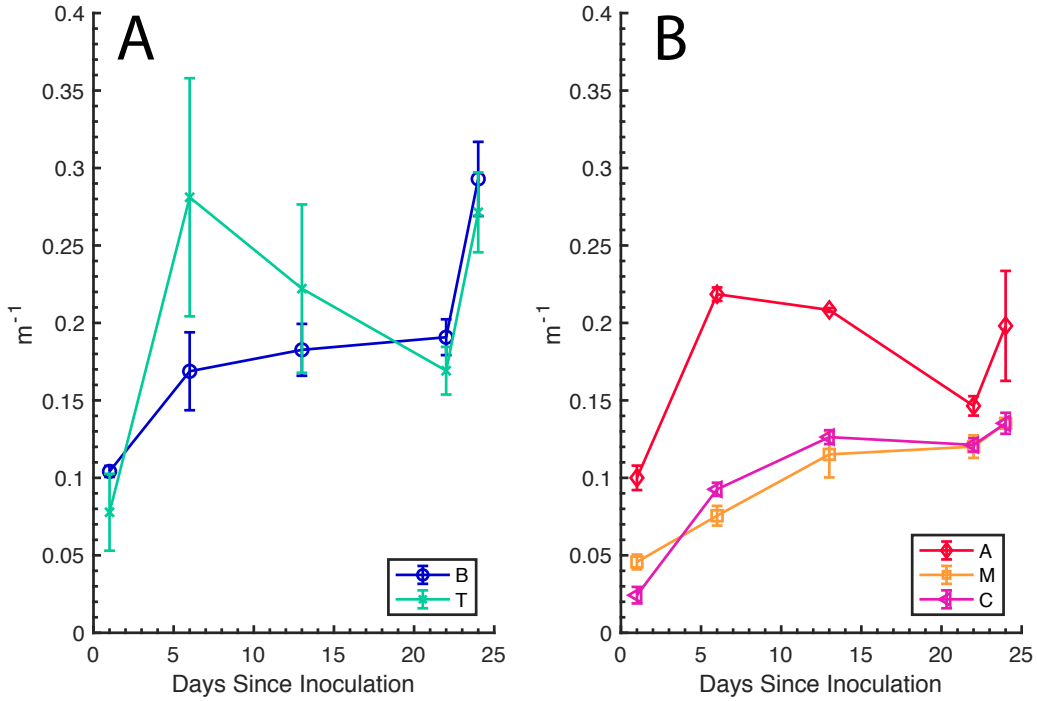

Figure 4.6: Colored dissolved organic matter absorbance of protein-like Coble's peaks (a) and humic-like Coble's peaks (b). Data points are mean value ± standard deviation, n = 3.

All reported nucleation temperatures (Figure 4.7) are from aerosol samples collected on Al foil discs. Most of the days had nucleation temperatures below -30 °C. However, Days 2 and 3 during the exponential phase showed much warmer freezing temperatures indicating the presence of ice nucleating particles. Day 3 had the warmest freezing temperature of any sample taken from cultures grown in the MART, with a mean freezing temperature of -18.0 ± 2.3 °C, while Day 2 had a slightly lower freezing temperature of -23.9 ± 1.9 °C. Past Day 3 the warmest freezing temperature was

measured with samples from Day 8, but this sample only had a mean freezing temperature of -30.7 ± 1.1 °C.

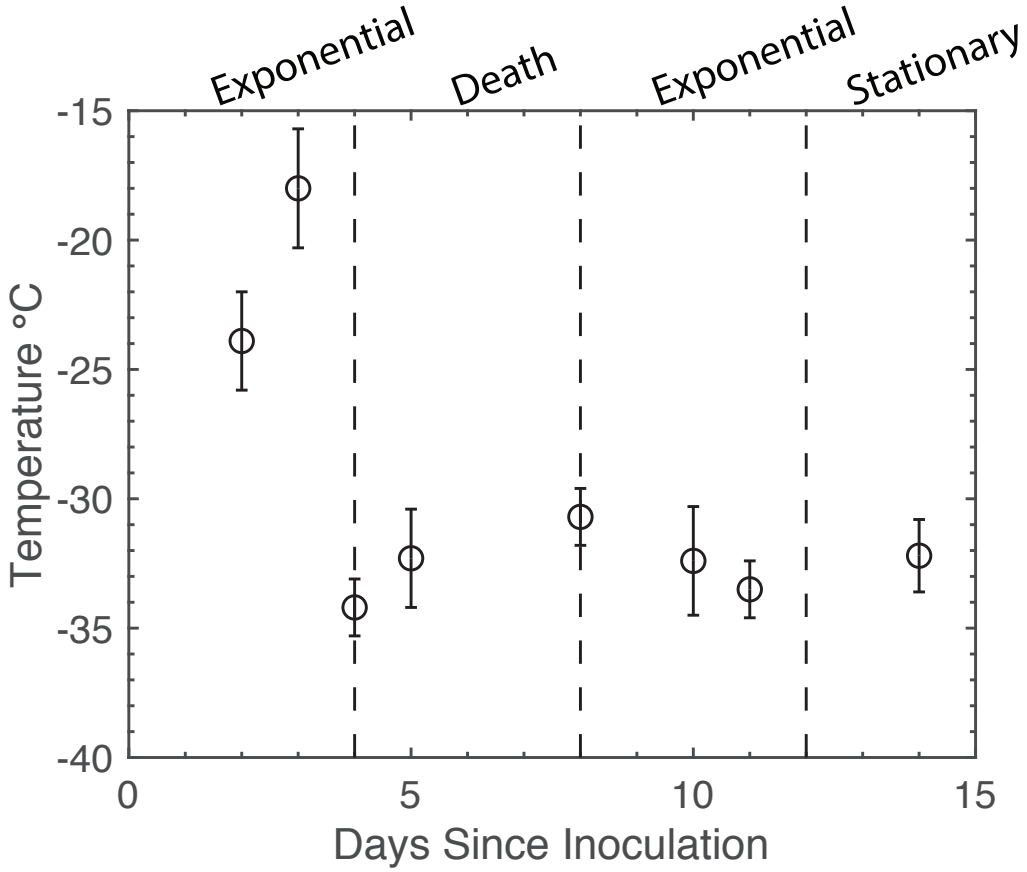

Figure 4.7: Mean freezing temperature of samples collected onto combusted aluminum foil discs. Data points are mean ± standard deviation, n ≥ 3.

Ambient aerosol concentrations (Figure 4.8) measured with a water-based condensation particle counter (model 3010, TSI) showed variability in the total number of aerosol particle numbers generated across the experiment, ranging from 838 ± 144

particles L^{-1} air on Day 2 to 2495 ± 531 particles L^{-1} air on Day 13. The aerosol concentrations increased for the first five days of the experiment, followed by a generally decreasing concentration during death phase and into stationary phase from Days 5 through 10 to a minimum concentration of 919 ± 165 particles L^{-1} air. The concentration then quickly increased to its maximum value on Day 13 at the beginning of stationary phase, followed by a decrease to approximately 1500 particles L^{-1} air for the remainder of the experiment.

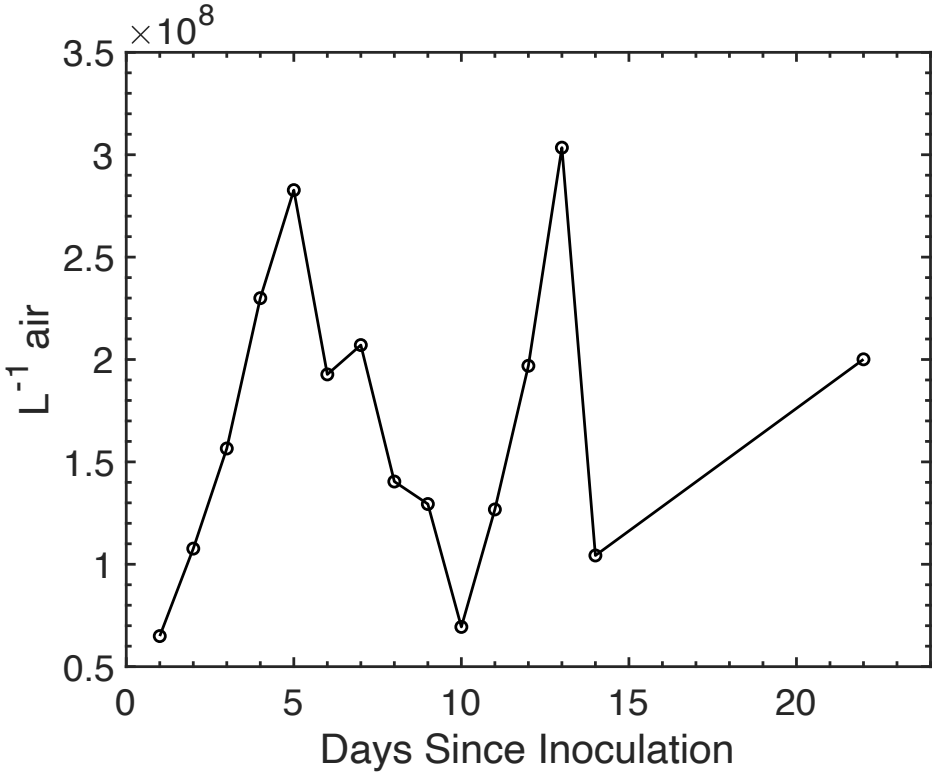

Figure 4.8: Average daily ambient aerosol concentrations across the approximately 2-hour long aerosol sample collection window. Measurements were taken every second. Data points show mean ± standard deviation, n ≥ 6640.

4.4. Discussion

Unlike the previous experiments with diatoms discussed in Chapter 3, the growth did not follow a standard growth curve in that it had two periods of exponential growth, a single death phase in the middle of the experiment, and a stationary phase at the end of the experiment. This may be due to interaction with heterotrophic bacteria as the tank was not axenic (although the experiments presented in Chapters 3 and 5 were also not axenic). Instead there were two distinct phases of exponential growth, the first following inoculation until Day 4. Although growth rates cannot be calculated prior to Day 4 due to calculation methods based on chlorophyll *a* concentrations which were only measured beginning on Day 3, the growth was likely high for the first four days. The tank contained the same amount of nitrogen, phosphorous and other nutrients as previous experiments, which was enough to fuel exponential growth in *Synechococcus* during the beginning of the experiment. The growth rate decreased after Day 4 as the total biomass (represented by chlorophyll *a* plotted in figure 4.1C) decreased and the proportion of dead cells (stained cells in Figure 4.4) increased. This may have been due to competition with a rapidly increasing bacterial population (Figure 4.1D). It is likely not due to a lack of nutrients, as the biomass then increases again after Day 8 for the rest of the experiment. The population may have adapted to the bacterial population and began to once again photosynthesize efficiently (Figure 4.1B) until Day 11, when the yield begins to decrease. This decrease was not followed by a decrease in chlorophyll concentration, but it is likely that a longer experiment would have shown this decrease.

When compared with exopolymer concentrations reported in Chapter 3 from *Thalassiosira weissflogii* populations, the TEP and CSP concentrations produced by *Synechococcus elongatus* were higher by nearly 300%, although when using chlorophyll as a proxy for biomass the diatom populations had a much higher biomass. It is possible that the chlorophyll per cell would be approximately the same, but cell counts are not available. Neither TEP nor CSP varied with biomass, but the concentrations of both were beginning to decrease by the end of the experiment. This would be expected if bacterial activity and consumption of exopolymers increased by the end of the experiment, which is supported by the increase in peak M of the colored dissolved organic matter. This peak has been used as an indicator of the level of bacterial activity (Kinsey, Corradino, Ziervogel, Schnetzer, & Osburn, 2018).

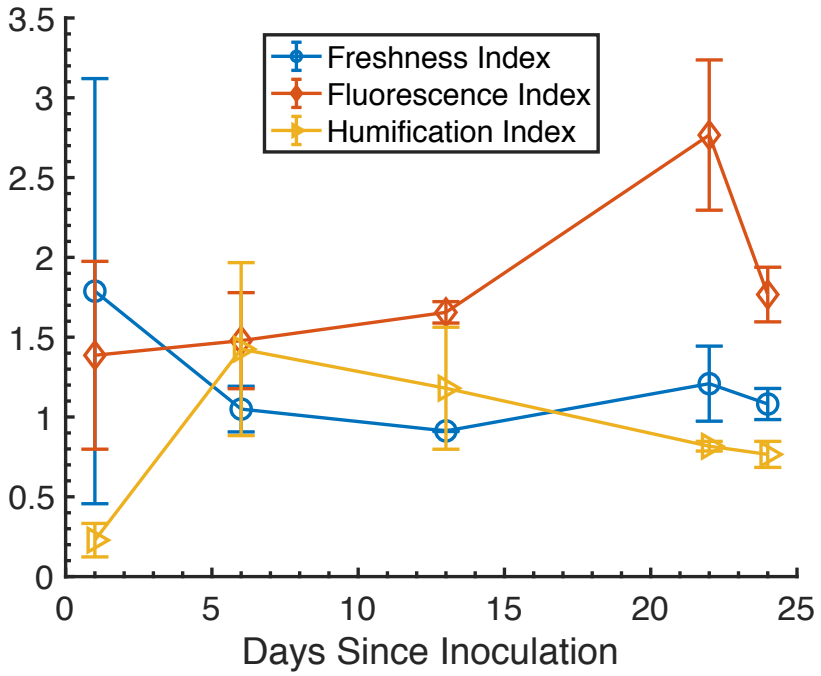

Figure 4.9: Colored dissolved organic matter Coble's peak ratios ± standard deviation, n = 3. Analysis performed by Gerado Gold Bouchot.

The ratios of fluorescent peaks can also be used to determine information about the dissolved material (Huguet et al., 2009). The humification index, representing the presence of large aromatic molecules (Kalbitz, Geyer, & Geyer, 2000; Kalbitz, Geyer, & Geyer, 1999), increased between Days 1 and 6, followed by a steady decrease until the end of the experiment. This would be expected if these large, high molecular weight compounds were being consumed by organisms within the tank. The fluorescence index indicates the source of the CDOM (Cory & McKnight, 2005; McKnight et al., 2001). The fluorescence index between Days 1 and 13 increased toward 1.8, indicating a shift toward a microbial source of CDOM. The CDOM source was highest on Day 22, but

was much higher than 1.8, indicating either a shift in the microbial source of the CDOM or a much different source than the other measurements. The fluorescence index decreased between Days 22 and 24, indicating a shift back to the same microbial CDOM source. The freshness index is also used as an indicator of the CDOM source (Huguet et al., 2009; Parlanti, Wörz, Geoffroy, & Lamotte, 2000; Wilson & Xenopoulos, 2009). The index is the ratio of microbial (newer) dissolved organic matter to more decomposed (older) dissolved organic matter, so a higher value indicates a newer source of CDOM. The freshness index is highest on Day 1, decreases and then remains approximately the same for the rest of the experiment. This is expected, as the amount of older organic matter increases as the culture in the tank ages. There was not much bacterial remineralization of organic matter, which would have been indicated by an increase in the freshness index.

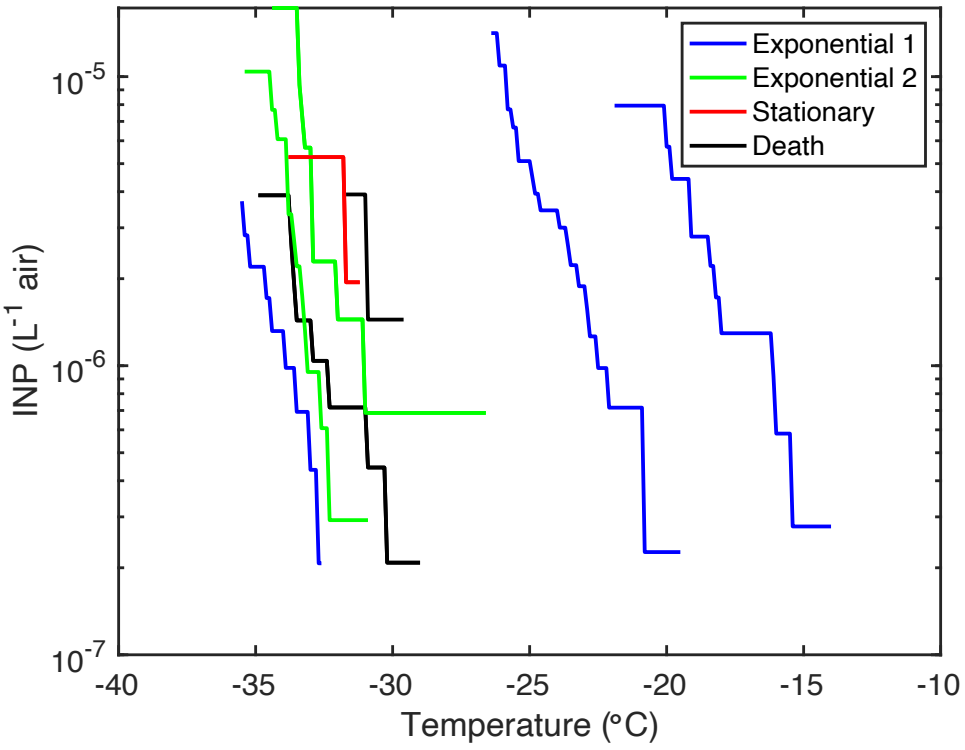

Figure 4.10: Ice nucleating particle concentrations per liter of air, calculated using Equation 4. See Section 2.6 for details on INP concentration calculations. The initial exponential phase is plotted in blue, the second exponential phase is plotted in green, the stationary phase is plotted in red, and the death phase is plotted in black.

Only two days of aerosol samples contained material that efficiently acted as INP, and as with the INPs produced by *Thalassiosira weissflogii* those samples were collected during the beginning of the first exponential phase. When INP concentrations (calculated from equation 4 modified from equations given in DeMott et al. [2016] and described in Chapter 2.6) are compared, Days 2 and 3 have much higher concentrations of INP at -25 °C than all other sampled days. Day 3 had both the warmest maximum

nucleation temperature at -14.0 °C and a higher concentration of INP at -20 °C, with 0.71 INP L^{-1} air.

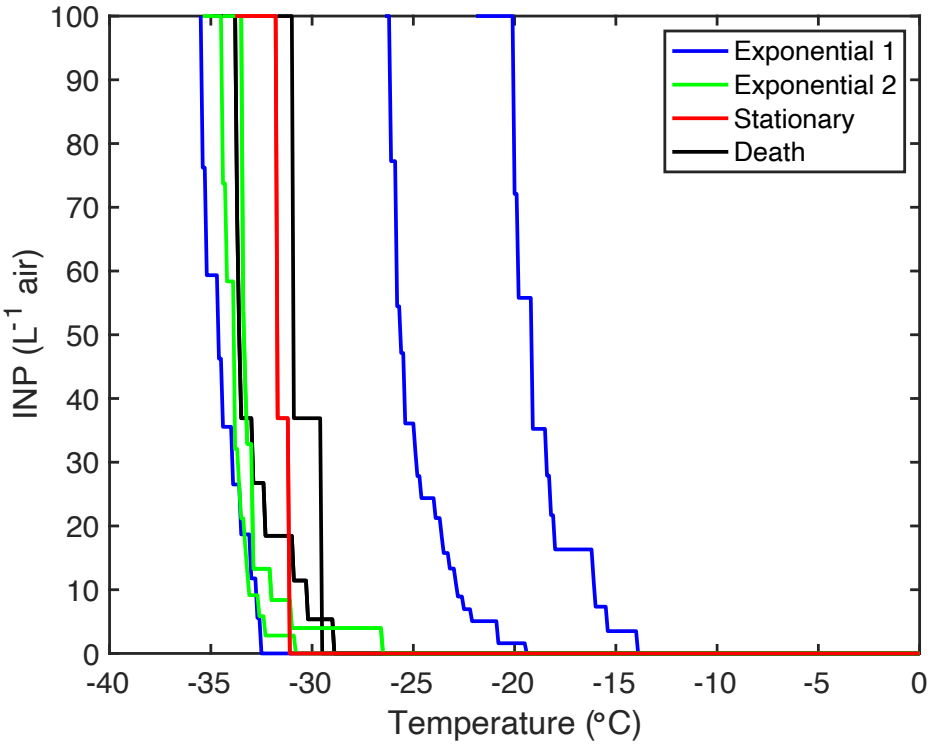

Figure 4.11: Percentage of INPs activated, calculated from equation 6 in Section 2.6. The initial exponential phase is plotted in blue, the second exponential phase is plotted in green, the stationary phase is plotted in red, and the death phase is plotted in black.

Figure 4.11 shows the fraction of particles activated as INP at a range of temperatures. Day 2 had the warmest initial activation temperature and contained INPs that nucleated at -19.6 °C. At this temperature, the sample contained 0.03 INP L^{-1} air, which is 1.6% of the total INPs. Following Day 3 the INP concentrations at temperatures warmer than -25

°C dropped sharply. None of the later samples tested had INP concentrations capable of nucleating at -20 °C.

None of the biological parameters were correlated with ice nucleation temperature (Pearson correlation, $p<0.05$). Although there were several parameters that were either high at the beginning of the experiment and decreased or low with an increasing value, most of the parameters measured varied throughout the experiment. The only characteristic that was highest at the beginning of the experiment, decreased, and stayed low for the rest of the experiment was the growth rate. This high growth rate with warm ice nucleation temperatures was also seen in the previous diatom-based MART experiments. However, the growth rate for this study was only able to be calculated starting on Day 4. By Day 4 the ice nucleation was occurring at much colder temperatures than Days 2 and 3. It is likely that the growth rate was higher on days prior to Day 4 (this would be expected due to the high nutrient concentrations and low bacterial population and thus low competition for nutrients).

It can be determined from these results that ice nucleation temperatures are much warmer at the very beginning of the experiment. This was also shown in the aerosol samples generated from the MART containing *Thalassiosira weissflogii*. Both species of phytoplankton only produced moderate INPs during the exponential phase. This is likely due to material that is produced by rapidly dividing cells that is then aerosolized and captured on Al foil discs. However, in samples generated from the MART containing *Synechococcus elongatus*, the INPs produced during the second exponential phase were

not active at the same warm temperatures as those generated on Days 2 and 3, suggesting a difference between the two exponential phases.

4.5. Conclusions

The MART containing *Synechococcus elongatus* did not show the same growth curve as *Thalassiosira weissflogii* grown in the MART under identical conditions, but both cultures were a source of moderate INP during the early days of their exponential phases. When comparing the INP and chlorophyll *a* concentrations of *Synechococcus* it can be concluded that chlorophyll *a* cannot be used as a predictor of INP activity, confirming what was reported in Chapter 4. Instead, high INP activity and concentrations were seen only during the first period of exponential growth just following inoculation, showing the presence of moderate INP in the aerosols produced from the culture. Like *Thalassiosira weissflogii*, *Synechococcus elongatus* produced the most effective INP on Days 2 and 3 of growth during exponential phase, followed by poor INP for the rest of the experiment. However, the presence of a second exponential phase that did not produce moderate INPs shows that it is important to consider how well the phytoplankton population is growing, but that a high growth rate is not the only indicator of the efficiency INPs produced. Due to the moderate efficiency of the INP produced on Days 2 and 3 and the ubiquitous nature of *Synechococcus* in marine ecosystems, it is possible that *Synechococcus* could be a source of INP in remote regions without terrestrial INP sources.

5. PRODUCTION OF ICE NUCLEATING PARTICLES BY THE COCCOLITHOPHORE *EMILIANIA HUXLEYI*

5.1. Introduction

Although a single phytoplankton cell is only a few micrometers in diameter, some phytoplankton blooms are visible on satellite imagery at a scale of kilometers. *Emiliania huxleyi*, a coccolithophore, produces blooms that can span thousands of kilometers (Brown & Yoder, 1994; Iglesias-Rodríguez et al., 2002; Poulton et al., 2013) and contain more than 10^5 cells mL^{-1} (Berge, 1962). In addition to consuming carbon dioxide through photosynthesis, these coccolithophore blooms are estimated to produce up to half the global oceanic calcium carbonate each year (Taylor, Brownlee, & Wheeler, 2017), some of which sinks and forms marine sediment (Bramlette, 1958; Broecker, Peng, Beng, & Observatory, 1982; Milliman, 1993) leading to burial of carbon and removal from the carbon cycle for thousands to millions of years. Due to the large scale of dense coccolithophore blooms (with concentrations as high as 10^5 cells mL^{-1} [Berge, 1962]) and their production of calcium carbonate coccoliths that reflect sunlight coccolithophore blooms can be observed in satellite imagery (Brown & Yoder, 1994; Holligan, Viollier, Harbour, Camus, & Champagne-Philippe, 1983; Holligan et al., 1993).

Coccolithophores are haptophytes that are found worldwide in temperate and tropical waters (Brown, 1995; Read et al., 2013). They evolved roughly 300 million years ago (Bown, Lees, & Young, 2004; Taylor et al., 2017) , later than many

phytoplankton species, but have high levels of genetic diversity both between species and between strains of the same species (Paasche, 2001; Read et al., 2013). One of the most abundant species of coccolithophore is *Emiliania huxleyi* (Iglesias-Rodríguez et al., 2002). There are two major cell types, both of which can be found within the same species. The most common cell type found in blooms is a diploid form with 10-15 calcium carbonate (calcite, $CaCO_3$) coccoliths surrounding the cell wall (Balch, Kilpatrick, M. Holligan, & Cucci, 1993; Paasche, 2001). The function of these plates is not fully understood. A variety of reasons have been proposed for their formation, including light scattering or focusing, stabilization of the cell surface, or defense against viruses and grazers (Taylor et al., 2017). The other cell type is a haploid cell without coccoliths. Haploid cells are seen in nutrient-limited or otherwise stressed populations (Nöel, Kawachi, & Inouye, 2004) and are especially common following viral infection (Frada, Probert, Allen, Wilson, & de Vargas, 2008; Frada, Bidle, Probert, & de Vargas, 2012). Haploid cells have flagella and are motile, while diploid cells have neither flagella nor a haptonema (Taylor et al., 2017).

Coccolithophore blooms are susceptible to viral infection by large double-stranded DNA viruses known as coccolithoviruses (Schroeder, Oke, Malin, & Wilson, 2002; Suttle, 2007). These viruses are in the family *Phycodnaviridae* and are much larger than most marine viruses—up to 200 nm in diameter (Schroeder et al., 2002a). It has been shown that these viruses can be transported via aerosolization across kilometer-scale distances, moving between coccolithophore blooms (Sharoni et al., 2015; Trainic et al., 2018). These large-scale blooms can collapse in only a few days following viral

infection (Gunnar Bratbak et al., 1993; Gunnar Bratbak, Wilson, & Heldal, 1996; Jacquet et al., 2002; Schroeder, Oke, Hall, Malin, & Wilson, 2003; Wilson et al., 2002), and likely produce large quantities of aerosols from both the lytic processes and the viruses themselves (Aller et al., 2005; Trainic et al., 2018).

Coccolithophores were one of the first phytoplankton species linked to cloud processes through their production of dimethylsulfoniopropionate (DMSP), dimethylsulfoxide (DMSO), and dimethyl sulfide (DMS) (Charlson et al., 1987; Keller, 1989; Patricia A. Matrai & Keller, 1993; P. A. Matrai & Keller, 1994). Although the exact role of DMSP in the cell is unknown, its primary role is thought to be osmoprotection (Paasche, 2001). DMSP is also a precursor to DMS, both inside the coccolithophore cell (Niki, Kunugi, & Otsuki, 2000; Van Boekel & Stefels, 1993; Yoch, Ansede, & Rabinowitz, 1997) and via bacterial degradation of DMSP (Levasseur et al., 1996; Stefels, 2000). DMS is released as part of the aerosols produced from phytoplankton blooms (Park et al., 2017), and it was proposed in 1987 that this DMS released could lead to cloud formation by acting as cloud condensation nuclei (CCN) (Charlson et al., 1987). However, more recent studies suggest that the environmental effects of DMS are more complicated than originally understood, and that in most cases the CCN and aerosols produced over a bloom cannot be tied directly to DMS production by coccolithophores and other phytoplankton (Matrai & Keller, 1993; Quinn & Bates, 2011). Instead, the DMS emitted by the coccolithophores themselves and through bacterial oxidation of DMSP is lofted to high altitudes prior to oxidation by OH radicals to form sulfate groups that act as CCN (Quinn & Bates, 2011). Although the amount of

CCN that can be tied directly to DMS production by coccolithophores is not known, recent work has shown that there is likely at least a weak positive relationship between the growth of DMS-producing phytoplankton, including coccolithophores, and an increase in CCN concentration in the atmosphere over the phytoplankton bloom (Sanchez et al., 2018).

Although there may be a slight link between coccolithophore primary productivity and increased CCN production, few studies have looked at coccolithophore production of ice nucleating particles. (Alpert et al., 2011b) found no different in freezing temperature between droplets containing *Emiliania huxleyi* and pure growth medium, with immersion mode freezing temperatures at -39 °C and lower. However, these results only consider cells harvested after a week of culture growth on a single day. In contrast, this chapter covers the INP activity and number concentration produced over the course of the entire bloom from inoculation to death and bloom collapse.

5.2. Methods

Cultures of *Emiliania huxleyi* (CCMP 374) were grown in ASW with the following nutrients added: 50 μM nitrate and 5 μM phosphate. In addition, trace metals and vitamins were added following the recipe for L1 medium (Hahn & Blobel, 1968; Harrison et al., 1980). All sampling methods remained the same as previous MART experiments (see Chapter 2 and Section 4.2.2). Unlike previous experiments, the tank was inoculated with a lower concentration of cells rather than 10% of the total tank volume. Inoculum was added to the tank for an initial concentration of 500 cells mL^{-1} (20 mL of dense culture was added). The following samples were analyzed by Alyssa

Alsante: chlorophyll *a* concentrations, β-glucosidase activity rates, and bacterial concentrations. Total aerosol concentration measurements were taken by Jessica Mirrielees. See Tables 2.1 and 5.1 for a complete list of samples taken during this experiment. Samples were taken from the tank full of ASW prior to the addition of any nutrients or organisms; these results are plotted as Day -1.

Table 5.1: Water samples taken during this experiment. Note that not all samples taken will be addressed by this chapter. See Table 2.1 for a complete list of MART samples and who they were taken by.

Sample	Sample type	Replications	Reference Section
Bacterial counts	Bottle, filter	3	2.3.1.2
Cell counts	Bottle	3	2.3.1.1
Fluorescence	Measurement	3	2.4.1
Zoff	Measurement	1	2.4.1
Bulk water ice	Microcentrifuge tube	3	2.6.2
Chlorophyll *a*	Filter (GF/C)	3	4.2.2
TEP	Filter (polycarbonate)	3	2.4.5
CSP	Filter (polycarbonate)	3	2.4.5
SYTOX green	Filter (polycarbonate)	3	2.4.2
Caspase	Pellet	3	2.4.3
CDOM	Bottle, filter (GF/F)	3	
DNA	Filter	3	Not addressed

The tank was cooled with an air conditioner, with a goal temperature of 17 °C. However, the average water temperature in the tank fluctuated between 16 and 19 °C. As in chapter 4, only samples collected via PIXE Impaction Samplers were analyzed for INP ability.

5.3. Results

Due to the low inoculation concentration, measurements show a pronounced lag phase that was not present in previous experiments. Although cell counts and chlorophyll concentrations remained low for the first three days of growth, the growth rate was positive for the first eight days as the cells moved through exponential phase (ending after the seventh day of sampling based on chlorophyll concentrations).

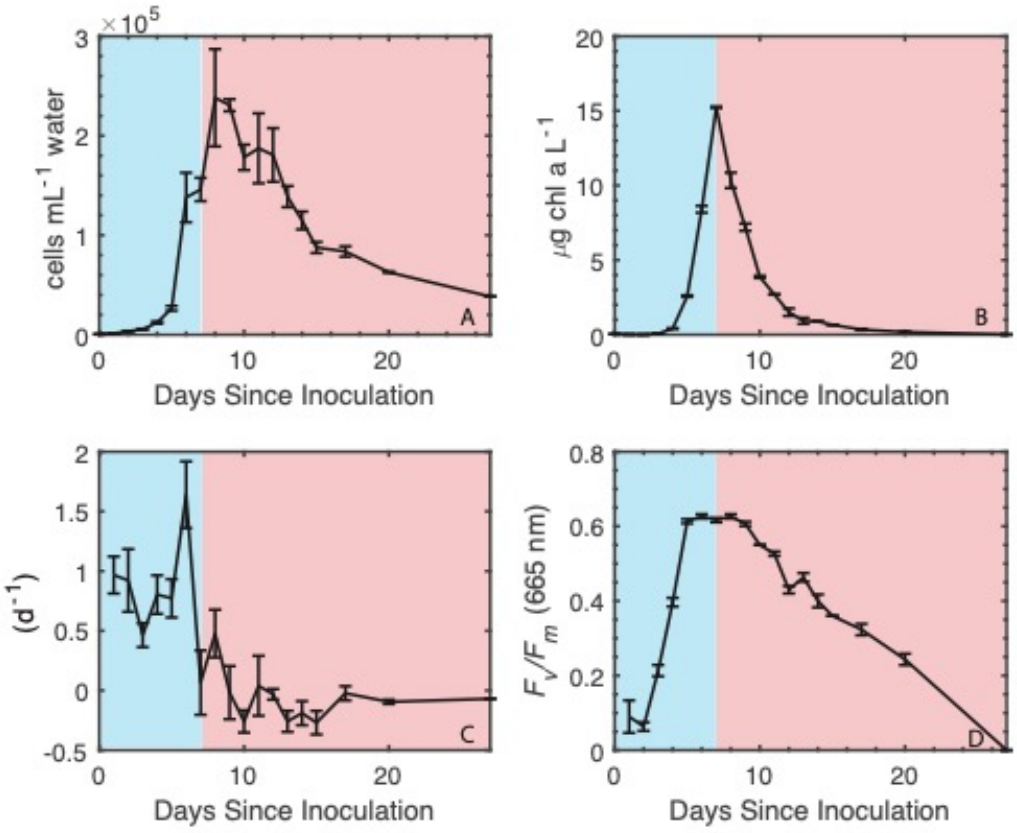

Figure 5.1: Physiological measurements of *Emiliania huxleyi*, including A) mean cell counts (n = 3), B) mean bulk chlorophyll *a* (μg L^{-1}, n = 3), C) growth rates (mean, n = 3), and D) mean photosynthetic yield (F_v/F_m at 665 nm, n = 3). Exponential phase is highlighted in blue and death phase is highlighted in red. All error bars are ± a single standard deviation from the mean value.

The initial cell concentration (Figure 5.1A) was 521 cells mL^{-1} immediately following inoculation. The cell concentration increased throughout exponential phase and slightly into death phase until Day 8, when the maximum cell concentration of 238000 ± 48900 cells mL^{-1} was measured. The maximum chlorophyll *a* concentration (Figure 5.1B) of 15.2 µg chl a mL^{-1} was measured one day prior on Day 7 and was used to define the start and end of exponential phase and death phase. The mean growth rate (n = 3) on Days 0-8 was positive, ranging from a low of 0.07 ± 0.30 day^{-1} on Day 7 to a maximum of 1.6 ± 0.28 day^{-1} on Day 6. Following Day 8 all growth rates were negative as the cell concentration declined until Day 27. The mean quantum yield of photosystem II was low for the first two days following inoculation (0.1 ± 0.05 on Day 1 and 0.1 ± 0.01 on Day 2, n = 3 for all yield measurements). It began rising on Day 3 and reached its highest value on Day 5 at 0.57 ± 0.01. The yield remained at or near its maximum value and above 0.55 until Day 10, when it began to decline. The minimum yield at the end of the experiment was seen on Day 20. The yield on Day 27 was essentially 0.

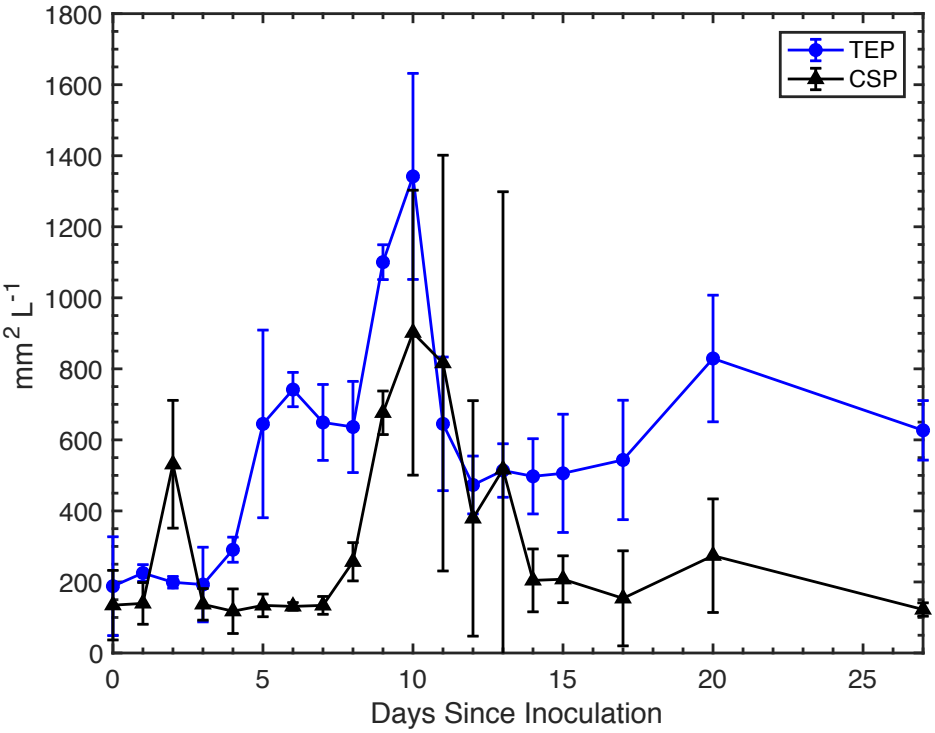

Figure 5.2: Mean exopolymer concentrations (n = 3). Transparent exopolymer particles (TEP) were stained with Alcian Blue and represent acidic polysaccharide concentrations in bulk water, while Coomassie staining particles (CSP) were stained with Coomassie Brilliant Blue dye and are proteinaceous. All data points show the mean area concentration ± a single standard deviation above and below the mean.

Transparent exopolymer particle area concentrations (TEP, Figure 5.2) were steady at approximately 200 mm^2 L^{-1} for the first four days, followed by an increase to a peak at 741 ± 48.3 mm^2 L^{-1} on Day 6. A second, higher peak was measured during death phase on Day 10 at 1340 ± 290 mm^2 L^{-1}. The TEP concentration stayed around 500 mm^2 L^{-1} for the rest of the days measured, except for an increase to 829 ± 178 mm^2 L^{-1} on Day 20. Coomassie staining particle area concentration (CSP, Figure 5.3) also peaked on Day

10 at 901 ± 401 mm^2 L^{-1}, with an earlier lower peak seen on Day 2 at 531 ± 180 mm^2 L^{-1}. CSP concentrations also increased between Days 17 and 20 to 274 ± 160 mm^2 L^{-1}.

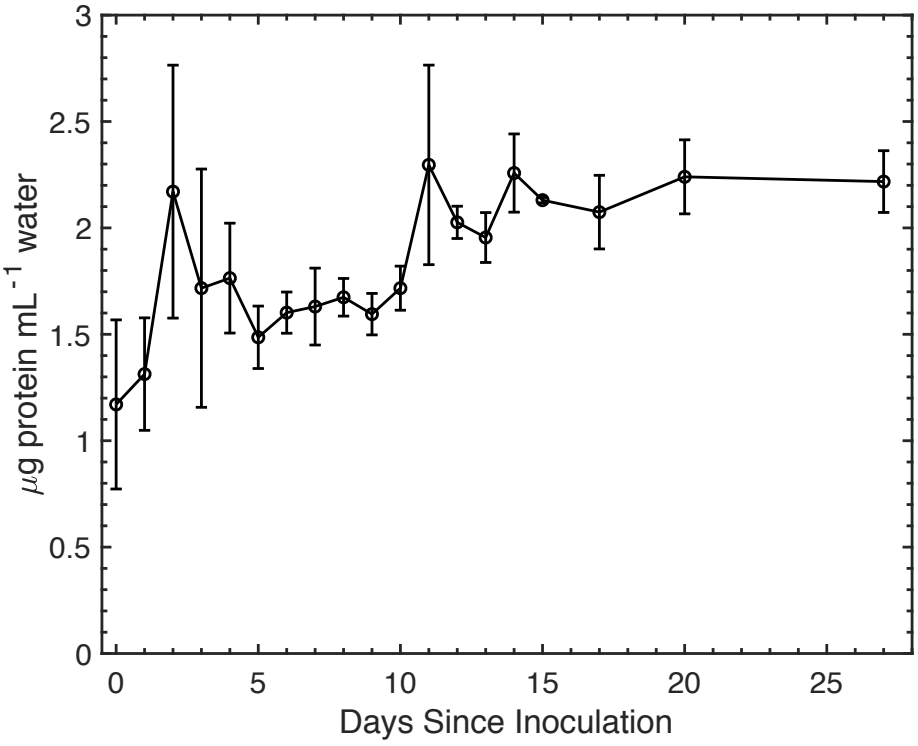

Figure 5.3: Mean bulk protein concentration (µg protein mL^{-1} water). Each data point shows the mean value ± a single standard deviation, n = 3.

The mean bulk protein concentration (Figure 5.3) showed a positive trend as the experiment progressed ($r^2 = 0.72$, $p < 0.05$), although there were times when the concentration decreased for a few days (the four measurements between Days 2 and 5 showed the longest decrease). The highest concentration was measured on Day 14 at

2.26 μg mL[1], and the lowest concentration was measured on Day 0 just following inoculation. The lowest measured concentration was 1.2 μg mL^{-1}.

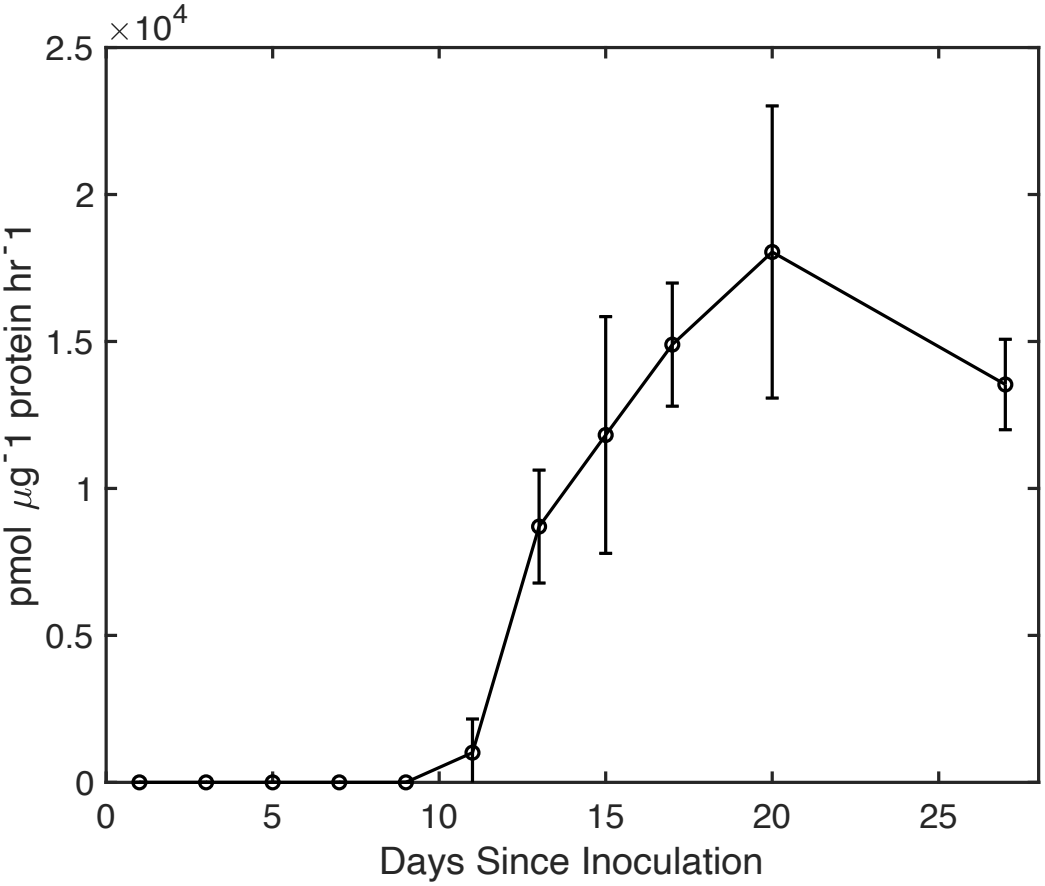

Figure 5.4: Rates of caspase-like enzyme activity (pmol μg^{-1} protein hr^{-1}, n = 3). Negative rates are assumed to be 0.

The rate of caspase-like enzyme production (Figure 5.4) is not measureable during the entirety of exponential phase. During death phase the first day it was measurable was in samples taken on Day 11 of growth. The caspase peaks on Day 20

although due to large sample standard deviations (n = 3) the rate from Day 15 onward cannot be said to be detectably lower or higher. It is also possible that there was a measurable rate of production on Day 10 when cell counts began to decline that cannot be seen due to sampling frequency.

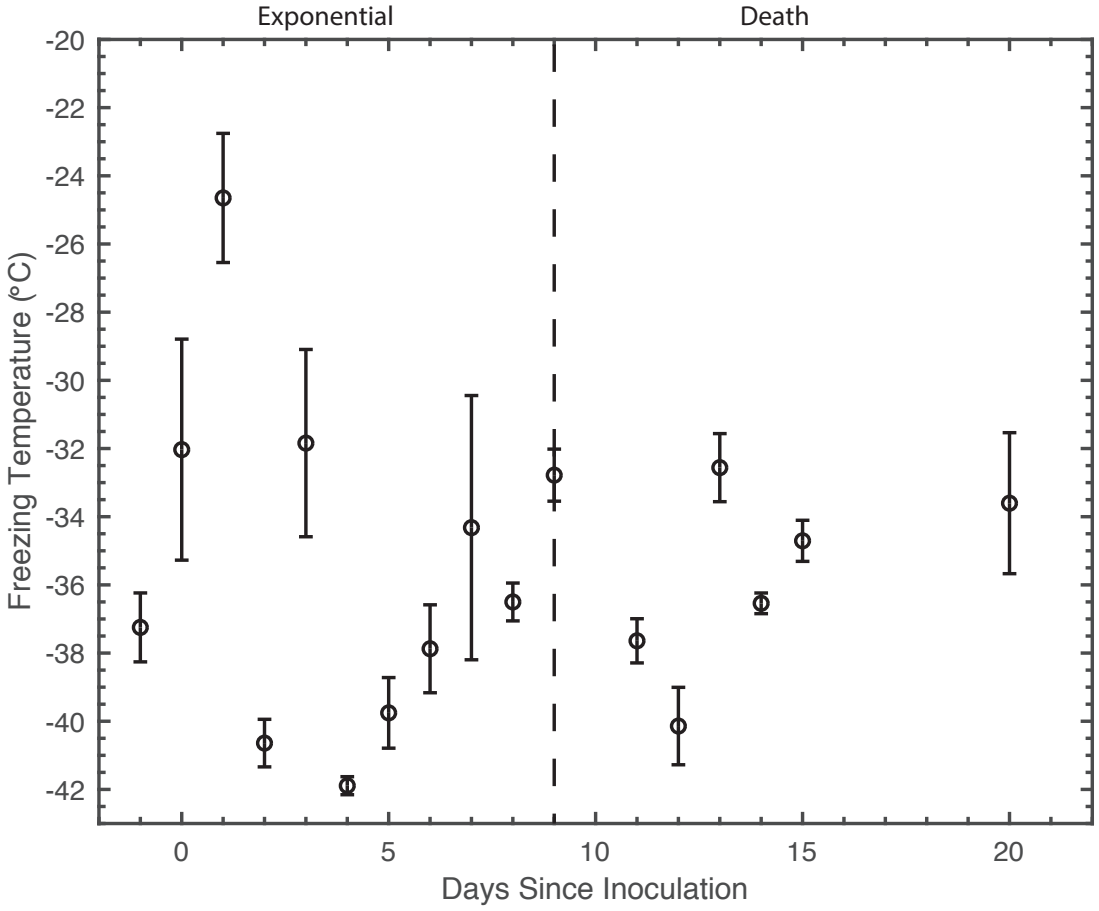

Figure 5.5: Mean freezing temperature (°C, n ≥ 3, mean ± standard deviation). Droplets (2 µL) of UHP water were placed over samples collected via impaction on to combust Al foil discs.

Overall, freezing temperatures of aerosol samples produced during an *E. huxleyi* bloom (Figure 5.5) were below -32 °C, with only Day 1 freezing at a temperature higher than -30 °C. Day 1 during exponential phase froze at -24.6 ± 1.9 °C (n = 12, mean ± standard deviation). However, the preceding day froze at -32.0 ± 3.2 °C (n = 12), and the day following froze at -40.6 ± 0.7 °C (n = 4). Seawater with no nutrients or coccolithophores froze at an average temperature of -32.8 ± 0.8 °C (n = 16). There was no trend in the freezing data as the culture progressed through the growth phases, other than a brief four-day warming trend from the coldest freezing temperatures measured (Day 4, -41.9 ± 0.3 °C, n = 4) to the slightly warmer freezing temperatures measured at the end of exponential phase on Day 7 (-34.3 ± 3.9 °C, n = 5). Like the other two MART experiments, the presence of moderate INP was only seen during exponential growth. However, unlike samples from *Thalassiosira weissflogii* and *Synechococcus elongatus*, there was only one day of warm freezing on Day 1, followed by freezing temperatures below -30 °C throughout the rest of exponential phase and the subsequent death phase.

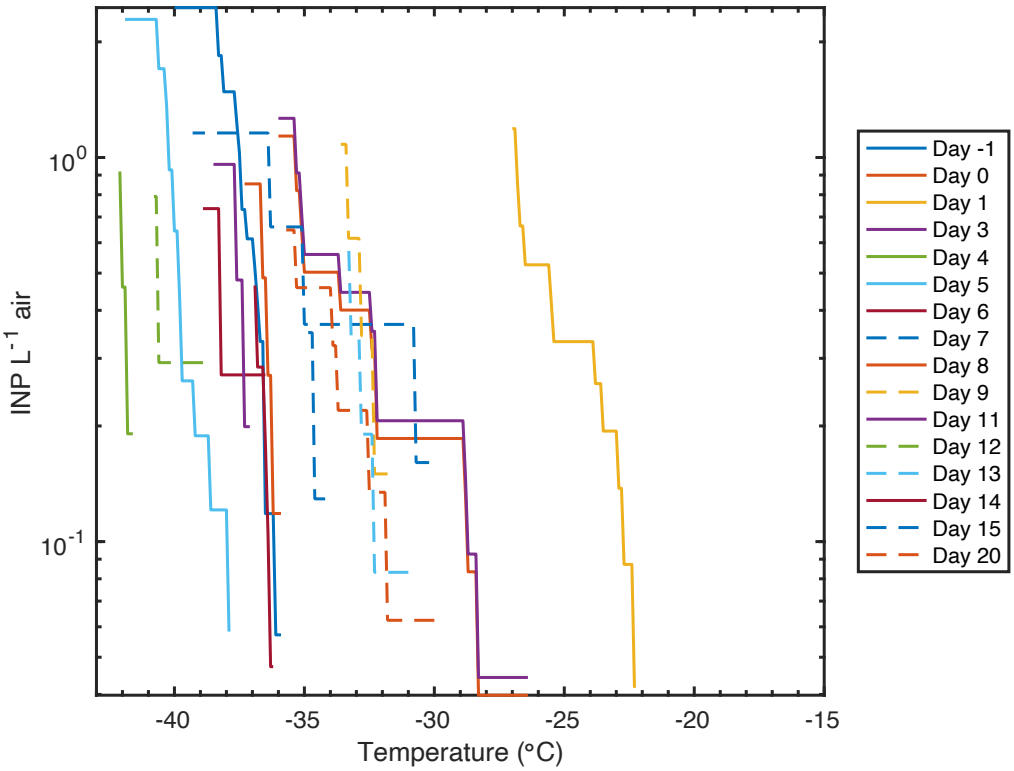

Figure 5.6: Ice nucleating particle concentrations (L^{-1} air) in each sample, calculated using equation 2 from DeMott et al., 2016 and normalized to total particles per liter of air. Samples (0.6 – 1 µm) were collected via impaction and total aerosols were measured with a TSI water CPC.

INP concentrations per liter of air are shown in Figure 5.6. The INP concentration at -25 °C was highest in the sample from Day 1 during exponential phase, with 2.8 x 10^{-6} INP L^{-1} air. Samples from later days of exponential phase and death phase did not contain any ice-active particles at -25 °C, and at -30 °C only five samples contained active INPs.

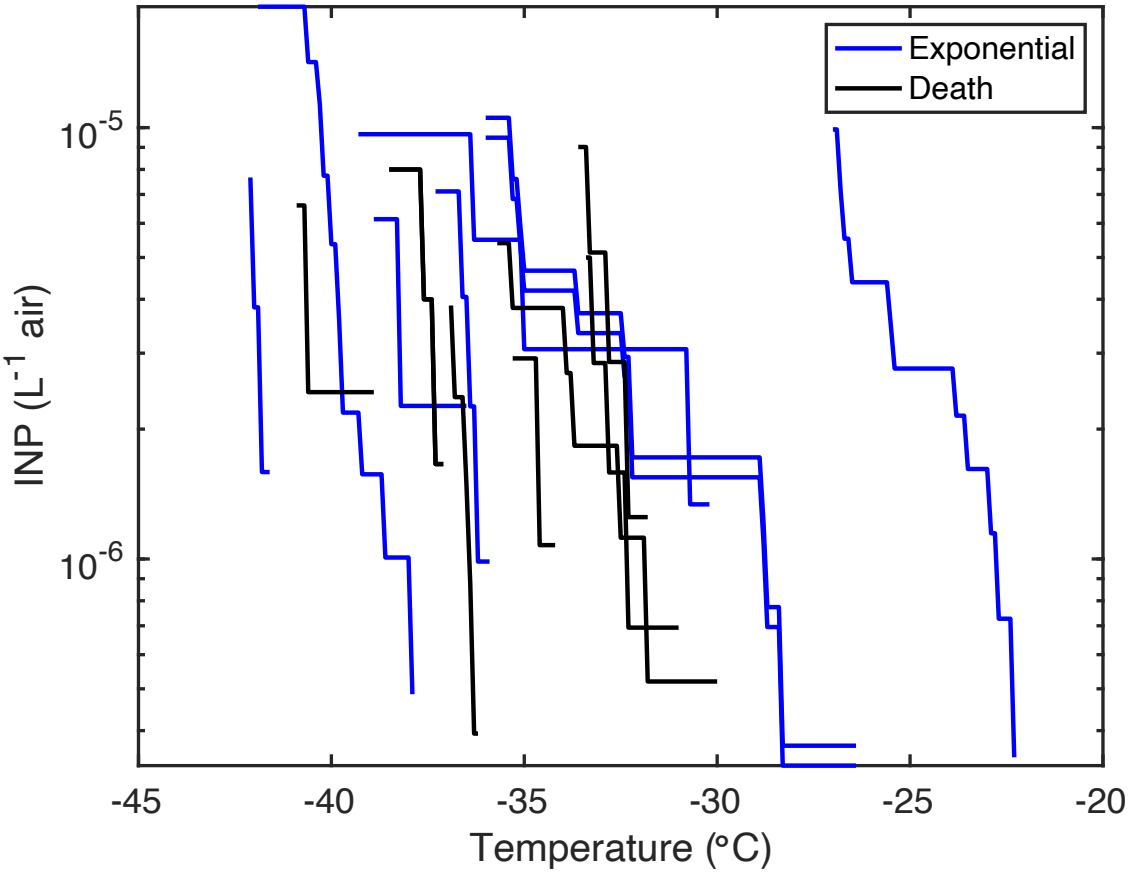

Figure 5.7: INP concentrations separated by growth phase (calculated from Equation 4 described in Section 2.6). Samples from exponential phase are plotted in blue and samples from death phase are plotted in black.

When comparing INP concentrations between growth phases, *Emiliania huxleyi* only produces INP active at -25 °C during exponential phase, but there are many samples from exponential phase that do not contain INP active at -25 °C or even -30 °C.

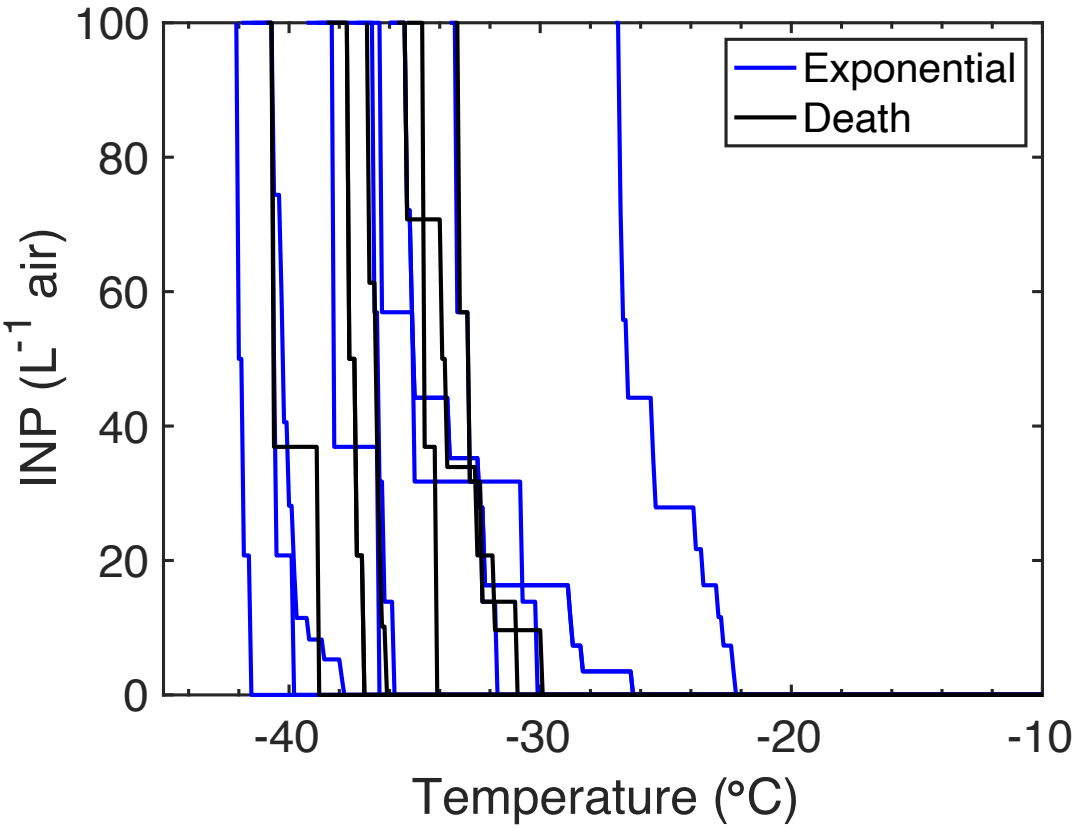

Figure 5.8: Percentage of INPs active at a range of temperatures. Fraction activated was calculated using equation 6 described in Section 2.6. Blue lines represent samples from exponential phase, while black lines represent samples from death phase.

The warmest-activating sample was collected during the exponential growth phase and first activated at -22.3 °C (with 3.5% of the INPs active at this temperature). The sample with the coldest activation temperature was also from the exponential phase, and did not have any INPs activate until -41.6 °C, below the temperature of homogeneous freezing.

5.4. Discussion

Unlike previous experiments the MART was inoculated with similar nutrient concentrations but much lower initial cell concentrations. This led to a much more pronounced lag phase that can be seen most easily in cell counts. The culture had an abundance of nutrients to begin with, leading to a positive growth rate as soon as the culture was added. Unlike previous experiments where the photosynthetic yield was high on Day 1, the yield was low on Day 1 and increased over the course of the lag phase for the first five days as the culture grew and entered exponential phase. The chlorophyll *a* concentration peaked on Day 7, well after the only day of high ice nucleation activity, and as with the *Thalassiosira weissflogii* and *Synechococcu elongatuss* cultures, there was no increase in INP activity as the chlorophyll concentration declined.

The production of caspase-like enzymes during the growth of *Emiliania. huxleyi* is well-known (Bidle, Haramaty, Barcelos, & Falkowski, 2007; Franklin et al., 2012), although different strains may produce different amounts under the same conditions (Kegel, John, Valentin, & Frickenhaus, 2013). Like other marine phytoplankton, *E. huxleyi* produces caspase as part of the process signaling the beginning of programmed cell death (PCD) when the cell declines in health. Therefore, a higher rate of caspase production indicates a higher rate of PCD. Caspase production is also strongly associated with viral infection in *E. huxleyi* and other phytoplankton (Berman-Frank, Bidle, Haramaty, & Falkowski, 2004; Bidle et al., 2007), but there were no viruses in the MART. In this MART experiment, nutrients were only added at the beginning and the culture declined in health due to nutrient limitation (rather than a decline due to viral

infection or predation). Franklin et al. (2012) showed that *E. huxleyi* has much higher rates of caspase-like enzyme production than a diatom culture (*Thalassiosira pseudonana*) grown under identical conditions. This high rate of caspase production by *Emiliania huxleyi* and *Thalassiosira weissflogii*. An increase in PCD (represented by an increase in the rate of capsase-like enzymes) could be one of the mechanisms leading to the hypothesized increase in INP during times of bloom decline due to an increase in DOM. However, caspase-like enzymes were not being produced at a measurable rate on Days 2 and 3, nor is there any correlation between INP activity and overall rate of caspase-like enzyme production.

Even though the cell concentration was much lower than previous experiments on Day 2 when the freezing temperature and INP concentration were the highest, the growth rate was positive, and the cells were dividing rapidly. However, the cell counts continued to increase and the growth rate remained positive but the average freezing temperature decreased by 15 °C between Days 2 and 3. The freezing temperature on Day 3 was below the temperature of homogeneous nucleation (-36 °C) and below the measured freezing temperature of aerosols generated in the MART from ASW with no nutrients or phytoplankton (-37.2 °C). It is known that salts in solution can greatly depress the freezing temperature even if droplets contain particles that would otherwise act as INP at atmospherically relevant temperatures (Whale et al., 2018) (see section 7.3.4 for more details on freezing of solutions containing both INP and salts). It is possible that the proportion of aerosolized material shifted between Days 2 and 3 towards a greater amount of aerosolized salts. However, the aerosols were resuspended

in 2 μL of UHP water, and even if every single aerosol particle generated was 100% salt, this would lead to a salinity of approximately 0.5 ppt, which would not lower the freezing temperature by 15 °C. It is also possible that the thermocouple within the freezing stage of the ice microscope registered a lower-than-accurate temperature, but freezing temperatures can still be compared to the freezing of ASW without any coccolithophores at -35.0 ± 1.0 °C. It is likely that the freezing temperatures of samples after Day 1 are low simply because there are not any INP present.

5.5. Conclusions

The pattern of production of INPs observed during the growth of *Thalassiosira* and *Synechococcus* was also seen in *Emiliania huxleyi*. A high INP freezing temperature of -24.6 ± 1.9 °C was measured on Day 2 of culture growth. However, unlike *Thalassiosira* and *Synechococcus* the freezing temperature on Day 3 had already dropped to a much lower average freezing temperature. the overall average freezing temperatures of samples generated from *Emiliania huxleyi* were also much lower than those measured during any previous or subsequent experiment, possibly due to high salt concentrations or instrumental error. There were no biological parameters measured that were highest on Day 1 when the highest INP activity and concentrations were measured.

6. MARINE PHYTOPLANKTON VIRUSES AS ICE NUCLEATING PARTICLES

6.1. Introduction

Viruses are abundant in seawater, with concentrations ranging from 10^7 to 10^8 mL^{-1} (Alonso, Jimenez-Gomez, Rodriguez, & Borrego, 2001; Bergh, Borsheim, Bratbak, & Heldal, 1989; Gunnar Bratbak, Heldal, Norland, & Thingstad, 1990; Hara, Terauchi, & Koike, 1991; Jiang & Paul, 1994). Virus particles can be an order of magnitude more abundant than bacteria (which have an average concentration of 10^6 cells mL^{-1} (Bezdek & Carlucci, 1972; Noble & Fuhrman, 1998)) and two to three orders of magnitude more abundant than phytoplankton (Bergh et al., 1989), but most are much smaller than even the smallest bacterium or phytoplankter, with diameters as small as 30 nm (Bergh et al., 1989). There are also much larger viruses that can range from 120 to 400 nm in diameter, with some having tails that are up to 2 μm long (Castberg et al., 2002; Gowing, 1993; Schroeder et al., 2002a).

Marine viruses can cause the collapse of phytoplankton blooms, therefore playing a direct role in the release of organic matter into surface waters. Virus infection pathways can be classified as lytic or lysogenic (Payet & Suttle, 2013; Wilcox & Fuhrman, 1994; Wilson & Mann, 1997). The infection pathway is classified as lytic if the viral particles begin to reproduce within the infected cell and cause cell lysis within a short time period (hours to days) following infection (Suttle, 2007). In contrast, during lysogenic pathways the viral genetic material is incorporated into the host genetic material, allowing the virus to exist undetected within the cell for much longer periods of

time (days to weeks or longer) (Suttle, 2007). After some time the lysogenic pathway converts to lytic and the virus begins to reproduce, followed by cell lysis and viral release (Hogg, 2005). It is not known exactly why the infection shifts between lysogenic and lytic, but possible explanations include reaction to environmental factors or stress (Payet & Suttle, 2013). Erez et al. (2017) found that lysis was induced in infected *Bacillus* cultures after the buildup of a communication peptide that was produced by cells. Production of this communication peptide was induced by genes encoded by the infecting phages during the earlier lysogenic cycle, suggesting a type of communication is possible between earlier and later generations of infecting phages.

The material released following viral lysis becomes part of the dissolved organic matter (DOM) pool that is aerosolized via wave action. This material may interact with water vapor in the atmosphere to form warm clouds (Andreae & Crutzen, 1997; Frossard et al., 2014; Huang et al., 2018; O'Dowd & de Leeuw, 2007). It has therefore been proposed that viral infection might contribute a significant portion of the organic aerosols produced over collapsing phytoplankton blooms (O'Dowd et al., 2015). Viruses themselves are also aerosolized, but the amount of viral particles aerosolized from the total population in the seawater is dependent on the type of virus. Aerosol virus particles per liter of air are also an order of magnitude fewer than the concentration per L of underlying seawater (Michaud et al., 2018).

One of the best-studied groups of large phytoplankton viruses are the coccolithoviruses (EhV) that infect *Emiliania huxleyi*. These double-stranded DNA virus are in the class *Phycodnaviridae* and have a diameter of approximately 160-180 nm

(Schroeder, Oke, Malin, & Wilson, 2002b). These viruses are known to increase the particulate organic matter within the water column (Nissimov et al., 2018), which may increase INP activity if the organics are then aerosolized and contain efficient INP. However, the effect of the presence of viruses in seawater as it relates to INP concentrations is not known.

The first step in determining whether or not viruses influence the INP activity of aerosols is to determine if the viruses themselves act as INP. This study tested the ability of three strains of viruses, including one coccolithovirus that infects *Emiliania huxleyi* (EhV 207) and two smaller viruses that infect *Chaetoceros tenuissimus* (CtenRNAV01 and CtenDNAV), to catalyze immersion mode freezing in samples containing viruses at two different concentrations. One concentration was chosen to represent the concentration of viruses in seawater, while the other is the approximate concentration of viruses in the atmosphere after seawater containing viruses is aerosolized.

6.2. Methods

Virus samples for this study were provided by Kay Bidle at Rutgers University. Viruses of known strains were first grown in artificial seawater (Hahn & Blobel, 1968; Harrison et al., 1980) along with phytoplankton cells from the species they infect. The first strain was EhV207, a *E. huxleyi* virus first described in Schroeder et al. (2002). The two *Chaetoceros tenuissimus* viruses included one with single-stranded DNA (CtenDNAV) (Tomaru, Shirai, Toyoda, & Nagasaki, 2011) and one with single-stranded RNA (CtenRNAV01) (Shirai et al., 2008). Viruses were grown and isolated by Kay Bidle's group at Rutgers University. Samples were filtered to remove all whole cells and

particles. Flow cytometry was used to concentrate the viruses to final concentrations that are shown in table 6.1. The viruses were then removed from the seawater based on their mass bands via density adjustment with CsCl, as described in Schroeder et al. (2002a). The density of the samples was first adjusted with CsCl. The samples then underwent ultracentrifugation to isolate mass bands, with a single band containing a single virus type. Bands were removed with a syringe. The seawater used to grow the viruses had a salt concentration of 35 ppt, high enough to depress the ice nucleation activity of the viruses. Since CsCl was added to adjust the density and salts were present in the growth medium, salt was removed from the samples by dialysis, with a final salt concentration of less than 1 ppt. Virus samples were then shipped to Texas A&M University at concentrations listed in Table 6.1. Samples were stored at 4 °C in the dark for no more than three months until their ice nucleation activity was tested. The sample of CtenRNAV01 had two mass bands, which were tested individually for ice nucleation ability. It was assumed that both mass bands were viruses, but it is not known if they were identical strains of the same virus. It is possible that they were two fragments of the same virus or two different viruses, but these viruses are all icosahedral and untailed, so it is difficult to determine what exactly composed the mass bands. Samples were stored at 4 °C until tested for ice nucleation.

Table 6.1: Viruses tested for ice nucleation ability and approximate starting concentration of viruses (measured via flow cytometry).

Virus	Virus type	Diameter	Infected organism	Sample Concentration (VLP mL^{-1} water)
CtenDNAV	ssDNA	31 nm	*C. tennuisimus*	1×10^{12}
CtenRNAV01	ssRNA	31 nm	*C. tennuisimus*	1×10^{12}
CtenRNAV01	ssRNA	37 nm	*C. tennuisimus*	1×10^{12}
EhV207	dsDNA	160-180 nm	*E. huxleyi*	3×10^{8}

Samples were diluted with UHP water to two concentrations just prior to testing the ice nucleation ability. These concentrations are referred to as seawater concentration (1×10^{8} VLP mL^{-1} water) and aerosol concentration (1×10^{5} VLP mL^{-1} water). The seawater concentration was chosen to approximate the real-world concentration of viruses in seawater (Alonso et al., 2001; Bergh et al., 1989; Gunnar Bratbak et al., 1990; Hara et al., 1991; Jiang & Paul, 1994). Although the measured concentration of viruses in seawater can be as low as 10^{3} VLP mL (Sharoni et al., 2015), the concentration of viruses in a phytoplankton bloom in the open ocean is generally closer to 10^{7}-10^{8} VLP mL^{-1} (Bratbak, Heldal, Thingstad, & Tuomi, 1996; Suttle, 2005).

The aerosol concentration was chosen to approximate the concentration of viruses in an aerosolized droplet acting as an INP through immersion freezing. This concentration was calculated assuming that all droplets containing INP are first diluted via activation as a CCN, followed by freezing. The samples were diluted from their initial concentrations (shown in Table 6.1) to the seawater and aerosol concentrations, but unlike the dilutions done in Chapter 7, there was no dilution of salt. The initial samples sent from Rutgers contained less than 1 ppt salt (it was removed through

dialysis). After dilution to either the seawater or aerosol concentration, this salt concentration can be assumed to be near 0 ppt. Each sample was gently shaken following dilution prior to a 2 µL droplet being placed on a silanized slide and tested using the same ice microscope setup and methods described in chapter 2.

6.3. Results

All of the samples tested contained moderately effective INP at atmospherically relevant temperatures. The warmest freezing point was the coccolithovirus at seawater concentrations with a freezing temperature of -20.8 ± 1.6 °C (Table 6.2). However, there was little difference between the freezing point of samples tested at different concentrations, although the seawater VLP concentrations were three orders of magnitude higher than the aerosol concentrations (10^5 vs 10^8 VLP mL^{-1} water). Only the coccolithoviruses froze at significantly different temperatures after the sample was diluted from seawater to aerosol concentrations, with the aerosol concentration sample freezing at -20.8 ± 1.6 and the seawater concentration sample freezing at -24.5 ± 0.9 °C.

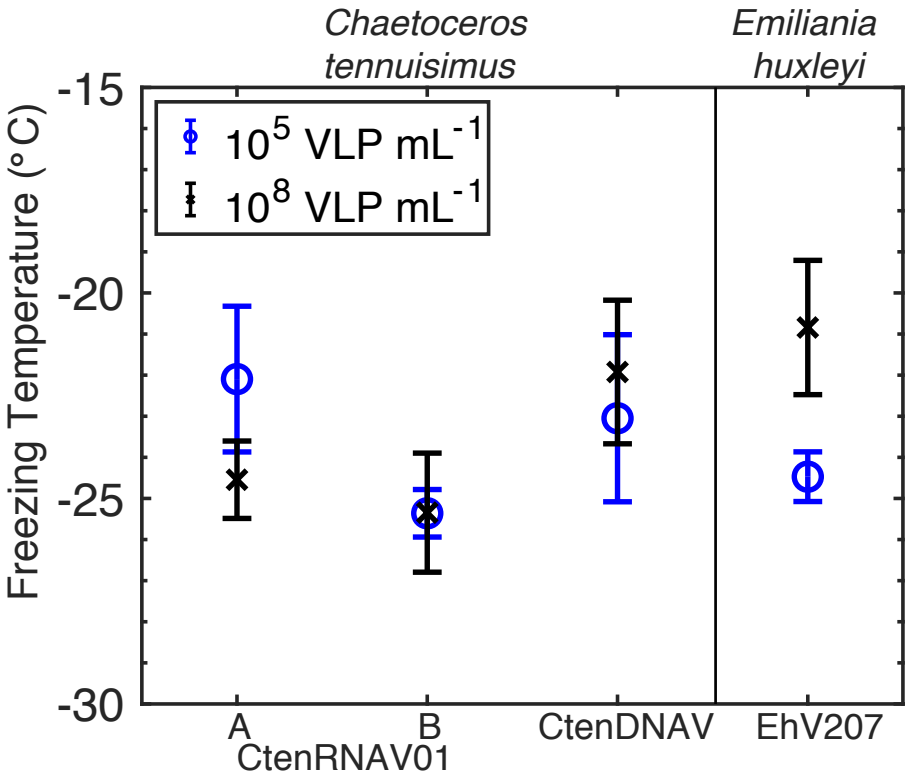

Figure 6.1: Average freezing temperature of viruses in desalinated water with salt concentrations of less than 1 ppt. Aerosol concentration (10^5 VLP mL^{-1} water) is shown with blue dots and seawater concentration (10^8 VLP mL^{-1} water) is plotted with black 'x's. The organisms infected with the viruses are indicated above the plot. All data points show mean ± a single standard deviation, n ≥ 3 .

All samples froze at temperatures warmer than homogeneous freezing (36 °C), but there was no statistically significant difference in freezing temperatures between samples even though the particle size was very different (One-Way ANOVA, $p < 0.01$, $n > 21$).

Table 6.2: Average freezing temperature reported as average freezing temperature ± standard deviation, n > 20) and INP concentration at -25 °C (N_{inp}, L^{-1} water) of droplets containing marine phytoplankton viruses. The two C. tennuisimus ssRNA differ in molar mass but it cannot be determined if they are the same virus or virus fragments.

Virus (*Organism Infected)*	**Virus concentration** (VLP mL^{-1})	**Freezing temperature** (°C)	**Number of freezing points**	**N_{inp}** (L^{-1} water, -25 °C)
CtenRNAV01-A(*C. tennuisimus*)	1 x 10^5	-21.9 ± 2.0	21	4.23 x 10^2
CtenRNAV01-B (*C. tennuisimus*)	1 x 10^5	-25.4 ± 0.6	25	7.71 x 10^1
CtenDNAV (*C. tennuisimus*)	1 x 10^5	-23.0 ± 2.0	27	1.22 x 10^3
EhV207 (*E. huxleyi*)	1 x 10^5	-24.5 ± 0.6	27	1.37x 10^3
CtenRNAV01-A(*C. tennuisimus*)	1 x 10^8	-24.5 ± 0.9	28	1.15 x 10^3
CtenRNAV01-B (*C. tennuisimus*)	1 x 10^8	-25.3 ± 1.4	21	1.37 x 10^2
CtenDNAV (*C. tennuisimus*)	1 x 10^8	-21.9 ± 1.7	23	7.52 x 10^2
EhV207 (*E. huxleyi*)	1 x 10^8	-20.8 ± 1.6	31	1.30 x 10^3

It is known that an increase in particle concentration generally leads to an increase in INP activity through an increase in surface area (Fletcher, 1969; Hoose & Mohler, 2012), so two virus concentrations were tested to see if this is the case for viral particles. However, the higher freezing temperatures did not correlate with increased VLP concentration in most samples (Pearson correlation, $n>21$, $p<0.05$), or the two concentrations were not statistically different. The higher concentration of *E. huxleyi* viruses led to significantly higher freezing temperature when all of the freezing data from a single virus type and concentration was pooled (One-Way ANOVA, $p <0.01$, $n >21$). The higher concentration of the first mass band of the CtenRNAV01 virus also led to a significantly higher freezing temperature than the lower concentration.

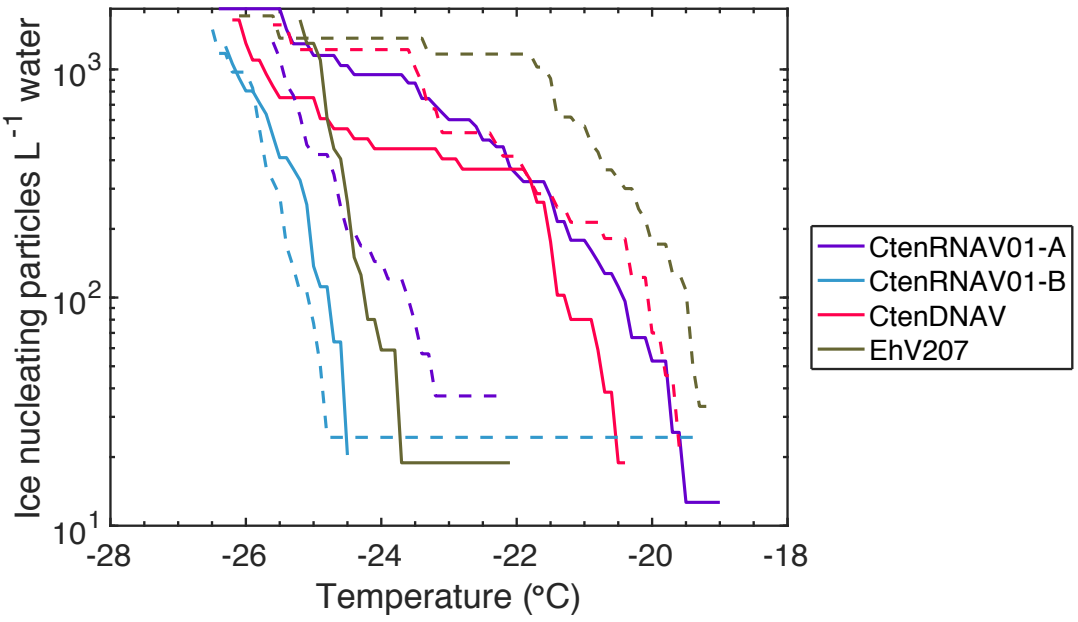

Figure 6.2: Number of ice nucleating particles per L of water, calculated based off equation 2 from DeMott et al., 2016. Seawater virus concentrations (10^8 VLP mL^{-1} water) are plotted with dashed lines, while aerosol virus concentrations (10^5 VLP mL^{-1} water) are plotted with solid lines. See section 2.6.3 for further detail on INP concentration calculations.

The highest concentration of INPs at -20.0 °C was in the EhV 207 samples (dsDNA virus) at seawater virus concentration (10^8 VLP mL^{-1}), with 1.7 x 10^2 INP L^{-1} water. INP per liter of air cannot be calculated since the samples were not aerosolized and no total aerosol counts are available. The INP concentration measured at -25 °C varied by up to two orders of magnitude, with the largest INP concentrations seen with the large coccolithovirus (dsDNA, EhV 207) with 1.3 x 10^3 INP L^{-1} water. The lowest INP concentration at -25 °C is in the second CtenRNAV01 (B) sample.

6.4. Discussion

It is well-known that viruses can be aerosolized both on land (Courault et al., 2017; Verreault, Moineau, & Duchaine, 2008) and from sea spray (Baylor, Baylor, Blanchard, Syzdek, & Appel, 1977; Blanchard, 1978; Sharoni et al., 2015). However, the only other study measuring the INP activity of viruses (Junge & Swanson, 2007) concluded that marine viruses are ineffective INP that are unlikely to have any impact on ice cloud formation in clean marine conditions. The results presented in this chapter instead suggest that although all the tested viruses froze at lower freezing temperatures than the best-known biological INP, all of the virus samples contained moderately effective INP.

The viruses tested in this study are moderate INP, with freezing temperatures ranging from -20.8 ± 1.6 °C to -25.4 ± 0.6 °C. The viruses tested froze at temperatures comparable to the measured range of freezing temperature of marine aerosols containing a mix of phytoplankton, bacteria, and viruses (DeMott et al., 2016; Irish et al., 2017; McCluskey et al., 2016; McCluskey, Hill, et al., 2018; McCluskey, Ovadnevaite, et al., 2018; Wilson et al., 2015). DeMott et al. (2016) reported freezing temperatures between -5 and -28 °C, while Irish, Hanna, Xi, et al. (2019) reported freezing temperatures between -10 and -36 °C and McCluskey et al. (2018) reported freezing between -12 and -30 °C. It is important to note that although each type of virus was also only tested for ice nucleation activity once at each concentration, each average freezing temperature was calculated from at least 21 individual freezing data points.

It is difficult to determine why there is only a concentration effect for two of the virus samples, as they were all isolated with the same methods and the samples should only contain whole virus particles at the time they were collected. However, it is possible that although they were stored at 4 °C in the dark there was some decomposition of virus particles that released organic material into the solution (Dell'Anno, Corinaldesi, & Danovaro, 2015). It is possible that the organic material released by the viruses that did not show a concentration effect was a more effective INP at lower concentrations while the material released by the EhV and one of the ssRNA *Chaetoceros* viruses was less effective and required a higher concentration to increase the probability of nucleation. It is more difficult to explain why only one mass band of the ssRNA *Chaetoceros* virus showed a concentration effect. It is possible that there was a difference in the material contained in each sample, but it is also possible that this difference would not be present if the freezing temperature was measured more times. When considering the average freezing temperature and INP concentration, the samples that freeze at the highest temperatures do not necessarily contain the highest concentration of INP at -25 °C. Although at aerosol concentrations the larger dsDNA *E. huxleyi* virus has the warmest average freezing temperature and highest INP concentrations at -25 °C, this may be due to its larger size. We can compare the fraction of INPs activated at a temperature to determine what range of temperatures the INPs in each sample were active at.

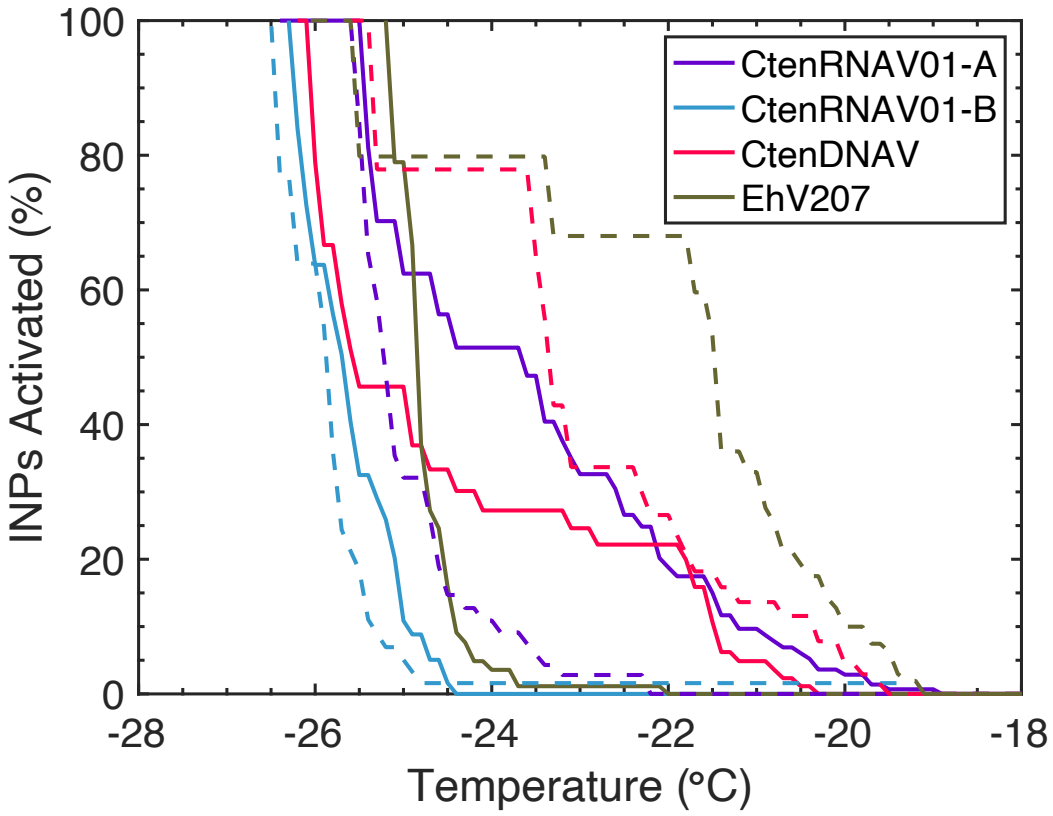

Figure 6.3: Fraction of ice nucleating particles that have activated at a given temperature (°C), calculated with Equation 6 from Chapter 2.6. Solid lines represent samples with 10^5 VLP mL^{-1}, while dashed lines represent samples with 10^8 VLP mL^{-1}.

The sample containing EhV207 at seawater concentrations of 10^8 VLP mL^{-1} showed the warmest initial activation temperature of -19.1 °C along with having the warmest average freezing temperature. At -19.1 °C, 1.9% of the INP present in the sample were active, and all of the INPs had activated by -26.2 °C. However, the next sample to activate was sample B containing CtenRNAV01 at seawater concentrations, which had 1.6% of the INP activated at -19.3 °C, even though this sample had one of the coldest

average freezing temperatures. In all of the samples all of the INPs were fully activated by -26.6 °C, with samples containing viruses at aerosol concentrations fully activated at -26.3 °C.

Junge and Swanson (2007) concluded that marine viruses were poor INP, with a measured freezing temperature at -41.9 °C (with 10^9 VLP mL^{-1} in phage lysis buffer). This was less than a degree warmer than the freezing temperatures they measured for phage lysis buffer with no VLP (-42.5 °C). This buffer contains several salts, included NaCl (0.5 M), $MgSO_4$ (8 mM), and $CaCl_2$ (2 mM), which is approximately 6 ppt salts. Based on results from section 7.3.4, this is enough salt to slightly depress the freezing temperature of the tested samples, but not enough to explain the nearly 20 °C difference between the freezing temperatures reported in section 6.2 and the freezing temperatures measured by Junge and Swanson (2007). However, there are several major differences between the *Chaetoceros* and *Emiliania huxleyi* viruses tested in this chapter and the *Colwellia* virus tested by Junge and Swanson (2007). The first difference is in the morphology of the viruses. All three *Chaetoceros* viruses tested are icosahedral, non-tailed viruses that range from 30-40 nm diameter (Shirai et al., 2008; Tomaru et al., 2011). The *Colwellia* virus tested was larger even than the 160-180 nm *Emiliania huxleyi* virus (Schroeder et al., 2002a), with head diameter of 90 nm and a 200 nm, non-contractile tail (Wells & Deming, 2006). All of the *Chaetoceros* viruses tested for INP activity contain single-stranded genetic material while the *Colwellia* virus contains double-stranded DNA, although the similarity between the freezing temperatures between the *Chaetoceros* and *Emiliania* viruses suggest that single-stranded and double-

stranded viruses of different sizes freeze at similar temperatures. The major difference of importance between the virus tested by Junge and Swanson (2007) and those tested here is the morphology, so common marine viruses of different morphologies should be compared further.

A rough calculation can be made to estimate the production of INP by *Emiliania huxleyi* blooms. Since we do not have measured aerosol concentrations of viruses, we can first consider how many of the viruses present in the seawater are acting as INP by comparing the calculated EhV207 virus INP concentration in water (plotted in Figure 6.2) to the total number of viruses per volume of water. If the seawater concentration of the viruses is 10^{11} VLP L^{-1} water, and there are only 1.7 x 10^{2} INP L^{-1} of water that catalyze freezing at -20 °C (using the INP concentrations calculated for EhV207), this suggests that only 1 virus in 10^{9} will act as an INP at -20 °C. However, the large extent of *Emiliania huxleyi* blooms could lead to a large number of potential INP in the seawater. *E. huxleyi* blooms can be hundreds of square kilometers (Brown & Yoder, 1994; P. Holligan et al., 1983; P. M. Holligan et al., 1993) and these blooms can collapse due to viral infection (Schroeder et al., 2002a; Suttle, 2007). If we consider a 1 km^2 portion of this bloom and assume that the upper 40 m of water contain EhV particles (as was seen in Sharoni et al. [2015]) at a concentration of 10^{11} VLP L^{-1}, this water parcel contains 4 x 10^{21} VLP. Although only 1 in 10^{9} VLP act as INP at -20 °C, this gives 10^{12} INP-active VLP at -20 °C within the water.

To calculate how many of the INP that are within the water parcel reach the atmosphere, we have to then consider how many of the virus particles are aerosolized

and then how many of those aerosolized particles contain INP active at -20 °C. Estimates of EhV aerosolization rates over a bloom suggest that seawater concentrations (10^{11} VLP L^{-1}) are approximately 10^6 VLP higher than the aerosol EhV concentration (10^5 VLP L^{-1}) (Sharoni et al., 2015), and if the INP are EhV we expect the same rate of aerosolization. If there are 10^{11} INP produced in the seawater parcel, this gives a total of 10^6 INP produced over a 1 km^2 area of an infected *E. huxleyi* bloom mixed to a depth of 40 m. While marine viruses are unlikely to drive ice cloud formation in areas with high concentrations of mineral dust or other, warmer-freezing INP, they are likely part of the INP population of importance in clean marine areas that freeze around -25 °C, as identified by Burrows et al. (2013).

6.5. Conclusions

Although viruses were first discovered in seawater decades ago and studies have shown that aerosolization of marine viruses can spread the viral infection across populations of phytoplankton kilometers apart (Sharoni et al., 2015), few studies have attempted to determine viral concentration in marine aerosols (Junge & Swanson, 2007; Michaud et al., 2018). This work shows that a range of icosahedral virus types and sizes are capable of acting as moderate effective INP. The results also show that in most cases the average freezing temperature and the INP concentration per liter of water are not dependent on the concentration of viruses in the sample. There is a possible enhancement of INP production over infected *Emiliania huxleyi* blooms, with 10^6 INP active at -20 °C produced per km^2. These results suggest that marine viruses, especially icosahedral viruses, may be capable of driving ice nucleation processes at temperatures

warmer than -25 °C, but only in clean marine areas, and that further study of viruses as INPs is warranted.

7. ICE NUCLEATION BY MARINE AEROSOLS OVER THE NORTH ATLANTIC OCEAN IN LATE SPRING

7.1. Introduction

Pure cloud water droplets form ice crystals homogeneously at temperatures below -36 °C (Hoose & Möhler, 2012; Kanji et al., 2017; Vali, DeMott, et al., 2015). Certain types of aerosol particles, referred to as ice nucleating particles (INPs), can catalyze ice nucleation at lower supersaturations and warmer temperatures. The four mechanisms of heterogeneous ice nucleation are deposition freezing, immersion freezing, condensation freezing, and contact freezing (Hoose & Möhler, 2012; Kanji et al., 2017; Murray, et al., 2012; Vali et al., 2015). Contact nucleation occurs when a particle is in contact with the surface of the droplet and induces freezing (Brooks, et al., 2014). Immersion freezing occurs when an INP becomes immersed in a droplet and subsequently freezes. Similarly, condensation freezing occurs when an INP becomes immersed in a supercooled droplet and freezing occurs concurrently with droplet formation (Kanji et al., 2017). In contrast, deposition freezing occurs when ice grows directly on the INP from the vapor phase.

Over the North Atlantic Ocean, ice is present in both mixed phase and cirrus clouds (Mace, 2010). Agreement between modeled immersion nucleation and satellite observations of ice water path are better when primary marine aerosol are included as sources of INPs at mixed phase clouds temperatures (Yun and Penner, 2013). Globally, a better understanding of cloud water phase is needed, particularly for mixed phase clouds

which form between -15 and -30 °C. For example, when the phase partitioning of cloud water determined by 6 global climate models and satellite retrievals were compared, the distribution of cloud phase according to temperature varied greatly (Komurco et al., 2014). In the mixed phase cloud regime where phase is highly sensitive to the choice of ice nucleation scheme, none of the models predicted realistic cloud phases.

Of the many studies of immersion mode nucleation, a wide variety of aerosol may be described as moderately effective INPs, facilitating freezing between 5 and 15 °C warmer than the homogenous threshold temperature (-36 °C) (Kanji et al., 2017; Hoose & Möhler, 2012; Murray et al., 2012). Relatively few compositions have been characterized as highly effective INP, catalyzing nucleation at temperatures at -5 °C and warmer (Creamean et al, 2019; Failor et al., 2017; Kim et al., 1987). Anthropogenic sources of INPs include soot particles and other industrial pollutants (Brooks et al., 2014; Collier & Brooks, 2016; DeMott, 1990), while natural INPs can come from a wider range of biological and abiotic sources (Kanji et al., 2017; Schnell and Vali, 1975, 1976) including maritime air masses (Rosinski, et al., 1986, 1987). Mineral dusts, especially K-feldspar, are very effective INPs with freezing temperatures as warm as -15 °C (Atkinson et al., 2013). Biological aerosols with ice nucleation potential include pollen (Hader, et al., 2014; Pummer, et al., 2012), diatoms (Alpert, et al., 2011a; Wilson et al., 2015) and bacteria (Failor, et al., 2017; Kim et al., 1987; Lindow, et al., 1978; Maki, et al., 1974). The bacteria *Pseudomonas syringae* is one of the most effective known biological INPs, with nucleation observed at temperatures as warm as -1.8 °C (Maki et al., 1974; Wex et al., 2015). Bacteria from several other taxa, including

Lysinibacillus, Xanthomonadaceae, Enterobacteriaceae, and additional members of *Pseudomonadaceae,* are also capable of acting as biological INPs at temperatures between -2 °C and -8 °C (Failor et al., 2017; Kim et al., 1987; Lindow et al., 1978). Growing interest in this topic has led to a number of observations on the ice nucleating behavior of marine aerosols (Brooks & Thornton, 2018; DeMott et al., 2016; Huang et al., 2018; Irish et al, 2017 & 2019; Ladino et al., 2016; McCluskey et al., 2016; McCluskey et al., 2018; Wilson et al., 2015; Creamean et al, 2019).

Studies of phytoplankton as a source of primary marine aerosols indicate that many phytoplankton and associated organic matter are sources of INPs in immersion and deposition mode (DeMott et al., 2016; Knopf, et al., 2011a; Ladino et al., 2016; Wilson et al., 2015, Wolf et al., 2019). For example, the diatom *Thalassiosira pseudonana* nucleated ice via immersion at temperatures of -23 °C and via deposition mode at colder temperatures in a laboratory study (Alpert et al., 2011a). In another study, a green alga (*Nannochloris atomus*) was observed to catalyze immersion ice nucleation at temperatures as high as -28 °C, whereas *Emiliania huxleyi* was a poor INP and did not catalyze immersion freezing. In contrast, in deposition mode experiments both were active catalysts. *Nannochloris atomus* activated freezing below -33 °C at ice saturation ratios as low as 1.21, and *Emiliania huxleyi* activated ice at ice saturation ratios as low as 1.19 at temperatures of -23 °C and below (Alpert et al, 2011b). Early work on the ice nucleating ability of phytoplankton-laden seawater was performed by Schnell and Vali (1976). In comparison, seawaters devoid of phytoplankton did not act as INP and facilitate freezing. In another study, Fall and Schnell (1985) surveyed 21 marine phytoplankton cultures and found that

one culture, *Heterocapsa niei* PY-5 facilitated freezing above -12 °C, whereas the rest of the cultures facilitated freezing between -19 to -21 °C. It should be noted that these freezing surveys were conducted in buffered media and the presence of salt in the droplets was not accounted for. Wolf et al. (2019) conducted a study on the deposition ice nucleation activity of *Prochlorococcus* and individual compounds selected to represent the organic contents of *Prochlorococcus*. The deposition nucleation efficiency of amylopectin, agarose, and aspartic acid were similar to aerosolized *Prochlorococcus* cultures, suggesting that these components may in part determine the ice nucleation activity of *Prochlorococcus* under cirrus cloud conditions.

In the natural environment, organic matter originating from phytoplankton reaches the atmosphere as a part of sea spray aerosols that are produced by bubble bursting and wave action (Russell, et al., 2010; Wilson et al., 2015). The sea surface microlayer (SML) is the thin layer of ocean at the air-sea interface, which is operationally defined as 1 to 1000 μm thick (Engel et al., 2017; Liss & Duce, 2005). Since the SML is selectively enriched in some classes of organic matter relative to the underlying water, it plays an important role in the introduction of INPs into the atmosphere (Aller et al. 2005 & 2017; Chance et al. 2018; Cunliffe et al. 2013; Hunter 1997; Irish et al., 2017 & 2019, Thornton, et al., 2016, Zeppenfeld et al., 2019). Enhancement in the concentrations of INPs active between -14 and -27 °C in the SML relative to bulk seawater have been observed in some cases, including Arctic melt ponds and marginal ice zones, (Zeppenfeld et al, 2019; Irish et al, 2019). However, enhancements in SML activity have not been observed in all sampling periods (Irish et al, 2017).

As a phytoplankton bloom progresses, senescence may result in an accumulation of leaky cells, dead cells, and fragments in the SML (Engel et al., 2017; Rahlff, 2019). Cell lysis can also result in a significant release of dissolved organic matter (DOM) into the water (O'Dowd et al., 2015; Thornton, 2014; Lenes et al, 2013). DOM is operationally defined as all organic materials which pass through a GF/F glass fiber filter, which have an average pore size of 0.7 μm, and thus DOM includes small particulates. Heterotrophic Bacteria and Archaea, while not a source of primary production, play an important role in the consumption and transformation of organic matter fixed by phytoplankton and released into the water (Jiao et al. 2010; Kujawinski, 2011). In addition, processes such as sloppy feeding by grazers (Møller, 2007; Møller, et al., 2003) and lytic viral infections (Bettarel et al., 2005; Bratbak, et al., 1993; Gobler, et al., 1997) contribute significant DOM and particulate organic matter (POM) to the water column. It follows that phytoplankton blooms may emit greater quantities of INPs during periods of bloom decline and collapse.

Measurements of INPs that isolate primary marine aerosols from the total aerosol population are uncommon (Ladino et al, 2016). Marine INP measurements that consider changes in plankton at different locations are also rare (Brooks & Thornton, 2018). Hence the measurements presented in this study on primary aerosols artificially generated from pristine waters of the North Atlantic Ocean far removed from coastal influences help to fill the gap in ice nucleation measurements. Further, an examination of ice nucleation from isolated phytoplankton components of seawater was also performed to compare the ice nucleating ability of aerosols to that of organisms in the ocean's

surface waters. The central hypothesis of this study is that phytoplankton, or organic matter aerosol derived from these organisms, represent a population of particles which catalyze atmospheric ice nucleation. Secondly, the nucleating temperatures and freezing efficiencies of marine INPs may vary depending on the organisms involved. Notably, *Synechococcus* is one of the most abundant and ubiquitous phytoplankton groups, with a global distribution, except in the polar oceans (Partensky, et al., 1999; Flombaum et al. 2013), but its potential to facilitate ice nucleation is unknown. The methods employed here enabled different phytoplankton groups, including *Synechococcus*, to be isolated from the environment and their propensities to contribute to atmospheric ice nucleation processes by immersion freezing were determined. The sampled phytoplankton were representative of *in situ* conditions, both in terms of assemblage composition and physiological status.

7.2. Measurements

Atmospheric aerosol and seawater samples analyzed in this study were collected in May 2016 onboard the R/V *Atlantis* during the second NASA North Atlantic Aerosols and Marine Ecosystems Study (NAAMES 2) research cruise. The overarching goal of the series of four NAAMES cruises was to determine links between the seasonal changes in phytoplankton populations and the production of marine aerosols (Behrenfeld et al., 2019). Within the NAAMES framework, the specific objective of this study was to characterize sources and atmospheric ice nucleating potential of marine aerosols.

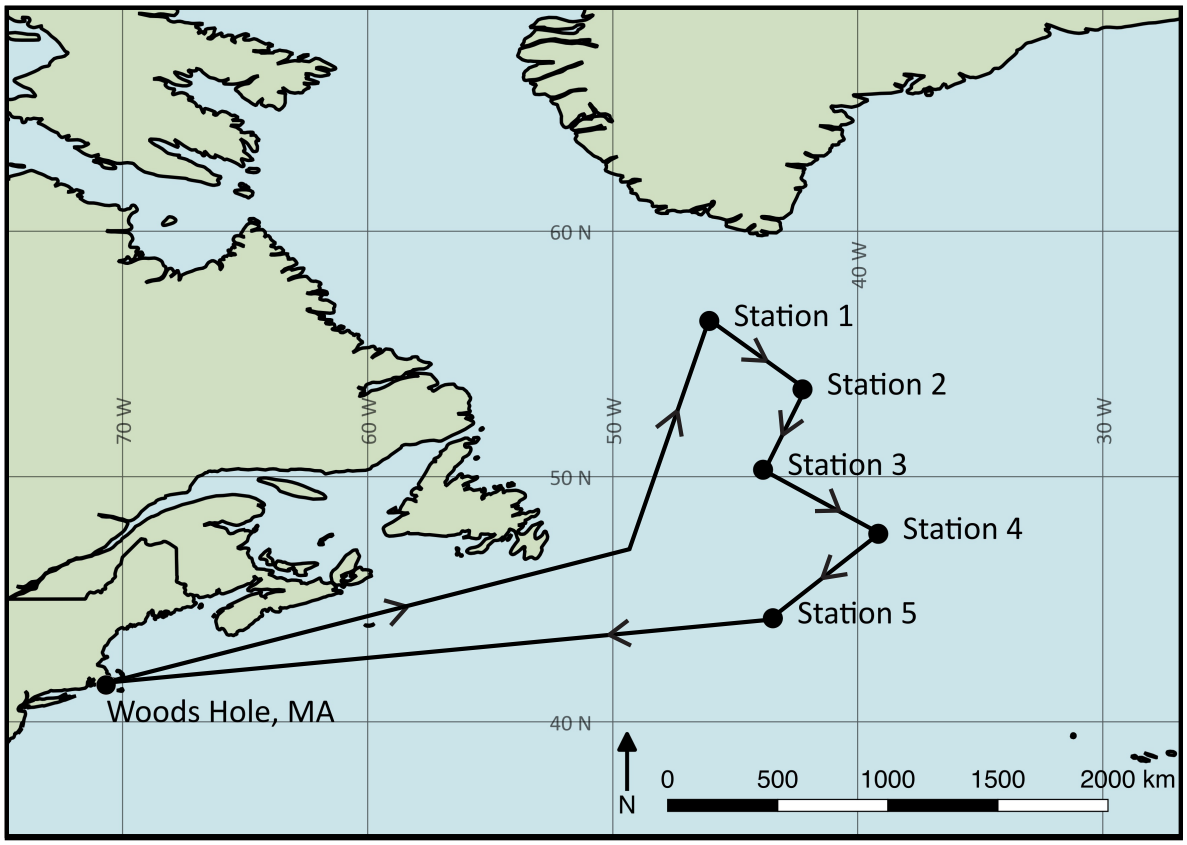

Figure 7.1: Ship track and sampling locations for the second leg of the North Atlantic Aerosol and Marine Ecosystem Study (NAAMES), which took place during May 2016. The ship stayed at each location for 24 hours with the exception of Station 4, where it stayed for approximately 96 hours.

NAAMES 2 consisted of five sampling stations (Figure 7.1). The R/V *Atlantis* remained at Stations 1, 2, 3, and 5 for approximately 24 hours and at Station 4 for approximately 96 hours. Multi-day sampling at Station 4 was conducted to investigate changes in atmospheric aerosols in the context of the ecosystem responding to a physical perturbation from a storm passing over the region (Graff & Behrenfeld, 2018). During May 22 to 24th, a low pressure storm system moved through the area causing ~9 m wave

heights and a deep water entrainment event (NOAA Ocean Prediction Center http:opc.ncep.noaa.gov/Atl_tab.shtml). The ship arrived on station on May 24th, immediately following the entrainment (Graff & Behrenfeld, 2018). Density, salinity, and temperature were used to estimate the surface mixing layer depth. As discussed in detail by Graff and Behrenfeld (2018), buoyancy frequency calculations and multiple mixed layer depth criteria indicated homogeneous physical properties to well below 200 m upon station occupation with rapid shoaling of the mixed layer to less than 25 m within 24-48 hours of arrival. A profiling Seabird Navis BGCi float and drifter operated by the University of California, Santa Barbara were deployed immediately prior to the first conductivity, temperature, and depth (CTD) cast and used to track the position of the water mass. Drifter reports (hourly) and float reports (every seven hours) were used to position the ship in the same water mass for the full 4 days.

This event changed the composition of surface waters available for aerosol production. When strong physical disturbances such as this occur in the ocean waters, phytoplankton communities can be abruptly vertically redistributed over depth. This results in an immediate change in the concentration and composition of the phytoplankton community of the surface layer. Secondly, the phytoplankton respond to their new environment by making rapid physiological adjustments. Specifically, changes in the availability of sunlight needed for photosynthesis cause phytoplankton to modify their photoacclimation state, resulting in observable changes in the chemical composition of the surface waters through changes in pigments and macromolecules. Graff and Behrenfeld (2018) observed significant increases in both phytoplankton

biomass and chlorophyll concentrations in the upper 25 m of seawater at Station 4 over a period of 4 days. These increases, however, did not occur at the same rate, indicating unbalanced growth of different cellular constituents (Shuter, 1979). It follows that changes in both the total biomass and the composition of marine aerosol ejected from these waters may occur as well, and that these changes may affect ice nucleation.

7.2.1. Primary Marine Aerosol Collection

Aerosol samples were collected with the Sea Sweep aerosol generator on every sampling day at each station. The Sea Sweep, built at NOAA's Pacific Marine Environmental Laboratory (PMEL), is an aerosol generator designed to replicate primary marine aerosol emissions by bubble bursting mechanisms (Bates et al., 2012). It cannot be said for certain whether the Sea Sweep aerosol generator which we use in this study generated jet drops or film drops. Compressed air was pumped through two coarse stainless steel frits 0.75 m below the ocean surface, causing bubbles to burst at the surface within the sealed hood of the Sea Sweep apparatus. Aerosol-laden flow leaving the Sea Sweep was transported at 1000 L min^{-1} via tubing (5.1 cm inner diameter) to a laboratory van on the 02 deck of the ship where the flow was distributed to a suite of instruments, including a PIXE impaction sampler used to collect samples for evaluation of the aerosols as INPs. The main sample line (16.7 VLPM) was directed to our instrumentation through a 1 ± 0.2 µm sharp-cut cyclone (SCC 2.229PM1, BGI Inc., Waltham, Massachusetts). An aliquot of flow, 1 VPLM, was drawn to the PIXE impaction sampler by a diaphragm pump downstream of the impactors. Size-sorted aerosol samples were collected on combusted aluminum foil discs (25 mm diameter)

inside PIXE sampler with the L1 and 3 stages installed to limit the size range to 0.06 μm to 1 μm diameter, representative of submicron aerosols with the potential to reach the upper troposphere and nucleate ice.

Each sample was collected for approximately two hours and immediately frozen at -80 °C, shipped to Texas A&M University on dry ice, and again stored at -80 °C until ice nucleation analysis. All samples were analyzed within 12 months of collection. We note that the time from generation to impaction was less than 20 seconds, which was insufficient time for secondary aerosols to form. Hence, the Sea Sweep aerosol samples were considered primary marine aerosols (Bates et al, 2012). Primary marine emissions are known to have complex compositions, including contributions from both salt and organic compounds (Barbaro et al, 2019).

The total number of aerosol particles produced by the Sea Sweep was counted using a condensation particle counter (TSI, Inc. Model 3010). Number size distributions were obtained by combining mobility distributions measurements from two Differential Mobility Particle Sizers (DMPS) and applying a data inversion algorithm according to the method of Stratmann and Wiendensohler (1996). In addition to Sea Sweep measurements, the concentration of ambient aerosol sampled directly from an open air inlet was continuously measured by a second TSI 3010 condensation particle counter. Sample air was drawn through an inlet 18 m above the sea surface to the ambient particle counter which was housed in the laboratory van beside instruments sampling the Sea Sweep output. Between stations, the Sea Sweep was removed from the water for travel and was flushed with filtered air before sampling and between each sampling

period. Since hours lapse between measurements, any aerosol remaining in the Sea Sweep apparatus and the supply line from the Sea Sweep to the instruments had sufficient time to settle. Bates et al. (2012) found that when sampling air inside the Sea Sweep at times when air was not running to the frits, aerosol counts were less than 20 particles per cubic centimeter. Thus, it is possible though unlikely that any aerosol from previous a station sampling periods contaminated samples from a subsequent station.

7.2.2. Seawater Phytoplankton Cell Collection

Phytoplankton were obtained from surface seawater samples in the surface mixed layer collected via Niskin bottles attached to a CTD rosette on 27 May 2016, the fourth day of Station 4, which represents a stable mixed layer in bloom conditions (Graff & Behrenfeld, 2018). A cell sorting flow cytometer (BD Influx, Becton Dickinson Biosciences) was used to enumerate, classify, and isolate microalgal groups (Graff, et al., 2012; Graff et al., 2015; Graff & Behrenfeld, 2018). Cells were sorted based on fluorescence emissions at 692 nm and 530 nm, and forward and side scattering intensity. The size ranges 0.5-1 µm, 1-3 µm, 3-50 µm corresponded to three groups of microorganisms: *Synechococcus,* photosynthetic picoeukaryotes, and photosynthetic nanoeukaryotes (Graff et al., 2015; Sieburth, et al., 1978). The flow cytometer was calibrated daily with fluorescent beads (Spherotech, SPHERO^{TM} 3.0 µm Ultra Rainbow Calibration Particles) (Graff & Behrenfeld, 2018). In addition to *Synechococcus*, *Prochlorococcus* is often an abundant cyanobacterium in the open ocean (Flombaum et al., 2013), though generally at lower latitudes in the North Atlantic Ocean than sampled during NAAMES 2 (Baer, et al., 2017). *Prochlorococcus* was not present at Station 4

(Graff & Behrenfeld, 2018), therefore no *Prochlorococcus* sample was produced for the INP analysis. For each sample, approximately 0.2 mL of sheath fluid (30 g L^{-1} NaCl solution (Graff et al., 2012) was enriched with cells in the specified size range to a concentration of approximately 50 cells μL^{-1}. We note that photosynthetic picoeukaryotes and nanoeukaryotes are larger than the upper limit of Sea Sweep aerosols collected by the impactor (1 μm diameter). Nevertheless, they are potential sources of INPs because their cells may leak, lyse, or fragment causing the internal materials and cell fragments to be emitted to the atmosphere (Lenes et al., 2013; O'Dowd et al., 2015).

The sorted seawater samples were stored at -80 °C until ice nucleation analysis at Texas A&M University. In addition, flow cytometry was used throughout the cruise to quantify concentrations of microorganisms in bulk waters collected from the cast of the CTD rosette at the shallowest collection depth (5 m). Samples were immediately passed through the flow cytometer, with between 6,000 and 10,000 cells counted per sample.

7.2.3. Immersion Mode Ice Nucleation Experiments

Ice nucleation measurements were conducted using a custom ice microscope apparatus built and operated at Texas A&M University (Brooks et al., 2014; Collier & Brooks, 2016; Fornea, et al., 2009). The well-established method is described in detail in our earlier work (Fornea et al., 2009) and is outlined briefly here. The major components of the apparatus were an Olympus optical microscope (Model BX51M), sealable Linkam cooling stage (LTS 350), and a digital camera (Q-Imaging Micropublisher 5.0 RTV). Accuracy in temperature control was maintained to within ± 0.1 °C by the Linkam stage

throughout freeze-thaw cycles from +5 to -40 °C. With this setup multiple ice nucleation data points were determined for each sample.

To set up an experiment, the aluminum foil impaction stage containing a Sea Sweep aerosol sample was placed on a hydrophobic glass microscope slide for support. In this study, experiments were conducted in immersion mode, in which a 2.0 µL drop of HPLC-grade water (VWR) was pipetted onto the center of the impaction stage and directly on top of the potential INPs, which are visible as a small circular spot. In the case of the sorted phytoplankton samples, a 2.0 µL droplet containing sorted organisms was placed directly on a silanized glass microscope slide pretreated with a 1% AquaSil solution (Pierce Chemical Company). The sample was then sealed into the stage and cooled at a rate of 1 °C min^{-1} from 0 °C to -40 °C. Photographs of the droplet were taken at 400x magnification every 6 seconds (corresponding to a 0.1 °C temperature change). Once the stage reached -40 °C it was heated at a rate of 5 °C min^{-1} until it reached 5 °C, where the temperature was held for 1 minute to ensure complete melting of the droplet. This cooling and warming process was repeated 25 times on the same sample to observe multiple ice nucleation events.

To prevent droplet evaporation throughout the experiment, a humidified flow was generated by combining a flow of saturated nitrogen from a glass bubbler containing ultra high purity (UHP) water (0.01 lpm) and a flow of dry nitrogen (0.6 lpm). A hygrometer (EdgeTech DewPrime II, Model 2000) was used to monitor the dew point. Maintaining a dewpoint at approximately -39 °C was optimal for preventing droplet evaporation while ensuring that condensation did not form inside the Linkam stage. In

the case of impactor samples collected on aluminium foil substrates, such as the Sea Sweep samples here, the dewpoint must not exceed this setting or condensation onto the foil will occur. Measurements collected with any evidence of condensation were excluded from the data set, resulting in less than 25 cycles in a data set.

After the experimental run, the CCD camera images were analyzed on a frame-by-frame basis to visibly determine the freezing temperature. All measurements reported in this study met the following quality control criteria: 1) a freezing point was observed during a minimum of three freeze-thaw cycles for the same sample, 2) freezing was clearly observed at a discrete temperature for each observation (i.e. in a single CCD image), 3) the droplet did not visibly change size, and 4) no condensation was observed adjacent to the droplet on the slide.

The ice nucleating temperature of microorganisms sorted with a flow cytometer was measured from samples collected at Station 4 on Day 4. These samples were representative of the smaller phytoplankton (< 50 μm diameter). It is well known that the presence of salt in water extends the temperature range of liquid water to colder temperatures (Bodnar, 1993). Some previous ice nucleation studies (Irish et al, 2017; Wilson et al, 2015), have adjusted the reported ice nucleating temperatures for salt concentration using the AIM model according to the water activity of the salt solution in equilibrium with ice (Koop & Zobrist, 2009). However, a recent study showed that the nucleating temperatures predicted for some compositions are inconsistent with laboratory measurements (Whale, et al., 2018). Therefore, rather than make adjustments

based on theory, we performed a series of dilutions to measure changes in concentration directly.

Assuming uniform distribution of organisms in the sorted samples (in 30 g L^{-1} NaCl), we estimate that each 2 µL droplet contained approximately 100 cells. Each sample was then diluted with UHP water to the following NaCl concentrations: 15 g L^{-1}, 7.5 g L^{-1}, and 3.75 g L^{-1}, resulting in particle counts of 50, 25 and 13 cells, respectively, per 2 µL droplet. Further dilutions were not performed as it was determined that there was a significant possibility that droplets at lower dilutions would contain no cells. Particles were not visible in the microscope photos, therefore it was not possible to confirm estimated particle counts in the drops.

7.2.4. Seawater Pigment Analysis

Samples for pigment analysis were collected from the 5 m Niskin bottle on the rosette. High Performance Liquid Chromatography (HPLC) was used to quantify individual phytoplankton pigments (Van Heukelem and Thomas 2001, Hooker et al., 2005). HPLC provides a precise measurement of chlorophyll *a* concentration in the surface water, coupled to measurements of accessory pigments that may be used as biomarkers for specific groups of phytoplankton. Casts were made between 8:00 and 9:00 am (local time), with the exception of the cast at Station 1, which was made at 12:20 pm. For pigment analysis, a known volume of sample (1 to 3 L) was filtered with combusted GF/F filters and stored at -80 °C until analysis at the NASA Goddard Space Flight Center Ocean Ecology Laboratory (Greenbelt, Maryland). Pigments were extracted in methanol and analyzed on a 4.6 x 150 mm HPLC Eclipse XDB column

using an Agilent RR1200 HPLC system (Agilent Technologies). In addition, vertical profiles of chlorophyll *a* concentration with depth were made for the upper 200 m using samples collected from the Niskin bottles on the CTD rosette. These water samples were filtered, extracted with 90 % acetone, and chlorophyll *a* concentrations were measured using a Turner Designs AU-10 fluorometer according to the methods outlined in Mueller et al. (2002).

7.3. Results and Discussion

7.3.1. Phytoplankton Bloom after a Storm

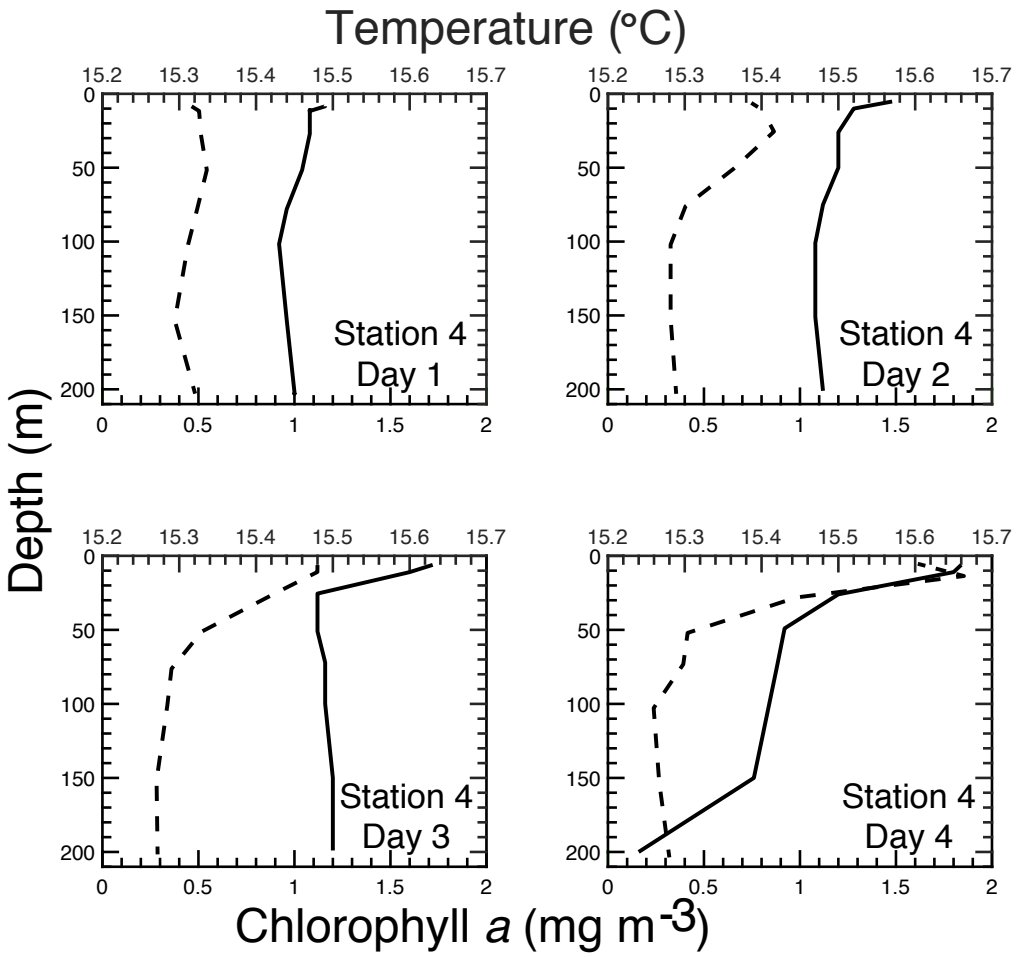

Figure 7.2: Daily chlorophyll a and temperature depth profiles. Chlorophyll *a* is plotted with a dashed line, while surface seawater temperature is plotted with a solid line. Panels A through D represent Days 1-4 of Station 4, respectively. Temperature was measured by the CTD thermometer and chlorophyll a by fluorescence after extraction of pigments with 90% acetone from samples collected in Niskin bottles at all available CTD depths.

Station 4 was occupied for approximately 96 hours. Temperature and chlorophyll *a* depth profiles measured each day at Station 4 are shown in Figure 7.2. Chlorophyll *a* concentrations were consistent with reestablishment of a phytoplankton bloom following storm-driven mixing. Temperature measurements showed warming of surface waters over the four days, resulting in a distinct thermocline from the surface to 25.5 m at Station 4 on Day 3 (Figure 7.2C), which increased in depth to 49 m on Day 4. On Day 1, chlorophyll *a* concentration was relatively constant (approximately 0.5 mg m^{-3}) throughout the epipelagic zone (Figure 7.2A). Surface chlorophyll *a* concentration increased to a maximum of 1.9 mg m^{-3} at 13.6 m depth on Day 4 (Figure 7.2D). For more details on bloom reestablishment processes and the phytoplankton response to the mixing event that occurred at this station and phytoplankton activity, see Graff and Behrenfeld (2018).

7.3.2. Primary Marine Aerosols as Ice Nucleating Particles

For each Sea Sweep aerosol sample, the droplet-sample set-up underwent a series of up to 25 freeze-thaw cycles. Due to issues of condensation on the aluminum substrates used to collect field samples, some experimental runs contain fewer data points than obtained in previous laboratory studies conducted on silanized glass microscope slides (Brooks et al., 2014; Collier & Brooks, 2016; Fornea et al., 2009). Ice nucleation measurements on HPLC-grade water droplets on the aluminum substrates used in the PIXE impactor were performed to test for any influence of the substrate on freezing temperatures. The average nucleation temperature was 33.5 $\pm$ 2.0 °C, in

agreement with the water droplet freezing on the silanized glass slides. The ice nucleation results are summarized in Figure 7.3 and Table 7.1.

Table 7.1: Pooled mean freezing temperatures and pooled standard deviation for each station.

Station number	Date	Lat.	Long.	No. of samples	No. of ice nucleation temp. data points	Mean nucleation temp. (°C) and standard deviation
Station 1	18 May	56° 20' 25.56"	46° 3' 37.80"	2	22	-28.0 ± 1.5
Station 2	20 May	53° 33' 3.84"	42° 15' 25.08"	2	16	-26.2 ± 1.2
Station 3	22 May	50° 16' 36.54"	43° 51' 58.20"	2	15	-28.0 ± 2.0
Station 4, all days	24-27 May	47° 40' 0.72"	39° 9' 55.86"	7	47	-25.1 ± 1.5
Station 4, Day 1	24-26 May	47° 40' 0.72"	39° 9' 55.86"	2	9	-29.5 ± 3.0
Station 4, Day 2	24-26 May	47° 40' 0.72"	39° 9' 55.86"	1	3	-31.5 ± 0.9*
Station 4, Day 3	24-26 May	47° 40' 0.72"	39° 9' 55.86"	2	6	-33.4 ± 1.2
Station 4, Day 4	27 May	47° 40' 0.72"	39° 9' 55.86"	2	29	-24.5 ± 0.9
Station 5	29 May	44° 13' 32.88"	43° 27' 59.10"	2	10	-27.1 ± 2.6
Impactor substrate	N/A	N/A	N/A	9	60	-33.5 ± 2.0

*Due to limited sample availability, mean and standard deviation were not pooled in this case.

Mean freezing temperatures ranged from -24.5 ± 0.9°C on Day 4 of Station 4 to as low as -33.4 ± 1.2°C on Day 3 of Station 4. Similar to our previous studies, a fairly high degree of variability was observed from one freezing event to the next, with individual freezing events occurring at temperatures as high as -21.4 °C and as low as -35.4 °C. The mean freezing temperature of Station 4 was -25.1 °C. The freezing temperature on the fourth day on Station 4, -24.5 ± 0.9 °C, was the warmest and was statistically different (at the 95% confidence limit) from the three days prior (Days 1-3). The Station 4 Day 4 freezing temperature was also the highest mean temperature observed throughout the cruise, and was statistically different at the 95% confidence

limit than the mean freezing temperature for all days at other stations with the exception of Station 2, -26.2 ± 1.2 °C.

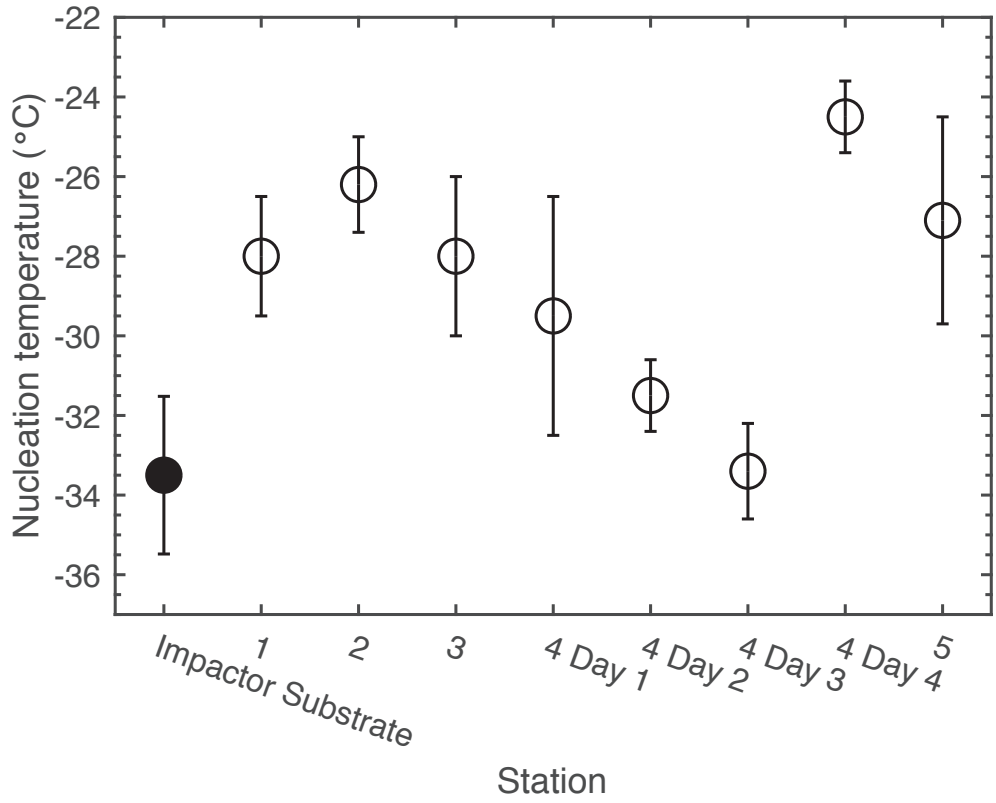

Figure 7.3: Mean immersion mode ice nucleation temperatures for Sea Sweep aerosol samples. Error bars represent the pooled standard deviation. For comparison, the nucleation temperature of a field blank (pre-cleaned Al foil PIXE substrate) is shown as a solid circle.

To determine the concentration of ice-active aerosols (those that freeze) relative to the total sample concentration, the probability of freezing, or fraction frozen, was calculated as:

$$\boldsymbol{P(T)} = \frac{\boldsymbol{N_f}}{\boldsymbol{N_o}}, \quad (1)$$

where N_0 is the total number of unfrozen water droplets (including the initial unfrozen droplet and subsequent thawed droplets) and N_f is the number of water droplets frozen at temperature, T (Brooks et al., 2014; Collier & Brooks, 2016; Shaw, Durant, & Mi, 2005). The fraction frozen for each sample is shown in Figure 7.4. In cases when multiple samples were available, all individual data points were compiled into a single data set and the fraction frozen was derived from the compilation. As the figure illustrates, the variation in freezing temperatures observed for any single day are much narrower than this. Broadly speaking, the aerosols available to act as INPs were the least efficient nucleators (characterized by the lowest fractions frozen) on the first three days at Station 4. In contrast, the most effective nucleators, with the highest fraction frozen at nearly all temperatures, were observed on Day 4 of Station 4. At the warmest observed droplet freezing temperature, -21.4 °C, freezing was only observed for Station 5. At the intermediate temperature of -25 °C, the fraction frozen for Station 4 Day 4 was 0.69, while the fraction frozen for both Day 2 and Day 3 was 0.0.

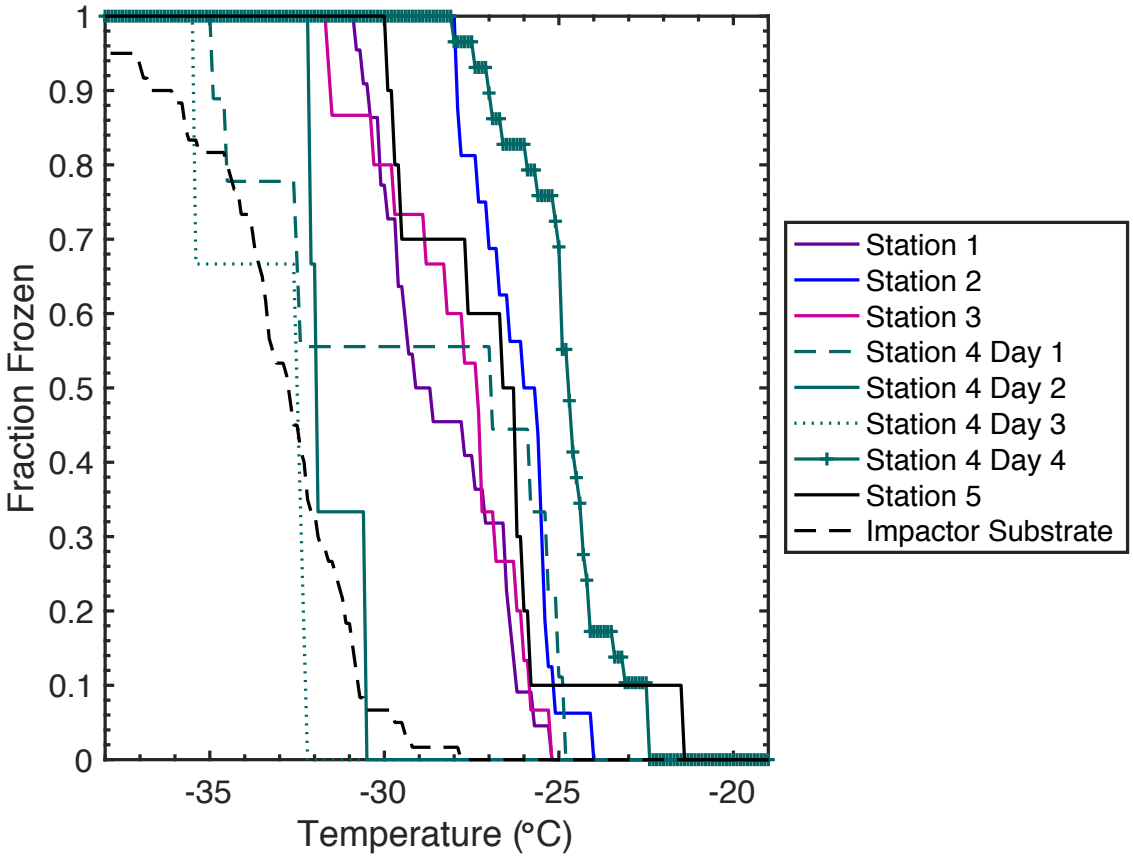

Figure 7.4: Fraction frozen (fraction of independent observations of sample freezing as a function of temperature). Each data set represents the fraction frozen for a single day of sampling.

The mean ice nucleation temperatures for Stations 1-5 indicate that marine sources produce moderately efficient INPs in general agreement with recent marine INP measurements in other locations (DeMott et al., 2016). The range in freezing temperatures is narrower than reported in other marine INP studies (DeMott, et al., 2016; Wilson, et al. 2015), perhaps because the Sea Sweep generates exclusively primary marine aerosol with no local secondary aerosol and no continental aerosol influences.

Some previous measurements on aerosols classified as marine INPs have observed freezing at higher temperatures than observed here, -27.5 to -6 °C (DeMott et al., 2016). However, it was later noted that all measurements above -12 °C were collected from onshore sampling sites in Puerto Rico and are likely influenced by continental sources of INPs (Brooks & Thornton, 2018). Highly effective marine INPs with immersion freezing temperatures as warm as -5 °C were also observed in aerosol samples collected over the Bering Sea, albeit for much larger aerosols (3 to >12 μm diameter) than sampled in the current study (Creamean et al, 2019). In comparison, we observed freezing at -21.5 °C and below for Sea Sweep samples (0.06 μm to 1 μm diameter). While the reason for this difference cannot be determined for certain, a clear difference is the size of the aerosol tested as potential INP. An additional contributing factor may be regional differences in the composition of the marine aerosols available to act as INPs. The possibility also exists that a low concentration of large aerosols with high ice nucleation potential were present during NAAMES but not sampled with our technique. In a separate study (Mason et al, 2016), the ice nucleation propensity of aerosols collected in the Labrador Sea and several continental locations in a range of sizes between 0.1 and 10 μm diameter were determined. Supermicron aerosol samples which nucleated ice at temperatures of -15 °C or colder represented a significant fraction of the total observed INP.

For reference, the aerosol concentrations and size distributions observed during Sea Sweep deployment are discussed in the Appendix and Figure A2. It should be noted that the absolute concentration of aerosols generated by the Sea Sweep varies with instrument operation and does not provide a measure of ambient aerosol concentration or size distribution. Over the course of the campaign, Sea Sweep aerosol concentrations

generated by the Sea Sweep were 2.3 – 17.2 times greater than ambient aerosol concentrations, with the highest concentrations produced at Station 2. By comparison, the size distributions and mean diameters of generated aerosols were much more consistent than concentrations. Given that the high INP freezing temperatures on Station 4 Day 4 do not coincide with high aerosol loading on the impaction stage or a change in generated size distribution, we conclude that the warmer observed nucleation temperature is likely due to a change in aerosol composition rather than a sampling artifact. In addition, the ambient aerosol concentration was relatively low on Station 4 Day 4, indicating that the warmer freezing temperatures did not coincide with an increase in aerosol concentration.

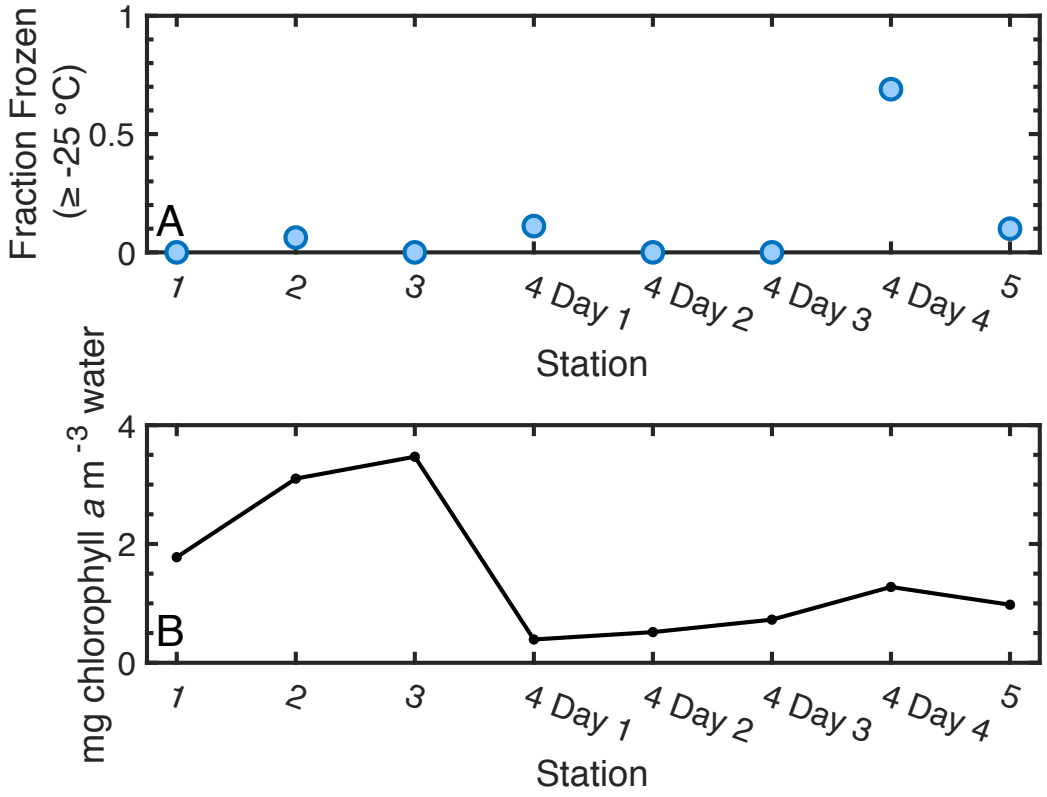

Figure 7.5: Changes in INP properties and phytoplankton biomass with sampling station. A) The fraction of droplets frozen at -25 °C or warmer. B. Surface (5 m depth) chlorophyll a concentrations (mg m-3), measured with High Performance Liquid Chromatography (HPLC) from samples collected at 5m during CTD casts made between 8:00 and 9:00 am local time, with the exception of Station 1, which was made at 12:20 pm.

To compare changes in INP activity with the composition of the underlying seawater, we first inspected the time series of INP freezing temperatures and the corresponding time series of daily mean chlorophyll concentrations in Figure 7.5. In Figure 7.5A, the fraction of sea sweep aerosols frozen by the moderate temperature of -25 °C or warmer are shown. For comparison, the concentration of chlorophyll a is shown

in 7.5B. Concentrations of chlorophyll *a* varied substantially throughout the cruise, ranging from 0.39 to 3.47 mg m-3 with the highest values observed at Station 3 and lowest on the first day of Station 4. No relationship between chlorophyll a and fraction frozen (> 25 °C) was evident in the data. There are several studies that have looked for a relationship between chlorophyll a concentration and INP production, and a consistent relationship was not reported across these studies (DeMott et al, 2016; Irish et al., 2019; McCluskey et al., 2017). In a mesocosm study, a positive relationship was found between chlorophyll *a* concentrations and INP concentrations at -26 °C and -30 °C but not at warmer temperatures (DeMott et al, 2016). McCluskey et al. (2017) report a lag between the highest INP concentrations active between -15 °C and -25 °C and chlorophyll *a* concentrations. In contrast, Irish et al. 2019 did not find a clear link between INP concentrations and chlorophyll *a* concentrations measured in the SML and bulk seawater in the Canadian Arctic. However, the possibility remains that certain components such as small phytoplankton are injected into the atmosphere and remain there long enough to induce freezing events. This subset of smaller marine organisms (< 50 μm diameter) includes a widely abundant single celled cyanobacteria, *Synechococcus*, as well as photosynthetic picoeukaryotes, and photosynthetic nanoeukaryote cells.

7.3.3. Community Composition

The concentrations of *Synechococcus*, picoeukaryotes, and nanoeukaryotes in sea water collected at 5 m depth during the daily CTD casts (taken between 8:00 am and 12:20 pm local time) were determined by flow cytometry (Figure 6) and, collectively,

represent the smaller chlorophyll-containing cells observed during the project. A complex and variable concentration of other chlorophyll-containing organisms were present as indicated by HPLC pigment data, discussed in the Appendix. The phytoplankton measured by flow cytometry (< 50 μm diameter) at the first four stations were dominated by picoeukaryotes in term of abundance, ranging from 52% during Station 3 to 85% during Day 4 of Station 4. *Synechococcus* concentrations increased from 2.76 x 106 L^{-1} on Day 1 of Station 4 to 9.24 x 10^6 L^{-1} on Day 4, while picoeukaryotes increased from 1.17 x 10^7 mL^{-1} to 9.13 x 10^7 L^{-1}, and nanoeukaryotes increased from 5.17 x 10^5 L^{-1} to 3.68 x 10^6 L^{-1}. However, on Station 5, *Synechococcus* concentrations increased six fold to 6.01 x 10^7 L^{-1}, while concentrations of picoeukaryotes and nanoeukaryotes dropped to 2.64 x 10^7 L^{-1} and 3.02 x 10^6 L^{-1}, respectively.

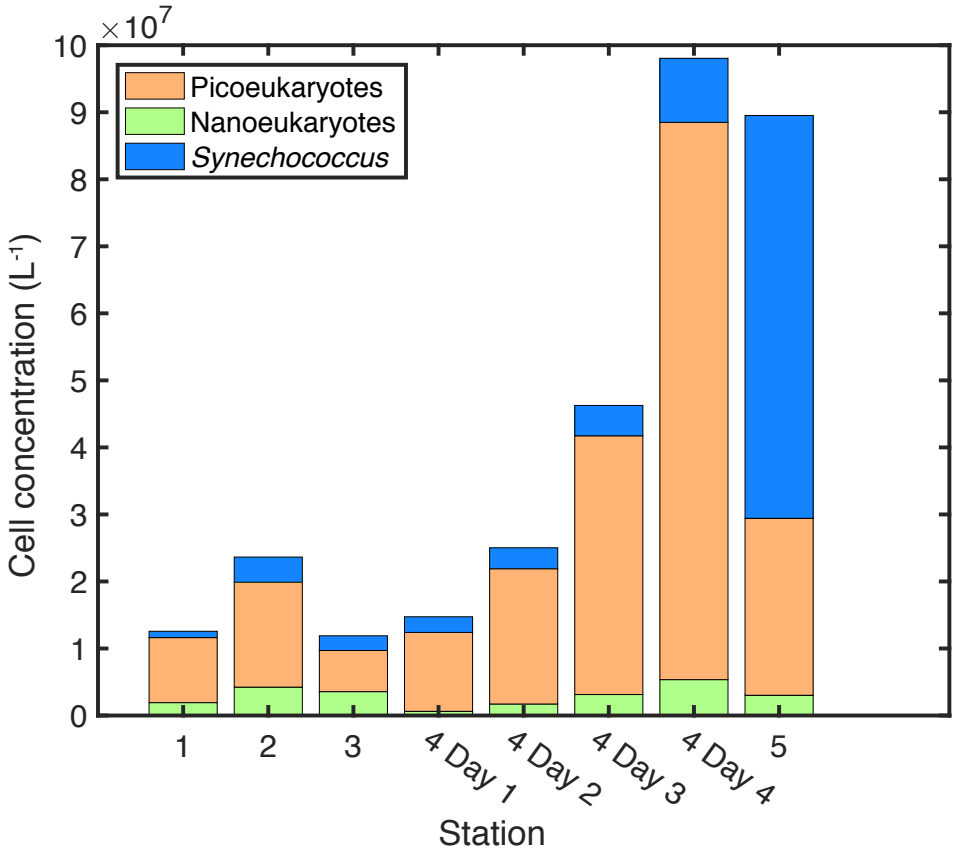

Figure 7.6: Bulk water cell concentrations sorted using the rapid sorting flow cytometer (BD Biosciences Influx Cell Sorter). Bulk water was taken from the 5 m Niskin bottle taken by CTD cast. Picoeukaryotes 1-3 µm) are represented in orange, nanoeukaryotes (3-50 µm) in green, and *Synechococcus* (0.5-1 µm) by blue.

Over the course of the 4 days on Station 4, there was less than a 5% difference in the relative proportions of *Synechococcus*, picoeukaryotes and nanoeukaryotes. For each organism type, the biggest increases were between Day 3 and Day 4. Over this period, the fraction of droplets frozen by -25 °C increased from 0.11 on Day 1 of Station 4 to

0.69 on Day 4 and chlorophyll *a* (determined by HPLC) rose from 0.39 mg m-3 on Day 1 to 1.28 mg m-3 on Day 4.

Both the increase in total cell concentration and the increase in picoeukaryote concentration paralleled the increase in INP activity (represented by the fraction frozen at -25 °C (Figure 5A) between Day 3 and Day 4 of Station 4). However, moving to Station 5, the picoeukaryote concentration dropped along with the reduction in fraction frozen, while the *Synechococcus* increased to the highest observed concentration throughout the cruise (Figure 6). The groups isolated here represent a possible source of INPs. *Synechococcus* (0.5-1 μm cell diameter) may be present in the Sea Sweep samples as a whole organism. In contrast picoeukaryotes, and nanoeukaryotes (size ranges of 1-3 μm and 3-50 μm diameter, respectively) would not be sampled by the Sea Sweep as whole organisms. Additional sources such as heterotrophic bacteria and other organic material in the water may also be part of the primary marine aerosols produced over the seawater.

7.3.4. Phytoplankton Cell Samples as Ice Nucleating Particles

Next we consider the ice nucleation temperatures of the cytometer-sorted seawater components *Synechococcus,* picoeukaryotes, and nanoeukaryotes individually. Pooled mean freezing temperatures and pooled standard deviations for sorted sea water samples are summarized in Figure 7.7 and Table 7.2.

Table 7.2: Pooled mean freezing temperatures and pooled standard deviations for sorted sea water samples.

INP Composition	Salt content (g L^{-1})	Particle concentration (cells per droplet)	No. of samples	No. of ice nucleation temp. data points	Mean nucleation temp. (°C) and standard deviation
Synechococcus	30	100	5	74	-33.1 ± 1.0
Synechococcus	15	50	2	26	-30.2 ± 0.5
Synechococcus	7.5	25	1	13	-27.0 ± 1.1
Synechococcus	3.75	13	1	15	-23.0 ± 0.2*
Nanoeukaryotes	30	100	6	92	-33.8 ± 1.5
Nanoeukaryotes	15	50	1	7	-30.4 ± 1.0*
Nanoeukaryotes	7.5	25	2	19	-26.2 ± 1.0
Nanoeukaryotes	3.75	13	1	6	-22.1 ± 0.9*
Picoeukaryotes	30	100	4	93	-31.8 ± 1.1
Picoeukaryotes	15	50	1	6	-27.6 ± 1.7*
Picoeukaryotes	7.5	25	1	23	-24.4 ± 2.1*
Picoeukaryotes	3.75	13	1	25	-25.2 ± 0.6*
Sheath fluid	30	0	3	45	-32.4 ± 1.0

*Due to limited sample availability, mean and standard deviation were not pooled in this case.

Amongst the 30 g L^{-1} NaCl samples, the warmest freezing occurred at -33.1 ± 1.0 °C for the *Synechococcus* samples, but there was no statistical difference between the three types of organisms in 30 g L^{-1} NaCl (95% confidence level). The temperature of homogeneous nucleation of pure water on a silanized glass microscope slide has been identified at -33.1 °C ± 0.6 °C standard deviation in our apparatus. In all three cases, we observed near-homogeneous freezing temperatures, suggesting only weak ice-nucleating properties of the microorganisms. However, the implications of these results in 30 g L^{-1} NaCl are inconclusive since the presence of the NaCl may inhibit nucleation

relative to pure water. For comparison, ice nucleation of the sheath fluid into which organisms were collected (30 g L^{-1} NaCl in deionized water supplied by the Barnstead deionized water system used on the ship) were also conducted. This sheath fluid was used for collection and storage of all *Synechococcus*, picoeukaryotes, and nanoeukaryotes. The sheath fluid froze at -32.4 $\pm$ 1.0 °C, which is slightly higher than expected for salt water but can be attributed to the presence of trace amounts of organics present in the deionized water source.

Figure 7.7 shows that overall trends toward warmer freezing temperatures were observed for each class of microorganism as salt content and cell concentrations decreased. The only exception was that the 3.75 g L^{-1} NaCl samples containing picoeukaryotes had a slightly lower freezing temperature than the 7.5 g L^{-1} NaCl containing picoeukaryote samples. The increase in freezing temperature varied between microorganism type, with the nanoeukaryotes showing the largest change from -33.8 ± 1.5 °C at 30 g L^{-1} NaCl to -22.1 ± 0.9°C at 3.75 g L^{-1} NaCl. Freezing data from each of the three groups of phytoplankton (*Synechococcus,* nanoeukaryotes, and picoeukaryotes) showed a statistically significant difference (95% confidence interval) between the 30 g L^{-1} NaCl data and the 3.75 g L^{-1} NaCl data. Additional dilutions were not conducted due to the lack of available sample and a concern that as salt content approaches that of pure water the microorganisms may lyse. It should be noted that lysing due to the dilutions performed here cannot be ruled out.

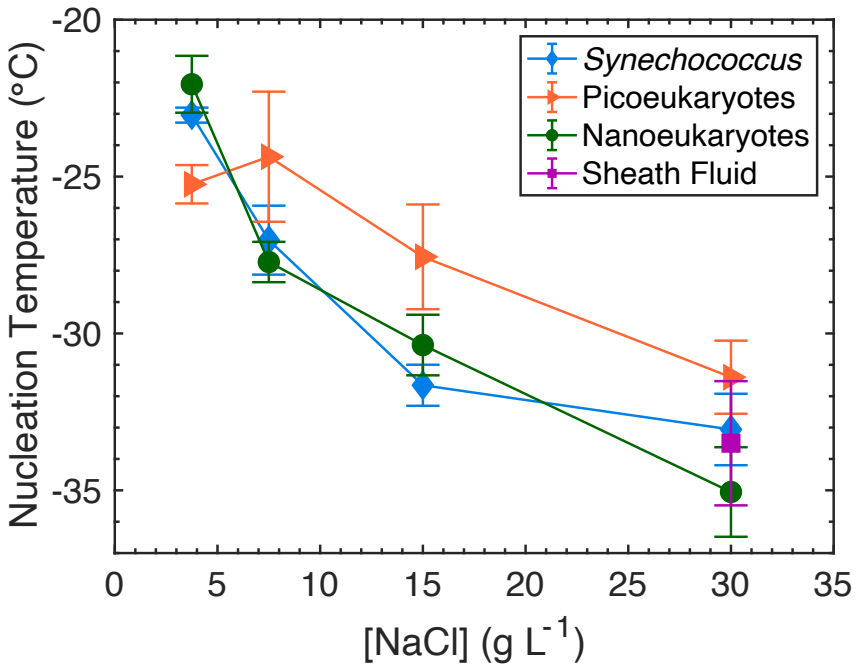

Figure 7.7: Mean immersion ice nucleation temperatures for sorted seawater samples. All samples were collected on Day 4 of sampling at Station 4 and sorted by the flow cytometer. *Synechococcus* is represented by blue diamonds, picoeukaryotes by orange triangles, and nanoeukaryotes by green circles, with error bars representing the pooled standard deviation. *Synechococcus,* picoeukaryotes, and nanoeukaryotes had the following size ranges, respectively: 0.5-1 µm, 1-3 µm, and 3-50 µm diameter.

Thirty g L^{-1} NaCl is the approximate salt content of freshly formed sea spray. However, during cloud formation, atmospheric particles rapidly uptake water and become more dilute under the humid conditions encountered in the marine environment. Assume that a sea spray droplet contains an initial NaCl mass of 10^{-19} kg (Wallace & Hobbs, 2006) and that the droplet activates as a cloud condensation nucleus (CCN), followed directly afterward by immersion freezing of the CCN. In this case, the droplet

would have a radius of 0.15 microns at the point of immersion freezing (Wallace & Hobbs, 2006), and the salt content would be reduced to approximately 1.1 g L^{-1} NaCl.

Therefore, of the experiments conducted in this study, the measurements at 3.75 g L^{-1} are the most realistic of atmospheric droplets at the point of freezing. The freezing temperatures of samples at 3.75 g L^{-1} NaCl may be considered as a lower limit to the temperature which needs to be reached for actual marine drops (containing the identified microorganisms) to freeze. At 3.75 g L^{-1} NaCl, *Synechococcus*, picoeukaryotes, and nanoeukaryotes samples froze at -23.0 ± 0.2, -25.2 ± 0.6, and -22.1 ± 0.9, respectively. These temperatures are well above the temperature of homogenous freezing, -36 °C. Thus, we conclude that marine aerosols containing *Synechococcus,* picoeukaryotes, and nanoeukaryotes in dilute salt solution are modestly effective INPs. These freezing temperatures fall within the range of the freezing temperatures of the Sea Sweep aerosolized samples collected at the same time (freezing temperatures of -33.4 °C to -24.5 °C). While *Synechococcus*, picoeukaryotes and nanoeukaryotes in salt solution droplets are all likely contributors to marine INP populations, no single class of microorganisms can be identified as the key nucleators of ice.

Flow cytometer sorting provides a limit on the size of organism considered, with an upper limit of ~50 μm (nanoeukaryotes). In a previous ice nucleation study conducted in the Canadian Arctic, samples of bulk sea water and the sea surface microlayer were filtered through PTFE filters with 10, 0.2 and 0.02 μm pore sizes (Irish et al., 2017). In the unfiltered bulk water and microlayer samples, a wide range of freezing temperatures were observed, with peak temperatures significantly higher than observed in our study.

While the possibility that larger organisms present at Station 4 also possess the physical properties conducive to nucleate ice, it is less likely that they will be present in the atmosphere due to low abundance in the ocean and their higher settling velocities. In fact, observations of sea spray diameters include particles ranging from 0.1 to 100 μm diameter (Blanchard & Woodcock, 1957), but the mean diameter is small (0.1 μm) (Clarke, et al., 2006). In the Irish et al. (2017) study, the freezing capacity of many (though not all) samples was significantly reduced after filtration, suggesting that the majority of INPs were between the sizes of 0.2 and 0.02 μm. While the possibility cannot be ruled out entirely, it is unlikely that larger particles and/or organisms represent a major unsampled marine INP source in our study.

7.4. Conclusions

At present, global coverage of INP measurements lack data from many locations. Our measurements indicate that North Atlantic aerosols have ice-nucleating temperatures between -22.4 °C and -35.4 °C, broadly consistent with the ice-nucleating properties of marine aerosol sampled in other clean marine locations (DeMott et al., 2016; Irish et al., 2017 & 2019; McCluskey et al., 2016; Wilson et al., 2015). In addition, this study provides marine INP measurements coordinated with detailed biological sorting by flow cytometry.

Using a flow cytometer we separated particles based on both fluorescence and size to isolates different groups of phytoplankton from the bulk water and other particles such as detritus. Ice nucleation measurements on these samples indicate three specific categories of phytoplankton (*Synechococcus*, picoeukaryotes, and nanoeukaryotes) are

moderately effective INPs. The ice nucleating activity of these three isolated types was observed to be very similar. Given that the cyanobacterium *Synechococcus* is one of the most abundant and ubiquitous phytoplankton taxa in surface waters of the ocean (Flombaum et al., 2013), it may have widespread influence on marine ice nucleation and mixed phase cloud formation. Our measurements also demonstrate that the ability of freshly generated spray aerosol to initiate freezing at warm temperatures is counterbalanced by the presence of sea salt until dilution by atmospheric water uptake occurs.

Our Sea Sweep aerosol measurements are the first series of INP measurements conducted on aerosol samples collected over the course of the reestablishment of a phytoplankton bloom after storm induced deep mixing. Interestingly, the daily mean freezing temperature and concentration of particles frozen at -25 °C or warmer were both significantly elevated on the fourth day of observations at a fixed sampling site (Station 4), in parallel with the reestablishment of a phytoplankton bloom. At Station 4, the warmest INP freezing temperatures were observed when the phytoplankton biomass was greatest, both in terms of chlorophyll *a* concentrations measured with HPLC from samples taken at 5 m depth (Figures 7.5B and A1) and the abundance of small (< 50 μm diameter) phytoplankton enumerated by flow cytometry. However, at Stations 1 to 3, higher chlorophyll *a* was observed while INP freezing temperatures were relatively colder, which indicates that biomass alone is not a driver of atmospheric ice nucleation. In contrast, the contribution of small phytoplankton (particularly picoeukaryotes) was relatively low at Stations 1 to 3 (compare Figures 7.6 and A1).

Mayol, et al. (2014) estimated aerosolization rates of microorganisms from the North Atlantic Ocean during summer to be 9 to 100 prokaryote cells m^{-2} s^{-1} and 0.01 to 0.1 eukaryote cells m^{-2} s^{-1}. Revisiting our central hypothesis, our results indicate that marine phytoplankton contribute to an effective population of atmospheric INPs. Moreover, our results suggest that smaller chlorophyll-containing cells (< 50 μm) may be key contributors to freezing in atmospheric droplets.

8. CONCLUSIONS

8.1. Summary of Research Questions and Results

Prior studies concluded that phytoplankton may be an underestimated source of INP (Alpert et al., 2011a, 2011b; Creamean et al., 2019; Knopf, Alpert, & Wang, 2018; Knopf et al., 2011; Knopf et al., 2014; Kong et al., 2018; McCluskey, Ovadnevaite, et al., 2018; Wilson et al., 2015), especially in clean marine conditions with no continental influence. Of these studies, only a few considered plankton populations as anything other than a whole, unchanging population. There was no consideration of the different species present in field measurements, and only chlorophyll was used to determine phytoplankton biomass, with no consideration of changing parameters other than overall biomass. The experiments presented here attempt to more closely link biological parameters including biomass and physiological status to atmospheric ice nucleation. There were four hypotheses presented in Chapter 1:

1. Phytoplankton and material produced by phytoplankton act as ice nucleating particles (INPs) at atmospherically relevant temperatures.
2. Different phytoplankton taxa change ice nucleation temperatures and INP concentrations.
3. There is a link between the processes associated with cell growth and physiological status and ice nucleation ability of cells and associated material.
4. Viruses act as ice nucleating particles in seawater samples.

The results addressing these hypotheses are discussed here.

8.1.1. Phytoplankton as INPs and INP Sources

Results from both laboratory and field samples suggest that phytoplankton and associated organic material act as INP at atmospherically relevant temperatures. Whole cells separated from North Atlantic seawater froze as warm as -22.1 ± 0.9 °C, while aerosols generated from single-species cultures froze even warmer (up to -18.0 ± 2.3 °C). These freezing temperatures are comparable to other studies of ice nucleation by marine phytoplankton (Alpert et al., 2011b; Irish, Hanna, Willis, et al., 2019; Knopf et al., 2011). Chapters 3, 4, and 5 showed that phytoplankton have significantly different freezing temperatures at different points in their growth, so it is important to fully characterize the growth rates of phytoplankton populations when taking natural marine organism samples. The lack of multiple time points at most stations is one of the major limitations of the results reported in Chapter 7—although the biology at each station was very well characterized, due to the short sampling time at most of the stations there was no way of determining phytoplankton growth rates over time. However, since the times of high INP ability corresponded with fast growth rates in all three individual taxa tested in the MART, it can be concluded that the INP that nucleate ice at the warmest temperatures are observed during periods of relatively fast growth.

Another thing that must be considered when planning experiments on the INP activity of marine phytoplankton is the salt concentrations of the droplets being tested. When the freezing temperatures of sorted whole cells in 35 ppt seawater collected in the North Atlantic and the freezing temperature of diatom cells in 30 ppt ASW is compared, it is apparent that droplets containing both salts at natural seawater concentrations and

organisms nucleate at quite low temperatures. All organisms tested in water droplets containing salts (*Thalassiosira weissflogii*, nanoeukaryotes, and picoeukaryotes) all act as INP at temperatures colder than -30 °C. In contrast, once the salt is removed by dilution or aerosolization of the sample the freezing temperatures are all significantly warmer, much warmer than can be explained by the removal of salt alone. Cells in 3.75 ppt NaCl solution freeze at -22.1 ± 0.9, -25.2 ± 0.6, and -23.0 ± 0.2 (sorted samples containing nanoeukaryotes, picoeukaryotes, and *Synechococcus* respectively). Material collected on Al foil and suspended in UHP water freeze at temperatures as high as -20.7± 0.4 (*Thalassiosira weissflogii*), -18.0 ± 2.3 (*Synechococcus elongatus*) and -24.6 ± 1.9 °C (*Emiliania huxleyi*).

When all of the single-species or group samples (from both lab-grown and field-collected samples) are compared, there are some differences in freezing temperature. The single-species samples had maximum freezing temperatures between 1.4 and 4.1 °C warmer than the samples collected during NAAMES 2 that were isolated using flow cytometry into 30 ppt NaCl solution rather than remaining in natural seawater. The samples both contained INP, but it is possible that the other material present in the single-species MART samples increased the freezing temperature. While the cell-sorted samples contained only whole organisms and NaCl, the single-species samples contained both whole and cell fragments, multiple types of salts from the ASW, and any other organic material that was aerosolized and collected on the Al foil. Therefore the range of possible INP is actually much broader in the samples generated by the MART,

suggesting that the INP activity of biological samples relies somewhat on both cell material and other biogenic material in the water.

8.1.2. Comparison of INP Activity Between Phytoplankton Groups

Although cyanobacteria, diatoms, and coccolithophores are all photosynthetic marine plankton, there are large differences in their physiology. The largest differences arise from the fact that cyanobacteria are prokaryotic and lack much of the internal organization found in the eukaryotic diatoms and coccolithophores. As well, they differ in size and composition of their cell wall. However, they have similar metabolisms and growth patterns, utilizing many of the same major nutrients (although diatoms require silica while cyanobacteria and coccolithophores do not).

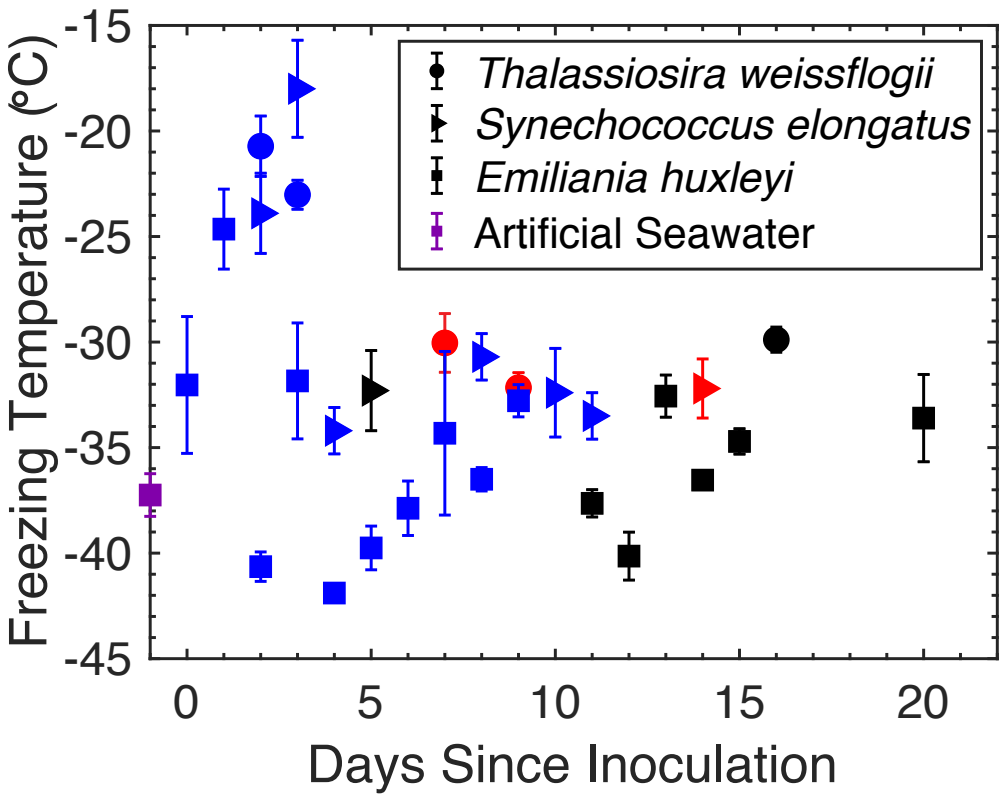

Figure 8.1: Mean freezing temperatures of aerosols generated from cultures grown in the MART. Each data point represents the mean freezing temperature ± standard deviation, n ≥ 3. *Thalassiosira weissflogii* is plotted with circles, *Synechococcus elongatus* with triangles, *Emiliania huxleyi* with squares, and artificial seawater with a purple square. Exponential phase samples are plotted in blue, stationary phase in red, and death phase in black.

For all the differences in physiology between the three species studied, when the freezing temperatures of samples from *Synechococcus elongatus* and *Thalassiosira weissflogii* are compared, a similar pattern emerges (shown in Figure 8.1). The freezing temperatures of samples from the first three days following inoculation are high, followed by very low freezing temperatures for the rest of the experiment. Samples

generated from *Emiliania huxleyi* culture show a similar high freezing temperature immediately following inoculation, but then the freezing temperature drops on Day 2. All of the warmest freezing temperatures are found in samples collected during exponential phase, but some of the coldest freezing temperatures are also from samples taken during the exponential phase of *Emiliania huxleyi*. In addition, the freezing temperatures of cyanobacteria and diatom samples are higher than the average coccolithophore sample freezing temperatures (mean freezing temperatures at -27.4 ± 4.5 °C, -29.7 ± 5.7 °C, and -34.9 ± 4.3 °C for diatoms, cyanobacteria, and coccolithophores respectively).

When a pairwise multiple comparison is performed (Holm-Sidak method, $p<0.05$) the difference between the coccolithophore sample freezing temperatures and the diatom and cyanobacteria sample freezing temperatures is even more apparent, as only the coccolithophore sample freezing temperatures vary significantly from the other two. As discussed in Chapter 5, this may be due to a fundamental difference between the INP produced by coccolithophores, as was seen in Alpert et al. (2011b). Alpert et al. (2001b) concluded that the lack of INPs was due to the calcareous plates produced by *Emiliania huxleyi*. However, this assumes that only the whole cells are capable of acting as INP, when the cells are much too large to act as INP in immersion mode freezing (Wilson et al., 2015). The strain of *Emiliania huxleyi* tested in Chapter 5 for INP ability had calcareous plates. Rather than the plates determining freezing temperatures, there is likely a difference in the organic material produced by coccolithophores versus the material produced during the growth of diatoms and cyanobacteria. Unfortunately,

further studies are needed to repeat ice nucleation experiments on the impact of the growth of calcified *Emiliania huxleyi*, as our experiment showed several days of freezing temperatures where the average freezing temperature was below the temperature of homogeneous nucleation, implying either an instrumental error producing erroneous data or a large increase in the salt content of the aerosols.

8.1.2.1. Chlorophyll *a* and Ice Nucleation

All three groups obtain energy through photosynthesis, and while eukaryotic thylakoids are enclosed within chloroplasts and cyanobacterial thylakoid membranes are not, the photosynthetic processes are very similar between the two types of organism. Each group does contain different accessory pigments, but all three contain chlorophyll *a*.

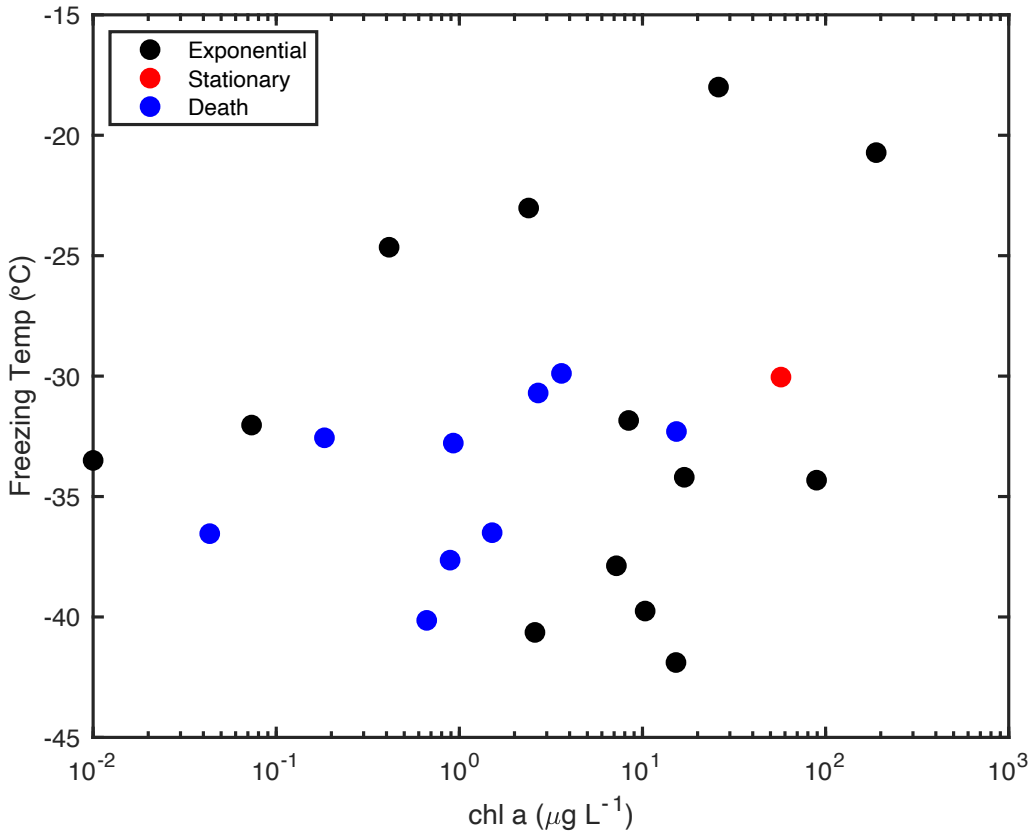

Figure 8.2: Average daily freezing temperature (°C) plotted against total chlorophyll content (µg L^{-1}) of the culture (measured daily with either fluorometry or spectrophotometry). As with previous studies, no relationship was observed between chlorophyll *a* concentration and freezing temperature of samples. Exponential phase samples are plotted in black, stationary phase in red, and death phase in black. Data is from MART experiments containing *Emiliania huxleyi*, *Thalassiosira weissflogii*, and *Synechococcus elongatus*.

While it has been proposed by some that there is a link between chlorophyll *a* concentrations and INP activity based on MART experiments containing natural seawater and phytoplankton (DeMott et al., 2016; McCluskey, Hill, et al., 2018; McCluskey, Ovadnevaite, et al., 2018), there is no relationship shown between the

amount of chlorophyll *a* in diatom or cyanobacterial cultures and INP activity (as addressed in Chapters 3 and 4 and seen in Figure 8.2). Samples from exponential phase when the culture was relatively fast-growing had some of the highest and some of the lowest freezing temperatures measured. We also did not see a relationship between chlorophyll *a* and INP activity in field samples that contained multiple different types of organisms (reported in Chapter 7). Irish, Hanna, Xi, et al. (2019) also did not see a relationship between chlorophyll *a* concentration and INP activity in field samples.

8.1.2.2. Photosynthetic Yield as a Possible Indicator of Ice Nucleation Activity

While previous studies have seen a relationship between bloom collapse and ice nucleation ability of the aerosols produced over the phytoplankton (McCluskey et al., 2018), our results show no correlation between the condition of the phytoplankton population and ice nucleation ability (Pearson Correlation, $p>0.05$).

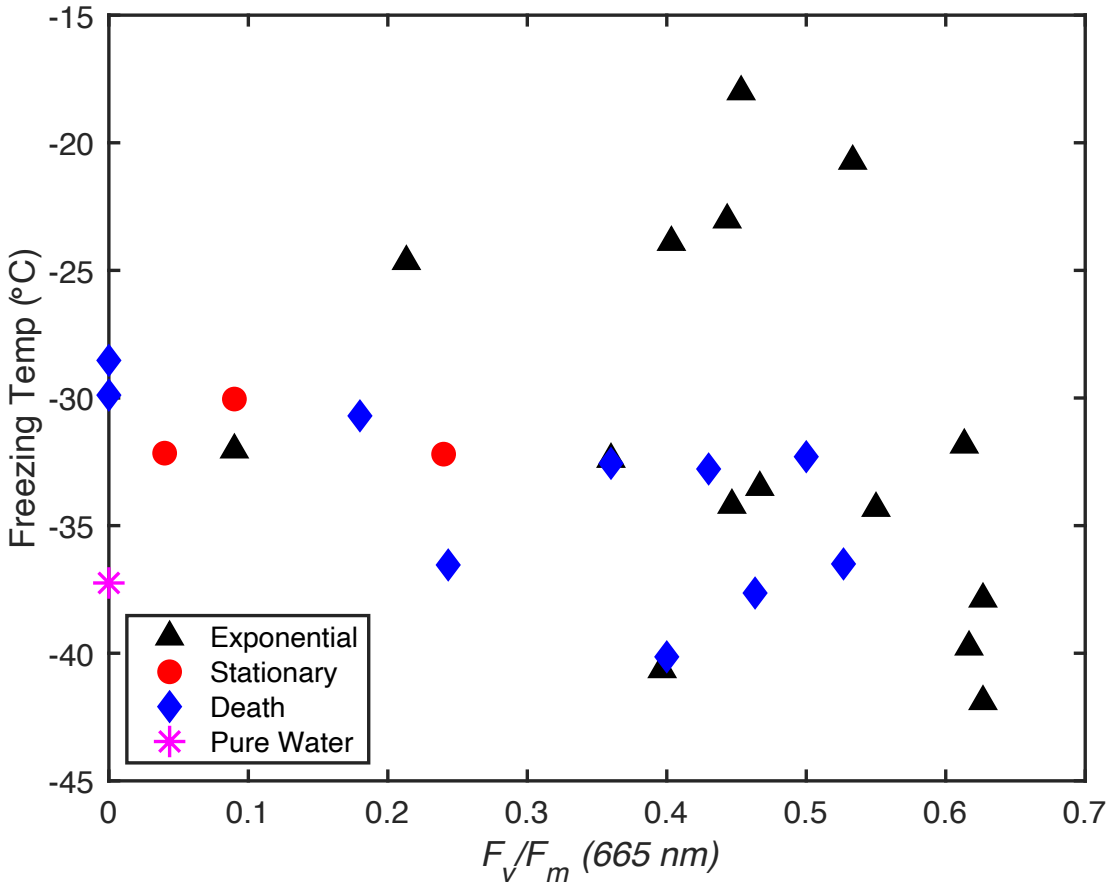

Figure 8.3: Average daily freezing temperature and average photosynthetic yield (measured by PAM fluorometry) on each day of three MART experiments. Exponential phase is plotted with black triangles, stationary phase with red dots, death phase with blue diamonds, and pure water with a purple star. Data is from MART experiments containing *Emiliania huxleyi*, *Thalassiosira weissflogii*, and *Synechococcus elongatus*.

One proposed explanation for the previously observed increase in INP efficiency with declining chlorophyll *a* concentrations is an increase in the production of extracellular material by phytoplankton. However, there was no relationship seen between either of

the two types of exopolymers measured and ice nucleation temperatures (Figure 8.4). Although exponential phase samples had higher yields, this did not correspond with higher freezing temperatures, and in fact the exponential phase samples with the highest yield did not have the highest freezing temperatures.

8.1.2.3. Exopolymers as a Possible Source of INPs

Although there was no relationship between TEP or CSP area and INP activity, what is apparent is that *Emiliania huxleyi* produced much lower quantities of both TEP and CSP than the other two species.

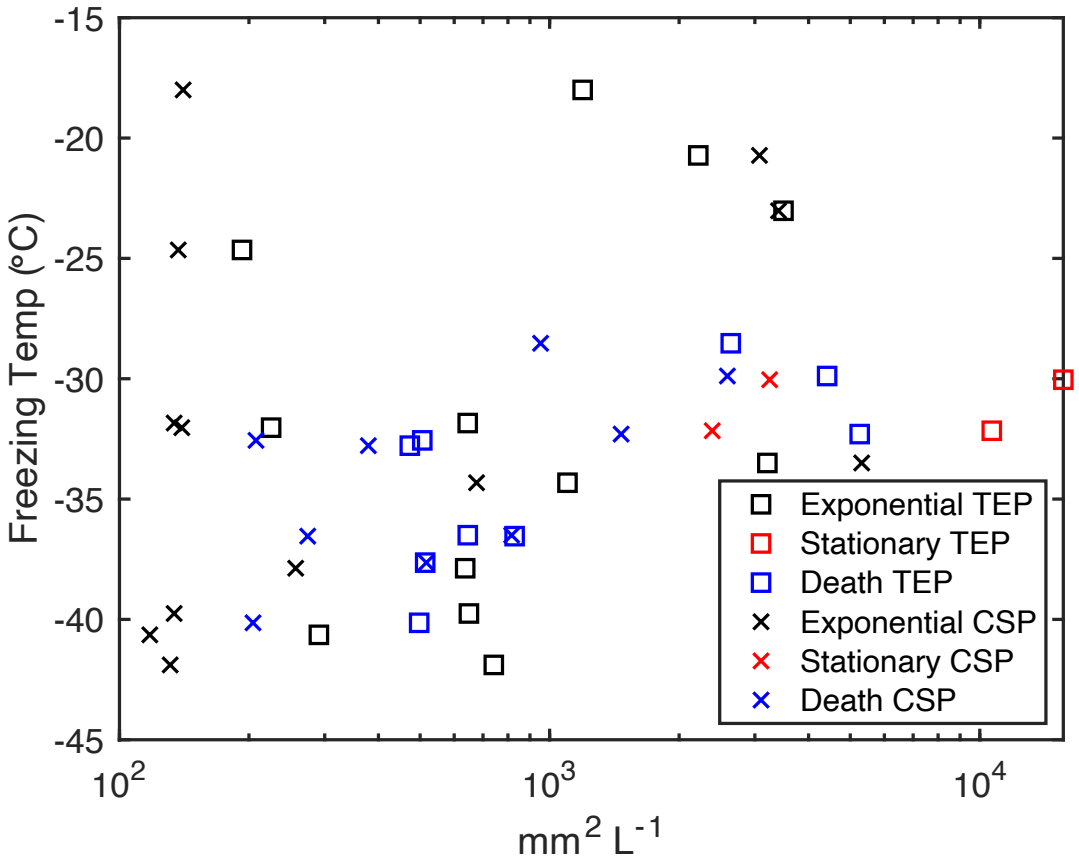

Figure 8.4: Average daily freezing temperatures for three MART experiments, plotted against the average transparent exopolymer (TEP) or Coomassie staining particle (CSP) area on each day. Data from Chapter 3 is plotted in blue, Chapter 4 in red, and Chapter 5 in blue, with TEP data points represented with squares and CSP with x's. Data is from MART experiments containing *Emiliania huxleyi*, *Thalassiosira weissflogii*, and *Synechococcus elongatus*.

However, the high TEP and CSP concentrations produced by *Synechococcus* and *Thalassiosira* did not lead to the higher INP activity that would be observed if the exopolymers were a source of INP. The highest TEP concentrations were seen in stationary phase samples, but these samples froze below -30 °C. There was no

relationship between the highest freezing temperatures observed in exponential phase and the concentration of TEP or CSP.

8.1.3. Marine Phytoplankton Viruses as INP

Two different sizes and three different types of virus were tested for ice nucleation ability: two that infect *Chaetoceros tenuissimus* and one that infects *Emiliania huxleyi*. The *C. tenuissimus* viruses both contained single-stranded genetic material (one with ssRNA and one with ssDNA) and were much smaller than the *E. huxleyi* virus at approximately 20 nm in diameter versus 180 nm in diameter. Both were shaped similarly, with icosahedral capsids lacking tails. Although all three types of virus tested are capable of causing the collapse of a phytoplankton bloom dominated by their respective target species, which could in turn increase aerosolized organic material (O'Dowd et al., 2015) and possibly INP concentrations, the INP activity of the viruses themselves was not clear. The only previous test of viruses as INP (Junge & Swanson, 2007) tested the ice nucleation activity of viruses in an extremely saline solution (more than 5% NaCl) which as shown in Chapter 7 can significantly depress the freezing point.

Results covered in Chapter 6 show that droplets containing marine viruses contain particles that act as INP. Two different concentrations of viruses in desalinated water were tested, and the smaller *C. tenuissimus* viruses froze at nearly identical temperatures (ranging from -21.9 ± 1.7 °C to -25.4 ± 0.6 °C) regardless of concentration. However, there was a concentration difference between the two tested concentrations of the larger *E. huxleyi* viruses, which froze at -24.5 ± 0.6 °C at 10^5 VLP mL^{-1} and -20.8 ± 1.6 °C at 10^8 VLP mL^{-1}. It is possible that the smaller viruses are more efficient INP, as

there was not a concentration effect, but further study is needed. As well, it is important that more than these two groups of viruses are tested. There are several different shapes and sizes of marine viruses that are present in multiple locations globally, and it is likely that large numbers of these viruses are aerosolized in sea spray aerosols (Michaud et al., 2018). If these viruses are capable of acting as INP, not accounting for viruses could lead to major underestimations in the number of INP present in sea spray aerosols.

8.1.4. Cell Growth and Ice Nucleation

When the freezing temperatures of daily aerosol samples taken from MART cultures are considered, there is a clear pattern in the *Thalassiosira*, *Synechococcus,* and *Emiliania* sample data. There are INP produced that raise the freezing temperature of the droplet by up to 15 °C, but those INP are only present at the very beginning of culture growth. After the first three days not only does the freezing temperature decrease, but it decreases to nearly the freezing temperature of pure water on the impactor substrate, which implies that the samples do not contain any INP. This directly contrasts the results from McCluskey et al. (2018) which saw high INP activity during times of phytoplankton population decline.

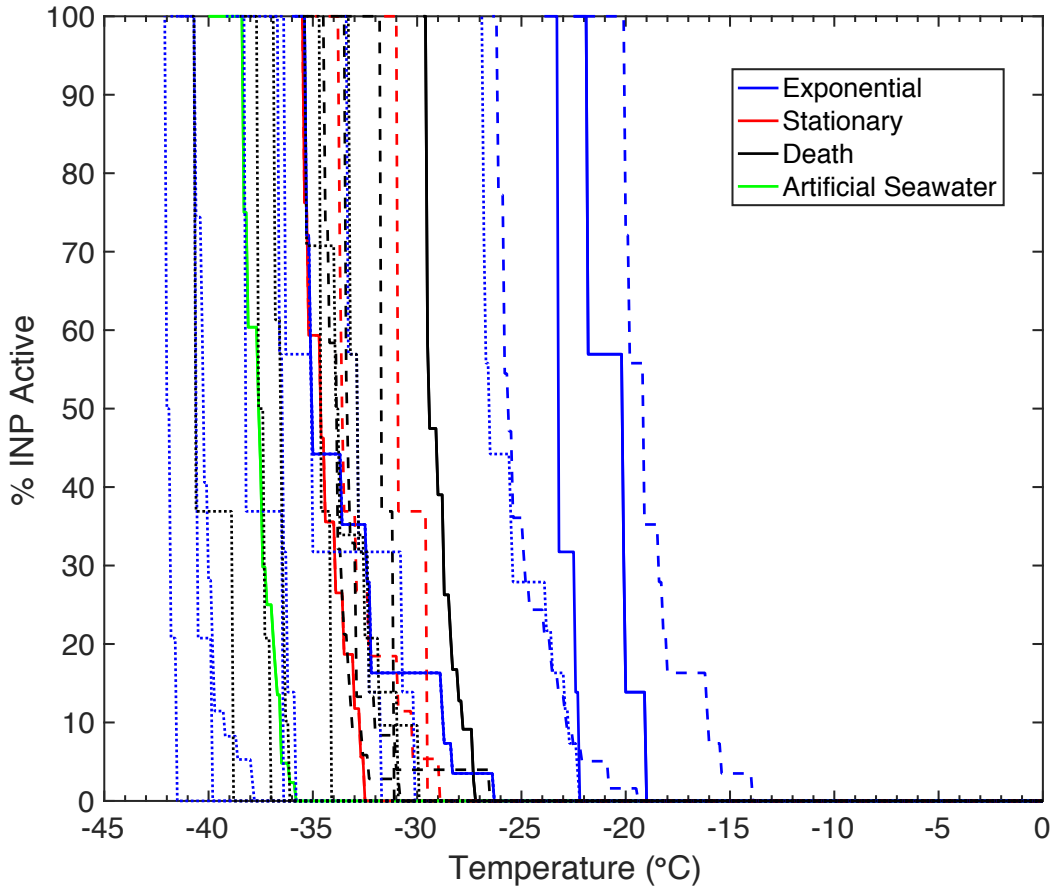

Figure 8.5: Fraction of INP active in each MART sample, separated by growth phase. Exponential phase samples are plotted in blue, stationary phase in red, and death phase in black. Artificial seawater with no organisms or nutrients is plotted in green. Samples containing *Thalassiosira weissflogii* are plotted with solid lines, samples containing *Synechococcus elongatus* are plotted with dashed lines, and samples containing *Emiliania huxleyi* are plotted with dotted lines.

Although growth rates are not significantly correlated with an increase in INP activity, the results in Chapters 3, 4, and 5 show that the best INPs are produced by exponentially growing phytoplankton. Figure 8.5 shows that the first samples to activate as INPs are all taken during exponential phase. However, not all exponential phase

samples contain INPs active at temperatures warmer than -25 °C. Veldhuis et al. (1986) showed that the highest growth rates (typically seen in exponentially growing organisms) are associated with high rates of protein production. However, there is no correlation between the INP activity of aerosols generated from diatoms, cyanobacteria, or coccolithophore species grown in the MART and protein concentrations. This suggests that the INP activity is not related to the entire population of proteins. However. we cannot concluded that the INP produced by phytoplankton are not proteinaceous, especially since the best-known INP produced by bacterial species such as *Pseudomonas syringae* are proteins (Graether & Jia, 2001; Maki et al., 1974; Schmid et al., 1997*)*. Although proteins are a known source of biological INP, faster-growing species (again indicated by growth rate) are also associated with lower N:P ratios and higher P concentrations in nutrient-rich situations which allow the cells to maintain high concentrations of rRNA (Elser et al., 2000; Sterner, 1995). No work has been done currently to determine the INP activity of RNA or other genetic material, but this should be an area of active study in the future.

8.2. Ice Nucleation by Marine Organisms, Organic Material, and Viruses

Comparing all of the median freezing temperatures (shown in Figure 8.5) we can see that each type of sample contained material that acted as moderately efficient INPs.

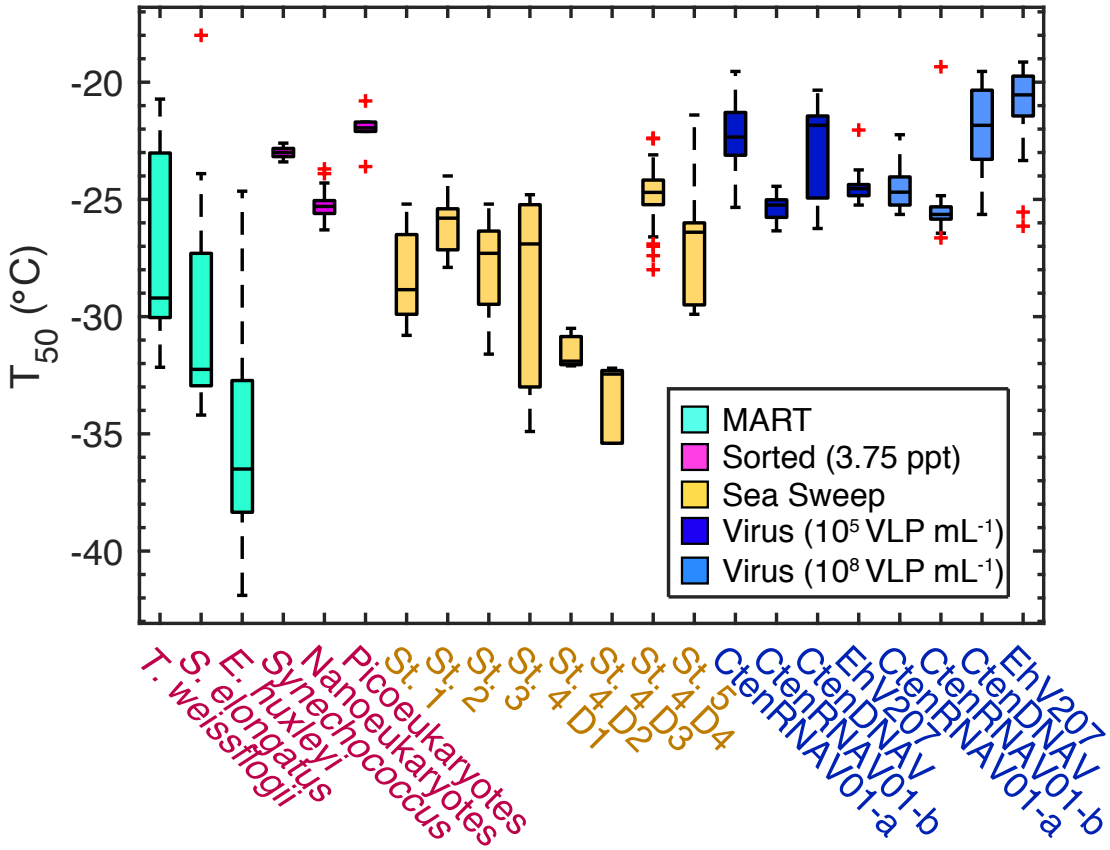

Figure 8.6: Average freezing temperatures of samples from MART experiments, the NAAMES II cruise in the North Atlantic, and three marine phytoplankton viruses. Samples from a specific organism or group are shown in red text. NAAMES station samples are shown in gold text, and viruses are shown in blue text. Boxes show the median freezing temperature (T_{50}, °C) spanned by the first and third quartile. Dashed lines represent the range of freezing temperatures, and outliers are shown with red crosses.

The EhV207 sample containing 10^8 VLP mL^{-1} seawater froze at the highest median temperature of -20.5 °C. The median freezing temperature of the samples generated from the MART containing *Emiliania huxleyi* was the lowest at -36.5 °C, lower than the temperature of homogeneous freezing. This sample also had the largest

range of freezing temperatures, and all three of the MART experiments when taken as a whole had very large ranges of freezing temperatures (more than 10 °C). Although these experiments had very warm freezing temperatures at the beginning of the experiments, the median freezing temperatures are skewed toward the lower end of the freezing range. However, we can also compare the growth phases for these experiments.

8.3. Recommendations for Future Work

Although this work addressed multiple groups and species of phytoplankton, it was by no means comprehensive. One of the largest groups missing from this study is the marine heterotrophic bacteria, which are small enough that whole cells might act as INP (Palumbo, Ferguson, & Rublee, 1984). Heterotrophic bacteria can also reduce the amount of labile organic matter within the surface ocean waters through remineralization, which may in turn reduce the number of INP produced.

In addition, there are thousands of phytoplankton species (Mann & Vanormelingen, 2013; Sournia, Chrdtiennot-Dinet, & Ricard, 1991). Although it would not be feasible or necessary to test every species, there are gaps in which marine phytoplankton phyla have been tested for ice nucleation ability. Two major taxa that are found worldwide are dinoflagellates and green algae. Although there have been studies of aerosol production over dinoflagellate blooms as they produce DMSP (Archer et al., 2013; Steinke, Brading, Kerrison, Warner, & Suggett, 2011), none of these studies have looked for INP production. Based on results from diatoms, cyanobacteria, and coccolithophores there seems to be a pattern in the times when marine phytoplankton produce INP, but further study is needed to clarify if this pattern is present in all species

as well as phytoplankton in natural systems. These measurements should include seasonal marine aerosol samples taken prior to, during, and following a phytoplankton bloom.

Further studies of the aerosolization of dissolved and particulate organic matter and the capacity of this material as INP is also needed. There have been several studies quantifying and describing the composition of dissolved and particulate organic matter as it relates to sea spray aerosols. However, studies determining the chemical composition of INP (either as individual particles or as a population of particles) are sorely lacking. This is primarily because there are limited methods for resolving chemical composition of any INP, let alone marine INPs. A single INP would need to be isolated following confirmation of its INP efficiency and then analyzed. Methods could include Raman spectroscopy, which has previously been used to analyze single particles within a water droplet (Buehler, Allen, & Davis, 1991; Deng, Brooks, Vidaurre, & Thornton, 2014; Sze, Siddique, Sloan, & Escribano, 2001) In addition, a single particle can have multiple components, especially if it is something like a TEP particle, so multiple spectra should be collected from different parts of the particle if there is concern that it contains a mixture of chemical compositions.

The results contained in Chapter 6 are very preliminary and need further confirmation. Although there was a statistical difference between the freezing temperatures of the viruses, their mean freezing temperatures were calculated from a single run on the ice microscope. For statistical validity, at least two more runs should be made with each type of virus. As well, attempts should be made to characterize any

differences between the two CtenRNAV01 samples. Although they were taken from two mass bands it is currently being assumed that they are the same virus, but this is based on analysis of the virus made when it was isolated with the assumption that no contamination has occurred. However, this should be confirmed. More experiments should also be performed with other virus shapes—these results only cover ice nucleation efficiency of icosahedral viruses, but other studies concluded that tailed viruses are not ice-nucleation active (Junge & Swanson, 2007), so a comparison of different virus shapes should be made.

The final step in determining the importance of marine phytoplankton as sources of INPs is to calculate their global importance while including that they are poor INP unless exponentially growing. Preliminary results suggest that viruses are also somewhat efficient INP. All of these results need to be applied globally to determine whether they should be included in global climate models. Increasing ice content in clouds can increase their greenhouse effect, as ice crystals are not opaque enough to reflect shortwave radiation but contain enough water to trap longwave radiation and increase the warming effect of the clouds (Lohmann, Lüönd, & Mahrt, 2016). If phytoplankton and viruses are a source of INPs that has not been accounted for, this could explain some of the uncertainty in aerosol effects on clouds, but this depends on the amount of INPs produced.

8.4. Conclusions

Overall, it is apparent that phytoplankton produce INPs that are active at atmospherically relevant temperatures, although none of the species produce INPs active

at temperatures comparable to the best biological INP (Amato et al., 2015; Maki et al., 1974). In addition, all of the marine viruses tested act as INP, again at atmospherically relevant temperatures. Both phytoplankton INPs and viral INPs have maximum average freezing temperatures between -18.0 °C and -24.5 °C. A freezing temperature 10 °C above the temperature of homogeneous nucleation could lower the altitude of formation of atmospheric ice crystals by approximately 2500 m (Brooks & Thornton, 2018; Russell, 2015), but the growth rate of the phytoplankton population must be considered to determine if they will be effective INP. Although biological INP are unlikely to be a major component of total global INP (Hoose, Kristjansson, & Burrows, 2010), based off the observed freezing temperatures of fast-growing phytoplankton and viruses, they may resolve some of the uncertainties arising from aerosol effects in clean marine conditions. Further study is warranted to determine what characteristics in fast-growing phytoplankton increase the production of INPs.

REFERENCES

Alldredge, A. L., Passow, U., & Logan, B. E. (1993). The abundance and significance of a class of large, transparent organic particles in the ocean. *Deep Sea Research Part I: Oceanographic Research Papers, 40*(6), 1131-1140. https://doi.org/10.1016/0967-0637(93)90129-Q

Aller, J. Y., Kuznetsova, M. R., Jahns, C. J., & Kemp, P. F. (2005). The sea surface microlayer as a source of viral and bacterial enrichment in marine aerosols. *Journal of Aerosol Science, 36*(5–6), 801-812. https://doi.org/10.1016/j.jaerosci.2004.10.012

Aller, J. Y., Radway, J. C., Kilthau, W. P., Bothe, D. W., Wilson, T. W., Vaillancourt, R. D., . . . Knopf, D. A. (2017). Size-resolved characterization of the polysaccharidic and proteinaceous components of sea spray aerosol. *Atmospheric Environment, 154*, 331-347. https://doi.org/10.1016/j.atmosenv.2017.01.053

Alonso, M. C., Jimenez-Gomez, F., Rodriguez, J., & Borrego, J. J. (2001). Distribution of virus-like particles in an oligotrophic marine environment (Alboran Sea, Western Mediterranean). *Microbial Ecology, 42*(3), 407-415. doi:10.1007/s00248-001-0015-y

Alpert, P. A., Aller, J. Y., & Knopf, D. A. (2011a). Ice nucleation from aqueous NaCl droplets with and without marine diatoms. *Atmospheric Chemistry & Physics, 11*(12), 5539-5555. doi:10.5194/acp-11-5539-2011

Alpert, P. A., Aller, J. Y., & Knopf, D. A. (2011b). Initiation of the ice phase by marine biogenic surfaces in supersaturated gas and supercooled aqueous phases. *Physical Chemistry Chemical Physics, 13*(44), 19882-19894. doi:10.1039/c1cp21844a

Amato, P., Joly, M., Schaupp, C., Attard, E., Möhler, O., Morris, C. E., . . . Delort, A. M. (2015). Survival and ice nucleation activity of bacteria as aerosols in a cloud simulation chamber. *Atmospheric Chemistry & Physics Discussions, 15*(3), 4055-4082. doi:10.5194/acpd-15-4055-2015

Andreae, M. O., & Crutzen, P. J. (1997). Atmospheric Aerosols: Biogeochemical Sources and Role in Atmospheric Chemistry. *Science, 276*(5315), 1052. doi:10.1126/science.276.5315.1052

Anning, T., MacIntyre, H. L., Pratt, S. M., Sammes, P. J., Gibb, S., & Geider, R. J. (2000). Photoacclimation in the marine diatom *Skeletonema costatum*. *Limnology and Oceanography, 45*(8), 1807-1817. doi:10.4319/lo.2000.45.8.1807

Arar, E. J. (1997). In vitro determination of chlorophylls *a*, *b*, *c1+ c2* and pheopigments in marine and freshwater algae by visible spectrophotometry. *USEPA Method, 446*(0).

Archer, S., Kimmance, S., Stephens, J., Hopkins, F., Bellerby, R., Schulz, K. G., . . . Engel, A. (2013). Contrasting responses of DMS and DMSP to ocean acidification in Arctic waters. *Biogeosciences, 10*, 1893-1908. doi:10.5194/bg-10-1893-2013

Atkinson, J. D., Murray, B. J., Woodhouse, M. T., Whale, T. F., Baustian, K. J., Carslaw, K. S., . . . Malkin, T. L. (2013). The importance of feldspar for ice nucleation by mineral dust in mixed-phase clouds. *Nature, 498*(7454), 355. doi:10.1038/nature12278

Ault, A. P., Moffet, R. C., Baltrusaitis, J., Collins, D. B., Ruppel, M. J., Cuadra-Rodriguez, L. A., . . . Grassian, V. H. (2013). Size-dependent changes in sea spray aerosol composition and properties with different seawater conditions. *Environmental Science and Technology, 47*(11), 5603-5612. doi:10.1021/es400416g

Baer, S. E., Lomas, M. W., Terpis, K. X., Mouginot, C., & Martiny, A. C. (2017). Stoichiometry of *Prochlorococcus*, *Synechococcus*, and small eukaryotic populations in the western North Atlantic Ocean. *Environmental Microbiology, 19*(4), 1568-1583. doi:10.1111/1462-2920.13672

Balch, W., Kilpatrick, K., M. Holligan, P., & Cucci, T. (1993). *Coccolith production and detachment by Emiliania huxleyi (Prymnesiophyceae)* (Vol. 29).

Barbaro, E., Feltracco, M., Cesari, D., Padoan, S., Zangrando, R., Contini, D., . . . Gambaro, A. (2019). Characterization of the water soluble fraction in ultrafine, fine, and coarse atmospheric aerosol. *Science of the Total Environment, 658*, 1423-1439. https://doi.org/10.1016/j.scitotenv.2018.12.298

Bates, T. S., Quinn, P. K., Frossard, A. A., Russell, L. M., Hakala, J., Petaja, T., . . . Keene, W. C. (2012). Measurements of ocean derived aerosol off the coast of California. *Journal of Geophysical Research-Atmospheres, 117*. doi:10.1029/2012jd017588

Baylor, E., Baylor, M., Blanchard, D. C., Syzdek, L. D., & Appel, C. (1977). Virus transfer from surf to wind. *Science, 198*(4317), 575-580. doi: 10.1126/science.918656

Behrenfeld, M. J., Halsey, K. H., & Milligan, A. J. (2008). Evolved physiological responses of phytoplankton to their integrated growth environment.

Philosophical Transactions of the Royal Society B: Biological Sciences, 363(1504), 2687-2703. https://doi.org/10.1098/rstb.2008.0019

Behrenfeld, M. J., Moore, R. H., Hostetler, C. A., Graff, J., Gaube, P., Russell, L. M., . . . Ziemba, L. (2019). The North Atlantic Aerosol and Marine Ecosystem Study (NAAMES): Science Motive and Mission Overview. *Frontiers in Marine Science, 6*(122). doi:10.3389/fmars.2019.00122

Behrenfeld, M. J., O'Malley, R. T., Siegel, D. A., McClain, C. R., Sarmiento, J. L., Feldman, G. C., . . . Boss, E. S. (2006). Climate-driven trends in contemporary ocean productivity. *Nature, 444*(7120), 752-755. doi:10.1038/nature05317

Beman, J. M., Arrigo, K. R., & Matson, P. A. (2005). Agricultural runoff fuels large phytoplankton blooms in vulnerable areas of the ocean. *Nature, 434*(7030), 211. doi:10.1038/nature03370

Berge, G. (1962). Discoloration of the sea due to *Coccolithus huxleyi* "bloom". *Sarsia, 6*(1), 27-40. https://doi.org/10.1080/00364827.1962.10410259

Bergh, O., Borsheim, K. Y., Bratbak, G., & Heldal, M. (1989). High abundance of viruses found in aquatic environments. *Nature, 340*(6233), 467-468. doi:10.1038/340467a0

Berman-Frank, I., Bidle, K. D., Haramaty, L., & Falkowski, P. G. (2004). The demise of the marine cyanobacterium, *Trichodesmium* spp., via an autocatalyzed cell death pathway. *Limnology and Oceanography, 49*(4), 997-1005. doi:10.4319/lo.2004.49.4.0997

Berman-Frank, I., Rosenberg, G., Levitan, O., Haramaty, L., & Mari, X. (2007). Coupling between autocatalytic cell death and transparent exopolymeric particle production in the marine cyanobacterium *Trichodesmium*. *Environmental Microbiology, 9*(6), 1415-1422. doi:10.1111/j.1462-2920.2007.01257.x

Berner, R. A. (1982). Burial of Organic-Carbon and Pyrite Sulfur in the Modern Ocean - Its Geochemical and Environmental Significance. *American Journal of Science, 282*(4), 451-473. doi:DOI 10.2475/ajs.282.4.451

Bettarel, Y., Kan, J., Wang, K., Williamson, K., Cooney, S., Ribblett, S., . . . Coats, D. (2005). Isolation and preliminary characterisation of a small nuclear inclusion virus infecting the diatom *Chaetoceros cf. gracilis*. *Aquatic Microbial Ecology, 40*(2), 103-114. doi:10.3354/ame040103

Bezdek, H., & Carlucci, A. (1972). Surface concentration of marine bacteria. *Limnology and Oceanography, 17*(4), 566-569. doi: 10.4319/lo.1972.17.4.0566

Bidle, K. D. (2015). The molecular ecophysiology of programmed cell death in marine phytoplankton. *Annual Review of Marine Science, 7*, 341-375. doi:10.1146/annurev-marine-010213-135014

Bidle, K. D., Haramaty, L., Barcelos, E. R. J., & Falkowski, P. (2007). Viral activation and recruitment of metacaspases in the unicellular coccolithophore, *Emiliania huxleyi*. *Proceedings of the National Academy of Science of the United States of America, 104*(14), 6049-6054. doi:10.1073/pnas.0701240104

Blanchard, D. C. (1978). Jet Drop Enrichment of Bacteria, Virus, and Dissolved Organic Material. *Pure and Applied Geophysics, 116*(2-3), 302-308. doi:Doi 10.1007/Bf01636887

Blanchard, D. C., & Woodcock, A. H. (1957). Bubble formation and modification in the sea and its meteorological significance. *Tellus, 9*(2), 145-158. doi:10.3402/tellusa.v9i2.9094

Blanchot, J., & Rodier, M. (1996). Picophytoplankton abundance and biomass in the western tropical Pacific Ocean during the 1992 El Niño year: results from flow cytometry. *Deep Sea Research Part I: Oceanographic Research Papers, 43*(6), 877-895. https://doi.org/10.1016/0967-0637(96)00026-X

Blanchot, J., Rodier, M., & Le Bouteiller, A. (1992). Effect of El Niño Southern Oscillation events on the distribution and abundance of phytoplankton in the Western Pacific Tropical Ocean along 165 E. *Journal of Plankton Research, 14*(1), 137-156. https://doi.org/10.1093/plankt/14.1.137

Bodnar, R. (1993). Revised equation and table for determining the freezing point depression of H_2O-NaCl solutions. *Geochimica et Cosmochimica acta, 57*(3), 683-684. doi: 10.1016/0016-7037(93)90378-A

Bopp, L., Aumont, O., Cadule, P., Alvain, S., & Gehlen, M. (2005). Response of diatoms distribution to global warming and potential implications: A global model study. *Geophysical Research Letters, 32*(19). doi:10.1029/2005gl023653

Bouchard, J. N., & Purdie, D. A. (2011). Effect of Elevated Temperature, Darkness, and Hydrogen Peroxide Treatment on Oxidative Stress and Cell Death in the Bloom-Forming Toxic Cyanobacterium *Microcystis aeruginosa*. *Journal of Phycology, 47*(6), 1316-1325. doi:10.1111/j.1529-8817.2011.01074.x

Boucher, O., Randall, D., Artaxo, P., Bretherton, C., Feingold, G., Forster, P., . . . Lohmann, U. (2013). Clouds and aerosols *Climate change 2013: the physical science basis. Contribution of Working Group I to the Fifth Assessment Report of the Intergovernmental Panel on Climate Change* (pp. 571-657): Cambridge University Press. doi: 10.1017/CBO9781107415324.016

Bown, P. R., Lees, J. A., & Young, J. R. (2004). Calcareous nannoplankton evolution and diversity through time. In H. R. Thierstein & J. R. Young (Eds.), *Coccolithophores: From Molecular Processes to Global Impact* (pp. 481-508). Berlin, Heidelberg: Springer Berlin Heidelberg. https://doi.org/10.1007/978-3-662-06278-4_18

Bradford, M. M. (1976). A rapid and sensitive method for the quantitation of microgram quantities of protein utilizing the principle of protein-dye binding. *Analytical Biochemistry, 72*(1), 248-254. https://doi.org/10.1016/0003-2697(76)90527-3

Bramlette, M. (1958). Significance of coccolithophorids in calcium-carbonate deposition. *Geological Society of America Bulletin, 69*(1), 121-126. https://doi.org/10.1130/0016-7606(1958)69[121:SOCICD]2.0.CO;2

Bratbak, G., Egge, J. K., & Heldal, M. (1993). Viral mortality of the marine alga *Emiliania huxleyi* (Haptophyceae) and termination of algal blooms. *Marine Ecology Progress Series*. https://doi.org/10.3354/meps093039

Bratbak, G., Heldal, M., Norland, S., & Thingstad, T. F. (1990). Viruses as partners in spring bloom microbial trophodynamics. *Applied Environmental Microbiology, 56*(5), 1400-1405.

Bratbak, G., Heldal, M., Thingstad, T. F., & Tuomi, P. (1996). Dynamics of virus abundance in coastal seawater. *FEMS Microbiology Ecology, 19*(4), 263-269. doi:https://doi.org/10.1016/0168-6496(96)00023-2

Bratbak, G., Wilson, W., & Heldal, M. J. (1996). Viral control of *Emiliania huxleyi* blooms? *Journal of Marine Systems, 9*(1-2), 75-81. https://doi.org/10.1016/0924-7963(96)00018-8

Broecker, W. S., Peng, T., Beng, Z., & Observatory, L.-D. G. (1982). *Tracers in the sea*: Lamont-Doherty Geological Observatory, Columbia University.

Brooks, S. D., Suter, K., & Olivarez, L. (2014). Effects of Chemical Aging on the Ice Nucleation Activity of Soot and Polycyclic Aromatic Hydrocarbon Aerosols. *The Journal of Physical Chemistry A, 118*(43), 10036-10047. doi:10.1021/jp508809y

Brooks, S. D., & Thornton, D. C. O. (2018). Marine Aerosols and Clouds. *Annual Review of Marine Science, 10*(1), 289-313. doi:10.1146/annurev-marine-121916-063148

Brown, C. W. (1995). Global distribution of coccolithophore blooms. *Oceanography, 8*(2), 59-60. https://doi.org/10.5670/oceanog.1995.21

Brown, C. W., & Yoder, J. A. (1994). Coccolithophorid Blooms in the Global Ocean. *Journal of Geophysical Research: Oceans, 99*(C4), 7467-7482. doi:10.1029/93jc02156

Brussaard, C. P. (2004). Viral Control of Phytoplankton Populations—a Review 1. *Journal of Eukaryotic Microbiology, 51*(2), 125-138. https://doi.org/10.1111/j.1550-7408.2004.tb00537.x

Buchanan, R. L., Whiting, R. C., & Damert, W. C. (1997). When is simple good enough: a comparison of the Gompertz, Baranyi, and three-phase linear models for fitting bacterial growth curves. *Food Microbiology, 14*(4), 313-326. https://doi.org/10.1006/fmic.1997.0125

Buehler, M. F., Allen, T. M., & Davis, E. J. (1991). Microparticle Raman spectroscopy of multicomponent aerosols. *Journal of Colloid and Interface Science, 146*(1), 79-89. https://doi.org/10.1016/0021-9797(91)90008-V

Bullerjahn, G. S., & Post, A. F. (2014). Physiology and molecular biology of aquatic cyanobacteria. *Frontiers in Microbiology, 5*(359). doi:10.3389/fmicb.2014.00359

Burrows, S. M., Hoose, C., Pöschl, U., & Lawrence, M. G. (2013). Ice nuclei in marine air: biogenic particles or dust? *Atmospheric Chemistry and Physics, 13*(1), 245-267. doi:10.5194/acp-13-245-2013

Calbet, A., & Landry, M. R. (2004). Phytoplankton growth, microzooplankton grazing, and carbon cycling in marine systems. *Limnology and Oceanography, 49*(1), 51-57. doi:10.4319/lo.2004.49.1.0051

Campbell, L., & Vaulot, D. (1993). Photosynthetic picoplankton community structure in the subtropical North Pacific Ocean near Hawaii (station ALOHA). *Deep Sea Research Part I: Oceanographic Research Papers, 40*(10), 2043-2060. doi: 10.1016/0967-0637(93)90044-4

Carlsson, P., & Granéli, E. (1993). Availability of humic bound nitrogen for coastal phytoplankton. *Estuarine, Coastal and Shelf Science, 36*(5), 433-447. https://doi.org/10.1006/ecss.1993.1026

Castberg, T., Thyrhaug, R., Larsen, A., Sandaa, R. A., Heldal, M., Van Etten, J. L., & Bratbak, G. (2002). Isolation and Characterization of a Virus That Infects *Emiliania huxleyi* (Haptophyta) 1. *Journal of Phycology, 38*(4), 767-774. doi:10.1046/j.1529-8817.2002.02015.x

Cavalli, F., Facchini, M., Decesari, S., Mircea, M., Emblico, L., Fuzzi, S., . . . Putaud, J. P. (2004). Advances in characterization of size-resolved organic matter in marine

aerosol over the North Atlantic. *Journal of Geophysical Research: Atmospheres, 109*(D24). doi:10.1029/2004JD005137

Chance, R. J., Hamilton, J. F., Carpenter, L. J., Hackenberg, S. C., Andrews, S. J., & Wilson, T. W. (2018). Water-soluble organic composition of the Arctic sea surface microlayer and association with ice nucleation ability. *Environmental Science & Technology, 52*(4), 1817-1826. doi:10.1021/acs.est.7b04072

Charlson, R. J., Lovelock, J. E., Andreae, M. O., & Warren, S. G. (1987). Oceanic phytoplankton, atmospheric sulphur, cloud albedo and climate. *Nature, 326*(6114), 655-661. doi: 10.1038/326655a0

Chen, J., & Thornton, D. C. (2015). Transparent exopolymer particle production and aggregation by a marine planktonic diatom (*Thalassiosira weissflogii*) at different growth rates. *Journal of Phycology, 51*(2), 381-393. https://doi.org/10.1111/jpy.12285

Clarke, A., D., Owens, S., R., & Zhou, J. (2006). An ultrafine sea-salt flux from breaking waves: Implications for cloud condensation nuclei in the remote marine atmosphere. *Journal of Geophysical Research: Atmospheres, 111*(D6). doi:10.1029/2005JD006565

Clarke, A. D., Owens, S. R., & Zhou, J. (2006). An ultrafine sea-salt flux from breaking waves: Implications for cloud condensation nuclei in the remote marine atmosphere. *Journal of Geophysical Research: Atmospheres, 111*(D6). doi:10.1029/2005JD006565

Coble, P. G. (1996). Characterization of marine and terrestrial DOM in seawater using excitation-emission matrix spectroscopy. *Marine Chemistry, 51*(4), 325-346.

Coble, P. G. (2007). Marine optical biogeochemistry: the chemistry of ocean color. *Chemical Reviews, 107*(2), 402-418. https://doi.org/10.1021/cr050350+

Cohn, S. A., & Weitzell, R. E. (1996). Ecological Considerations of Diatom Cell Motility. I. Characterization of Motility and Adhesion in Four Diatom Species1. *Journal of Phycology, 32*(6), 928-939. doi:10.1111/j.0022-3646.1996.00928.x

Collier, K. N., & Brooks, S. D. (2016). Role of organic hydrocarbons in atmospheric ice formation via contact freezing. *The Journal of Physical Chemistry A, 120*(51), 10169-10180. doi:10.1021/acs.jpca.6b11890

Cooper, W. A., & Vali, G. (1981). The origin of ice in mountain cap clouds. *Journal of The Atmospheric Sciences, 38*, 1244-1259. doi:10.1175/1520-0469(1981)038<1244:TOOIIM>2.0.CO;2

Cory, R. M., & McKnight, D. M. (2005). Fluorescence spectroscopy reveals ubiquitous presence of oxidized and reduced quinones in dissolved organic matter. *Environmental Science & Technology, 39*(21), 8142-8149. doi:10.1021/es0506962

Courault, D., Albert, I., Perelle, S., Fraisse, A., Renault, P., Salemkour, A., & Amato, P. (2017). Assessment and risk modeling of airborne enteric viruses emitted from wastewater reused for irrigation. *Science of the Total Environment, 592*, 512-526. https://doi.org/10.1016/j.scitotenv.2017.03.105

Crawford, I., Möhler, O., Schnaiter, M., Saathoff, H., Liu, D., McMeeking, G., . . . Connolly, P. (2011). Studies of propane flame soot acting as heterogeneous ice nuclei in conjunction with single particle soot photometer measurements. *Atmospheric Chemistry and Physics, 11*(18), 9549-9561. https://doi.org/10.5194/acp-11-9549-2011

Creamean, J. M., Cross, J. N., Pickart, R., McRaven, L., Lin, P., Pacini, A., . . . DeMott, P. J. (2019). Ice nucleating particles carried from below a phytoplankton bloom to the Arctic atmosphere. *Geophysical Research Letters, 46*(14), 8572-8581. doi:10.1029/2019GL083039

Cunliffe, M., Engel, A., Frka, S., Gasparovic, B., Guitart, C., Murrell, J. C., . . . Wurl, O. (2013). Sea surface microlayers: A unified physicochemical and biological perspective of the air-ocean interface. *Progress in Oceanography, 109*, 104-116. doi:10.1016/j.pocean.2012.08.004

Dell'Anno, A., Corinaldesi, C., & Danovaro, R. (2015). Virus decomposition provides an important contribution to benthic deep-sea ecosystem functioning. *Proceedings Of The National Academy Of Sciences Of The United States Of America, 112*(16), E2014-E2019. doi:10.1073/pnas.1422234112

Demott, P. J. (1990). An Exploratory-Study of Ice Nucleation by Soot Aerosols. *Journal of Applied Meteorology, 29*(10), 1072-1079. doi:10.1175/1520-0450(1990)029<1072:Aesoin>2.0.Co;2

DeMott, P. J., Chen, Y., Kreidenweis, S. M., Rogers, D. C., & Sherman, D. E. (1999). Ice formation by black carbon particles. *Geophysical Research Letters, 26*(16), 2429-2432. doi:10.1029/1999gl900580

DeMott, P. J., Hill, T. C., McCluskey, C. S., Prather, K. A., Collins, D. B., Sullivan, R. C., . . . Franc, G. D. (2016). Sea spray aerosol as a unique source of ice nucleating particles. *Proceedings of the National Academy of Science of the United States of America, 113*(21), 5797-5803. doi:10.1073/pnas.1514034112

DeMott, P. J., Mason, R. H., McCluskey, C. S., Hill, T. C. J., Perkins, R. J., Desyaterik, Y., . . . Prather, K. A. (2018). Ice nucleation by particles containing long-chain fatty acids of relevance to freezing by sea spray aerosols. *Environmental Science Process Impacts, 20*(11), 1559-1569. doi:10.1039/c8em00386f

DeMott, P. J., Prenni, A. J., Liu, X., Kreidenweis, S. M., Petters, M. D., Twohy, C. H., …Rogers, D. C. (2010). Predicting global atmospheric ice nuclei distributions and their impacts on climate. *Proceedings of the National Academy of Science of the United States of America, 107*(25), 11217-11222. doi:10.1073/pnas.0910818107

Deng, C. H., Brooks, S. D., Vidaurre, G., & Thornton, D. C. O. (2014). Using Raman Microspectroscopy to Determine Chemical Composition and Mixing State of Airborne Marine Aerosols over the Pacific Ocean. *Aerosol Science and Technology, 48*(2), 193-206. doi:10.1080/02786826.2013.867297

Deng, W., Cruz, B. N., & Neuer, S. (2016). Effects of nutrient limitation on cell growth, TEP production and aggregate formation of marine Synechococcus. *Aquatic Microbial Ecology, 78*(1), 39-49. doi:10.3354/ame01803

Diehl, K., Matthias-Maser, S., Jaenicke, R., & Mitra, S. K. (2002). The ice nucleating ability of pollen:: Part II. Laboratory studies in immersion and contact freezing modes. *Atmospheric Research, 61*(2), 125-133. http://dx.doi.org/10.1016/S0169-8095(01)00132-6

Diehl, K., & Mitra, S. K. (1998). A laboratory study of the effects of a kerosene-burner exhaust on ice nucleation and the evaporation rate of ice crystals. *Atmospheric Environment, 32*(18), 3145-3151. doi:10.1016/S1352-2310(97)00467-6

DiTullio, G. R., Hutchins, D. A., & Bruland, K. W. (1993). Interaction of iron and major nutrients controls phytoplankton growth and species composition in the tropical North Pacific Ocean. *Limnology and Oceanography, 38*(3), 495-508. https://doi.org/10.4319/lo.1993.38.3.0495

Duarte, C. M., & Cebrián, J. (1996). The fate of marine autotrophic production. *Limnology and Oceanography, 41*(8), 1758-1766. doi:10.4319/lo.1996.41.8.1758

Dubinsky, Z., & Stambler, N. (2009). Photoacclimation processes in phytoplankton: mechanisms, consequences, and applications. *Aquatic Microbial Ecology, 56*(2-3), 163-176. doi:10.3354/ame01345

DuBois, M., Gilles, K. A., Hamilton, J. K., Rebers, P. A., & Smith, F. (1956). Colorimetric Method for Determination of Sugars and Related Substances. *Analytical Chemistry, 28*(3), 350-356. doi:10.1021/ac60111a017

Dugdale, R. C., & Wilkerson, F. P. (1998). Silicate regulation of new production in the equatorial Pacific upwelling. *Nature, 391*(6664), 270. https://doi.org/10.1038/34630

DuRand, M. D., Olson, R. J., & Chisholm, S. W. (2001). Phytoplankton population dynamics at the Bermuda Atlantic Time-series station in the Sargasso Sea. *Deep-Sea Research Part II-Topical Studies in Oceanography, 48*(8-9), 1983-2003. doi:10.1016/S0967-0645(00)00166-1

Durant, A. J., & Shaw, R. A. (2005). Evaporation freezing by contact nucleation inside-out. *Geophysical Research Letters, 32*(20). doi:10.1029/2005gl024175

Durant, A. J., Shaw, R. A., Rose, W. I., Mi, Y., & Ernst, G. G. J. (2008). Ice nucleation and overseeding of ice in volcanic clouds. *Journal of Geophysical Research: Atmospheres, 113*(D9). doi:10.1029/2007JD009064

Dvořák, P., Casamatta, D. A., Poulíčková, A., Hašler, P., Ondřej, V., & Sanges, R. (2014). *Synechococcus*: 3 billion years of global dominance. *Molecular Ecology, 23*(22), 5538-5551. doi:10.1111/mec.12948

Dvořák, P., Hindák, F., Hašler, P., Hindakova, A., & Poulíčková, A. (2014). Morphological and molecular studies of *Neosynechococcus sphagnicola*, *gen*. et *sp*. nov. (Cyanobacteria, Synechococcales). *Phytotaxa, 170*(1), 24-34. http://dx.doi.org/10.11646/phytotaxa.170.1.3

Elser, J., Sterner, R., Gorokhova, E. a., Fagan, W., Markow, T., Cotner, J., . . . Weider, L. (2000). Biological stoichiometry from genes to ecosystems. *Ecology Letters, 3*(6), 540-550. https://doi.org/10.1111/j.1461-0248.2000.00185.x

Emerson, S., & Hedges, J. (2008). *Chemical oceanography and the marine carbon cycle*: Cambridge University Press.

Engel, A., Bange, H. W., Cunliffe, M., Burrows, S. M., Friedrichs, G., Galgani, L., . . . Zäncker, B. (2017). The Ocean's Vital Skin: Toward an Integrated Understanding of the Sea Surface Microlayer. *Frontiers in Marine Science, 4*(165). doi:10.3389/fmars.2017.00165

Eppley, R. W. (1972). Temperature and phytoplankton growth in the sea. *Fishery bulletin, 70*(4), 1063-1085.

Erez, Z., Steinberger-Levy, I., Shamir, M., Doron, S., Stokar-Avihail, A., Peleg, Y., . . . Sorek, R. (2017). Communication between viruses guides lysis-lysogeny decisions. *Nature, 541*(7638), 488-493. doi:10.1038/nature21049

Erwin, P. M., & Thacker, R. W. (2008). Cryptic diversity of the symbiotic cyanobacterium *Synechococcus spongiarum* among sponge hosts. *Molecular Ecology, 17*(12), 2937-2947. https://doi.org/10.1111/j.1365-294X.2008.03808.x

Failor, K. C., Schmale III, D. G., Vinatzer, B. A., & Monteil, C. L. (2017). Ice nucleation active bacteria in precipitation are genetically diverse and nucleate ice by employing different mechanisms. *The ISME Journal, 11*, 2740. doi:10.1038/ismej.2017.124

Falkowski, Scholes, R. J., Boyle, E., Canadell, J., Canfield, D., Elser, J., . . . Steffen, W. (2000). The global carbon cycle: a test of our knowledge of earth as a system. *Science, 290*(5490), 291-296. doi:10.1126/science.290.5490.291

Falkowski, P., Barber, R. T., & Smetacek, V. V. (1998). Biogeochemical Controls and Feedbacks on Ocean Primary Production. *Science, 281*(5374), 200-207. doi:10.1126/science.281.5374.200

Falkowski, P. G. (1980). Light-shade adaptation in marine phytoplankton *Primary productivity in the sea* (pp. 99-119): Springer.

Fall, R., & Schnell, R. C. (1985). Association of an ice-nucleating pseudomonad with cultures of the marine dinoflagellate, *Heterocapsa niei*. *Journal of Marine Research*, *43*(1), 257-265. doi: 0.1357/002224085788437370

Fan, S. M., Moxim, W. J., & Levy, H. (2006). Aeolian input of bioavailable iron to the ocean. *Geophysical Research Letters, 33*(7). doi: 10.1029/2005GL024852

Fay, P. (1992). Oxygen relations of nitrogen fixation in cyanobacteria. *Microbiological Reviews, 56*(2), 340-373.

Ferguson, R. L., Collier, A., & Meeter, D. A. (1976). Growth response of *Thalassiosira pseudonana* Hasle and Heimdal clone 3H to illumination, temperature and nitrogen source. *Chesapeake Science, 17*(3), 148-158. https://doi.org/10.2307/1351192

Field, C. B., Behrenfeld, M. J., Randerson, J. T., & Falkowski, P. (1998). Primary production of the biosphere: integrating terrestrial and oceanic components. *Science, 281*(5374), 237-240. doi:10.1126/science.281.5374.237

Field, P. R., Heymsfield, A. J., Shipway, B. J., DeMott, P. J., Pratt, K. A., Rogers, D. C., . . . Prather, K. A. (2012). Ice in Clouds Experiment-Layer Clouds. Part II: Testing Characteristics of Heterogeneous Ice Formation in Lee Wave Clouds. *Journal of the Atmospheric Sciences, 69*(3), 1066-1079. doi:10.1175/Jas-D-11-026.1

Fletcher, N. H. (1969). Active Sites and Ice Crystal Nucleation. *Journal of the Atmospheric Sciences, 26*(6), 1266-1271. doi:10.1175/1520-0469(1969)026<1266:ASAICN>2.0.CO;2

Flombaum, P., Gallegos, J. L., Gordillo, R. A., Rincon, J., Zabala, L. L., Jiao, N., . . . Martiny, A. C. (2013). Present and future global distributions of the marine Cyanobacteria *Prochlorococcus* and *Synechococcus*. *Proceedings of the National Academy of Sciences of the United States of America, 110*(24), 9824-9829. doi:10.1073/pnas.1307701110

Fornea, A. P., Brooks, S. D., Dooley, J. B., & Saha, A. (2009). Heterogeneous freezing of ice on atmospheric aerosols containing ash, soot, and soil. *Journal of Geophysical Research. Atmospheres, 114*(D13), https://doi.org/10.1029/2009JD011958

Frada, M., Probert, I., Allen, M. J., Wilson, W. H., & de Vargas, C. (2008). The "Cheshire Cat" escape strategy of the coccolithophore *Emiliania huxleyi* in response to viral infection. *Proceedings of the National Academy of Sciences, 105*(41), 15944-15949. https://doi.org/10.1073/pnas.0807707105

Frada, M. J., Bidle, K. D., Probert, I., & de Vargas, C. (2012). In situ survey of life cycle phases of the coccolithophore *Emiliania huxleyi* (Haptophyta). *Environmental Microbiology, 14*(6), 1558-1569. doi: 10.1111/j.1462-2920.2012.02745.x

Franklin, D. J., Airs, R. L., Fernandes, M., Bell, T. G., Bongaerts, R. J., Berges, J. A., & Malin, G. (2012). Identification of senescence and death in Emiliania huxleyi and *Thalassiosira pseudonana*: Cell staining, chlorophyll alterations, and dimethylsulfoniopropionate (DMSP) metabolism. *Limnology and Oceanography, 57*(1), 305-317. doi:10.4319/lo.2012.57.1.0305

Frey, B. E., & Small, L. F. (1980). Effects of micro-nutrients and major nutrients on natural phytoplankton populations. *Journal of Plankton Research, 2*(1), 1-22. https://doi.org/10.1093/plankt/2.1.1

Friedman, B., Kulkarni, G., Beránek, J., Zelenyuk, A., Thornton, J. A., & Cziczo, D. J. (2011). Ice nucleation and droplet formation by bare and coated soot particles. *Journal of Geophysical Research: Atmospheres, 116*(D17). https://doi.org/10.1029/2011JD015999

Fröhlich-Nowoisky, J., Kampf, C. J., Weber, B., Huffman, J. A., Pöhlker, C., Andreae, M. O., . . . Pöschl, U. (2016). Bioaerosols in the Earth system: Climate, health, and ecosystem interactions. *Atmospheric Research, 182*, 346-376. https://doi.org/10.1016/j.atmosres.2016.07.018

Frossard, A. A., Russell, L. M., Burrows, S. M., Elliott, S. M., Bates, T. S., & Quinn, P. K. (2014). Sources and composition of submicron organic mass in marine aerosol particles. *Journal of Geophysical Research: Atmospheres, 119*(22), 12,977-913,003. doi:10.1002/2014JD021913

Fukao, T., Kimoto, K., & Kotani, Y. (2010). Production of transparent exopolymer particles by four diatom species. *Fisheries Science, 76*(5), 755-760.

Fukuta, N. (1958). Experimental investigations on the ice-forming ability of various chemical substances. *Journal of Meteorology, 15*(1), 17-26. doi:10.1175/1520-0469(1958)015<0017:Eiotif>2.0.Co;2

Fullerton, C. M., Garcia, C., & Langer, G. (1975). Nine months of ice nucleus monitoring at Mauna Loa, Hawaii. *Meteorologische Rundschau, 28*, 178-190.

Furey, P. C., Lowe, R. L., & Johansen, J. R. (2007). Wet wall algal community response to in-field nutrient manipulation in the Great Smoky Mountains National Park, USA. *Algological Studies, 125*(1), 17-43. https://doi.org/10.1127/1864-1318%2F11%2F0125-017

Gantt, B., & Meskhidze, N. (2013). The physical and chemical characteristics of marine primary organic aerosol: a review. *Atmospheric Chemistry and Physics, 13*(8), 3979-3996. doi:10.5194/acp-13-3979-2013

Garcia, H. E., & Gordon, L. I. (1992). Oxygen solubility in seawater: Better fitting equations. *Limnology and Oceanography*, 37(6), 1307-1312. doi:10.4319/lo.1992.37.6.1307

Gobler, C. J., Hutchins, D. A., Fisher, N. S., Cosper, E. M., & Saňudo-Wilhelmy, S. A. (1997). Release and bioavailability of C, N, P Se, and Fe following viral lysis of a marine chrysophyte. *Limnology and Oceanography, 42*(7), 1492-1504. https://doi.org/10.4319/lo.1997.42.7.1492

Gokhale, N. R., & Goold Jr, J. (1968). Droplet freezing by surface nucleation. *Journal of Applied Meteorology, 7*(5), 870-874. https://doi.org/10.1175/1520-0450(1968)007%3C0870:DFBSN%3E2.0.CO;2

Goldman, J. C. (1980). Physiological processes, nutrient availability, and the concept of relative growth rate in marine phytoplankton ecology *Primary productivity in the sea* (pp. 179-194): Springer.

Gowing, M. M. (1993). Large virus-like particles from vacuoles of phaeodarian radiolarians and from other marine samples. *Marine Ecology-Progress Series, 101*, 33-33.

Graether, S. P., & Jia, Z. (2001). Modeling *Pseudomonas syringae* ice-nucleation protein as a β-helical protein. *Biophysical journal, 80*(3), 1169-1173. https://doi.org/10.1016/S0006-3495(01)76093-6

Graff, J. R., & Behrenfeld, M. J. (2018). Photoacclimation responses in subarctic Atlantic phytoplankton following a natural mixing-restratification event. *Frontiers in Marine Science 5*(209). doi:10.3389/fmars.2018.00209

Graff, J. R., Milligan, A. J., & Behrenfeld, M. J. (2012). The measurement of phytoplankton biomass using flow-cytometric sorting and elemental analysis of carbon. *Limnology and Oceanography: Methods, 10*(11), 910-920. doi:10.4319/lom.2012.10.910

Graff, J. R., Westberry, T. K., Milligan, A. J., Brown, M. B., Dall'Olmo, G., Dongen-Vogels, V. v., . . . Behrenfeld, M. J. (2015). Analytical phytoplankton carbon measurements spanning diverse ecosystems. *Deep Sea Research Part I: Oceanographic Research Papers, 102*, 16-25. doi:http://dx.doi.org/10.1016/j.dsr.2015.04.006

Graham, L. E., Graham, J. M., Wilcox, L. W., & Cook, M. E. (2016). Photosynthetic Stramenopiles I *Algae* (3rd ed., pp. 233-261): Benjamin Cummings.

Guillard, R. R., & Sieracki, M. S. (2005). Counting cells in cultures with the light microscope. In R. A. Andersen (Ed.), *Algal culturing techniques* (pp. 239-252): Elsevier Academic Press.

Hader, J. D., Wright, T. P., & Petters, M. D. (2014). Contribution of pollen to atmospheric ice nuclei concentrations. *Atmospheric Chemistry and Physics, 14*(11), 5433-5449. doi:10.5194/acp-14-5433-2014

Hara, S., Terauchi, K., & Koike, I. (1991). Abundance of viruses in marine waters: assessment by epifluorescence and transmission electron microscopy. *Applied and Environmental Microbiology, 57*(9), 2731-2734.

Harrison, P. J., Waters, R. E., & Taylor, F. J. R. (1980). A broad spectrum artificial sea water medium for coastal and open ocean phytoplankton1. *Journal of Phycology, 16*(1), 28-35. doi:10.1111/j.0022-3646.1980.00028.x

Heymsfield, A. J., & Sabin, R. M. (1989). Cirrus crystal nucleation by homogeneous freezing of solution droplets. *Journal of the Atmospheric Sciences, 46*(14), 2252-2264. doi:10.1175/1520-0469(1989)046<2252:Ccnbhf>2.0.Co;2

Hill, T. C. J., Moffett, B. F., DeMott, P. J., Georgakopoulos, D. G., Stump, W. L., & Franc, G. D. (2014). Measurement of ice nucleation-active bacteria on plants and

in precipitation by quantitative PCR. *Applied and Environmental Microbiology 80*(4), 1256-1267. doi:10.1128/AEM.02967-13

Hiranuma, N., Adachi, K., Bell, D. M., Belosi, F., Beydoun, H., Bhaduri, B., . . . Mohler, O. (2019). A comprehensive characterization of ice nucleation by three different types of cellulose particles immersed in water. *Atmospheric Chemistry and Physics, 19*(7), 4823-4849. doi:10.5194/acp-19-4823-2019

Hiranuma, N., Mohler, O., Yamashita, K., Tajiri, T., Saito, A., Kiselev, A., . . . Murakami, M. (2015). Ice nucleation by cellulose and its potential contribution to ice formation in clouds. *Nature Geoscience, 8*(4), 273-277. doi:10.1038/Ngeo2374

Hogan, A. W. (1967). Ice nuclei from direct reaction of iodine vapor with vapors from leaded gasoline. *Science, 158*(3802), 800-800. doi:10.1126/science.158.3802.800

Hogg, S. (2005). *Essential Microbiology*: John Wiley & Sons.

Holligan, P., Viollier, M., Harbour, D., Camus, P., & Champagne-Philippe, M. (1983). Satellite and ship studies of coccolithophore production along a continental shelf edge. *Nature, 304*(5924), 339. https://doi.org/10.1038/304339a0

Holligan, P. M., Fernández, E., Aiken, J., Balch, W. M., Boyd, P., Burkill, P. H., . . . van der Wal, P. (1993). A biogeochemical study of the coccolithophore, *Emiliania huxleyi*, in the North Atlantic. *Global Biogeochemical Cycles, 7*(4), 879-900. doi:10.1029/93gb01731

Hooker, S. B., Van Heukelem, L., Thomas, C. S., Claustre, H., Ras, J., Barlow, R., . . . Trees, C. (2005). The second SeaWiFS HPLC analysis round-robin experiment (SeaHARRE-2). *NASA Technical Memo, 212785*, 124.

Hoose, C., Kristjansson, J. E., & Burrows, S. M. (2010). How important is biological ice nucleation in clouds on a global scale? *Environmental Research Letters, 5*(2). doi:10.1088/1748-9326/5/2/024009

Hoose, C., Kristjansson, J. E., Chen, J. P., & Hazra, A. (2010). A Classical-Theory-Based Parameterization of Heterogeneous Ice Nucleation by Mineral Dust, Soot, and Biological Particles in a Global Climate Model. *Journal of the Atmospheric Sciences, 67*(8), 2483-2503. doi:10.1175/2010jas3425.1

Hoose, C., & Mohler, O. (2012). Heterogeneous ice nucleation on atmospheric aerosols: a review of results from laboratory experiments. *Atmospheric Chemistry and Physics, 12*(20), 9817-9854. doi:10.5194/acp-12-9817-2012

Hoppe, H. G. (1983). Significance of exoenzymatic activities in the ecology of brackish water - measurements by means of methylumbelliferyl-substrates. *Marine Ecology Progress Series, 11*(3), 299-308. doi:10.3354/meps011299

Hou, J.-J., Huang, B.-Q., Cao, Z.-R., Chen, J.-X., & Hong, H.-S. (2007). Effects of Nutrient limitation on pigments in *Thalassiosira weissflogii* and *Prorocentrum donghaiense*. *49*(5), 686-697. doi:10.1111/j.1744-7909.2007.00449.x

Hoyle, C. R., Pinti, V., Welti, A., Zobrist, B., Marcolli, C., Luo, B., . . . Peter, T. (2011). Ice nucleation properties of volcanic ash from Eyjafjallajökull. *Atmospheric Chemistry and Physics, 11*(18), 9911-9926. doi:10.5194/acp-11-9911-2011

Huang, W. T. K., Ickes, L., Tegen, I., Rinaldi, M., Ceburnis, D., & Lohmann, U. (2018). Global relevance of marine organic aerosol as ice nucleating particles. *Atmospheric Chemistry and Physics, 18*(15), 11423-11445. doi:10.5194/acp-18-11423-2018

Huguet, A., Vacher, L., Relexans, S., Saubusse, S., Froidefond, J. M., & Parlanti, E. (2009). Properties of fluorescent dissolved organic matter in the Gironde Estuary. *Organic Geochemistry, 40*(6), 706-719. https://doi.org/10.1016/j.orggeochem.2009.03.002

Hunter, K. A. (1997). Chemistry of the sea-surface microlayer. *The sea surface and global change*, 287-319. Cambridge University Press https://doi.org/10.1017/CBO9780511525025.010

Iannone, R., Chernoff, D., Pringle, A., Martin, S., & Bertram, A. (2011). The ice nucleation ability of one of the most abundant types of fungal spores found in the atmosphere. *Atmospheric Chemistry and Physics, 11*(3), 1191-1201. http://dx.doi.org/10.5194/acp-11-1191-2011

Iglesias-Rodriguez, M. D., Halloran, P. R., Rickaby, R. E., Hall, I. R., Colmenero-Hidalgo, E., Gittins, J. R., . . . Boessenkool, K. P. (2008). Phytoplankton calcification in a high-CO_2 world. *Science, 320*(5874), 336-340. doi:10.1126/science.1154122

Iglesias-Rodríguez, M. D., Brown, C. W., Doney, S. C., Kleypas, J., Kolber, D., Kolber, Z., . . . Falkowski, P. G. (2002). Representing key phytoplankton functional groups in ocean carbon cycle models: Coccolithophorids. *Global Biogeochemical Cycles, 16*(4), 47-41-47-20. http://dx.doi.org/10.5194/acp-11-1191-2011

Irish, V. E., Elizondo, P., Chen, J., Chou, C., Charette, J., Lizotte, M., . . . Bertram, A. K. (2017). Ice-nucleating particles in Canadian Arctic sea-surface microlayer and bulk seawater. *Atmospheric Chemistry and Physics, 17*(17), 10583-10595. doi:10.5194/acp-17-10583-2017

Irish, V. E., Hanna, S. J., Willis, M. D., China, S., Thomas, J. L., Wentzell, J. J. B., . . . Bertram, A. K. (2019). Ice nucleating particles in the marine boundary layer in the Canadian Arctic during summer 2014. *Atmospheric Chemistry and Physics, 19*(2), 1027-1039. doi:10.5194/acp-19-1027-2019

Irish, V. E., Hanna, S. J., Xi, Y., Boyer, M., Polishchuk, E., Ahmed, M., . . . Bertram, A. K. (2019). Revisiting properties and concentrations of ice-nucleating particles in the sea surface microlayer and bulk seawater in the Canadian Arctic during summer. *Atmospheric Chemistry and Physics, 19*(11), 7775-7787. doi:10.5194/acp-19-7775-2019

Jacquet, S., Heldal, M., Iglesias-Rodriguez, D., Larsen, A., Wilson, W., & Bratbak, G. (2002). Flow cytometric analysis of an *Emiliana huxleyi* bloom terminated by viral infection. *Aquatic Microbial Ecology, 27*(2), 111-124. doi:10.3354/ame027111

Jeffrey, S. W., & Humphrey, G. F. (1975). New spectrophotometric equations for determining chlorophylls *a, b, c1* and *c2* in higher plants, algae and natural phytoplankton. *Biochemie und Physiologie der Pflanzen, 167*(2), 191-194. https://doi.org/10.1016/S0015-3796(17)30778-3

Jensen, E. J., & Toon, O. B. (1997). The potential impact of soot particles from aircraft exhaust on cirrus clouds. *Geophysical Research Letters, 24*(3), 249-252. doi:10.1029/96gl03235

Jiang, S. C., & Paul, J. H. (1994). Seasonal and diel abundance of viruses and occurrence of lysogeny/bacteriocinogeny in the marine environment. *Marine Ecology Progress Series, 104*(1), 163-172. doi: 10.3354/meps104163

Jiao, N., Herndl, G. J., Hansell, D. A., Benner, R., Kattner, G., Wilhelm, S. W., . . . Azam, F. (2010). Microbial production of recalcitrant dissolved organic matter: long-term carbon storage in the global ocean. *Nature Reviews Microbiology, 8*(8), 593-599. doi:10.1038/nrmicro2386

Jochem, F. (1988). On the distribution and importance of picocyanobacteria in a boreal inshore area (Kiel Bight, Western Baltic). *Journal of Plankton Research, 10*(5), 1009-1022. doi: 10.1093/plankt/10.5.1009

Johansen, J. R. (2010). Diatoms of aerial habitats *The diatoms: applications for the environmental and earth sciences* (Vol. 465).

Junge, K., & Swanson, B. D. (2007). High-resolution ice nucleation spectra of sea-ice bacteria: implications for cloud formation and life in frozen environments. *Biogeosciences Discussions, 4*(6), 4261-4282. https://doi.org/10.5194/bg-5-865-2008

Kalbitz, K., Geyer, S., & Geyer, W. (2000). A comparative characterization of dissolved organic matter by means of original aqueous samples and isolated humic substances. *Chemosphere, 40*(12), 1305-1312. http://dx.doi.org/10.1016/S0045-6535(99)00238-6

Kalbitz, K., Geyer, W., & Geyer, S. (1999). Spectroscopic properties of dissolved humic substances—a reflection of land use history in a fen area. *Biogeochemistry, 47*(2), 219-238. https://doi.org/10.1007/bf00994924

Kanji, Z. A., Ladino, L. A., Wex, H., Boose, Y., Burkert-Kohn, M., Cziczo, D. J., & Kramer, M. (2017). Overview of Ice Nucleating Particles. *Ice Formation and Evolution in Clouds and Precipitation: Measurement and Modeling Challenges, 58*, 1.1-1.33. doi:10.1175/Amsmonographs-D-16-0006.1

Keene, W. C., Maring, H., Maben, J. R., Kieber, D. J., Pszenny, A. A., Dahl, E. E., . . . Zhou, X. (2007). Chemical and physical characteristics of nascent aerosols produced by bursting bubbles at a model air-sea interface. *Journal of Geophysical Research: Atmospheres, 112*(D21). doi: 10.1029/2007JD008464

Kegel, J. U., John, U., Valentin, K., & Frickenhaus, S. (2013). Genome variations associated with viral susceptibility and calcification in *Emiliania huxleyi*. *PLOS ONE, 8*(11), e80684. doi:10.1371/journal.pone.0080684

Keller, M. D. (1989). Dimethyl sulfide production and marine phytoplankton: the importance of species composition and cell size. *Biological oceanography, 6*(5-6), 375-382. doi: 10.1021/bk-1989-0393.ch011

Kieft, T. L. (1988). Ice nucleation activity in lichens. *Appl Environ Microbiol, 54*(7), 1678-1681.

Kieft, T. L., & Ahmadjian, V. (1989). Biological ice nucleation activity in lichen mycobionts and photobionts. *Lichenologist, 21*(4), 355-362. doi:10.1017/S0024282989000599

Kim, H., Orser, C., Lindow, S., & Sands, D. (1987). *Xanthomonas campestris* pv. *translucens* strains active in ice nucleation. *Plant Disease, 71*(11), 994-997. doi: 10.1094/PD-71-0994

Kinsey, J. D., Corradino, G., Ziervogel, K., Schnetzer, A., & Osburn, C. L. (2018). Formation of Chromophoric Dissolved Organic Matter by Bacterial Degradation of Phytoplankton-Derived Aggregates. *Frontiers in Marine Science, 4*(430). doi:10.3389/fmars.2017.00430

Kiselev, A., Bachmann, F., Pedevilla, P., Cox, S. J., Michaelides, A., Gerthsen, D., & Leisner, T. (2017). Active sites in heterogeneous ice nucleation—the example of K-rich feldspars. *Science, 355*(6323), 367-371. doi:10.1126/science.aai8034

Klughammer, C., & Schreiber, U. (2008). Complementary PS II quantum yields calculated from simple fluorescence parameters measured by PAM fluorometry and the Saturation Pulse method. *PAM Application Notes, 1*(2), 201-247.

Knopf, D. A., Alpert, P. A., & Wang, B. (2018). The Role of Organic Aerosol in Atmospheric ice nucleation: A review. *ACS Earth and Space Chemistry, 2*(3), 168-202. doi:10.1021/acsearthspacechem.7b00120

Knopf, D. A., Alpert, P. A., Wang, B., & Aller, J. Y. (2011). Stimulation of ice nucleation by marine diatoms. *Nature Geosciences, 4*(2), 88-90. doi: 10.1038/ngeo1037

Knopf, D. A., Alpert, P. A., Wang, B., O'Brien, R. E., Kelly, S. T., Laskin, A., . . . Moffet, R. C. (2014). Microspectroscopic imaging and characterization of individually identified ice nucleating particles from a case field study. *Journal of Geophysical Research: Atmospheres, 119*(17), 10,365-310,381. https://doi.org/10.1002/2014JD021866

Knopf, D. A., Wang, B., Laskin, A., Moffet, R. C., & Gilles, M. K. (2010). Heterogeneous nucleation of ice on anthropogenic organic particles collected in Mexico City. *Geophysical Research Letters, 37*(11). doi:10.1029/2010gl043362

Kociolek, J. P., Stepanek, J. G., Lowe, R. L., Johansen, J. R., & Sherwood, A. R. (2013). Molecular data show the enigmatic cave-dwelling diatom *Diprora* (Bacillariophyceae) to be a raphid diatom. *European Journal of Phycology, 48*(4), 474-484. doi: 0.1080/09670262.2013.860239

Komurcu, M., Storelvmo, T., Tan, I., Lohmann, U., Yun, Y., Penner, J. E., . . . Takemura, T. (2014). Intercomparison of the cloud water phase among global climate models. *Journal of Geophysical Research: Atmospheres, 119*(6), 3372-3400. https://doi.org/10.1002/2013JD021119

Kong, X., Wolf, M. J., Roesch, M., Thomson, E. S., Bartels-Rausch, T., Alpert, P. A., . . . Cziczo, D. J. (2018). A continuous flow diffusion chamber study of sea salt particles acting as cloud nuclei: deliquescence and ice nucleation. *Tellus B: Chemical and Physical Meteorology, 70*(1), 1463806. doi:10.1080/16000889.2018.1463806

Kono, T. (1968). Kinetics of microbial cell growth. *Biotechnology and Bioengineering, 10*(2), 105-131. doi:10.1002/bit.260100202

Kooistra, W., Gersonde, R., Medlin, L., & Mann, D. (2007). *The Origin and Evolution of the Diatoms. Their Adaptation to a Planktonic Existence*.

Koop, T. (2004). Homogeneous ice nucleation in water and aqueous solutions. *Zeitschrift Fur Physikalische Chemie-International Journal of Research in Physical Chemistry & Chemical Physics, 218*(11), 1231-1258. doi:10.1524/zpch.218.11.1231.50812

Koop, T., & Zobrist, B. (2009). Parameterizations for ice nucleation in biological and atmospheric systems. *Physical Chemistry Chemical Physics, 11*(46), 10839-10850. doi:10.1039/b914289d

Kujawinski, E. B. (2011). The impact of microbial metabolism on marine dissolved organic matter. *Annual Review of Marine Science, 3*, 567-599. doi:10.1146/annurev-marine-120308-081003

Kumar, A., Marcolli, C., & Peter, T. (2019). Ice nucleation activity of silicates and aluminosilicates in pure water and aqueous solutions - Part 2: Quartz and amorphous silica. *Atmospheric Chemistry and Physics, 19*(9), 6035-6058. doi:10.5194/acp-19-6035-2019

Ladino, L. A., Yakobi-Hancock, J. D., Kilthau, W. P., Mason, R. H., Si, M., Li, J., . . . Abbatt, J. P. D. (2016). Addressing the ice nucleating abilities of marine aerosol: A combination of deposition mode laboratory and field measurements. *Atmospheric Environment, 132*, 1-10. https://doi.org/10.1016/j.atmosenv.2016.02.028

Lalli, C., & Parsons, T. R. (1997). *Biological oceanography: an introduction*: Elsevier.

Lebaron, P., Catala, P., & Parthuisot, N. (1998). Effectiveness of SYTOX Green stain for bacterial viability assessment. *Applied and Environmental Microbiology, 64*(7), 2697-2700.

Leblanc, K., Arístegui, J., Armand, L., Assmy, P., Beker, B., Bode, A., . . . Yallop, M. (2012). A global diatom database–abundance, biovolume and biomass in the world ocean. *Earth Systems Science Data*, *4*, 149–165, https://doi.org/10.5194/essd-4-149-2012, 2012

Leck, C., & Bigg, E. K. (2005). Biogenic particles in the surface microlayer and overlaying atmosphere in the central Arctic Ocean during summer. *Tellus Series B-Chemical and Physical Meteorology, 57*(4), 305-316. doi:10.1111/j.1600-0889.2005.00148.x

Lee, L. A., Reddington, C. L., & Carslaw, K. S. (2016). On the relationship between aerosol model uncertainty and radiative forcing uncertainty. *Proceedings of the*

National Academy of Sciences, 113(21), 5820-5827. doi:10.1073/pnas.1507050113

Lenes, J. M., Walsh, J. J., Darrow, B. P. (2013) Simulating cell death in the termination of Karenia brevis blooms: implications for predicting aerosol toxicity vectors to humans. *Marine Ecology Progress Series, 493*, 71-81. https://doi.org/10.3354/meps10515.

Levasseur, M., Michaud, S., Egge, J., Cantin, G., Nejstgaard, J. C., Sanders, R., . . . Gosselin, M. (1996). Production of DMSP and DMS during a mesocosm study of an *Emiliania huxleyi* bloom: influence of bacteria and *Calanus finmarchicus* grazing. *Marine Biology, 126*(4), 609-618. doi:10.1007/bf00351328

Levin, Z., & Yankofsky, S. A. (1983). Contact Versus Immersion Freezing of Freely Suspended Droplets by Bacterial Ice Nuclei. *Journal of Climate and Applied Meteorology, 22*(11), 1964-1966. doi:10.1175/15200450(1983)022<1964:Cvifof>2.0.Co;2

Li, W. (1995). Composition of ultraphytoplankton in the central North Atlantic. *Marine Ecology Progress Series, 122*, 1-8. https://doi.org/10.3354/meps122001

Lindow, S., Arny, D., & Upper, C. (1978). *Erwinia herbicola*: a bacterial ice nucleus active in increasing frost injury to corn. *Phytopathology, 68*(3), 523-527.

Ling, M. L., Wex, H., Grawe, S., Jakobsson, J., Löndahl, J., Hartmann, S., . . . Šantl-Temkiv, T. (2018). Effects of ice nucleation protein repeat number and oligomerization level on ice nucleation activity. *Journal of Geophysical Research: Atmospheres, 123*(3), 1802-1810. doi:10.1002/2017JD027307

Liss, P. S., & Duce, R. A. (2005). *The sea surface and global change*: Cambridge University Press.

Lohmann, U. (2002). A glaciation indirect aerosol effect caused by soot aerosols. *Geophysical Research Letters, 29*(4). doi:10.1029/2001gl014357

Lohmann, U., & Diehl, K. (2006). Sensitivity studies of the importance of dust ice nuclei for the indirect aerosol effect on stratiform mixed-phase clouds. *Journal of the Atmospheric Sciences, 63*(3), 968-982. doi:10.1175/JAS3662.1

Lohmann, U., & Ferrachat, S. (2010). Impact of parametric uncertainties on the present-day climate and on the anthropogenic aerosol effect. *Atmospheric Chemistry and Physics, 10*(23), 11373-11383. doi:10.5194/acp-10-11373-2010

Lohmann, U., Lüönd, F., & Mahrt, F. (2016). *An introduction to clouds: From the microscale to climate*: Cambridge University Press.

Long, R. A., & Azam, F. (1996). Abundant protein-containing particles in the sea. *Aquatic Microbial Ecology, 10*, 213. doi: 10.3354/ame010213

Macdonald, J. D. (1869). I.—On the structure of the Diatomaceous frustule, and its genetic cycle. *Journal of Natural History, 3*(13), 1-8. https://doi.org/10.1080/00222936908695866

Mace, G. G. (2010). Cloud properties and radiative forcing over the maritime storm tracks of the Southern Ocean and North Atlantic derived from A-Train. *Journal of Geophysical Research: Atmospheres, 115*(D10). http://dx.doi.org/10.1029/2009JD012517

Mace, G. G., Zhang, Q., Vaughan, M., Marchand, R., Stephens, G., Trepte, C., & Winker, D. (2009). A description of hydrometeor layer occurrence statistics derived from the first year of merged Cloudsat and CALIPSO data. *Journal of Geophysical Research: Atmospheres, 114*(D8). doi: 10.1029/2007JD009755

Mahowald, N. M., Baker, A. R., Bergametti, G., Brooks, N., Duce, R. A., Jickells, T. D., . . . Tegen, I. (2005). Atmospheric global dust cycle and iron inputs to the ocean. *Global Biogeochemical Cycles, 19*(4). doi: 10.1029/2004GB002402

Maki, L. R., Galyan, E. L., Chang-Chien, M.-M., & Caldwell, D. R. (1974). Ice Nucleation induced by *Pseudomonas syringae*. *Applied Microbiology, 28*(3), 456-459.

Malviya, S., Scalco, E., Audic, S., Vincent, F., Veluchamy, A., Poulain, J., . . . Bowler, C. (2016). Insights into global diatom distribution and diversity in the world's ocean. *Proceedings of the National Academy of Sciences, 113*(11), E1516-1525. doi:10.1073/pnas.1509523113

Mann, D. G., & Vanormelingen, P. (2013). An inordinate fondness? The number, distributions, and origins of diatom species. *Journal of Eukaryotic Microbiology, 60*(4), 414-420. doi:10.1111/jeu.12047

Marks, R., Górecka, E., McCartney, K., & Borkowski, W. (2019). Rising bubbles as mechanism for scavenging and aerosolization of diatoms. *Journal of Aerosol Science, 128*, 79-88. https://doi.org/10.1016/j.jaerosci.2018.12.003

Marx, M.-C., Wood, M., & Jarvis, S. (2001). A microplate fluorimetric assay for the study of enzyme diversity in soils. *Soil Biology and Biochemistry, 33*(12-13), 1633-1640. http://dx.doi.org/10.1016/S0038-0717(01)00079-7

Mason, B. J., & Maybank, J. (1958). Ice-nucleating properties of some natural mineral dusts. *Quarterly Journal of the Royal Meteorological Society, 84*(361), 235-241. doi:10.1002/qj.49708436104

Mason, R. H., Si, M., Chou, C., Irish, V. E., Dickie, R., Elizondo, P., . . . Bertram, A. K. (2016). Size-resolved measurements of ice-nucleating particles at six locations in North America and one in Europe. *Atmospheric Chemistry and Physics, 16*(3), 1637-1651. doi:10.5194/acp-16-1637-2016

Matrai, P. A., & Keller, M. D. (1993). Dimethylsulfide in a large-scale coccolithophore bloom in the Gulf of Maine. *Continental Shelf Research, 13*(8), 831-843. https://doi.org/10.1016/0278-4343(93)90012-M

Matrai, P. A., & Keller, M. D. (1994). Total organic sulfur and dimethylsulfoniopropionate in marine phytoplankton: intracellular variations. *Marine Biology, 119*(1), 61-68. doi:10.1007/bf00350107

Mayol, E., Jimenez, M. A., Herndl, G. J., Duarte, C. M., & Arrieta, J. M. (2014). Resolving the abundance and air-sea fluxes of airborne microorganisms in the North Atlantic Ocean. *Frontiers in Microbiology, 5*, 557. doi:10.3389/fmicb.2014.00557

McCarthy, A., Rogers, S. P., Duffy, S. J., & Campbell, D. A. (2012). Elevated Carbon Dioxide Differentially Alters the Photophysiology of *Thalassiosira pseudonana* (Bacillariophyceae) and *Emiliania huxleyi* (Haptophyta)(1). *Journal of Phycology, 48*(3), 635-646. doi:10.1111/j.1529-8817.2012.01171.x

McCluskey, C. S., Hill, T. C. J., Malfatti, F., Sultana, C. M., Lee, C., Santander, M. V., . . . DeMott, P. J. (2016). A dynamic link between ice nucleating particles released in nascent sea spray aerosol and oceanic biological activity during two mesocosm experiments. *Journal of the Atmospheric Sciences, 74*(1), 151-166. doi:10.1175/JAS-D-16-0087.1

McCluskey, C. S., Hill, T. C. J., Sultana, C. M., Laskina, O., Trueblood, J., Santander, M. V., . . . DeMott, P. (2018). A mesocosm double feature: Insights into the chemical make-up of marine ice nucleating particles. *Journal of the Atmospheric Sciences*. *75*(7), doi:10.1175/JAS-D-17-0155.1

McCluskey, C. S., Ovadnevaite, J., Rinaldi, M., Atkinson, J., Belosi, F., Ceburnis, D., . . . DeMott, P. J. (2018). Marine and terrestrial organic ice-nucleating particles in pristine marine to continentally influenced Northeast Atlantic air masses. *Journal of Geophysical Research: Atmospheres, 123*(11), 6196-6212. doi:10.1029/2017JD028033

McKnight, D. M., Boyer, E. W., Westerhoff, P. K., Doran, P. T., Kulbe, T., & Andersen, D. T. (2001). Spectrofluorometric characterization of dissolved organic matter for indication of precursor organic material and aromaticity. *Limnology and Oceanography, 46*(1), 38-48. doi:10.4319/lo.2001.46.1.0038

Michaud, J. M., Thompson, L. R., Kaul, D., Espinoza, J. L., Richter, R. A., Xu, Z. Z., . . . Prather, K. A. (2018). Taxon-specific aerosolization of bacteria and viruses in an experimental ocean-atmosphere mesocosm. *Nature Communications, 9*(1), 2017. doi:10.1038/s41467-018-04409-z

Milliman, J. D. (1993). Production and accumulation of calcium carbonate in the ocean: budget of a nonsteady state. *Global Biogeochemical Cycles, 7*(4), 927-957. https://doi.org/10.1029/93GB02524

Moffet, B., Getti, G., Henderson-Begg, S., & Hill, T. (2015). Ubiquity of ice nucleation in lichen–possible atmospheric implications. *Lindbergia, 38*, 39-43. https://doi.org/10.25227/linbg.01070

Möhler, O., Büttner, S., Linke, C., Schnaiter, M., Saathoff, H., Stetzer, O., . . . Ebert, V. (2005). Effect of sulfuric acid coating on heterogeneous ice nucleation by soot aerosol particles. *Journal of Geophysical Research: Atmospheres, 110*(11). doi: 10.1029/2004JD005169

Möhler, O., Field, P. R., Connolly, P., Benz, S., Saathoff, H., Schnaiter, M., . . . Heymsfield, A. J. (2006). Efficiency of the deposition mode ice nucleation on mineral dust particles. *Atmospheric Chemistry and Physics, 6*(10), 3007-3021. doi:10.5194/acp-6-3007-2006

Møller, E. F. (2007). Production of dissolved organic carbon by sloppy feeding in the copepods *Acartia tonsa, Centropages typicus,* and *Temora longicornis*. *Limnology and Oceanography, 52*(1), 79-84. http://dx.doi.org/10.4319/lo.2007.52.1.0079

Møller, E. F., Thor, P., & Nielsen, T. G. (2003). Production of DOC by *Calanus finmarchicus, C. glacialis* and *C. hyperboreus* through sloppy feeding and leakage from fecal pellets. *Marine Ecology Progress Series, 262*, 185-191. https://doi.org/10.3354/meps262185

Monod, J. (1949). The growth of bacterial cultures. *Annual review of microbiology, 3*(1), 371-394. http://dx.doi.org/10.1146/annurev.mi.03.100149.002103

Morgan, G. M., & Allee, P. A. (1968). The production of potential ice nuclei by gasoline engines. *Journal of Applied Meteorology, 7*(2), 241-246. doi:10.1175/1520-0450(1968)007<0241:Tpopin>2.0.Co;2

Morris, C., Georgakopoulos, D., & Sands, D. (2004). *Ice nucleation active bacteria and their potential role in precipitation.* Paper presented at the Journal de Physique IV (Proceedings). doi:10.1051/jp4:2004121004

Morris, C. E., Sands, D. C., Glaux, C., Samsatly, J., Asaad, S., Moukahel, A. R., . . . Bigg, E. K. (2013). Urediospores of rust fungi are ice nucleation active at >-10 degrees C and harbor ice nucleation active bacteria. *Atmospheric Chemistry and Physics, 13*(8), 4223-4233. doi:10.5194/acp-13-4223-2013

Morrison, H., & Milbrandt, J. A. (2015). Parameterization of cloud microphysics based on the prediction of bulk ice particle properties. Part I: Scheme description and idealized tests. *Journal of the Atmospheric Sciences, 72*(1), 287-311. doi:10.1175/Jas-D-14-0065.1

Müller, P. J., & Suess, E. (1979). Productivity, sedimentation rate, and sedimentary organic matter in the oceans—I. Organic carbon preservation. *Deep Sea Research Part A. Oceanographic Research Papers, 26*(12), 1347-1362. https://doi.org/10.1016/0198-0149(79)90003-7

Murphy, L., & Haugen, E. (1985). The distribution and abundance of phototrophic ultraplankton in the North Atlantic 1, 2. *Limnology and Oceanography, 30*(1), 47-58. https://doi.org/10.4319/lo.1985.30.1.0047

Murray, B. J., O'Sullivan, D., Atkinson, J. D., & Webb, M. E. (2012). Ice nucleation by particles immersed in supercooled cloud droplets. *Chemical Society Reviews, 41*(19), 6519-6554. http://dx.doi.org/10.1039/c2cs35200a

Murray, B. J., Wilson, T. W., Dobbie, S., Cui, Z. Q., Al-Jumur, S. M. R. K., Mohler, O., . . . Karcher, B. (2010). Heterogeneous nucleation of ice particles on glassy aerosols under cirrus conditions. *Nature Geoscience, 3*(4), 233-237. doi:10.1038/Ngeo817

Myklestad, S. M. (1995). Release of extracellular products by phytoplankton with special emphasis on polysaccharides. *Science of The Total Environment, 165*(1), 155-164. https://doi.org/10.1016/0048-9697(95)04549-G

Nelson, D. M., Treguer, P., Brzezinski, M. A., Leynaert, A., & Queguiner, B. (1995). Production and dissolution of biogenic silica in the ocean - Revised global estimates, comparison with regional data and relationship to biogenic sedimentation. *Global Biogeochemical Cycles, 9*(3), 359-372. doi:10.1029/95gb01070

Niehaus, J., Becker, J. G., Kostinski, A., & Cantrell, W. (2014). Laboratory Measurements of contact freezing by dust and bacteria at temperatures of mixed-phase clouds. *Journal of the Atmospheric Sciences, 71*(10), 3659-3667. doi:10.1175/JAS-D-14-0022.1

Niki, T., Kunugi, M., & Otsuki, A. (2000). DMSP-lyase activity in five marine phytoplankton species: its potential importance in DMS production. *Marine Biology, 136*(5), 759-764. doi:10.1007/s002279900235

Noble, R. T., & Fuhrman, J. A. (1998). Use of SYBR Green I for rapid epifluorescence counts of marine viruses and bacteria. *Aquatic Microbial Ecology, 14*(2), 113-118. doi:10.3354/ame014113

Nöel, M. H., Kawachi, M., & Inouye, I. (2004). Induced dimorphic life cycle of a coccolithophorid, *Calyptrosphaera sphaeroidea* (Prymnesiophyceae, Haptophyta) 1. *Journal of Phycology, 40*(1), 112-129. http://dx.doi.org/10.1046/j.1529-8817.2004.03053.x

O'Dowd, C. D., Ceburnis, D., Ovadnevaite, J., Bialek, J., Stengel, D. B., Zacharias, M., . . . Danovaro, R. (2015). Connecting marine productivity to sea-spray via nanoscale biological processes: Phytoplankton Dance or Death Disco? *Science Reports, 5*, 14883. doi:10.1038/srep14883

O'Dowd, C. D., & de Leeuw, G. (2007). Marine aerosol production: a review of the current knowledge. *Philosophical Transactions of the Royal Society A: Mathematical, Physical, and Engineering Sciences, 365*(1856), 1753-1774. doi:10.1098/rsta.2007.2043

Olson, R. J., Chisholm, S. W., Zettler, E. R., & Armbrust, E. V. (1988). Analysis of *Synechococcus* pigment types in the sea using single and dual beam flow-cytometry. *Deep-Sea Research Part a-Oceanographic Research Papers, 35*(3), 425-440. doi:10.1016/0198-0149(88)90019-2

Olson, R. J., Chisholm, S. W., Zettler, E. R., & Armbrust, E. V. (1990). Pigments, Size, and Distribution of *Synechococcus* in the North-Atlantic and Pacific Oceans. *Limnology and Oceanography, 35*(1), 45-58. doi:10.4319/lo.1990.35.1.0045

Owens, O. V. H., & Esaias, W. E. (1976). Physiological responses of phytoplankton to major environmental factors. *Annual Review of Plant Physiology and Plant Molecular Biology, 27*(1), 461-483. doi:10.1146/annurev.pp.27.060176.002333

Paasche, E. (2001). A review of the coccolithophorid *Emiliania huxleyi* (Prymnesiophyceae), with particular reference to growth, coccolith formation, and calcification-photosynthesis interactions. *Phycologia, 40*(6), 503. https://doi.org/10.2216/i0031-8884-40-6-503.1

Palumbo, A. V., Ferguson, R. L., & Rublee, P. A. (1984). Size of suspended bacterial cells and association of heterotrophic activity with size fractions of particles in estuarine and coastal waters. *Applied and Environmental Microbiology, 48*(1), 157-164.

Park, K. T., Jang, S., Lee, K., Yoon, Y. J., Kim, M. S., Park, K., . . . Shin, K. H. (2017). Observational evidence for the formation of DMS-derived aerosols during Arctic phytoplankton blooms. *Atmospheric Chemistry and Physics, 17*(15), 9665-9675. doi:10.5194/acp-17-9665-2017

Parkhill, J. P., Maillet, G., & Cullen, J. J. (2001). Fluorescence-based maximal quantum yield for PSII as a diagnostic of nutrient stress. *Journal of Phycology, 37*(4), 517-529. doi:DOI 10.1046/j.1529-8817.2001.037004517.x

Parlanti, E., Wörz, K., Geoffroy, L., & Lamotte, M. (2000). Dissolved organic matter fluorescence spectroscopy as a tool to estimate biological activity in a coastal zone submitted to anthropogenic inputs. *Organic Geochemistry, 31*(12), 1765-1781. http://dx.doi.org/10.1016/S0146-6380(00)00124-8

Partensky, F., Blanchot, J., & Vaulot, D. J. B.-I. O. M.-N. S.-. (1999). Differential distribution and ecology of *Prochlorococcus* and *Synechococcus* in oceanic waters: a review. 457-476.

Passow, U., & Alldredge, A. L. (1995). A dye-binding assay for the spectrophotometric measurement of transparent exopolymer particles (TEP). *Limnology and Oceanography, 40*(7), 1326-1335. doi:10.4319/lo.1995.40.7.1326

Passow, U., & Laws, E. A. (2015). Ocean acidification as one of multiple stressors: growth response of Thalassiosira weissflogii (diatom) under temperature and light stress. *Marine Ecology Progress Series, 541*, 75-90. https://doi.org/10.3354/meps11541

Payet, J. P., & Suttle, C. A. (2013). To kill or not to kill: the balance between lytic and lysogenic viral infection is driven by trophic status. *Limnology and Oceanography, 58*(2), 465-474. doi:10.4319/lo.2013.58.2.0465

Perry, M. J., Talbot, M. C., & Alberte, R. S. (1981). Photoadaption in marine phytoplankton: Response of the photosynthetic unit. *Marine Biology, 62*(2), 91-101. doi:10.1007/bf00388170

Pfitzer, E. (1869). Über den Bau und die Zellteilung der Diatomeen. *Botanische Zeitung, 27*, 774-776.

Pitter, R. L., & Pruppacher, H. R. (1973). A wind tunnel investigation of freezing of small water drops falling at terminal velocity in air. *Quarterly Journal of the Royal Meteorological Society, 99*(421), 540-550. http://dx.doi.org/10.1002/qj.49709942111

Post, A. F., Dubinsky, Z., Wyman, K., & Falkowski, P. G. (1984). Kinetics of light-intensity adaptation in a marine planktonic diatom. *Marine Biology, 83*(3), 231-238. doi:10.1007/bf00397454

Pouleur, S., Richard, C., Martin, J.-G., & Antoun, H. (1992). Ice Nucleation Activity in *Fusarium acuminatum* and *Fusarium avenaceum*. *Applied and Environmental Microbiology, 58*(9), 2960-2964.

Poulton, A. J., Painter, S. C., Young, J. R., Bates, N. R., Bowler, B., Drapeau, D., . . . Balch, W. M. (2013). The 2008 *Emiliania huxleyi* bloom along the Patagonian Shelf: Ecology, biogeochemistry, and cellular calcification. *Global Biogeochemical Cycles, 27*(4), 1023-1033. doi:10.1002/2013gb004641

Prather, K. A., Bertram, T. H., Grassian, V. H., Deane, G. B., Stokes, M. D., DeMott, P. J., . . . Corrigan, C. E. (2013). Bringing the ocean into the laboratory to probe the chemical complexity of sea spray aerosol. *Proceedings of the National Academy of Sciences of the United States of America, 110*(19), 7550-7555. doi:10.1073/pnas.1300262110

Pruppacher, H. R., & Klett, J. D. (2012). *Microphysics of Clouds and Precipitation*: Springer Science & Business Media.

Pummer, B. G., Bauer, H., Bernardi, J., Bleicher, S., & Grothe, H. (2012). Suspendable macromolecules are responsible for ice nucleation activity of birch and conifer pollen. *Atmospheric Chemistry and Physics, 12*(5), 2541-2550. doi:10.5194/acp-12-2541-2012

Quinn, P. K., & Bates, T. S. (2011). The case against climate regulation via oceanic phytoplankton sulphur emissions. *Nature, 480*(7375), 51-56. http://dx.doi.org/10.1038/nature10580

Quinn, P. K., Bates, T. S., Schulz, K. S., Coffman, D. J., Frossard, A. A., Russell, L. M., . . . Kieber, D. J. (2014). Contribution of sea surface carbon pool to organic matter enrichment in sea spray aerosol. *Nature Geoscience, 7*(3), 228-232. doi:10.1038/Ngeo2092

Quinn, P. K., Collins, D. B., Grassian, V. H., Prather, K. A., & Bates, T. S. (2015). Chemistry and related properties of freshly emitted sea spray aerosol. *Chemical Reviews, 115*(10), 4383-4399. doi:10.1021/cr500713g

Rahlff, J. (2019). The Virioneuston: A review on viral–bacterial associations at air–water interfaces. *Viruses, 11*(2), 191. https://dx.doi.org/10.3390%2Fv11020191

Rastelli, E., Corinaldesi, C., Dell'Anno, A., Lo Martire, M., Greco, S., Cristina Facchini, M., . . . Danovaro, R. (2017). Transfer of labile organic matter and microbes

from the ocean surface to the marine aerosol: an experimental approach. *Scientific Reports, 7*(1), 11475. doi:10.1038/s41598-017-10563-z

Read, B. A., Kegel, J., Klute, M. J., Kuo, A., Lefebvre, S. C., Maumus, F., . . . Salamov, A. (2013). Pan genome of the phytoplankton *Emiliania* underpins its global distribution. *Nature, 499*(7457), 209. doi:10.1038/nature12221

Reche, I., D'Orta, G., Mladenov, N., Winget, D. M., & Suttle, C. A. (2018). Deposition rates of viruses and bacteria above the atmospheric boundary layer. *The ISME Journal, 12*(4), 1154-1162. doi:10.1038/s41396-017-0042-4

Redfield, A. C. (1934). On the proportions of organic derivatives in sea water and their relation to the composition of plankton. *James Johnstone memorial volume*, 176-192.

Redfield, A. C. (1958). The biological control of chemical factors in the environment. *American Scientist, 46*(3), 230A-221.

Riebesell, U., Schulz, K. G., Bellerby, R., Botros, M., Fritsche, P., Meyerhöfer, M., . . . Wohlers, J. (2007). Enhanced biological carbon consumption in a high CO_2 ocean. *Nature, 450*(7169), 545. doi:10.1038/nature06267

Riebesell, U., & Tortell, P. D. (2011). Effects of ocean acidification on pelagic organisms and ecosystems. *Ocean acidification* 99-121. Oxford University Press

Robertson, B. R., Tezuka, N., & Watanabe, M. M. (2001). Phylogenetic analyses of *Synechococcus* strains (cyanobacteria) using sequences of 16S rDNA and part of the phycocyanin operon reveal multiple evolutionary lines and reflect phycobilin content. *International Journal of Systematic and Evolutionary Microbiology, 51*(3), 861-871. doi:10.1099/00207713-51-3-861

Rogers, R. R., & Yau, M. K. (1996). *A short course in cloud physics* (3rd ed.): Elsevier.

Romera-Castillo, C., Sarmento, H., Álvarez-Salgado, X. A., Gasol, J. M., Marrasé, C. (2011). Net production/consumption of fluorescent coloured dissolved organic matter by natural bacterial assemblages growing on marine phytoplankton exudates. *Applied and Environmental Microbiology 77*(21) 7490-7498. doi: 10.1128/AEM.00200-11

Rosinski, J., Haagenson, P., Nagamoto, C., & Parungo, F. (1986). Ice-forming nuclei of maritime origin. *Journal of Aerosol Science, 17*(1), 23-46. https://doi.org/10.1016/0021-8502(86)90004-2

Rosinski, J., Haagenson, P., Nagamoto, C., & Parungo, F. (1987). Nature of ice-forming nuclei in marine air masses. *Journal of Aerosol Science, 18*(3), 291-309. https://doi.org/10.1016/0021-8502(87)90024-3

Russell, L. M. (2015). Sea-spray particles cause freezing in clouds. *Nature, 525*, 194. doi:10.1038/525194a

Russell, L. M., Hawkins, L. N., Frossard, A. A., Quinn, P. K., & Bates, T. S. (2010). Carbohydrate-like composition of submicron atmospheric particles and their production from ocean bubble bursting. *Proceedings of the National Academy of Sciences, 107*(15), 6652-6657. https://doi.org/10.1073/pnas.0908905107

Sanchez, K. J., Chen, C.-L., Russell, L. M., Betha, R., Liu, J., Price, D. J., . . . Moore, R. H. (2018). Substantial seasonal contribution of observed biogenic sulfate particles to cloud condensation nuclei. *Scientific Reports, 8*(1), 3235. doi:10.1038/s41598-018-21590-9

Schaefer, V. J. (1966). Ice nuclei from automobile exhaust and iodine vapor. *Science, 154*(3756), 1555-1557. doi:10.1126/science.154.3756.1555-a

Schmid, D., Pridmore, D., Capitani, G., Battistutta, R., Neeser, J.-R., & Jann, A. (1997). Molecular organisation of the ice nucleation protein InaV from *Pseudomonas syringae*. *FEBS Letters, 414*(3), 590-594. https://doi.org/10.1016/S0014-5793(97)01079-X

Schmitt-Kopplin, P., Liger-Belair, G., Koch, B. P., Flerus, R., Kattner, G., Harir, M., . . . Hertkorn, N. (2012). Dissolved organic matter in sea spray: a transfer study from marine surface water to aerosols. *Biogeosciences, 9*(4), 1571-1582. doi:10.5194/bg-9-1571-2012

Schnell, R. C., & Vali, G. (1975). Freezing nuclei in marine waters. *Tellus, 27*(3), 321-323. doi:10.1111/j.2153-3490.1975.tb01682.x

Schnell, R. C., & Vali, G. (1976). Biogenic ice nuclei: Part I. Terrestrial and marine sources. *Journal of the Atmospheric Sciences, 33*(8), 1554-1564. doi:10.1175/1520-0469(1976)033<1554:BINPIT>2.0.CO;2

Schreiber, U. (1998). Chlorophyll fluorescence: new instruments for special applications. *Photosynthesis: mechanisms and effects, 5*, 4253-4258. doi: 10.1007/978-94-011-3953-3_984

Schreiber, U. (2004). Pulse-amplitude-modulation (PAM) fluorometry and saturation pulse method: an overview *Chlorophyll a fluorescence* (pp. 279-319): Springer.

Schreiber, U., Schliwa, U., & Bilger, W. (1986). Continuous recording of photochemical and non-photochemical chlorophyll fluorescence quenching with a new type of modulation fluorometer. *Photosynthesis Research, 10*(1), 51-62. doi:10.1007/bf00024185

Schroeder, D. C., Oke, J., Hall, M., Malin, G., & Wilson, W. H. (2003). Virus succession observed during an *Emiliania huxleyi* bloom. *Appl Environ Microbiol, 69*(5), 2484-2490. doi:10.1128/aem.69.5.2484-2490.2003

Schroeder, D. C., Oke, J., Malin, G., & Wilson, W. H. (2002). Coccolithovirus (Phycodnaviridae): characterisation of a new large dsDNA algal virus that infects *Emiliana huxleyi*. *Arch Virol, 147*(9), 1685-1698. doi:10.1007/s00705-002-0841-3

Seifert, P., Ansmann, A., Groß, S., Freudenthaler, V., Heinold, B., Hiebsch, A., . . . Wiegner, M. (2011). Ice formation in ash-influenced clouds after the eruption of the Eyjafjallajökull volcano in April 2010. *Journal of Geophysical Research: Atmospheres, 116*(D20). doi:10.1029/2011jd015702

Seinfeld, J. H., Bretherton, C., Carslaw, K. S., Coe, H., DeMott, P. J., Dunlea, E. J., . . . Wood, R. (2016). Improving our fundamental understanding of the role of aerosol-cloud interactions in the climate system. *Proceedings of the National Academy of Science of the United States of America, 113*(21), 5781-5790. doi:10.1073/pnas.1514043113

Shapiro, L. P., & Haugen, E. M. (1988). Seasonal distribution and temperature tolerance of *Synechococcus* in Boothbay Harbor, Maine. *Estuarine, Coastal and Shelf Science, 26*(5), 517-525. https://doi.org/10.1016/0272-7714(88)90004-2

Sharoni, S., Trainic, M., Schatz, D., Lehahn, Y., Flores, M. J., Bidle, K. D., . . . Vardi, A. (2015). Infection of phytoplankton by aerosolized marine viruses. *Proceedings of the National Academy of Science of the United States of America, 112*(21), 6643-6647. doi: 10.1073/pnas.1423667112

Shaw, R. A., Durant, A. J., & Mi, Y. (2005). Heterogeneous surface crystallization observed in undercooled water. *The Journal of Physical Chemistry B, 109*(20), 9865-9868. http://dx.doi.org/10.1021/jp0506336

Shimotori, K., Omori, Y., & Hama, T. (2009). Bacterial production of marine humic-like fluorescent dissolved organic matter and its biogeochemical importance. *Aquatic Microbial Ecology 58*(1), 55-66. https://doi.org/10.3354/ame01350

Shirai, Y., Tomaru, Y., Takao, Y., Suzuki, H., Nagumo, T., & Nagasaki, K. (2008). Isolation and characterization of a single-stranded RNA virus infecting the

marine planktonic diatom *Chaetoceros tenuissimus* Meunier. *Applied Environmental Microbiology, 74*(13), 4022-4027. doi:10.1128/AEM.00509-08

Shuter, B (1979), A model of physiological adaptation in unicellular algae. *Journal of Theoretical Biology. 78*, 519-552, doi:10.10/0022-5193(79)90189-9

Sieburth, J. M., Smetacek, V., & Lenz, J. (1978). Pelagic ecosystem structure: Heterotrophic compartments of the plankton and their relationship to plankton size fractions 1. *Limnology and Oceanography, 23*(6), 1256-1263. https://doi.org/10.4319/lo.1978.23.6.1256

Sournia, A., Chrdtiennot-Dinet, M.-J., & Ricard, M. (1991). Marine phytoplankton: how many species in the world ocean? *Journal of Plankton Research, 13*(5), 1093-1099. https://doi.org/10.1093/plankt/13.5.1093

Stefels, J. (2000). Physiological aspects of the production and conversion of DMSP in marine algae and higher plants. *Journal of Sea Research, 43*(3–4), 183-197. http://doi.org/10.1016/S1385-1101(00)00030-7

Steinke, I., Möhler, O., Kiselev, A., Niemand, M., Saathoff, H., Schnaiter, M., . . . Leisner, T. (2011). Ice nucleation properties of fine ash particles from the Eyjafjallajökull eruption in April 2010. *Atmospheric Chemistry and Physics, 11*(24), 12945-12958. doi:10.5194/acp-11-12945-2011

Steinke, M., Brading, P., Kerrison, P., Warner, M. E., & Suggett, D. J. (2011). Concentrations of dimethylsulfoniopropionate and dimethyl sulfide are strain-specific in symbiotic dinoflagellates (*Symbiodinium* Sp., Dinophyceae)(1). *Journal of Phycology, 47*(4), 775-783. doi:10.1111/j.1529-8817.2011.01011.x

Sterner, R. W. (1995). Elemental stoichiometry of species in ecosystems *Linking Species & Ecosystems* (pp. 240-252): Springer.

Stratmann, F., & Wiedensohler, A. (1996). A new data inversion algorithm for DMPS-measurements. *Journal of Aerosol Science* (27), 339-340 https://doi.org/10.1016/0021-8502(96)00242-X

Sumper, M., & Brunner, E. (2008). Silica biomineralisation in diatoms: The model organism *Thalassiosira pseudonana*. *ChemBioChem, 9*(8), 1187-1194. doi:10.1002/cbic.200700764

Suttle, C. A. (2005). Viruses in the sea. *Nature, 437*(7057), 356. doi:10.1038/nature04160

Suttle, C. A. (2007). Marine viruses--major players in the global ecosystem. *Nature Reviews: Microbiology, 5*(10), 801-812. doi:10.1038/nrmicro1750

Sze, S. K., Siddique, N., Sloan, J. J., & Escribano, R. (2001). Raman spectroscopic characterization of carbonaceous aerosols. *Atmospheric Environment, 35*(3), 561-568. doi:10.1016/S1352-2310(00)00325-3

Taylor, A. R., Brownlee, C., & Wheeler, G. (2017). Coccolithophore cell biology: Chalking up progress. *Annual Review of Marine Science, 9*(1), 283-310. http://dx.doi.org/10.1146/annurev-marine-122414-034032

Teller, A., Xue, L., & Levin, Z. (2012). The effects of mineral dust particles, aerosol regeneration and ice nucleation parameterizations on clouds and precipitation. *Atmospheric Chemistry & Physics, 12*(19). doi: 10.5194/acpd-12-8225-2012

Thornton, D. C. O. (2014). Dissolved organic matter (DOM) release by phytoplankton in the contemporary and future ocean. *European Journal of Phycology, 49*(1), 20-46. doi:10.1080/09670262.2013.875596

Thornton, D. C. O., Brooks, S. D., & Chen, J. (2016). Protein and carbohydrate exopolymer particles in the sea surface microlayer (SML). *Frontiers in Marine Science, 3*, 135. http://dx.doi.org/10.3389/fmars.2016.00135

Thornton, D. C. O., & Chen, J. (2017). Exopolymer production as a function of cell permeability and death in a diatom (*Thalassiosira weissflogii*) and a cyanobacterium (*Synechococcus elongatus*). *Journal of Phycology, 53*(2), 245-260. doi:10.1111/jpy.12470

Thurman, H. V., Trujillo, A. P., Abel, D. C., & McConnell, R. (1999). *Essentials of oceanography*: Prentice Hall Upper Saddle River, NJ.

Tomaru, Y., Shirai, Y., Toyoda, K., & Nagasaki, K. (2011). Isolation and characterisation of a single-stranded DNA virus infecting the marine planktonic diatom *Chaetoceros tenuissimus*. *Aquatic Microbial Ecology, 64*(2), 175-184. doi: 10.1128/AEM.00202-11

Trainic, M., Koren, I., Sharoni, S., Frada, M., Segev, L., Rudich, Y., & Vardi, A. (2018). Infection dynamics of a bloom-forming alga and its virus determine airborne coccolith emission from seawater. *iScience, 6*, 327-335. https://doi.org/10.1016/j.isci.2018.07.017

Turnbull, D., & Vonnegut, B. (1952). Nucleation catalysis. *Industrial & Engineering Chemistry, 44*(6), 1292-1298. https://doi.org/10.1021/ie50510a031

Uitz, J., Claustre, H., Morel, A., & Hooker, S. B. (2006). Vertical distribution of phytoplankton communities in open ocean: An assessment based on surface chlorophyll. *Journal of Geophysical Research: Oceans 111*(C8). doi:10.1029/2005JC003207

Usher, K., Fromont, J., Sutton, D., & Toze, S. (2004). The biogeography and phylogeny of unicellular cyanobacterial symbionts in sponges from Australia and the Mediterranean. *Microbial Ecology, 48*(2), 167-177. doi: 10.1007/s00248-003-1062-3

Vali, G. (1971). Quantitative evaluation of experimental results an the heterogeneous freezing nucleation of supercooled liquids. *Journal of the Atmospheric Sciences, 28*(3), 402-409. doi:10.1175/15200469(1971)028<0402:QEOERA>2.0.CO;2

Vali, G. (1985). Nucleation terminology. *Bulletin of the American Meteorological Society, 66*(11), 1426-1427.

Vali, G. (1994). Freezing rate due to heterogeneous nucleation. *Journal of the Atmospheric Sciences, 51*(13), 1843-1856. doi:10.1175/15200469(1994)051<1843:FRDTHN>2.0.CO;2

Vali, G., DeMott, P., Möhler, O., & Whale, T. (2015). A proposal for ice nucleation terminology. *Atmospheric Chemistry and Physics, 15*(18), 10263-10270. https://doi.org/10.5194/acp-15-10263-2015

Van Boekel, J., & Stefels, W. (1993). Production of DMS from dissolved DMSP in axenic cultures of the marine phytoplankton species *Phaeocystis* sp. *Marine Ecology Progress Series, 97*, 11-18. doi: 10.3354/meps097011

van de Poll, W. H., Alderkamp, A.-C., Janknegt, P. J., Roggeveld, J., & Buma, A. G. J. (2006). Photoacclimation modulates excessive photosynthetically active and ultraviolet radiation effects in a temperate and an Antarctic marine diatom. *Limnology and Oceanography, 51*(3), 1239-1248. doi:10.4319/lo.2006.51.3.1239

Van Heukelem, L., & Thomas, C. S. (2001). Computer-assisted high-performance liquid chromatography method development with applications to the isolation and analysis of phytoplankton pigments. *Journal of Chromatography A, 910*(1), 31-49. doi:10.1016/s0378-4347(00)00603-4

van Kooten, O., & Snel, J. F. H. (1990). The use of chlorophyll fluorescence nomenclature in plant stress physiology. *Photosynthesis Research, 25*(3), 147-150. doi:10.1007/bf00033156

Vaulot, D., & Xiuren, N. (1988). Abundance and cellular characteristics of marine *Synechococcus* spp. in the dilution zone of the Changjiang (Yangtze River, China). *Continental Shelf Research, 8*(10), 1171-1186. doi: 10.1016/0278-4343(88)90018-0

Veldhuis, M. J. W., Admiraal, W., & Colijn, F. (1986). Chemical and physiological changes of phytoplankton during the spring bloom, dominated by *Phaeocystis*

pouchetii (Haptophyceae): Observations in Dutch coastal waters of the North Sea. *Netherlands Journal of Sea Research, 20*(1), 49-60. https://doi.org/10.1016/0077-7579(86)90060-8

Veldhuis, M. J. W., Cucci, T. L., & Sieracki, M. E. (1997). Cellular DNA content of marine phytoplankton using two new fluorochromes: Taxonomic and ecological implications 1. *Journal of Phycology, 33*(3), 527-541. doi:10.1111/j.0022-3646.1997.00527.x

Veldhuis, M. J. W., Kraay, G. W., & Timmermans, K. R. (2001). Cell death in phytoplankton: correlation between changes in membrane permeability, photosynthetic activity, pigmentation and growth. *European Journal of Phycology, 36*(2), 167-177. doi:10.1017/S0967026201003110

Vergara-Temprado, J., Miltenberger, A. K., Furtado, K., Grosvenor, D. P., Shipway, B. J., Hill, A. A., . . . Carslaw, K. S. (2018). Strong control of Southern Ocean cloud reflectivity by ice-nucleating particles. *Proceedings of the National Academy of Science of the United States of America, 115*(11), 2687-2692. doi:10.1073/pnas.1721627115

Vergara-Temprado, J., Murray, B. J., Wilson, T. W., O'Sullivan, D., Browse, J., Pringle, K. J., . . . Carslaw, K. S. (2017). Contribution of feldspar and marine organic aerosols to global ice nucleating particle concentrations. *Atmospheric Chemistry and Physics, 17*(5), 3637-3658. doi:10.5194/acp-17-3637-2017

Verreault, D., Moineau, S., & Duchaine, C. (2008). Methods for sampling of airborne viruses. *Microbiology and molecular biology reviews : MMBR, 72*(3), 413-444. doi:10.1128/MMBR.00002-08

Vonnegut, B. (1947). The nucleation of ice formation by silver iodide. *Journal of Applied Physics, 18*(7), 593-595. doi:10.1063/1.1697813

Wallace, J. M., & Hobbs, P. V. (2006). *Atmospheric science: an introductory survey* (Vol. 92): Elsevier.

Wang, X., Deane, G. B., Moore, K. A., Ryder, O. S., Stokes, M. D., Beall, C. M., . . . Prather, K. A. (2017). The role of jet and film drops in controlling the mixing state of submicron sea spray aerosol particles. *Proceedings of the National Academy of Science of the United States of America, 114*(27), 6978-6983. doi:10.1073/pnas.1702420114

Wang, X., Sultana, C. M., Trueblood, J., Hill, T. C., Malfatti, F., Lee, C., . . . Prather, K. A. (2015). Microbial Control of Sea Spray Aerosol Composition: A Tale of Two Blooms. *ACS Central Science, 1*(3), 124-131. doi:10.1021/acscentsci.5b00148

Waterbury, J. B., Watson, S. W., Guillard, R. R., & Brand, L. E. (1979). Widespread occurrence of a unicellular, marine, planktonic, cyanobacterium. *Nature, 277*(5694), 293. https://doi.org/10.1038/277293a0

Wells, L. E., & Deming, J. W. (2006). Characterization of a cold-active bacteriophage on two psychrophilic marine hosts. *Aquatic Microbial Ecology, 45*(1), 15-29. doi:DOI 10.3354/ame045015

Welti, A., Lohmann, U., & Kanji, Z. A. (2019). Ice nucleation properties of K-feldspar polymorphs and plagioclase feldspars. *Atmospheric Chemistry and Physics Discuss., 2019*, 1-25. doi:10.5194/acp-2018-1271

Welti, A., Lüönd, F., Stetzer, O., & Lohmann, U. (2009). Influence of particle size on the ice nucleating ability of mineral dusts. *Atmospheric Chemistry and Physics, 9*(18), 6705-6715. doi:10.5194/acp-9-6705-2009

Wex, H., Augustin-Bauditz, S., Boose, Y., Budke, C., Curtius, J., Diehl, K., . . . Hiranuma, N. (2015). Intercomparing different devices for the investigation of ice nucleating particles using Snomax® as test substance. *Atmospheric Chemistry and Physics, 15*(3), 1463-1485. http://dx.doi.org/10.5194/acp-15-1463-2015

Whale, T. F., Holden, M. A., Kulak, A. N., Kim, Y. Y., Meldrum, F. C., Christenson, H. K., & Murray, B. J. (2017). The role of phase separation and related topography in the exceptional ice-nucleating ability of alkali feldspars. *Physical Chemistry Chemical Physics, 19*(46), 31186-31193. doi:10.1039/c7cp04898j

Whale, T. F., Holden, M. A., Wilson, T. W., O'Sullivan, D., & Murray, B. J. (2018). The enhancement and suppression of immersion mode heterogeneous ice-nucleation by solutes. *Chemical Science, 9*(17), 4142-4151. doi:10.1039/c7sc05421a

Whiting, R. C., & Cygnarowicz-Provost, M. (1992). A quantitative model for bacterial growth and decline. *Food Microbiology, 9*(4), 269-277. https://doi.org/10.1016/0740-0020(92)80036-4

Whitman, W. B., Coleman, D. C., & Wiebe, W. J. (1998). Prokaryotes: the unseen majority. *Proceedings of the National Academy of Science of the United States of America, 95*(12), 6578-6583. doi:10.1073/pnas.95.12.6578

Wilcox, R. M., & Fuhrman, J. A. (1994). Bacterial viruses in coastal seawater: lytic rather than lysogenic production. *Marine Ecology-Progress Series, 114*, 35-35. https://doi.org/10.3354/meps114035

Wilson, H. F., & Xenopoulos, M. A. (2009). Effects of agricultural land use on the composition of fluvial dissolved organic matter. *Nature Geoscience, 2*(1), 37. doi:10.1038/ngeo391

Wilson, T. W., Ladino, L. A., Alpert, P. A., Breckels, M. N., Brooks, I. M., Browse, J., . . . Murray, B. J. (2015). A marine biogenic source of atmospheric ice-nucleating particles. *Nature, 525*(7568), 234-238. doi:10.1038/nature14986

Wilson, T. W., Murray, B. J., Wagner, R., Mohler, O., Saathoff, H., Schnaiter, M., . . . Al-Jumur, S. M. R. K. (2012). Glassy aerosols with a range of compositions nucleate ice heterogeneously at cirrus temperatures. *Atmospheric Chemistry and Physics, 12*(18), 8611-8632. doi:10.5194/acp-12-8611-2012

Wilson, W. H., & Mann, N. H. (1997). Lysogenic and lytic viral production in marine microbial communities. *Aquatic Microbial Ecology, 13*(1), 95-100. doi:10.3354/ame013095

Wilson, W. H., Tarran, G. A., Schroeder, D., Cox, M., Oke, J., & Malin, G. (2002). Isolation of viruses responsible for the demise of an *Emiliania huxleyi* bloom in the English Channel. *Journal of the Marine Biological Association of the United Kingdom, 82*(3), 369-377. https://doi.org/10.1017/S002531540200560X

Wolf, M. J., Coe, A., Dove, L. A., Zawadowicz, M. A., Dooley, K., Biller, S. J., . . . Cziczo, D. J. (2019). Investigating the heterogeneous ice nucleation of sea spray aerosols using *Prochlorococcus* as a model source of marine organic matter. *Environmental Science & Technology, 53*(3), 1139-1149. doi:10.1021/acs.est.8b05150

Yamada, Y., Tomaru, Y., Fukuda, H., & Nagata, T. (2018). Aggregate formation during the viral lysis of a marine diatom. *Frontiers in Marine Science, 5*, 167. https://doi.org/10.3389/fmars.2018.00167

Yau, M. K., & Rogers, R. R. (1996). Observed properties of clouds *A short course in cloud physics* (pp. 60-80): Elsevier.

Yoch, D. C., Ansede, J. H., & Rabinowitz, K. S. (1997). Evidence for intracellular and extracellular dimethylsulfoniopropionate (DMSP) lyases and DMSP uptake sites in two species of marine bacteria. *Applied Environmental Microbiology, 63*(8), 3182-3188.

Yun, Y., & Penner, J. E. (2013). An evaluation of the potential radiative forcing and climatic impact of marine organic aerosols as heterogeneous ice nuclei. *Geophysical Research Letters, 40*(15), 4121-4126. doi:10.1002/grl.50794

Zeppenfeld, S., van Pinxteren, M., Hartmann, M., Bracher, A., Stratmann, F., & Herrmann, H. (2019). Glucose as a Potential Chemical Marker for Ice Nucleating Activity in Arctic Seawater and Melt Pond Samples. *Environmental Science & Technology, 53*(15), 8747-8756. doi: 10.1021/acs.est.9b01469

Zhao, M., Golaz, J. C., Held, I. M., Ramaswamy, V., Lin, S. J., Ming, Y., . . . Guo, H. (2016). Uncertainty in model climate sensitivity traced to representations of cumulus precipitation microphysics. *Journal of Climate, 29*(2), 543-560. doi:10.1175/Jcli-D-15-0191.1

Zimmermann, F., Weinbruch, S., Schutz, L., Hofmann, H., Ebert, M., Kandler, K., & Worringen, A. (2008). Ice nucleation properties of the most abundant mineral dust phases. *Journal of Geophysical Research: Atmospheres, 113*(D23). doi:10.1029/2008jd010655

Zobrist, B., Marcolli, C., Koop, T., Luo, B., Murphy, D., Lohmann, U., . . . Cziczo, D. (2006). Oxalic acid as a heterogeneous ice nucleus in the upper troposphere and its indirect aerosol effect. *Atmospheric Chemistry and Physics, 6*(10), 3115-3129. doi: 10.5194/acp-6-3115-2006

Zwietering, M. H., Jongenburger, I., Rombouts, F. M., & van 't Riet, K. (1990). Modeling of the bacterial growth curve. *Applied and Environmental Microbiology, 56*(6), 1875-1881.

APPENDIX

Introduction

The Appendix herein contains a report of phytoplankton pigment concentrations quantified at each station through High Performance Liquid Chromatography (HPLC) analysis of seawater collected at 5 m depth (Text A1 and Fig. A1). Secondly, aerosol concentrations and size distributions observed during Sea Sweep deployments are reported in Fig. A2 and discussed in Text A2.

Text A1

HPLC pigment analysis (Fig. A1) indicated that phytoplankton biomass was greatest at the first three stations, with maximum surface (5 m depth) chlorophyll *a* concentration observed at Station 3 (3.47 mg m^{-3}). Deep mixing due to the storm resulted in relatively low chlorophyll *a* concentration at Station 4 (0.39 mg m^{-3}). During the next four days, the water column stabilized and phytoplankton bloomed. Chlorophyll *a* concentration increased over this period to 1.28 mg m^{-3} (Fig. A2). The pigment profiles at all sampling stations indicate that the phytoplankton assemblage was composed of several major eukaryote taxonomic groups (diatoms, dinoflagellates, prymnesiophytes, cryptophytes, prasinophytes and chlorophytes), whose relative contribution to the phytoplankton biomass changed from station to station. The presence of fucoxanthin indicates that diatoms were a significant component of the phytoplankton throughout the cruise, an observation confirmed by FlowCam imaging. Alloxanthin is a biomarker for cryptophytes, while the presence of 19'-hexanoyloxyfucoxanthin and 19'-

butanoyloxyfucoxanthin indicate prymnesiophytes. Violaxanthin is a biomarker for prasinophytes and chlorophytes, which were likely a significant component of the photosynthetic picoeukaryotes enumerated by flow cytometry (Figure 6). Violaxanthin was present in concentrations between 0.008 and 0.04 mg m^{-3} on Station 4 Day 1 and Station 4 Day 4, respectively. For clarity, Figure A1 only lists primary pigments (defined in Hooker et al. 2005), and therefore violaxanthin is not included in the figure. Peridinin, a biomarker of dinoflagellates, was found at relatively high concentrations at Station 1 (0.409 mg m^{-3}), Station 2 (0.420 mg m^{-3}), and Station 3 (0.136 mg m^{-3}). Peridinin concentrations were low at stations sampled after the storm (0.004 – 0.034 mg m^{-3}). Peridinin to chlorophyll ratios decreased from 0.230 at Station 1 to 0.010 at Station 4 on the day after the storm.

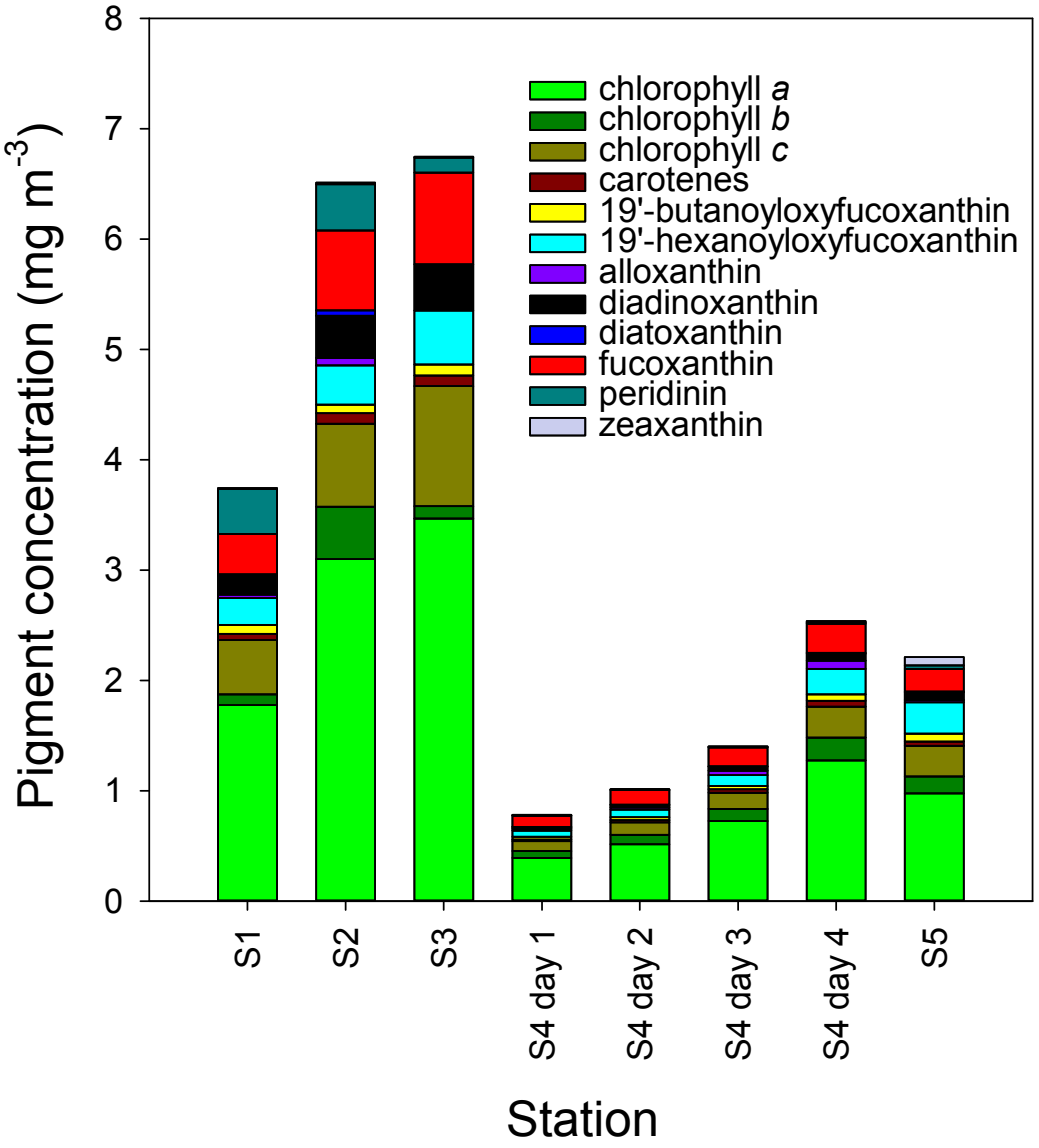

Figure A1: Phytoplankton pigment concentrations at each station measured with High Performance Liquid Chromatography (HPLC). Seawater samples were collected during CTD casts made between 8:00 and 9:00 am (local time), with the exception of Station 1, which was made at 12:20 pm.

Text A2

Aerosol concentrations and size distributions observed during Sea Sweep deployment are discussed here. Sea Sweep aerosol concentrations and ambient aerosol concentrations were simultaneously measured by two condensation particle counters (TSI, Inc. Model 3010). We note that Sea Sweep concentrations depend on instrument operation (the number of bubbles captured by the hood), rather than ambient concentrations. In fact, over the course of the campaign, Sea Sweep aerosol concentrations were 2.3 – 17.2 times greater that ambient aerosol concentrations. Mean aerosol concentrations are shown in Figure A2. The aerosol number size distribution generated by the Sea Sweep was determined by combining mobility distributions measurements from two Differential Mobility Particle Sizers (DMPSs) and applying a data inversion algorithm according to the method of Stratmann and Wiedensohler (1996). In general, generated aerosol size distributions were much more consistent than concentrations. During each deployment, the Sea Sweep produced broad unimodal size distributions of particles with the majority of particles in the range of 20 and 200 nm diameter with a tail of few particles detected in all size bins measured by the DMPS's (up to 1 micron diameter). The daily modal diameter was between ~100 nm to 200 nm

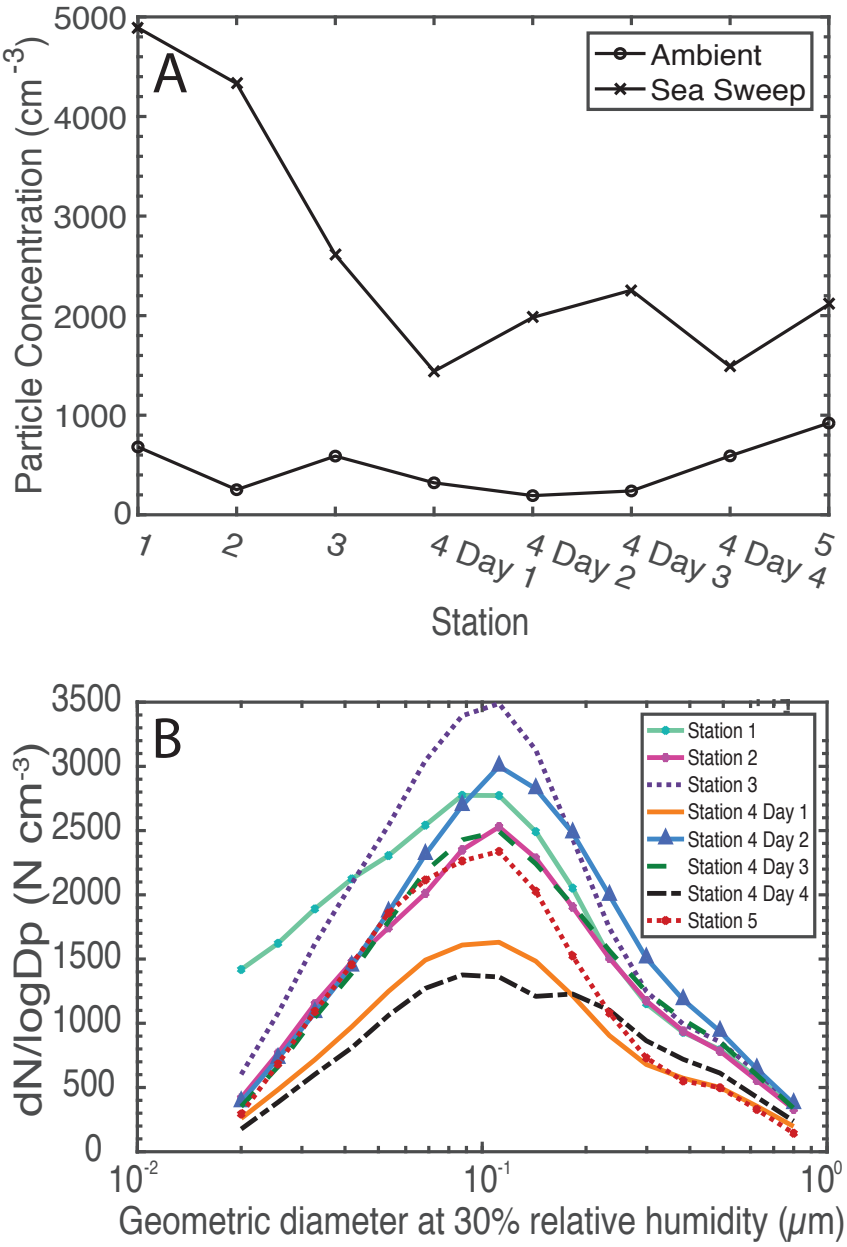

Figure A2: A) Ambient aerosol concentrations and Sea Sweep aerosol concentrations, each measured with a condensation particle counter (TSI, Inc. Model 3010) onboard the R/V Atlantis. B) DMPS Number size distributions (dN/dlogDp) of aerosols generated by the Sea Sweep. We note that Sea Sweep aerosol concentrations and size distributions are strongly influenced by operating conditions of the Sea Sweep, and do not represent variations in the ambient aerosol population.